N84-28066

Final Technical Report

covering period from July 1, 1978 to June 30, 1983

National Aeronautics and Space aAdministration

for

NAG 2-48

University of California
Santa Barbara, CA 93106

"Long Range Coherence in Free Electron Lasers"

Principal Investigator: W. B. Colson
Quantum Institute
University of California
Santa Barbara, CA 93106

FINAL TECHNICAL REPORT

Summary:

This research started in July 1978 at Rice University, Houston TX as NASA-Ames Grant NSG 7490 with Ken Billman as technical monitor. In July 1980, the grant terminated at Rice and the effort was moved to the University of California at Santa Barbara, CA under NASA-Ames Grant NAG 2-48 for its completion in June 1983; the technical monitor then was R. L. McKenzie. The research goal was the theoretical understanding of free electron lasers (FELs).

In 1978, FELs were just barely an idea; the first experiment at Stanford University had just been completed months before, there had been only one publication, and no other theoretical or experimental groups were even aware of the concepts. At present, there are many major experiments around the world and the funding level in the U.S. alone exceeds $40,000,000/year. The simple FEL design uses a static, periodic, transverse magnetic field to undulate relativistic electrons traveling along it's axis; this allows coupling to a co-propagating optical wave and results in bunching to produce coherent radiation. The advantages of the FEL are continuous tunability, operation at unique wavelengths ranging from centimeters to angstroms, and high efficiency resulting from the fact that the interaction region only contains light, relativistic electrons, and a

magnetic field.

This grant initiated and developed the basic theoretical concepts that are now the most widely used in the FEL field. While the title of the grant indicates a narrow application to the initial storage-ring FEL design, the research quickly became generalized to full FEL theory. The theoretical approach is related to those of accelerator physics, plasma physics, and conventional atomic laser theory, but with important distinctions. First of all, the fundamental mechanism is classical. The electrons entering the interaction region of an operating FEL respond to the combined forces of the static magnetic field and the light wave. We have shown that the resulting electron motion is governed by the phase-space of the simple pendulum. In an atomic laser, the electron equations of motion are quite different, the Bloch equations. It is appropriate to assume that even from spontaneous emission there is enough initial coherence to use the slowly-varying amplitude and phase approximation in the optical wave equation. This reduces it to the parabolic wave equation. While the pendulum equation shows up often in accelerator and plasma physics, those fields do not usually use the parabolic wave equation to describe electromagnetic radiation. In accelerators, the electromagnetic wave typically does not evolve since it is confined to an RF cavity. In plasma physics, the fields are

electrostatic as well as freely propagating, and are usually more broad-band.

After several years of development the basic theory using the coupling pendulum for electrons and the parabolic wave equation for light has grown more sophisticated. The range of validity includes high gain, low gain, collective effects, strong and weak optical fields, Coulomb forces, exotic undulator designs, short optical pulse effects, transverse mode optical resonator design, higher optical harmonics, and multimode operation in each dimension. We feel a particularly deep knowledge of the theory is justified for two reasons. First, FELs are typically $10,000,000 investments so that design improvements and guidance are well worth a substantial effort. Secondly, a fairly simple theory seems to work very well, indicating that many detailed measurements are possible and that the comparison between theory and experiment can be made complete.

Research:

The main emphasis of the work accomplished under this grant was the development of the basic equations and theoretical concepts which describe FEL operation. During the course of the research some other closely related topics were also explored. The research resulted in eleven refereed publications and five non-refereed publications and reports.

In collaboration with S.K. Ride, we explored the possibility of creating an FEL in a uniform magnetic field [1]. In was found that the interaction of free electrons and free electromagnetic radiation, in the presence of a uniform magnetic field, can result in stimulated emission or absorption. We analyzed the dynamics of single electrons by solving the classical, relativistic Lorentz force equations of motion in these combined fields. An electron may gain energy from, or lose energy to, the radiation field, depending crucially on the phase and oscillation frequency of the electron's helical motion within the superposed, circularly polarized light wave. To first order in the radiation field strength, electrons in a monoenergetic, uniformly distributed beam become spatially bunched, but there is no net energy change. To second order, however, the beam may experience a gain or loss of energy, corresponding to attenuation or amplification of radiation. We compared the bunching of this laser process to the bunching processes involved in (1) the Stanford free-electron laser and (2) the cyclotron maser, and find significant differences in each case. Our analytic results provide a clear, simple picture of the interaction process, and can be useful in exploring light amplification in astrophysical magnetic fields, the magnetosphere, or in laboratory devices.

With a group in the Space Solar Power Research Program

at Rice University, J. Freedman and S. Simons, we explored [2] two new devices which may have application to space deployed solar energy conversion and transmission systems, the "photoklystron" and the FEL. The photoklystron converts solar energy directly to R.F. power. It operates on the principle of the klystron with the cathode replaced by a photoemitting surface. We tested a model at Rice University which oscillated at 30 MHz. The laboratory model required two low-voltage bias voltages. Concepts for a self-biasing device are also being considered. The photoklystron is expected to be an alternative to solid state solar cells which produce DC current. The second device, the FEL, converts energy from relativistic electrons to narrow band electromagnetic energy which is tunable from the infared to the ultraviolet. Such a system is now being studied at NASA Lewis Research Center for space communications applications.

Again in collaboration with S.K. Ride [3], it was shown that a laser can efficiently accelerate charged particles if a magnetic field is introduced to improve the coupling between the particle and the wave. Solving the relativistic equations of motion for an electron in a uniform magnetic field and superposed, circularly polarized electromagnetic wave, we found that in energy-position phase-space an electron traces out a curtate cycloid: it alternately gains and loses energy. If, however, the parameters are chosen so

that the electron's oscillations in the two fields are resonant, it will continually accelerate or decelerate depending on its initial position within a wavelength of light. A laboratory accelerator operating under these resonant conditions appears attractive: in a magnetic field of 100 kGauss, and the fields of a 5 teraWatt, 10 micron wavelength laser, an optimally positioned electron would accelerate to 700 MeV in only 10 meters.

In collaboration with S. K. Ride [4], the spontaneous emission properties of FELs where explored and related to those of synchrotron radiation from relativistic electrons in a bending magnet. The modes of an FEL evolve from the spontaneous radiation emitted by relativistic electrons traveling in "small pitch angle" helical orbits in a magnetic field. The details of FEL operation depend on the angular and spectral characteristics of the emission spectrum, and laser gain is proportional to the slope of the spontaneous emission line. We first obtained an exact, fully relativistic expression for the radiation emitted by a charge traveling in finite helical trajectory (the finite length of the trajectory determines the spectral line width). We then examine the specific case of spontaneous emission in an FEL where the narrow radiation cone continually excites a detector on-axis at infinity. The result is a spectrum of sharp, well-separated harmonics. We discussed the spectrum

for electrons guided by (1) a periodic, transverse magnetic field, and (2) a uniform, longitudinal magnetic field, and show that a knowledge of the spontaneous spectrum, and its dependence on the field parameters, could be exploited to tune the laser, or induce gain in the higher harmonics.

In collaboration with J. Freedman, S. Simons, F. Brotzen, and J. Hester of Rice University, we again explored the photoklystron device [5]. Now we were able to make the device oscillates at R.F. frequencies simply by illuminating it by light. It was originally conceived as reflex klystron with the termionic electron source replaced by a photoemitter. In practice, the photoklystron has been found to have different properties from what might be expected by simply scaling a reflex klystron to lower electron energies and oscillation frequencies. These include electron energy exchange with the R.F. field on multiple oscillations and plasma effects. The device can be made to "self-oscillate"; that is, no external accelerating bias voltage is necessary. The energy to sustain oscillation is derived solely from the photoelectrons. An electrical efficiency of 1% has been demonstated for the first test model photoklystron. An ultimate efficiency of 10% appears possible.

In collaboration with S. Segall of KMS Fusion, Inc. a simple single-particle model of an FEL amplifier [6] was used in a computer simulation to determine the maximum fractional

conversion of electron kinetic energy to laser energy. The simulation results can be represented by a single universal curve. A simple scaling relationship for the length of the optimized constant period helix together with the universal curve permit one to predict maximum fractional energy conversion for any set of values of initial electron energy, initial laser intensity, magnetic field amplitude, and magnet period.

In collaboration with S. K. Ride, we developed a self-consistent, nonlinear description of the free electron laser using single-particle dynamics and Maxwell's wave equation [7]. Microscopic electron bunching drives the amplitude and phase of the optical wave. This is the first paper where the wave equation was self-consistently coupled to the electron pendulum equation. A method of sampling only a few particles was developed to save computer time in numerical approaches. The system of equations contains the non-linear aspects of the FEL mechanism.

In a subsequent, more complete papers we applied the coupled wave and pendulum equations to a variety of problems to show their capabilities [8,9]. The short optical pulse problem is solved to show a wide range of exotic effects in FELs. Several of these effects were observed in the original Stanford experiments. The excellent comparison between theory and experiment gave the first implication that the approach

was going to be exceptionally useful.

There is also an analysis of how electron beam energy spread and emittance can decrease the gain process in FELs. This had practical applications in the design of experiments. A long time-scale averaging procedure was developed which allowed us to relate the FEL oscillator to a second order phase transition. As coherence grows in the laser field, the long range order grows as in a magnetic solid. The generalized potential for the evolution of the FEL optical field is presented.

In 1981 a review article was written for the McGraw-Hill Yearbook of Science and Technology [10]. The basic mechanism was described in simple terms and the advantages over conventional atomic lasers was outlined. Several of the existing experimental configurations were mentioned.

As another extension of our basic theory the nonlinear wave equation and self-consistent pendulum equation were used to generalize FEL operation to higher harmonics [11]. This can significantly extend their tunable range to shorter wavelengths. The practical application of this technique is reviewed in this paper. The coupling to higher harmonics depends only the magnetic field strength and the magnet wavelength. For most experiments the coupling is not small. In fact, of the four experiments that have now operated as oscillators, three have observed emission in higher

harmonics. Another experiment has measured gain in the third harmonic.

In further work [12] the theory is used to explore the dynamics of the laser field's amplitude and phase for a wide range of parameters using families of normalized gain curves applicable to both the fundamental and higher harmonics. The electron phase-space displays the fundamental physics driving the wave, and we use this picture to distinguish between the effects of high gain and Coulomb forces. It is shown that Coulomb forces can be included in a generalized pendulum equation and collect effects in FELs are typically not caused be plasma oscillations.

In collaboration with P. Elleaume of University of Paris, Orsay, France, we study [13] the electron phase-space evolution and gain of FELs whose short-wavelength radiation has Gaussian spherical wavefronts. Several FEL designs are considered: the periodic magnetic field undulator, tapered wavelength undulator, and the optical klystron with a gap between two short undulators. We find that the gain spectrum is not proportional to the slope of the forward spontaneous emission spectrum as had been predicted by a previously published theorem, and we found the design of the Gaussian mode which maximizes the energy extraction from the electron beam in FELs.

Several years after the initial short pulse experiments

at Stanford University, another round of more sophisticated measurements were being made. Now the credibility of the theory had grow to the extent that the experimentalists were using simulations to help design the measurement technique. Predictions had been made by our research effort [14] as to the results. Observations involved a shift in optical frequency as the FEL reaches saturation power levels and a dramatic change in the optical spectrum and pulse shape when the resonator length is adjusted by a few microns out of 12 meters. The agreement with theory on these matters was good; all qualitative effects agreed with theory and the quantitative comparison was with experimental uncertainty. In the review of these results, some predictions were made for short pulse effects in tapered wavelength undulators [13]. This kind of magnetic undulator design was being explored at the National Labs to extend the saturation level to higher powers.

In collaboration with P. Bosco, a graduate student supported by this grant in the last year, and R. Freedman, the problem of oscillator evolution and mode competition in FELs was studied [15]. Relativistic quantum field theory was used to calculate the electron wave functions, the angular distribution of spontaneous emission, and the transition rates for stimulated emission and absorption in each frequency mode. The photon rate equation for the weak-field

regime was presented. This rate equation was applied to oscillator evolution with a conventional undulator, the two-stage optical klystron, and the tapered undulator. The effects of classical shot noise and optical quantum noise are briefly discussed. In each case, noise is found to have only a small effect on laser operation.

With the NASA supported graduate student, P. Bosco, the spectrum, angular distribution, polarization and coherence properties of the radiation emitted by relativistic electrons undulating through a quasiperiodic tapered magnetic field were studied [16]. Tapering the wavelength and/or field strength along the undulator's axis has the effect of spreading the spectral line to higher frequencies; interference over this broader spectral range results in a more complex line shape. The angular dependence, on the other hand, is not affected by the amount of taper. The polarization of the radiation in the forward direction is determined by the transverse polarization of the undulator, but the polarization changes off axis. The radiation patterns predicted are distinct from those of untapered undulators, and their detection is now feasible. They will provide useful diagnostics of electron trajectories and threshold behavior in free-electron-laser oscillators using tapered undulators.

Publications:

1. S. K. Ride and W. B. Colson, "A Free Electron Laser in a Uniform Magnetic Field", Appl. Phys. 20, 41 (1979).

2. J. W. Freeman, W. B. Colson and S. Simons, "New Methods for the Conversion of Solar Radiation to R.F. and Laser Power", Fourth Princeton AIAA Conference on Space Manufacturing Facilities III, 79-1416, p. 1 (May 1979).

3. W. B. Colson and S. K. Ride, "A Laser Accelerator", Appl. Phys. 20, 61 (1979).

4. S. K. Ride and W. B. Colson, "Spontaneous Emission in a Free Electron Laser", Stanford University High Energy Physics Lab Report #858 (1979).

5. J. W. Freeman, S. Simons, W. B. Colson, F. R. Brotzen, and J. Hester, "The Photoklystron", The Space Solar Power Review 1, 145 (1980).

6. W. B. Colson and S. B. Segall, "Energy Transfer in Constant Period Free Electron Lasers", Appl. Phys. 22, 219 (1980).

7. W.B. Colson and S. K. Ride, "The Non-Linear Wave Equation for Free Electron Lasers Driven by Single Particle Currents", Phys. Lett. A76, 379 (1980).

8. W. B. Colson and S. K. Ride, "The Free Electron Laser: Maxwell's Equations Driven by Single-Particle Currents", Invited Chapter in "Physics of Quantum Electronics", Vol. 7, Chapter 13, p. 377, Addison-Wesley Publishing Co., 1980, ed. Jacobs, Pilloff, Sargent, Scully, Spitzer.

9. W. B. Colson, "Free Electron Laser Wave and Particle Dynamics", Invited Chapter at the International Summer School of Quantum Electronics, Erice (Sicily), " Free Electron Lasers", eds. S. Martellucci and A.N. Chester (Plenum Publishing, 1983).

10. W. B. Colson, "Free Electron Lasers", 1981 McGraw-Hill Yearbook of Science and Technology, p. 218.

11. W. B. Colson, "Free Electron Lasers Operating in Higher Harmonics", Phys. Rev. Rapid Communications A24, 639 (1981).

12. W. B. Colson, "The Non-Linear Wave Equation for Higher Harmonics in Free Electron Lasers", IEEE J. Quantum Electronics QE-17, 1417 (1981).

13. W. B. Colson and P. Elleaume, "Electron Dynamics in Free Electron Laser Resonator Modes," Applied Physics B29, 101 (1982).

14. W. B. Colson, "Optical Pulse Evolution in the Stanford Free Electron Laser and in a Tapered Wiggler", Invited Chapter in "Physics of Quantum Electronics", Vol. 8, Chapter 19, p. 457, Addison-Wesley, 1982, ed. Jacobs, Moore, Pilloff, Sargent III, Spitzer.

15. P. Bosco, W. B. Colson, and Roger A. Freedman, "Quantum/Classical Mode Evolution in Free Electron Laser Oscillators," IEEE J. Quantum Electronics QE-19, 272 (1983).

16. P. Bosco and W. B. Colson, "Spontaneous Radiation from Relativistic Electrons in a Tapered Undulator", Phys. Rev. A28, 319 (1983).

Appl. Phys. 20, 41–50 (1979)

Applied Physics

A Free-Electron Laser in a Uniform Magnetic Field

S. K. Ride

NASA, Johnson Space Center, Houston, TX 77058, USA

*W. B. Colson**

Space Physics, Rice University, Houston, TX 77001, USA

Received 18 December 1978/Accepted 2 May 1979

Abstract. The interaction of free electrons and free electromagnetic radiation, in the presence of a uniform magnetic field, can result in stimulated emission or absorption. We analyze the dynamics of single electrons by solving the classical, relativistic Lorentz force equations of motion in these combined fields. An electron may gain energy from, or lose energy to, the radiation field, depending crucially on the phase and oscillation frequency of the electron's helical motion within the superposed, circularly polarized light wave. To first order in the radiation field strength, electrons in a monoenergetic, uniformly distributed beam become spatially bunched, but there is no net energy change. To second order, however, the beam may experience a gain or loss of energy, corresponding to attenuation or amplification of radiation. We compare the bunching of this laser process to the bunching processes involved in 1) the Stanford free-electron laser and 2) the cyclotron maser, and find significant differences in each case. Our analytic results provide a clear, simple picture of the interaction process, and can be useful in exploring light amplification in astrophysical magnetic fields, the magnetosphere, or in laboratory devices.

PACS: 41, 42.55, 95

Recently there has been a great deal of interest in the development of a free-electron laser, a device in which ultra-relativistic electrons, following helical orbits in a periodic, transverse magnetic field, amplify coherent radiation [1]. This laser operates on the principle that the free spontaneous radiation, emitted in a narrow cone about the forward direction, remains in the interaction volume with the electrons and is therefore available to stimulate subsequent radiation processes. The energetic electron beam need only lose a small fraction of its energy to amplify a powerful short-wavelength pulse stored in an optical cavity. In 1976, Madey built a prototype free-electron laser, which has operated both as an oscillator [2] and amplifier [3].

Can a free-electron laser operate in static fields other than the periodic transverse field? In this paper, we will show that this type of laser action is also possible in a uniform, longitudinal magnetic field (symbolized $\vec{B}_\parallel$). The characteristics of such a laser differ both qualitatively and quantitatively from those of the laser employing a periodic, transverse magnetic field (symbolized $\vec{B}_\perp$).

The process we investigate is shown schematically in Fig. 1. Relativistic electrons spiral with small pitch

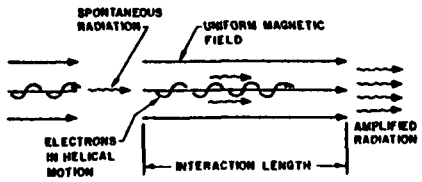

Fig. 1. Relativistic electrons spiral along the field lines of a uniform magnetic field, and emit circularly-polarized monoenergetic radiation in the forward direction. The radiation induces the emission of laser light from electrons further along in the beam

* Supported in part by Army Contract No. DASG 60-77-C-0083 and NASA Grant NSG-7490.

0340-3793/79/0020/0041/$02.00

angles in a uniform magnetic field. Circularly polarized radiation (like that emitted spontaneously) passes over these electrons, and stimulates further radiation processes. It should be noted that the device proposed here is different from a well-known cyclotron maser [4–7]. The stimulating fields are free radiation fields, not modes of a cavity operating near cutoff (as with the cyclotron maser); the result is a different gain mechanism and a correspondingly different gain curve. The two devices are compared in detail in Appendix A.

In this paper, we adopt a single particle approach similar to that used by Lamb [8] and Gaponov [9] to model conventional lasers and the cyclotron maser, and by Colson [10] to model the $\vec{B}_\perp$-field free-electron laser. We examine the fully relativistic Lorentz force equations and solve them order by order in the radiation field strength to obtain analytic expressions for the electron trajectory and energy as functions of its initial position within a wavelength of light. To first order, a dilute, spatially uniform, monoenergetic electron beam becomes bunched, but there is no net energy transfer. To second order, however, the energy change of the beam does not average to zero, and if the parameters of the device are chosen judiciously, the system should lase. We derive analytic expressions for the longitudinal and transverse bunching (both are important), and for laser gain.

This general procedure can be employed to derive the low gain behavior of other free-electron devices. We have used it to derive the particle trajectories and gain equation of the cyclotron maser and $\vec{B}_\perp$-field free-electron laser. The results of these calculations are presented in Appendices A and B, respectively; the bunching mechanisms and gain curves of these devices are compared to those of the "uniform field free-electron laser".

By investigating laser action in a $\vec{B}_\parallel$-field, we are exploring a process which, like the cyclotron maser and $\vec{B}_\perp$-field laser, has potential as a laboratory device; more intriguing, however, is the possibility that this process, which requires neither a cavity nor an intricate field structure, could occur spontaneously outside the laboratory. The basic ingredients, relativistic electrons and uniform magnetic fields, are present, for example, in the earth's magnetosphere, the radiation belts of Jupiter, the magnetospheres of pulsars, and other astrophysical situations.

1. Physical Problem

To examine whether laser action could be sustained in a uniform magnetic field ($\vec{B}_\parallel$) we will consider the following model problem: a single relativistic electron entering a region of space containing a circularly polarized electromagnetic wave, of well defined frequency and phase, and travelling along the axis of the $\vec{B}_\parallel$-field. The dynamics of the electron are described by the Lorentz force equations

$$\frac{d}{dt}(\gamma\boldsymbol{\beta}) = -\frac{|e|}{mc}[\mathbf{E}_r + \boldsymbol{\beta}\times(\mathbf{B}_m + \mathbf{B}_r)] \tag{1}$$

$$\frac{d}{dt}\gamma \equiv \dot{\gamma} = -\frac{|e|}{mc}\boldsymbol{\beta}\cdot\mathbf{E}_r\,, \tag{2}$$

where $\boldsymbol{\beta}c$ is the velocity of the electron of charge $e = -|e|$, mass m, and energy γmc^2. $\mathbf{B}_m$ is the magnetic field in the $\hat{z}$-direction,

$$\mathbf{B}_m = (0, 0, B_0)\,. \tag{3}$$

$\mathbf{E}_r$ and $\mathbf{B}_r$ are the radiation electric and magnetic fields. Equation (2) shows that the work done on the electron by the radiation field is proportional to $\boldsymbol{\beta}\cdot\mathbf{E}_r$, the orientation of the vectors determines whether the electron loses or gains energy. If it loses energy, there has been stimulated emission; if it gains energy, there has been absorption. The longer $\boldsymbol{\beta}\cdot\mathbf{E}_r$ retains a particular value, the more energy will be transferred between the radiation field and electron. This suggests that to maximize the energy transfer rate, we should choose the radiation to be circularly polarized such that the electron sees an electric field which rotates in the same sense as its velocity vector. We therefore take the radiation field to be of the form[1]

$$\begin{aligned}\mathbf{E}_r &= E_0[\cos(k_r z - \omega_r t + \phi), -\sin(k_r z - \omega_r t + \phi), 0]\,,\\ \mathbf{B}_r &= E_0[\sin(k_r z - \omega_r t + \phi), \cos(k_r z - \omega_r t + \phi), 0]\,.\end{aligned} \tag{4}$$

Equation (4) describes a plane wave of constant amplitude E_0, frequency $\omega_r = k_r c$, and phase ϕ, travelling with velocity $c\hat{z}$. It is assumed that (a) E_0 is large enough that it (and the phase ϕ) remains substantially constant during the amplification process (low gain), yet (b) E_0 is small enough that the effect of radiation on the electron dynamics may be handled perturbatively.

We perform the analysis for a light wave of arbitrary frequency, but show that only frequencies near a "resonant" value will result in significant energy transfer. Near resonance $\boldsymbol{\beta}_\perp$ and $\mathbf{E}_r$ rotate together and retain their orientation through many oscillations. The frequency of oscillation is given by the cyclotron frequency $\omega_c = |e|B_0/\gamma mc$, and the frequency at which radiation passes over the electron is $(1 - \boldsymbol{\beta}\cdot\hat{z})k_r$. The "resonance parameter" is defined as

$$\Delta\omega \equiv \frac{|e|B_0}{\gamma mc} - \omega_r(1 - \boldsymbol{\beta}\cdot\hat{z})\,. \tag{5}$$

[1] If the particles were positively charged, or if the magnetic field were reversed, polarization of the opposite sense would be appropriate.

"On resonance" ($\Delta\omega = 0$), exactly one wavelength of light will pass over the electron as it travels through one oscillation in the magnetic field. For ultrarelativistic electrons (γ large, $\beta \cdot \hat{z} \simeq 1$), and reasonable laboratory magnetic fields, the radiation wavelength can be made quite small.

In a laser oscillator, or free-space laser, the initial radiation would be spontaneously emitted by the electrons accelerating through helical orbits with small pitch angles. We emphasize that such radiation has just the right direction, polarization, and frequency to initiate amplification when passing over electrons further "upstream" in the uniform magnetic field. The radiation is emitted into a small range of frequencies about the resonance frequency given in (5), and into a narrow forward cone of angular width γ^{-1}. The radiation yielding the highest net gain will establish the final laser line. In an amplifier, the initial stimulating radiation is specified. In this calculation, we assume an initial electromagnetic wave of arbitrary frequency and phase, and search for the conditions necessary for amplification (gain) as the wave passes over an electron beam travelling through a uniform magnetic field.

The Lorentz force equations describing an electron's motion in the combined fields (3) and (4) form a complicated set of coupled, nonlinear differential equations. We will employ a perturbation approach to obtain a solution. Before turning to this approximation method, we can make some progress toward an exact solution. The $\hat{z}$-component of (1) can be combined with (2) to yield a relation between the energy and the velocity in the $\hat{z}$-direction

$$\gamma(t)[1 - \beta_z(t)] = \text{const}. \tag{6}$$

Therefore, if the energy of the electron is changed, its velocity in the $\hat{z}$-direction is necessarily changed; since γ, β_z, and $\beta_\perp$ are related through $\gamma^{-2} = (1 - \beta_z^2 - \beta_\perp^2)$, the velocity in the transverse direction must also change.

As a second step towards solution of the equations of motion, we can integrate the $\hat{x}$- and $\hat{y}$-components of (1) immediately by noting that the right-hand sides are perfect time derivatives. We therefore have the following set of exact equations

$$\text{(a)}\quad \gamma\beta_x = \frac{|e|E_0}{mc\omega_c}[\sin(k_z z - \omega_c t + \phi) - \sin(k_z z_0 + \phi)] - \frac{|e|B_0 y}{mc^2} + \text{const.},$$

$$\text{(b)}\quad \gamma\beta_y = \frac{|e|E_0}{mc\omega_c}[\cos(k_z z - \omega_c t + \phi) - \cos(k_z z_0 + \phi)] + \frac{|e|B_0 x}{mc^2} + \text{const.}, \tag{7}$$

$$\text{(c)}\quad \gamma(1 - \beta_z) = \text{const.},$$

$$\text{(d)}\quad \dot{\gamma} = -\frac{|e|E_0}{mc}[\beta_x \cos(k_z z - \omega_c t + \phi) - \beta_y \sin(k_z z - \omega_c t + \phi)].$$

Unable to integrate further, we seek a solution by means of a perturbation expansion in the field strength E_0. That is, we assume that the electron's trajectory is determined by the static field, and that the radiation field produces small perturbations about this motion. We choose to perform our analysis in weak radiation fields where the energy transfer is small, and require only that the amplitude be large enough that we are dealing with a classical wave.

It is possible to self-consistently solve the equations of motion (7) order by order in E_0. To zeroth order, the electron moves in the uniform magnetic field alone with trajectory $\mathbf{r}_0 = (x_0, y_0, z_0)$

$$x_0(t) = \frac{\beta_{\perp 0} c}{\omega_c}\sin(\omega_c t + \theta_0),$$

$$y_0(t) = -\frac{\beta_{\perp 0} c}{\omega_c}\cos(\omega_c t + \theta_0),$$

$$z_0(t) = z_0 + \beta_{z0} c t,$$

$$\gamma_0 = \text{const.} = (1 - \beta_{\perp 0}^2 - \beta_{z0}^2)^{-1/2},$$

where $\omega_c = |e|B_0/\gamma_0 mc$ is the relativistic cyclotron frequency; the arbitrary constants $\beta_{z0}c$, z_0, $\beta_{\perp 0}c$, and θ_0 are the electron's initial longitudinal velocity and position, and transverse velocity and phase, respectively. These constants of motion define a class of trajectories which spiral symmetrically about the $\hat{z}$-axis.

We now proceed to first order in the radiation field strength, and write the solutions in the form

$$\mathbf{r}(t) = \mathbf{r}_0(t) + \delta\mathbf{r}_1(t) + \ldots,$$
$$\gamma(t) = \gamma_0 + \delta\gamma_1(t) + \ldots, \tag{9}$$

where $\delta\mathbf{r}_1 = (\delta x_1, \delta y_1, \delta z_1)$ and $\delta\gamma_1$ are small, proportional to E_0, and must vanish at $t = 0$. Substitute these expressions into the Lorentz force equations, and retain terms only to first order in small parameters. Equation (7d) becomes

$$\frac{\delta\dot{\gamma}_1}{\dot{\gamma}_0} = -\omega_E \beta_{\perp 0}\cos(\Delta\omega t + \theta), \tag{10}$$

where $\theta \equiv k_z z_0 + \phi + \theta_0$, $\omega_E = |e|E_0/\dot{\gamma}_0 mc$, and $\Delta\omega = \omega_c - \omega_c(1 - \beta_{z0})$. Equation (10) can be integrated immediately to give the first order change in the electron energy

$$\frac{\delta\gamma_1(t)}{\dot{\gamma}_0} = -\frac{\beta_{\perp 0}\omega_E}{\Delta\omega}[\sin(\Delta\omega t + \theta) - \sin\theta]. \tag{11}$$

From (6) it is clear that we can relate $\delta\dot{\gamma}_n$ to $\delta\dot{z}_n$ order by order. In particular, after evaluating the constant $\gamma(1 - \beta_z)$ at $t = 0$, we find

$$\frac{\delta\dot{z}_1}{c} = (1 - \beta_{z0})\frac{\delta\dot{\gamma}_1}{\dot{\gamma}_0}.$$

Therefore,

$$\frac{\delta z_1}{c} = \beta_{\perp 0}(1 - \beta_{z0})\frac{\omega_E}{\Delta\omega^2} \cdot [\cos(\Delta\omega t + \theta) - \cos\theta + \Delta\omega t \sin\theta]. \tag{12}$$

δx_1 and δy_1 can be found from combining 7(a) and (b) into an exponential form. They are

$$\frac{\delta x_1}{c} = \frac{\omega_E}{\omega_c}\left[\frac{\cos(k_z z_0 + \phi - \omega_c t) - \cos[k_z z_0 + \phi - \omega_z(1 - \beta_{z0})t]}{\Delta\omega} + \frac{\cos(k_z z_0 + \phi) - \cos(k_z z_0 + \phi - \omega_c t)}{\omega_c}\right] + \frac{\omega_E \beta_{\perp 0}^2}{\Delta\omega^2}\cos(\omega_c t + \theta_0)[-\cos(\Delta\omega t + \theta) + \cos\theta - \Delta\omega t \sin\theta] \tag{13}$$

and,

$$\frac{\delta y_1}{c} = \frac{\omega_E}{\omega_c}\left[\frac{\sin[k_z z_0 + \phi - \omega_z(1 - \beta_{z0})t] - \sin(k_z z_0 + \phi - \omega_c t)}{\Delta\omega} + \frac{\sin(k_z z_0 + \phi - \omega_c t) - \sin(k_z z_0 + \phi)}{\omega_c}\right] + \frac{\omega_E \beta_{\perp 0}^2}{\Delta\omega^2}\sin(\omega_c t + \theta_0)[-\cos(\Delta\omega t + \theta) + \cos\theta - \Delta\omega t \sin\theta]. \tag{14}$$

The expansion can now be extended to second order in a similar fashion.

$$\frac{\delta\dot{\gamma}_2}{\gamma_0} = \omega_E \cos[k_z z_0 + \phi - \omega_z(1 - \beta_{z0})t] \cdot \left[\frac{\dot{y}_0}{c}k_z \delta z_1 - \frac{\delta\dot{x}_1}{c}\right] + \omega_E \sin[k_z z_0 + \phi - \omega_z(1 - \beta_{z0})t] \cdot \left[\frac{\dot{x}_0}{c}k_z \delta z_1 + \frac{\delta\dot{y}_1}{c}\right]. \tag{15}$$

When the zero-order and first-order results are inserted, (15) can be integrated directly.

$$\frac{\delta\gamma_2}{\dot{\gamma}_0} = \frac{\omega_E^2 \beta_{\perp 0}^2}{\Delta\omega^2}[-\cos(\Delta\omega t + \theta)\cos\theta + \cos^2\theta + \tfrac{1}{2}\cos(2\theta + \Delta\omega t) - \tfrac{1}{2}\cos 2\theta + \Delta\omega t \cos(\Delta\omega t + \theta)\sin\theta] + \frac{\omega_E^2}{\Delta\omega^2}(1 - \beta_{z0})(1 - \cos\Delta\omega t). \tag{16}$$

Note that the second-order change in energy results from first-order changes in both longitudinal and transverse position. Also, all phases (z_0, ϕ, and θ_0) have combined into the single phase θ.

2. Particle Dynamics

To second order in the radiation field, the fractional change in the electron energy evolves as

$$\frac{\Delta\dot{\gamma}(t)}{\dot{\gamma}_0} = \frac{\dot{\gamma}(t) - \dot{\gamma}_0}{\dot{\gamma}_0} = \frac{\delta\dot{\gamma}_1}{\dot{\gamma}_0} + \frac{\delta\dot{\gamma}_2}{\dot{\gamma}_0} + \ldots \tag{17}$$

A particle's evolution depends, in a complicated way, on its initial parameters $\beta_{\perp 0}$, β_{z0}, and z_0.

In a real electron beam, particles enter the interaction region with a range of initial conditions. Dilute beams (where Coulomb forces may be neglected) can be accurately described by summing over all electrons in the beam. We assume that realistic beams are not "prebunched", and therefore consider, as a specific example, a monoenergetic, uniformly spread beam entering the interaction region at a particular angle. The initial positions are uniformly populated over many wavelengths of light so that the phase should be averaged over intervals of 2π. At any given time, to first order in the radiation field exactly half the electrons within a radiation wavelength gain energy and move ahead of the average beam flow; the other half lose energy and fall behind. This causes spatial bunching of the beam and a spreading of the initially narrow energy distribution.

To first order in fields, the form of the electron energy distribution is given by $[\delta\gamma_{max}^2(t) - \Delta\gamma^2]^{-1/2}$ where $\Delta\dot{\gamma}_{max}^2(t) = (\omega_E^2 \gamma_z^2 \beta_{\perp 0}^2/2\Delta\omega^2)(1 - \cos\Delta\omega t)$ with two spikes at $\pm\Delta\gamma_{max}(t)$, and oscillates with frequency $\Delta\omega$. The second-order corrections (proportional to ω_E^2) are asymmetric and cause the distribution to become slightly distorted. It is these distortions that are responsible for net amplification or laser gain.

If the electron beam is initially bunched, gain may result from the first-order energy changes. This gain mechanism can be important in long wavelength applications. In short wavelength radiations fields, gain can

only be obtained by means of "self-bunching" at the radiation wavelength, as described above.

As an aside, we wish to stress the importance of the "bunched" electron beam produced by the free-electron laser. This analysis shows that an external laser (or the laser oscillator) may be used in combination with a uniform longitudinal magnetic field to coherently modulate a relativistic electron beam at optical wavelengths [10]. Such a beam may be used, for example, to drive a high gain, powerful optical klystron [11].

3. Gain Equation

To calculate "gain", the fractional change in radiation energy, we must compute the energy gained or lost by the electron beam as a whole. The energy change per electron, $\langle \Delta\gamma \rangle mc^2$, is obtained by averaging (17) over a weighted distribution of initial positions and velocities; multiplying this by the number of electrons yields the energy change of the beam. We now identify the energy lost (or gained) by a section of the beam of volume V, containing $\varrho_e V$ electrons, as the energy gained (or lost) by radiation field in that volume. Gain, $G(t)$, can therefore be written

$$G(t) \equiv -\frac{\langle \Delta\gamma \rangle mc^2 \varrho_e V}{(2E_0^2 V/8\pi)}, \tag{18}$$

where $2E_0^2 V/8\pi$ is the radiation energy (in cgs units) orginally present in volume V. Thus, using energy conservation, the small growth of the field amplitude is

$$E_0(t) \simeq E_0 \exp[G(t)/2]. \tag{19}$$

In general, growth is not exponential, since $G(t)$ is not necessarily linear in time.

We perform the average for a uniformly spread, monoenergetic beam. In short-wavelength (large γ_z) applications, even short electron pulses are spread, approximately uniformly, over many optical wavelengths. Note that averaging over all initial longitudinal phases $k_z z_0$, or over all initial transverse phases θ_0, is equivalent and renders the result independent of any phase. Thus, $\langle\ \rangle \equiv \int_0^{2\pi} d\theta(\ )$. The first-order terms in Eq. (17) average to zero, but the second-order do not. The result is

$$G(t) = \frac{2\pi\varrho_e e^2}{\gamma_z m \Delta\omega^3}\{[\beta_{\perp 0}^2 + 2(1-\beta_{z0})](\cos\Delta\omega t - 1) + \beta_{\perp 0}^2 \Delta\omega t \sin\Delta\omega t\}. \tag{20}$$

This is the fractional change in the energy of the radiation field as it passes over an electron beam spiralling through a uniform magnetic field ($\vec{B}_0$). Under the proper conditions, energy *can* be transferred to the radiation field.

The gain is proportional to the electron density, inversely proportional to particle mass and kinetic energy, and decreases if far from resonance ($\Delta\omega$ large). We can acquire insight into the gain mechanism by examining the nonrelativistic limit of Eq. (20)

$$G(t) = \frac{4\pi\varrho_e e^2}{m\Delta\omega^3}(\cos\Delta\omega t - 1), \tag{21}$$

where $\beta_{\perp 0}, \beta_{z0} \ll 1$. $\Delta\omega = \omega_c - \omega_r$. Resonance occurs when the electron cyclotron frequency equals the radiation frequency. Note that in this limit gain cannot be positive – net stimulated emission is not possible for any choice of parameters.

We can understand this result by considering the electron beam as a system of classical oscillators. It is well known that a set of randomly phased *harmonic* oscillators absorbs energy from an electromagnetic wave – net stimulated emission can only occur if the oscillators are anharmonic [12, 9]. In the nonrelativistic limit of our problem, the electron beam is just a collection of harmonic oscillators; if, however, the electrons are even slightly relativistic, they are anharmonic oscillators – then, as indicated in (20), stimulated emission can dominate.

It is appropriate to examine gain at the end of an interaction region of length L. The time required by the unperturbed beam to traverse this length is $L/\beta_{z0}c$. Since shifts in the position and velocity are small, this is very nearly the time required by each electron to cover that length.

The final gain is then,

$$G_{final}(\omega) = \frac{2\pi\varrho_e e^2 L^2}{\gamma_z mc^2}\left|\frac{[\beta_{\perp 0}^2 + 2(1-\beta_{z0})]}{\beta_{z0}^3\omega^2}(\cos\omega - 1) + \frac{\beta_{\perp 0}^2 \omega \sin\omega}{\beta_{z0}^3\omega^2}\right|, \tag{22}$$

where ω is a dimensionless resonance parameter,

$$\omega \equiv \frac{\Delta\omega L}{\beta_{z0}c} = \left|\frac{|e|B_0}{\gamma_z mc} - \omega_r(1-\beta_{z0})\right|\frac{L}{\beta_{z0}c}. \tag{23}$$

Note that, for a fixed L, ω can be changed by varying any of the parameters γ_z, β_{z0}, ω_r, or B_0.

We can examine $G(\omega)$ in (22) by fixing, for example, γ_z, β_{z0}, and ω_r, and sampling various resonance parameters by changing the magnetic filed strength. In Fig. 2, $G(\omega)$ (in units of $2\pi\varrho_e e^2 L^2/\gamma_z mc^2$) is plotted versus ω. Maximum attainable gain is proportional to L^2. We have chosen $\gamma_z = 50$ and show the gain curves for three different injected pitch angles, $\theta_p \simeq \beta_{\perp 0}/\beta_{z0}$. Exactly on

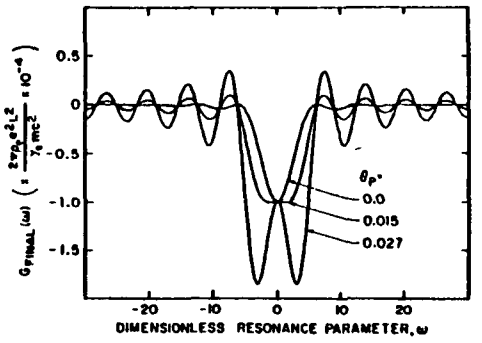

Fig. 2. When injected at a small pitch angle, $\theta_p \simeq \beta_{\perp 0}/\beta_{z0}$, the relativistic electron beam shows several gain peaks on either side of resonance. "On-resonance" ($\omega = 0$) only absorption can occur

resonance ($\omega = 0$) the "gain" is negative; in the specific limit $\beta_{z0} \simeq 1$, it is independent of the injection angle

$$G_{final}(0) = -\frac{\pi\varrho_e e^2 L^2}{\gamma_z^3 mc^2}. \tag{24}$$

Further, if the beam is injected exactly on-axis, there is no value of ω which can lead to net stimulated emission.

If however, the beam is injected slightly off-axis, net stimulated emission is possible for certain values of ω. The device will then operate as a laser if gain is larger than the losses. Maximum gain is achieved if $\omega \simeq \pm 7.5$. The principle of operation is the same as that which governs the Stanford free-electron laser: if the narrow spontaneous radiation cone (of angular width γ_z^{-1}, [10]) remains on-axis (that is, if $\beta_{\perp 0}\gamma_z^{-1} \lesssim 1$), it will excite a narrow fundamental emission line in the resonant cavity.

In contrast to the $\vec{B}_\perp$-field laser and the cyclotron maser, the gain curve of the $\vec{B}_\parallel$-field laser is symmetric in the resonance parameter. Although to zero order the electrons in each of these devices move in helical trajectories, the trajectories evolve differently. In the cyclotron maser, the electrons become azimuthally bunched (this is sometimes called "phase bunching") and the second-order changes in energy (i.e., gain) result from these transverse pertubations, $\delta x_\perp$, and $\delta y_\perp$ (see Appendix A). In the $\vec{B}_\perp$-field free-electron laser, the electrons become longitudinally bunched, and second-order energy changes arise from perturbations $\delta z_\perp$ (see Appendix B). Again, the result is an antisymmetric gain curve. However, in the $\vec{B}_\parallel$-field laser, both transverse and longitudinal bunching contribute to $\delta\gamma_z$, or gain. Their contributions oppose, and eliminate the usual cyclotron maser gain mechanism. There is however another (less efficient) mechanism at work; that mechanism is the one described in this paper.

In all these free-electron processes (and, in fact, any laser process), the length of the interaction region is a crucial factor in determining the conditions required for positive gain. This can be understood by referring to Fig. 2, and noting that the resonance parameter ω depends on the product of L and $\Delta\omega$. If L is fixed, as is usually the case in laboratory situations, $\Delta\omega$ can be chosen to maximize the gain. Creating a laser is therefore simply a matter of extracting the electron beam and radiation field at the right time.

Conclusions

We have presented a calculation which demonstrates that under certain conditions laser action can be sustained by relativistic electrons spiralling through a uniform magnetic field. We find that to first order in radiation field strength, the electron beam becomes spatially bunched in both the longitudinal and transverse directions, and spread in energy. The net energy transfer is zero to first order (for a uniformly spread, monoenergetic beam), but the self-bunching achieved to this order results in gain to second order. To achieve laser action in the uniform magnetic field, the electrons must be relativistic, they must be injected slightly off-axis, and they must oscillate slightly off-resonance. The gain mechanism is not that of a cyclotron maser or the periodic-field laser.

A laboratory device similar to the periodic, transverse field free-electron laser currently operating at Stanford could be made by placing mirrors of a resonant cavity beyond each end of the region of the uniform axial magnetic field. The condition $\beta_{\perp 0}\gamma_z^{-1} \simeq 1$ would maximize available gain, yet allow the narrow spontaneous emission cone to excite the resonator on-axis. The uniform-field laser would enjoy the same potential

advantages [13] as the periodic-field device: it would be continuously tunable, and capable of high power with good efficiency. However, for a given field strength and electron energy, the uniform field laser typically produces less gain and operates at longer wavelengths. Since the ultra-relativistic electron beam has such a high energy density, even this low gain can sustain a powerful laser pulse. The exciting possibility, of course, is that the uniform field laser mechanism described in this paper may operate in nature. Although a specific relationship between the electron motion and the radiation field is required for laser gain, the spontaneous emission produced by electrons in relativistic helical motion will pass over electrons further along in a beam, and bathe them in radiation which has the right properties to induce stimulated emission. Resonant interaction might therefore occur naturally for a whole range of magnetic field strengths, from weak interstellar fields to the huge fields near the surfaces of neutron stars.

The signature of this laser process would be anomalously bright, directional radiation featuring a narrow emission line; the emission frequency would be related to the magnetic field strength and electron kinematics through the resonance condition (5). It must be emphasized, however, that these properties may be disguised or distorted as the radiation propagates from its source to our detectors. This suggests that more specific analyses ought to be performed, and the model problem adapted to particular physical situations, in order to explore the importance of this radiation mechanism.

Appendix A

In order to compare the uniform-field free-electron laser to the cyclotron maser, we will describe the latter device using the one-body analysis of the text. Both devices use a static uniform magnetic field, but because we propose an experimental configuration similar to the Stanford free-electron laser [2, 3] (making use of Doppler shifted free radiation), the gain mechanisms are quite different. We adopt a simple model of the cyclotron maser, employed by several previous authors [5, 6, 9, 14], choosing the stimulating field to be a mode of a rectangular waveguide operating near cutoff. This choice simplifies the mathematics, yet illustrates the essential physics of the device. In particular, it describes the "transverse bunching mechanism" [6, 7, 15].

Again we begin with the relativistic equations of motion (1) and (2). The oscillating field of the cyclotron maser is

$$\mathbf{E}_w = E_w(\cos(\omega_w t + \phi), 0, 0)\,, \tag{25}$$

and there is no associated magnetic field. The static magnetic field is the same as that in the uniform-field free-electron laser,

$$\mathbf{B}_w = (0, 0, B_w)\,. \tag{26}$$

The problem can now be solved as outlined in the text. The zero order solutions are

$$\begin{aligned} x_1 &= -\frac{\beta_{\perp 0} c}{\omega_c}\sin(\omega_c t + \theta_0)\,,\\ v_{x_1} &= -\frac{\beta_{\perp 0} c}{\omega_c}\cos(\omega_c t + \theta_0)\,,\\ z_1 &= z_0 + \beta_{z0} c t\,,\\ \gamma_1^{-1} &= 1 - \beta_{\perp 0}^2 - \beta_{z0}^2 = \text{const.}\,, \end{aligned} \tag{27}$$

where again $\omega_c = |e|B_w/\gamma_1 mc$, and the electrons are initially located at angular phases θ_0 and longitudinal positions z_0.

As the electrons oscillate through their helical orbits, the oscillating wave does work on them. The largest energy transfer is possible near resonance, defined by

$$\Delta\omega = \omega_w - \omega_c = 0\,. \tag{28}$$

Note that this is similar to the resonance parameter for the uniform field laser, but the frequency of the oscillating field is not Doppler shifted.

To first order in E_w, the fractional change in energy is

$$\begin{aligned} \frac{\delta\gamma_1}{\gamma_1} = &-\frac{\omega_w e B_w}{2\Delta\omega}\{\sin(\Delta\omega t - \phi + \theta_0) - \sin(-\phi + \theta_0)\}\\ &+ (\text{non-resonant terms})\,, \end{aligned} \tag{29}$$

where $\omega_w = |e|E_w/\gamma_1 mc$. Since the maser will be operated near resonance, the resonant pieces in (29) (proportional to $\Delta\omega^{-1}t$) will dominate. For brevity we do not write out the non-resonant terms. Work can be done on or by the electron; the sign of $\delta\gamma_1$ depends on the electron's initial phase θ_0 relative to the phase of the oscillating field, ϕ.

The first-order changes in position are

$$\begin{aligned} \frac{\delta x_1}{c} = &-\frac{\beta_{\perp 0}^2\omega_w}{2\Delta\omega^2}\cos(\omega_c t + \theta_0)[\cos(\Delta\omega t - \phi + \theta_0)\\ &-\cos(-\phi + \theta_0) - \Delta\omega t\sin(-\phi + \theta_0)] + \dots,\\ \frac{\delta y_1}{c} = &-\frac{\beta_{\perp 0}^2\omega_w}{2\Delta\omega^2}\sin(\omega_c t + \theta_0)[\cos(\Delta\omega t - \phi + \theta_0)\\ &-\cos(-\phi + \theta_0) - \Delta\omega t\sin(-\phi + \theta_0)] + \dots,\\ \frac{\delta z_1}{c} = &-\beta_{z0}\frac{\beta_{\perp 0}\omega_w}{2\Delta\omega^2}[\cos(\Delta\omega t - \phi + \theta_0)\\ &-\cos(-\phi + \theta_0) - \Delta\omega t\sin(-\phi + \theta_0)] + \dots\,. \end{aligned} \tag{30}$$

We have not included the non-resonant terms.

We use these first-order changes in position to calculate the second-order change in energy. Here we find the important difference between the cyclotron maser and the $\hat{B}_0$-field free-electron laser. In the laser analyzed in the text, contributions to $\delta\gamma_2$ were found to result from both transverse shifts (δx_1 and δy_1) and longitudinal shifts (δz_1). These contributions nearly cancelled, leaving only a small residual energy shift. The cyclotron maser, however, employs a cavity mode (bound radiation) to upset this cancellation. In this oscillating field, longitudinal bunching cannot affect the energy flow ($\delta\dot{\gamma}_2$) between the electrons and the oscillating field; energy flow is a result of transverse bunching alone[3].

[3] It is possible to choose a cavity mode with a phase velocity less than c, and recover the longitudinal bunching mechanism, but losing the transverse mechanism [6, 7, 15]. The form of the results are similar.

The average rate of energy change of a beam is obtained by averaging $\delta\dot{\gamma}$ over the initial phases: $\langle\ \rangle = \int_0^{2\pi} d\theta_0/2\pi$. Performing the average renders $\langle\delta\dot{\gamma}\rangle$ independent of the initial longitudinal position, z_0, and the phase ϕ. $\delta\gamma_1$ averages to zero, therefore

$$\begin{aligned} \frac{\langle\delta\dot{\gamma}_2\rangle}{\gamma_2} &= \frac{\langle\delta\gamma_2\rangle}{\gamma_2}\cdot\\ &= \frac{\beta_{\perp 0}^2\omega_w^2 e B_w}{8\Delta\omega^2}(\sin\Delta\omega t - \Delta\omega t\cos\Delta\omega t) + \frac{\omega_w^2\omega_c}{4\omega_c\Delta\omega}\sin\Delta\omega t\\ &\quad + (\text{smaller, non-resonant terms})\,. \end{aligned} \tag{31}$$

Here, the leading non-resonant term has been written out for comparison with published results. It is convenient to rewrite this equation for the fractional energy flow rate as

$$\begin{aligned} \frac{\langle\Delta\dot{\gamma}\rangle}{\gamma_2} &= \frac{\omega_w^2\omega_c t}{4\omega_c}\left(1 - \beta_{\perp 0}^2\frac{\omega_c t}{2}\frac{d}{dx}\right)\left(\frac{\sin x}{x}\right)_{x=\omega_c t}\\ &\quad + (\text{smaller non-resonant terms})\,. \end{aligned} \tag{32}$$

In this form, we can see that our expression agrees with those obtained using (a) the linearized Boltzmann equation or (b) quantum mechanics [7, 14]. To compare (32) to Schneider's original quantum mechanical result [5, 7] it is necessary to identify the interaction time t with his "collision time" τ; Schneider also assumed a Lorentzian "response function", which differs from the $(\sin x/x)$ explicitly derived here. The first term in (32) is symmetric, and always positive (corresponding to absorption); the second term, resulting from relativistic corrections is anti-symmetric and can lead to gain. Maximizing the second term with respect to the first can produce a net flow of energy from the electron beam into the oscillating field (this is maximized if $x = \Delta\omega t \simeq 1$). Note that (32) is fully relativistic, and that gain is only possible for relativistic beams [see the discussion following (21) in the text].

The rate of energy change can be integrated to describe maser gain. The parameters of a working cyclotron maser would be chosen such that the absorption term in (32) (the first term) would be small compared to the "gain term". Considering only this second term, we find that the gain (the fractional change in the energy of the oscillating wave) is

$$G(t) = \frac{2\omega_p e^2\beta_{\perp 0}^2\omega_c}{\gamma_2 mc\omega^2}\left(\cos\Delta\omega t - 1 + \frac{\Delta\omega t}{2}\sin\Delta\omega t\right)$$
$$+ (\text{non-resonant terms})\,, \tag{33}$$

where ρ_e is the electron beam density. If we fix the length of the interaction region, $t = L/\beta_{z0}c$, the gain function is anti-symmetric in $\Delta\omega$. This is in striking contrast to the gain curve of the uniform-field free-electron laser, which is symmetric in the resonance parameters (see Fig. 2).

The operation of the cyclotron maser is intimately tied to its cavity design. If the cavity mode is chosen properly [6, 7, 15], the device is an excellent, and highly efficient amplifier. In a device similar to the Stanford laser [1-3] (co-axial free radiation and ultra-relativistic electrons), the normal cyclotron maser mechanism is not possible. The derivation in the text shows that even after the cancellation of the longitudinal and transverse bunching mechanism, a useful low-gain mechanism still exists (Earlier, Petelin [16] has discussed another ultra-relativistic mechanism using stationary electrons ($\beta_{z0} = 0$) but this does not make use of the Doppler shift to shorten wavelengths as does the Stanford scheme.)

Appendix B

In this appendix, we use the single particle, perturbative analysis to derive the gain equation of a transverse, periodic field ($\hat{B}_\perp$) free-electron laser. This will further demonstrate the validity of the technique (the results we obtain in this low gain regime accurately describe the device currently operating at Stanford), and will enable us to draw a direct comparison between the $\hat{B}_\perp$-field laser and the $\hat{B}_0$-field laser.

In the $\hat{B}_\perp$-field laser, the relativistic electrons travel along the axis of a transverse, periodic magnetic field of the form

$$\mathbf{B}_w = B_w(\cos k_w z, \sin k_w z, 0)\,, \tag{34}$$

where B_w is the field strength, and $\lambda_w = 2\pi/k_w$ is the wavelength. If there is no light present, stationary solutions describing the helical motion along the magnet axis are

$$\begin{aligned} \frac{x_1}{c} &= \frac{\omega_c}{\beta_{z0}\omega_w^2}\sin(k_w z_0 + \beta_{z0}\omega_w t + \theta_0)\,,\\ \frac{y_1}{c} &= -\frac{\omega_c}{\beta_{z0}\omega_w^2}\cos(k_w z_0 + \beta_{z0}\omega_w t + \theta_0)\,,\\ z_1 &= z_0 + \beta_{z0} c t\,,\\ \gamma_1^2 &= (1 + e^2 B_w^2/m^2 c^2\omega_w^2)(1 - \beta_{z0}^2)\,, \end{aligned} \tag{35}$$

where z_0 and θ_0 are the initial longitudinal position and phase of the particle, $\omega_c = |e|B_w/\gamma_1 mc$, and $\omega_w = k_w c$. This particular solution has no transverse drift.

The electromagnetic wave is taken to be of the form

$$\begin{aligned} \mathbf{E}_w &= E_w\{\cos(k_w z - \omega_w t + \phi),\ -\sin(k_w z - \omega_w t + \phi), 0\}\,,\\ \mathbf{B}_w &= E_w\{\sin(k_w z - \omega_w t + \phi), \cos(k_w z - \omega_w t + \phi), 0\}\,. \end{aligned} \tag{36}$$

This wave, identical to the one employed in the text, satisfies Maxwell's equations with frequency $\omega_w = k_w c$, and amplitude E_w. The polarization and direction are appropriate for the light emitted spontaneously by an electron in helical orbit of (35). As before, this oscillating wave alters the electron's orbit slightly, and can do work. In this laser, the electron's orbital frequency is determined by the wavelength of the helical field; the resonance condition (where $\mathbf{E}_w$, $\mathbf{B}_w$, and $\hat{\beta}_z$ rotate with the same frequency) is given by

$$\Delta\omega = \beta_{z0}\omega_w - \omega_c(1 - \beta_{z0}) = 0\,. \tag{37}$$

The next step is to solve the equations of motion. The transverse components can be integrated by inspection. The constants of integration are chosen such that the stationary solutions satisfy the equations of motion at $t = 0$. Proceeding as in the text, assume that the radiation field induces small perturbations about the zero-order solutions, and calculate these changes to first, then second, order in the radiation field strength. (In previously published works [10, 17], the $\hat{z}$-component of the momentum Eq. (1) and the energy Eq. (2) were combined, resulting in the pendulum equation.)

Expanding to first order, and retaining only the resonant terms (those proportional to $\Delta\omega^{-1}t$) we find that the change in an electron's energy is

$$\begin{aligned} \frac{\delta\gamma_1}{\gamma_1} = &-\frac{\omega_p\omega_c}{\omega_w\Delta\omega}\{\sin(\Delta\omega t + \theta) - \sin\theta\}\\ &+ (\text{non-resonant terms})\,, \end{aligned} \tag{38}$$

where $\theta \equiv (k_z + k_0)z_0 + \theta_0 + \phi$. The first-order shifts in position are

$$\frac{\delta z_1}{c} = -\frac{\omega_0^2 \omega_s}{\omega_0 \omega_z^2 \Delta\omega^3}\{\omega_0 + \omega_z(1-\beta_{z0})\}$$
$$[\cos(\Delta\omega t + \theta) - \cos\theta + \Delta\omega t \sin\theta]$$
$$+ \text{(non-resonant terms)},$$
$$\frac{\delta x_1}{c} = \frac{\omega_0}{\omega_z^2(1-\beta_{z0})}\{\cos[\omega_z(1-\beta_{z0})t - \zeta]$$
$$- \cos\zeta - \omega_z(1-\beta_{z0})t\sin\zeta\}, \tag{39}$$
$$\frac{\delta y_1}{c} = \frac{\omega_0}{\omega_z^2(1-\beta_{z0})}\{\sin[\omega_z(1-\beta_{z0}) - \zeta]$$
$$+ \sin\zeta - \omega_z(1-\beta_{z0})t\cos\zeta\},$$

where $\zeta = k_z z_0 + \phi$. Note that the transverse perturbations are rapidly varying, and are small (non-resonant) compared to the longitudinal perturbations. In this laser, unlike the uniform-field laser, it is only longitudinal bunching that results in laser action; the transverse bunching is negligible.
The second-order change in electron energy is,

$$\frac{\delta\gamma_2}{\gamma_z} = \frac{2\omega_0^2\omega_s^2}{\omega_0\Delta\omega^3}\left\{-\frac{\cos(2\Delta\omega t + 2\theta) - \cos 2\theta}{4} - 1\right.$$
$$\left. + \cos\Delta\omega t - \Delta\omega t\sin\theta\cos(\Delta\omega t + \theta)\right|$$
$$+ \text{(non-resonant terms)}, \tag{40}$$

where $\Delta\omega$ is given in (37) for this field configuration, and we have dropped the non-resonant terms.
In a realistic beam, the electrons enter the interaction region with a random distribution of phases. To describe the evolution of the entire beam, we may average over either azimuthal phases, θ_0, or longitudinal phases, $(k_z + k_0)z_0 \simeq k_z z_0$ (since $k_z \gg k_0$ in the ultra-relativistic case). These are equivalent, and performing either average yields an answer independent of all initial phases. As usual, the first order energy shift averages to zero, but the second-order energy change does not

$$\frac{\langle\Delta\gamma\rangle}{\gamma_z} = \frac{\langle\delta\gamma_2\rangle}{\gamma_z} = \frac{2\omega_0^2\omega_s^2}{\omega_0\Delta\omega^3}\left(\cos\Delta\omega t - 1 + \frac{\Delta\omega t}{2}\sin\Delta\omega t\right)$$
$$+ \text{(non-resonant terms)}. \tag{41}$$

The gain [defined by (18)] is

$$G(t) = \frac{8\pi e^2 B_0^2 a_0}{\omega_0 m^2 c^2 \gamma_z^3 \Delta\omega^3}\left(1 - \cos\Delta\omega t - \frac{\Delta\omega t}{2}\sin\Delta\omega t\right). \tag{42}$$

An extensive discussion of this gain equation can be found in [10]. It has previously been derived using semiclassical radiation theory [1, 10, 18], quantum electrodynamics [10], the coupled Maxwell-Boltzmann equations [19], and the single particle equations of motion [10, 17, 20]. Although (42) is similar in form to the gain equation of the cyclotron maser (33), the detailed mechanisms are quite distinct: the cyclotron maser relies on azimuthal bunching, while the $\hat{B}_z$-field laser relies on longitudinal bunching. In the $\hat{B}_0$-field laser of the text, both these mechanisms are present, but cancel to leave a smaller, but non-zero remnant as the gain process.

Acknowledgments. We would like to thank J.D. Walecka, J.M.J. Madey, R. Kompfner, M. Chodorow, and P.F. Michelson for many helpful discussions related to this work. We are particularly grateful for the friendship and guidance offered by Peggy and Rudi Kompfner, who will remain an inspiration.

References

1. J.M.J.Madey: J. Appl. Phys. 42, 1906 (1971)
2. L.R.Elias, W.M.Fairbank, J.M.J.Madey, H.A.Schwettman, T.I.Smith: Phys. Rev. Lett. 36, 717 (1976); reported in Phys Today (February 1976) p. 17
3. D.A.G.Deacon, L.R.Elias, J.M.J.Madey, G.J.Ramian, H.A.Schwettman, T.I.Smith: Phys. Rev. Lett 38, 892 (1977); reported in Sci. Am. (June 1977) p. 63
4. R.Q.Twiss: Aust. J. Phys. 11, 564 (1958)
5. J.Schneider: Phys. Rev. Lett. 2, 504 (1959)
6. A.B.Goponov: Izv. Vyssh. Uchebn. Zaved. Radiofiz. 2, 837 (1959)
7. J.L.Hirshfield, V.L.Granatstein: IEEE Trans. MTT-25, 522 (1977)
   V.A.Flyagin, A.V.Gaponov, M.I.Petelin, V.K.Yulpatov: IEEE Trans. MTT-25, 514 (1972)
8. M. Borenstein, W.E.Lamb, Jr.: Phys. Rev. A5, 1298 (1972)
   W.E.Lamb, Jr.: Phys. Rev. A6, 1429 (1964)
9. A.V.Gaponov, M.I.Petelin, V.K.Yulpatov: Izv. Vyssh. Uchebn. Zaved. Radiofiz. 10, 1414 (1967)
10. W.B.Colson: Phys. Lett. A64, 190 (1977)
    W.B.Colson: "Free Electron Laser Theory", Ph.D. Thesis Stanford University (1977)
    W.B.Colson: *Physics of Quantum Electronics*, Vol. 5, Chapt. 4, ed. by S. Jacobs, M. Sargent, and M. Scully (Addison-Wesley Reading, Mass. (1978)
11. N.A.Vinokurov, A.N.Skrinskii: preprint (private communication)
    N.A.Vinokurov, A.N.Skrinskii: Siberian Department of the Institute of Nuclear Physics of the USSR Academy of Science (7 July 1977)
    D.F.Alferov, Ye.G.Bessonov: preprint No. 162, USSR Academy of Sciences, Order of Lenin Physics Institute imeni P. N. Lebedev, Photomeson Processes Laboratory of the Department of High Energy and Cosmic Ray Physics, Moscow (1977)
    S.K.Chen, J.C.Sheppard, M.A.Piestrup, R.H.Pantell: J. Appl. Phys. 49, 41 (1978)
12. W.Heitler: *The Quantum Theory of Radiation* (Oxford Univ. Press, Oxford 1954) p. 39
13. L.R.Elias, W.M.Fairbank, J.M.J.Madey, H.A.Schwettman, T.I.Smith: "A Discussion of the Potential of the Free Electron Laser as a High Power Tuneable Source of Infrared, Visible and Ultraviolet Radiation", *Proc. Synchrotron Radiation Facilities Quebec Summer Workshop*, Université Laval, Québec, Canada (15-18 June 1976)
    D.A.G.Deacon, L.R.Elias, J.M.J.Madey, H.A.Schwettman, T.I.Smith: *Laser Spectroscopy*, ed. by J. L. Hall and J. L. Carlsten, Springer Series in Opt. Sciences, Vol. 7 (Springer, Berlin, Heidelberg, New York 1977)
    J.M.J.Madey, D.A.G Deacon: "Free Electron Lasers", in *Cooperative Effects in Matter and Radiation* (Plenum Press, New York 1977) p. 313
    D.A.G.Deacon, L.R.Elias, J.M.J.Madey, H.A.Schwettman, T.I.Smith: "The Free Electron Laser", SPIE, Optics in Adverse Environments 121, 89 (1977)
14. P.Sprangle, W.M.Manheimer: Phys. Fluids 18, 224 (1975)
    P Sprangle, A.T.Drobot: IEEE Trans. MTT-25, 528 (1977)
    J.D Coccoli: Research Lab of Electronics, M.I.T., Cambridge, MA., Quart. Prog. Rept. No. 67 (1962)

15. K.R.Chu, J.L.Hirshfield: Naval Research Laboratory Memorandum Report 3607, Washinton D.C. (1977)
    J.L.Hirshfield, I.B.Bernstein, J.M.Wachtel: IEEE J. QE-1, 237 (1965)
    K.K.Chow, R.H.Pantell: IRE Trans. ED-9, 351 (1962)
16. M.I.Petelin: Izv. Vyssh Uchebn. Zaved Radiofiz. 17, 686 (1974)
17. W.H.Louisell, J.Lam, D.A.Copeland, W.B.Colson: Phys. Rev. A. (1979)
18. V.P.Sukhatme, P.A.Wolff: J. Appl. Phys. 44, 2331 (1973)
19. F.A.Hopf, P.Meystre, M.O.Scully, W.H.Louisell: Opt. Commun. 18, 413 (1976)
    F.A.Hopf, P.Meystre, M.O.Scully, W.H.Louisell: Phys Rev Lett. 37, 1342 (1976)
    H Al Abawi, F.A.Hopf, P.Meystre: Phys. Rev. A16, 666 (1977)
    N.M.Kroll, W.A.McMullin: Phys. Rev. A17, 300 (1978)
20. A.Bambini, A.Renieri: Lett. Nuovo Cimento 21, 399 (1978)
    T.Kwan, J.M.Dawson, T.Lin: Phys. Fluids 20, 581 (1977)
    G.Mayer: Opt. Commun. 20, 200 (1977)
    V.N.Baier, A.I.Milstein: Phys. Lett. A65, 319 (1978)

Sponsored by:
Princeton University Conference
American Institute of Aeronautics and Astronautics (AIAA)

79-1416

New Methods for the Conversion of Solar Energy to Radio Frequency and Laser Power

J.W. Freeman, W.B. Colson and S. Simons
Rice University, Houston, Texas

FOURTH PRINCETON/AIAA CONFERENCE ON SPACE MANUFACTURING FACILITIES

Princeton, N.J./May 14-17, 1979

-- NOTES --

NEW METHODS FOR THE CONVERSION OF SOLAR ENERGY TO R. F. AND LASER POWER

by

John W. Freeman*

William B. Colson

and

Sedgwick Simons

Space Solar Power Research Program
and
Department of Space Physics and Astronomy
Rice University
Houston, Texas 77001

Abstract

This paper discusses two new devices which may have application to space deployed solar energy conversion and transmission systems, the photoklystron* and the free electron laser. The photoklystron converts solar energy directly to R.F. radiation. It operates on the principle of the klystron with the cathode replaced by a photoemitting surface. We have tested a model which oscillates at 30 MHz. This laboratory model requires two low-voltage bias voltages which can be supplied by D.C. solar cells. Concepts for a self-biasing device are also being considered. The photoklystron is expected to be easier and less expensive to manufacture than solid state solar cells. A photoklystron array could replace the high voltage solar cell array, slipring and klystron transmitter in the SPS. The second device, the free electron laser (FEL), converts energy from a relativistic electron beam to narrow band electromagnetic energy, tuneable from the infrared to the ultraviolet. Because the lasing electrons are not bound in atomic energy levels the ultimate efficiency of the FEL is expected to exceed that of conventional lasers, possibly making lasers a practical means of energy conversion and transmission in space systems.

Introduction

As presently conceived, the solar power satellite (SPS) requires a high voltage D.C. solar cell array, a massive bus bar and slipring D.C. current distribution system, and high power klystrons to generate an ultra-high-frequency radio energy beam. The use of high voltage solar cell systems in space is, at best, challenging and will certainly lead to losses from parasitic currents, even at the geostationary orbit! The massive slipring concepts being considered appear awkward and demanding of technology and resources. For this reason, the Rice Space Solar Power Research Program has focused on other possible approaches to the solar to R.F. conversion problem and has examined free electron lasers (FEL) as an alternative concept, should the microwave beam prove impractical.

The Photoklystron

We have designed a working model of a device which converts sunlight into coherent narrowband R.F. radiation. The device, called a photoklystron*, takes an electron beam from a photoemitting surface and through electron bunching allows the beam to reinforce oscillations in a resonant circuit. The mechanism is that of a reflex klystron with a photocathode as the electron source.

Because of the simplicity of the photoklystron, the cost of production is expected to be lower than that of solar cells, and manufacture in space is conceivably possible.

A Solar power Satellite configuration is envisioned where the R.F. radiation from each photoklystron is beamed directly to the earth. The potential advantages of the photoklystron as applied to the Solar Power Satellite are as follows:

1. High voltage solar cell arrays are eliminated.
2. D.C. bus bars are greatly reduced in quantity.
3. The necessity for sliprings is eliminated.
4. Lifetime problems associated with with high power klystrons are eliminated.
5. Heat rejection of the R.F. elements becomes less important.
6. The cost of manufacture of the photoklystron should be much less than that of solar cells.

*Professor, Space Physics and Astronomy
Member AIAA

How the Photoklystron Works

Figure 1 is a schematic of the photoklystron. In version (a) solar photons pass through a transparent substrate and emit electrons from a photoemitting material. The photoelectrons are then accelerated and pass through a pair of grids connected to an inductor and on which an oscillating voltage is established. After passing through the two grids the electrons are repelled by a negative-biased reflector electrode. They return to the two grids and are bunched according to reflex klystron theory[2]. When the reflection voltage is adjusted properly the returning bunched electrons will be phased such as to add energy to the A.C. electric field between the grids. This energy from the electron beam reinforces the oscillations in the tuned resonant circuit. Energy can be extracted from the resonant circuit by transformer coupling or by an antenna stub in the case of very high frequencies. The version of this device being tested is designed to oscillate at about 30 MHz. The frequency is determined by the time of flight of the electrons during relection. The resonant frequency of the LC circuit must be tuned to match this frequency. Fine tuning is accomplished by adjusting the accelerating or reflection electrode voltage.

An alternative photoemitter configuration is shown in Figure 1b. In this case, the principle of operation is the same except the photoemitter is now coated on an opaque metallic plate and the photons pass through the grids first. (a) is called the transmission type and (b) the reflection type. It appears possible to design a device that uses both the transmission and reflection photoemission processes simultaneously to optimize the photoelectron yield. For operation at higher frequencies, the A.C. grids may be replaced by a resonant cavity which is part of a waveguide. As a vacuum tube the device is ideal for space application without a vaccum enclosure.

A motivation leading to the conception of the photoklystron was to increase the useable portion of the photoelectron energy spectrum over D.C. solar cells. While not all the photoelectrons in the photoklystron contribute energy to the R.F. power (because bunching cannot be made perfect) we have an approach for optimizing the averaged photoelectron energy contribution and the final output is in a desirable energy form, R.F. energy.

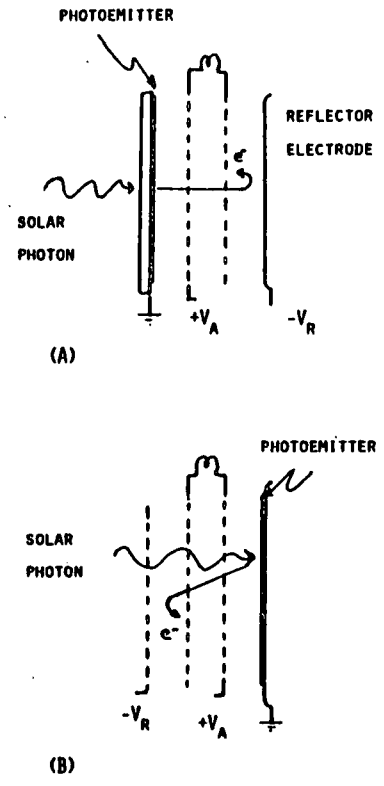

FIGURE 1: SCHEMATICS OF TWO VERSIONS OF THE PHOTOKLYSTRON

Status

Rice University has designed a proof-of-concept working model of the photoklystron. The device, pictured in Figure 2, operates at about 30 MHz. Multiple modes at higher and lower frequencies can be obtained by tuning the bias voltages. It has also been operated at higher frequencies by employing a smaller inductor. Energy conversion efficiency data are not yet available, however the R.F. signal from the first and second upper harmonics

is readily detected by a small transistor radio several meters from the photoklystron without a tuned antenna and with 10 mW of light input. The oscillations are strong and oscillation begins readily without a trigger pulse.

The proof-of-concept model described above uses an S-4 CsSb photocathode. In order for the photoklystron to be used in space an efficient photocathode of high stability at high light levels and temperatures will be required.

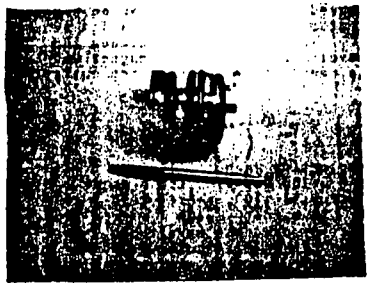

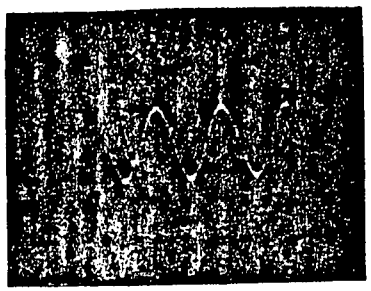

FIGURE 2: THE PHOTOKLYSTRON TEST MODEL AND IT'S RF SIGNAL

An SPS Configuration Suitable for the Photoklystron

With the photoklystron, the R.F. is generated near the point of incidence of the solar energy. Each photoklystron is a transmitter. Moreover, the propagation vector of the R.F. wave is at a right angle to the direction of incidence of the solar radiation. A configuration must be found in which the entire photoklystron array can serve as a large transmitter array and the R.F. wavefront can propagate to the earth. This requires that either the solar radiation or the R.F. radiation be reflected through 90°. One configuration in which the sunlight is reflected is shown in Figure 3. The photoklystron array need not be connected to the reflector/concentrator. Moreover, with the attachment of a suitable counter-weight, gravity-gradient torques could be used to maintain aligment of the photoklystron array toward the earth. Furthermore the larger transmitter area should allow a more efficient microwave beam than the conventional 1 km diameter klystron array.

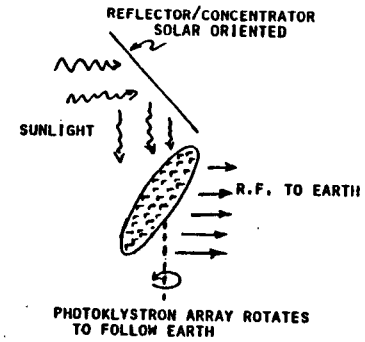

FIGURE 3: A SOLAR POWER SATELLITE CONFIGURATION THAT EMPLOYS A PHOTOKLYSTRON ARRAY. SUNLIGHT IS REFLECTED THROUGH 90° BY AN OVAL REFLECTOR WHICH MAY ALSO SERVE AS A CONCENTRATOR. THE REFLECTOR/CONCENTRATOR PRODUCES A VERTICAL CYLINDRICAL BEAM OF LIGHT WHICH FALLS ON AN OVAL PHOTOKLYSTRON ARRAY TILTED AT 45°. THE PHOTOKLYSTRON ARRAY ROTATES ABOUT AN AXIS PARALLEL TO THE LIGHT BEAM AXIS SO THAT THE ULTRA-HIGH-FREQUENCY RADIO BEAM REMAINS POINTED AT THE EARTH. THE ENTIRE PHOTOKLYSTRON ARRAY IS THE TRANSMITTING ANTENNA.

The Free Electron Laser

As man begins spending more time in space, there will be a growing need for transmitting energy over great distances. R.F. and microwave beams spread out in relatively short distances, but short wavelength light enables us to beam energy over larger distances. The distances z over which laser light may be transmitted without spreading more than 40% is determined by its wavelength, λ, and the sender size, s.

$$z = \pi s^2/\lambda$$

For a fixed sender size s, the distance over which laser energy can be efficiently beamed decreases in proportion to the wavelength of light. Generally, speaking lasers give an advantage of 10^4 over microwaves. This can be used to increase the distance and/or decrease the sender-receiver sizes. Many ideas utilizing lasers in space[1] depend crucially on the compact size of the beams; some of the specific ideas involve powering airbreathing aircraft from space solar power stations, laser propulsion of spacecraft, materials processing, and beaming large amounts of energy from space to earth for electrical power generation.

Several practical questions remain unanswered regarding the use of microwave beams for the SPS. These include bioeffects, ionosphere and troposphere effects, R.F. and electromagnetic interference and the availability of land. Should microwaves prove impractical, lasers might offer a suitable alternative. Conventional lasers are generally considered too inefficient. A new device, the free electron laser (FEL) offers promise of higher efficiency. For this reason, we are examining the use of the FEL for the solar power satellite.

How The Free Electron Laser Works

The free electron laser[4] uses an ultra-relativistic electron beam traveling through a static, periodic magnetic field in a laser cavity to efficiently produce continously tuneable, powerful optical radiation. To understand some of the advantages of the FEL, it is useful to view it as an advanced, relativistic electron tube. Both avoid the problems of dealing with atomic structure, which fixes the wavelength of most lasers, and causes inherent inefficiencies. The FEL is a laser reduced to its bare essentials; only the electrons and a static magnet field are present in the laser cavity.

Figure 4 describes the operation of the FEL. Successive electron pulses (or a continous beam) are guided through the periodic, transverse magnetic field. The source of these electrons may be a storage ring, a linear accelerator, or electrostatic accelerator. As relativistic electrons pass through the periodic magnet, they oscillate and radiate primarily in the forward direction. This light is stored in a resonant cavity formed by two mirrors; one at each end of a long periodic magnet. When pulsed, subsequent electrons are synchronized so that the stored light pulse and electron pulse merge together when entering the magnet. The emission of light in the presence of light is "stimulated emission"; lasing occurs and energy from the electron beam is converted into coherent radiation. It should be noted that the energy density in a relativistic electron beam is large. If any reasonable fraction of the electron energy is converted into coherent radiation, the laser is powerful. Typically, the fractional energy loss of the electron beam is small (~1%), so the electrons retain most of their original energy. The unused electron energy can be recycled in a storage ring or deceleration system.

The relationship between the laser wavelength, λ, and the magnet wavelength λ_0, depends on the electron energy E:

$$\lambda = \lambda_0/8E^2(\text{MeV}),$$

neglecting magnetic field corrections. For a 100 MeV electron beam, the reduction factor is $\sim 10^4$, therefore a 1 cm wavelength magnet yields 1 micron radiation. Furthermore, the wavelength is continously tuneable by merely changing the electron energy. Since the lasing medium consists of electrons, and a static magnetic field in a vacuum, the device is inherently efficient and powerful.

Free Electron Lasers for Space Systems

The only existing laser of this kind is presently at Stanford University[5]. The laser wavelength obtained in these experiments was 3 microns from a 3 cm wavelength magnet with an overall length of 5 meters; the magnetic field strength was 2.4 kilogauss. The electron energy was 40 MeV with peak current of about 1 amp. This produced $\sim 10^9$ watts/cm^2 peak power in short pulses. The average power was low due to the limited current available from the accelerator. These experiments serve to prove the concept and lead the way toward more powerful systems. The Stanford effort is directed towards more efficient operation of the FEL in a storage ring. Other alternative recovery designs are being proposed. Studies show promise that future FEL systems may approach the efficiencies of their predecessors, the microwave electron tubes. A recent report by Bain[6] reviews lasers applied to space systems and discusses the FEL. Improvements are immanent in the peripheral technologies needed for FEL development, particle accelerators and storage rings.

The efficiency of the FEL depends on recovery of the electron beam energy. One of the ideas for an efficient FEL is to incorporate it as part of a storage ring as shown in Figure 5. After passing through the periodic magnet the electron beam is re-accelerated by an R.F. field

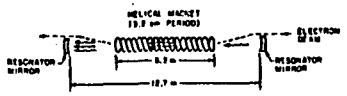

FIGURE 1: A BEAM OF RELATIVISTIC ELECTRONS IS GUIDED THROUGH A PERIODIC MAGNETIC FIELD AND AMPLIFIES THE RADIATION PRESENT IN A RESONANT CAVITY.

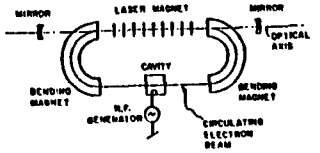

FIGURE 5: IN A STORAGE RING, RECIRCULATING ELECTRONS TRANSFER ENERGY FROM AN ACCELERATOR SECTION TO THE LASER SECTION.

to replace the energy lost to radiation. The FEL then operates as a frequency converter which transfers R.F. power directly to optical power. (By the way, the photoklystron is a possible source of R.F. energy for this purpose.)

The efficiency of the FEL and storage ring combination has been estimated at around 50%, based on existing storage rings. The ultimate feasibility of the storage ring FEL rests on the laser's interaction with the circulating electron beam, and its final operating efficiency is yet to be determined. Even though storage rings are quite massive, it has been estimated[8] that the power/weight ratio might be 0.1 kg/kW. This is significantly less than the total solar power satellite which has been estimated at 10 kg/kW.

Another system under consideration recirculates the electron beam through an electrostatic decelerator.[7] This recovery scheme is used in non-relativistic electron tubes. The power may be collected as a D.C. voltage, or as R.F. using a series of accelerator cavities in reverse. Estimates suggest it may be possible to produce 10 to 50 kW of CW power with an overall efficiency of about 50%.

In parallel with the above, several researchers are studying improved periodic magnets with the hope of extracting more energy from electrons on a single pass. This is an opportunity which is not feasible in atomic lasers. The magnet wavelength, or field strength can be modified slowly along its length. As an electron pulse travels down the magnet, and the electrons changes their energy, the magnet design can change appropriately. This is equivalent to changing atomic structure during the emission process in normal lasers. While the constant period helical design typically extracts approximately 1% of the electron energy, studies of improved designs have achieved 30% extraction for a large fraction of the beam[8].

While lasers are becoming an important consideration for transmission of power in space, the FEL is developing into a promising laser. The FEL is in it's infancy, and basic research is needed to allow the device to reach it's full potential. When compared to R.F. methods for transmitting power in space, klystrons, the FEL can be considered an extension to optical transmission which reduces the sender-receiver sizes and/or increases the range. In essence, the FEL creates a lasing medium in a more efficient, and controllable manner than does an atomic laser; it is a laser with the advantages of a klystron. Moreover, when used in tandem with the photoklystron, we have a system which converts broad band incoherent solar radiation into high power, narrow band, coherent radiation and which is tuneable form ultraviolet to infrared frequencies.

Summary

We have described here the photoklystron and the free electron laser, two devices which we feel should be more completely investigated for their potential application to space energy conversion and transmission. These devices, used separately or together, seem to offer considerable promise of simplicity, high efficiency and flexibility in choice of transmission wavelength.

---

* Patent applied for

References

1. Freeman, J.W., P. Reiff, and D. Cooke. Space Environmental Effects and the Solar Power Satellite, presented at the Spacecraft Charging Conference, Colorado Springs, Nov., 1978

2. Hamilton, J.J., "Reflex Klystron" (The MacMillan Co.) 1959, Chapter 3

3. Billman, K.W. (ed) Radiation Energy in Space, Progress in Astronautics and Aeronautics series, vol. 61, AIAA, New York, N.Y., 1978

4. Madey, J.M.J., J. Appl. Phys. 42,1906 (1971)

   Elias, L.R., Fairbank, W.M., Madey, J.M.J., Schwetteman, H.A., Smith, T.I. "A Discussion of the Potential of the Free Electron Laser as a High Power Tuneable Source of Infrared, Visible and Ultraviolet Radiation," published Proceedings of the Synchrotron Radiation Facilities Quebec Summer Workshop, Université Laval, Quebec, Canada, 15-18 June, 1976

   Colson, W.B.: Physics of Quantum Electronics, vol. 5, Chapter 4 (Addison-Wesley Pub. Co., 1978) ed. S. Jacobs, M. Sargent, and M. Scully

5. Elias, L.R., Fairbank, W.M., Madey, J.M.J., Schwettman, and Smith, T.I., Phys. Rev. Letts. 36, 717 (1976); Physics Today, 17 (Feb. 1976)

   Deacon, D.A.G., Elias, L.R., Madey, J.M.J., Ramian, G.J., Schwettman, H.A. and Smith, T.I., Phys. Rev. Letts. 38 892 (1977); Scientific American, 63 (June, 1977)

6. Bain, C.N., "Potential of Laser for SPS Power Transmission," PRC Energy Analysis Co., Ref. No. 1861, Sept., 1978 prepared for DOE under contract no. EG-77-C-01-4024, and issued as DOE MPS/ER-4024-07

7. Elias, L.R., "A High Power, C.E. Tuneable Efficient, UV-visible and IR Free Electron Laser Using Low Energy Beams," Jan., 1979, Stanford Preprint, Submitted to Phys. Rev. Letters.

8. Kroll, N., M. Rosenbluth, and P. Morton, "Variable Parameter Wiggler Devices," presented March, 1979 at the Stanford Free Electron Laser Workshop.

Appl. Phys. 20, 61–65 (1979)

Applied Physics

A Laser Accelerator

*W. B. Colson**

Space Physics, Rice University, Houston, TX 77001, USA

S. K. Ride

Johnson Space Center, Houston, TX 77058, USA

Received 2 February 1979/Accepted 25 April 1979

Abstract. We show that a laser can efficiently accelerate charged particles if a magnetic field is introduced to improve the coupling between the particle and the wave. Solving the relativistic equations of motion for an electron in a uniform magnetic field and superposed, circularly polarized electromagnetic wave, we find that in energy-position phase space an electron traces out a curtate cycloid: it alternately gains and loses energy. If, however, the parameters are chosen so that the electron's oscillations in the two fields are resonant, it will continually accelerate or decelerate depending on its initial position within a wavelength of light.

A laboratory accelerator operating under these resonant conditions appears attractive: in a magnetic field of 10^9 Gauss, and the fields of a 5×10^{12} W, 10 μm wavelength laser, an optimally positioned electron would accelerate to 700 MeV in only 10 m.

PACS: 42.55

High-energy accelerators use electromagnetic fields to transfer energy to charged particles. The field strength in a typical rf accelerating cavity is considerably smaller than can be achieved in modern lasers, so we might expect lasers to be useful as particle accelerators; in a typical laser-particle interaction, however, little energy is exchanged. The energy transfer rate is proportional to $\boldsymbol{\beta}\cdot\mathbf{E}_r$, where $\boldsymbol{\beta}c$ is the particles' velocity vector, and $\mathbf{E}_r$ is the radiation electric field. $\mathbf{E}_r$ oscillates so rapidly that $|\boldsymbol{\beta}\cdot\mathbf{E}_r|$ nearly averages to zero over any macroscopic time scale. The key to achieving large energy transfers is to make $\boldsymbol{\beta}$ rotate rapidly (with $\mathbf{E}_r$) for long times. Palmer [1], and later Kompfner and Chowdorow [2], showed that a periodic, static, transverse magnetic field could be used to "guide" relativistic particles in a helical path, and increase the distance over which the interaction can efficiently transfer energy.

In this paper, we investigate another "laser accelerator" scheme: one in which the guiding field is a static, uniform magnetic field, parallel to the direction of propagation of the light. Here, too, the magnetic field guides the charge in a helical path; if the radiation is circularly polarized, it is possible to choose initial parameters such that $\boldsymbol{\beta}$ and $\mathbf{E}_r$ retain their relative orientation through many oscillations, and allow significant energy transfer to occur.

We solve the relativistic Lorentz force equations, describing the motion of a charge in a static, uniform magnetic field, and a superimposed circularly polarized plane wave of constant amplitude (Fig. 1). We were able to obtain the analytic solution, and determine the energy of a particle as it travels through the interaction region. For most choices of initial parameters, the energy is an oscillatory function of time; a particle alternately gains and loses energy. If the parameters are such that $\boldsymbol{\beta}$ and $\mathbf{E}_r$ rotate synchronously, the particle's energy is not a periodic function but increases or decreases monotonically (the sign depending on the initial orientation of $\boldsymbol{\beta}$ and $\mathbf{E}_r$). If we choose the electromagnetic field strength and frequency of the laser light such that the interaction is resonant, then inject a monoenergetic beam of electrons, half the electrons will decelerate, half will accelerate. The final energies, and the spread in those energies, depend on the length of the interaction region and the values of the initial parameters.

* Supported by NASA Grant NSG-7490

0340-3793/79/0020/0061/$01.00

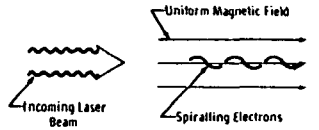

Fig. 1. A circularly polarized laser beam can accelerate electrons spiralling in a uniform magnetic field

I. Particle Dynamics

The dynamics and energy change of a single charged particle in the fields produced by the solenoid and laser are governed by the relativistic Lorentz force equations

$$\frac{d}{dt}(\gamma\boldsymbol{\beta}) = \frac{e}{mc}[\mathbf{E}_r + \boldsymbol{\beta}\times(\mathbf{B}_m + \mathbf{B}_r)], \tag{1}$$

$$\frac{d\gamma}{dt} \equiv \dot{\gamma} = \frac{e}{mc}\boldsymbol{\beta}\cdot\mathbf{E}_r, \tag{2}$$

where e and m are the particle's charge and mass, c is the speed of light, $\boldsymbol{\beta}c$ and γmc^2 are the particle's velocity and energy, respectively, and $\gamma^{-2} = 1-\boldsymbol{\beta}\cdot\boldsymbol{\beta}$. The motion is influenced by both the uniform magnetic field, $\mathbf{B}_m = (0, 0, B_0)$, and the radiation fields, $\mathbf{E}_r$ and $\mathbf{B}_r$. Equation (2) shows that the energy transferred to the particle will be maximized if the vectors $\boldsymbol{\beta}$ and $\mathbf{E}_r$ are parallel, and retain their orientation over many oscillations. In this magnetic field, an electron's velocity vector and the electric field vector rotate in the same sense if the radiation is circularly polarized, with positive helicity[1]

$$\begin{aligned}\mathbf{E}_r &= E_0(\cos(k_r z-\omega_r t+\phi), -\sin(k_r z-\omega_r t+\phi), 0),\\ \mathbf{B}_r &= E_0(\sin(k_r z-\omega_r t+\phi), \cos(k_r z-\omega_r t+\phi), 0).\end{aligned} \tag{3}$$

These are the fields of a plane wave traveling in the z-direction with frequency $\omega_r = k_r c$, phase ϕ, and constant amplitude E_0. We assume that only a small fraction of the laser energy is transferred to the particles.

Using the fields above, the Lorentz force equations become

$$\frac{d}{dt}(\gamma\beta_x) = -\frac{|e|E_0}{mc}(1-\beta_z)\cos\zeta - \frac{|e|B_0}{mc}\beta_y, \tag{4a}$$

$$\frac{d}{dt}(\gamma\beta_y) = \frac{|e|E_0}{mc}(1-\beta_z)\sin\zeta + \frac{|e|B_0}{mc}\beta_x, \tag{4b}$$

$$\frac{d}{dt}(\gamma\beta_z) = -\frac{|e|E_0}{mc}(\beta_x\cos\zeta - \beta_y\sin\zeta), \tag{4c}$$

$$\frac{d}{dt}(\gamma) = -\frac{|e|E_0}{mc}(\beta_x\cos\zeta - \beta_y\sin\zeta), \tag{4d}$$

[1] Above, we consider the motion of negatively charged particles. Since positive particles spiral in the opposite sense in $\mathbf{B}_m$, a radiation field of negative helicity would be required

where $\zeta = k_r z - \omega_r t + \phi$. The last two equations can be combined to produce a relation between energy and z-velocity

$$\gamma(1-\beta_z) = \text{const} \equiv \varepsilon. \tag{5}$$

This constant of motion, determined by initial conditions, describes the velocity of a particle as a function of its energy. If the energy increases, $\beta_\perp$ increases: the transverse velocity which can be expressed in terms of ε and γ.

$$\beta_\perp^2 \equiv \beta_x^2 + \beta_y^2 = \frac{2\varepsilon\gamma - \varepsilon^2 - 1}{\gamma^2} \tag{6}$$

decreases. The pitch angle of an accelerating particle therefore decreases as it moves through the interaction region.

We can construct a second constant of motion by taking β_x and β_y from (4b) and (4a), respectively, substituting these results into (4c), and extracting the overall time derivative. The result is

$$\eta \equiv \gamma(t)\left|1 - \frac{\omega_R}{\Delta\omega}\beta_\perp(t)\sin\theta(t)\right| = \text{const}, \tag{7}$$

where

$$\Delta\omega = |e|B_0/\gamma_0 mc - (1-\beta_{z_0})\omega_r,$$

$\omega_R = |e|E_0/\gamma_0 mc$, and $\gamma_0 mc^2$ and $\beta_{z_0}c$ are the electron's initial energy and z-velocity. $\theta(t)$ is the angle between the rotating electric field vector and the rotating perpendicular component of the electron's velocity vector: $\boldsymbol{\beta}\cdot\mathbf{E}_r = \beta_\perp E_0\cos\theta$. As the energy of the particle changes, the orientation of these vectors must also change. The nonlinear character of the system is apparent: this changing orientation feeds back to alter the rate of change of energy.

We can use (6) and (7) to write $\beta_\perp(t)$ and $\theta(t)$ in terms of $\gamma(t)$, then substitute these results into (2) to get a first-order differential equation for the electron energy as a function of time

$$\frac{d\gamma(t)}{dt} = \frac{\gamma_0}{\gamma}[\omega_R^2(2\varepsilon\gamma - \varepsilon^2 - 1) - \Delta\omega^2(\gamma-\eta)^2]^{1/2}. \tag{8}$$

The more relevant quantity is the energy of the electron as a function of its distance down the accelerating region. From (5),

$$dt = [\gamma/(\gamma-\varepsilon)]dz/c.$$

Then, integrating,

$$\left(\frac{\gamma_0-\eta\omega}{c}\right)z = \left|-(q+2r\gamma-\gamma^2)^{1/2} - (r-\varepsilon)\sin^{-1}\left(\frac{r-\gamma}{\sqrt{r^2+q}}\right)\right|_{\gamma_0}^{\gamma}. \tag{9}$$

where

$$q = -\eta^2 - (\varepsilon^2 + 1)\frac{\omega_g^2}{\Delta\omega^2}, \quad r = \eta + \varepsilon\omega_g^2/\Delta\omega^2,$$

and the right-hand side must be evaluated at the limits of integration γ and γ_0.

This form of the solution is rather unwieldly, and cannot be inverted analytically. However, it is possible to rewrite (9) as two equivalent parametric equations

$$\begin{aligned} \zeta - \zeta_0 &= a\psi - b\cos\psi, \\ \Gamma &= a + b\sin\psi, \end{aligned} \tag{10}$$

where

$$\zeta = \gamma_0\Delta\omega z/c, \quad \Gamma = \gamma - \varepsilon, \quad a = r - \varepsilon,$$

and

$$b = (r^2 + q)^{1/2};$$

ζ_0, determined from the initial conditions, is

$$\zeta_0 = [b^2 - (a + \varepsilon - \gamma_0)^2]^{1/2} + a\sin^{-1}[(a + \varepsilon - \gamma_0)/b],$$

and ψ is an arbitrary angle. These are equations of a "curtate cycloid", and generate the curve shown in Fig. 2. From the properties of curtate cycloids, we can immediately extract valuable information on the behavior of γ as a function of z. First, the curve is periodic in z. The electron alternately gains and loses energy, and the distance between energy maxima (minima) is $2\pi a$. The maximum energy obtained is $\Gamma_{max} = a + b$, or

$$\gamma_{max} = \eta + \varepsilon\omega_g^2/\Delta\omega^2 + \frac{\omega_g}{\Delta\omega}\left(\varepsilon^2\frac{\omega_g^2}{\Delta\omega^2} - \varepsilon^2 - 1 + 2\varepsilon\eta\right)^{1/2}. \tag{11}$$

Similarly, $\gamma_{min} = a - b + \varepsilon$. The maxima occur at $\zeta = (4n+1)\pi/2 + \zeta_0$, or

$$z_{\gamma=\gamma_{max}} = \frac{c}{\gamma_0\Delta\omega}\left[(4n+1)\frac{a\pi}{2} + \zeta_0\right], \quad n = 0, 1, 2, \ldots. \tag{12}$$

The maximum of the curtate cycloid depends on several parameters. In particular,

(a) γ_{max} will increase if the power of the laser is increased.

(b) γ_{max} will increase if the injection angle (and therefore ε) is increased. This is apparent from (2) and (6). As γ grows, $\beta_\perp$ asymptotically becomes proportional to $\gamma^{-1/2}$. As the electron accelerates, it loses transverse velocity, and the acceleration process "turns off". Therefore, if two electrons are injected with the same energy but different pitch angles, the electron with the larger pitch angle can accelerate longer, and achieve a higher energy.

(c) γ_{max} increases if $|\Delta\omega|$ is decreased. This is illustrated in Fig. 3, and will be discussed in detail below.

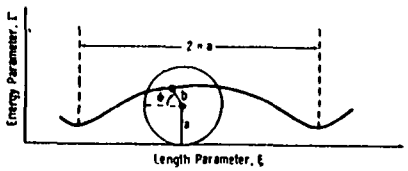

Fig. 2. Equations (10) generate a curtate cycloid, the path traced by a point inside a circle as that circle rolls along the ζ-axis

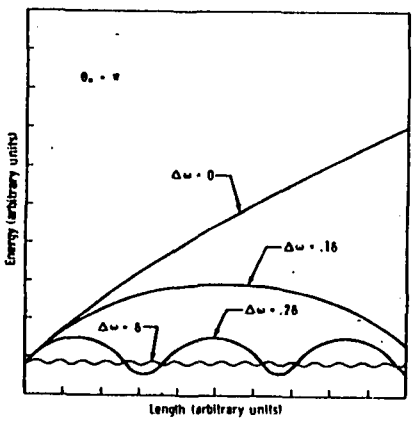

Fig. 3. This family of curves illustrates the influence of the parameter $\Delta\omega = |e|B_0/\gamma_0 mc - (1 - \beta_{z_0})k\omega$, on the amplitude and period of the energy cycloid. If $B_0 = 0$, $|\Delta\omega| = \delta$ is large, and the particle energy oscillates rapidly. If $|\Delta\omega|$ is decreased (e.g., by increasing B_0), the amplitude and period of the cycloid increase. Maximum acceleration is achieved if $\Delta\omega = 0$

From (2), we expect maximum acceleration for negative particles ($e = -|e|$) if β and $\mathbf{E}_\perp$ antialigned ($\theta = \pi$). In general, their relative phase evolves in time, but under certain conditions that evolution will be slow, and the two vectors can rotate nearly synchronously. Physically, we expect them to be synchronous if exactly one wavelength of light passes over the electron as it travels through one complete oscillation. In the magnetic field alone, the electron would oscillate with the cyclotron frequency $\omega_c = |e|B_0/\gamma_0 mc$; as it spirals down the z-axis, it sees a Doppler-shifted radiation field of frequency $\omega_c(1 - \beta_z)$. The parameter $\Delta\omega$ is the difference between these frequencies.

The family of curves in Fig. 3 shows the dependence of $\gamma(z)$ on $\Delta\omega$. For a given laser and electron injection, $\Delta\omega$ can be varied by varying the magnetic field strength. If

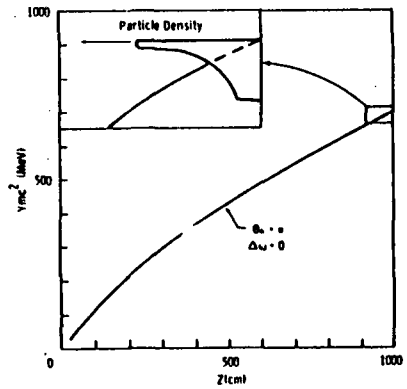

Fig. 4. An electron entering the interaction region with $\theta_0 = \pi$ and $\Delta\omega = 0$ experiences maximum acceleration. $\gamma(z)$ is plotted assuming $\varepsilon = 0.01$ and $\gamma_0 = 50$. The electron reaches an energy of 700 MeV in 10 m. All electrons with initial phases between $\pi/2$ and $3\pi/2$ are accelerated. The inset shows their final energy distribution (~0.1% FWHM)

$B_0 = 0$, $|\Delta\omega|$ is large; the cycloid period is short, and only minimal acceleration occurs[2]. As B_0 is increased, $|\Delta\omega|$ becomes smaller; both the cycloid period and maximum electron energy then increase. Finally, if B_0 is chosen such that $\Delta\omega = 0$, we find that $\gamma(z)$ is described by a cycloid of infinite wavelength, and continues to increase with z. We can examine this case further by setting $\Delta\omega = 0$ in (8) and integrating

$$z = \left(\frac{c}{\gamma_0\omega_g}\right)\frac{(\varepsilon\gamma - 2\varepsilon - 2)}{3\varepsilon^3}(2\varepsilon\gamma - \varepsilon^2 - 1)^{1/2}_{\gamma_0}, \tag{13}$$

where $\gamma_f mc^2$ is the final energy of the electron. In the limit that γ_f is large, the energy increases as $z^{2/3}$.

If a homogeneous, monoenergetic beam of electrons is injected into the interaction region with $\Delta\omega = 0$, the energy change of a particular electron depends on its initial position within a wavelength of light: those with θ_0 between $\pi/2$ and $3\pi/2$ are accelerated, the others are decelerated. From the synchronism argument, we know that those with $\theta_0 = \pi$ initially experience the greatest acceleration. But (7) indicates that if $\Delta\omega = 0$ and $\theta_0 = \pi$, $\theta(z)$ is constant: β and $\mathbf{E}_\perp$ rotate at exactly the same rate, and the electron continues to experience acceleration. This would be true for all initial phases if the electron's oscillation frequency were determined solely by the static field. But the laser fields influence its trajectory, and, in general, $\theta(z)$ evolves as the electron travels down the interaction region. In the special case $\Delta\omega = 0$, $\theta(z)$ does not oscillate, but evolves monotonically toward π. Although the accelerations felt by electrons with different initial phases can be initially quite different, their phases evolve rapidly and are soon all near π. The electrons' energies then evolve at nearly the same rate. Figure 4 shows the energy as a function of interaction length of an electron injected "on-resonance" ($\Delta\omega = 0$, $\theta_0 = \pi$); *the sketch in the upper corner shows the final* energy distribution of the electrons from a homogeneous, monoenergetic beam with initial phases between $\pi/2$ and $3\pi/2$. Assuming a static magnetic field of 10^5 Gauss and a 5×10^{12} W laser with a wavelength of 10 μm, we find that an electron injected with $\gamma_0 = 50$ could be accelerated to 700 MeV in only 10 m[3]. The distribution of final energies of those accelerated electrons is narrow: ~0.1% in the above example.

2. Discussion

Equation (9) is an exact analytical result, describing the acceleration of an electron in a uniform magnetic field and a circularly polarized laser field. Efficient energy transfer is possible because the magnetic field guides the electron through a spiral trajectory, and thereby improves the coupling between the particle and the radiation field. The electron's energy is, in general, a periodic function of z; as the rate of rotation of β approaches that of $\mathbf{E}_\perp$, the maximum energy that the electron can attain increases. If β and $\mathbf{E}_\perp$ rotate synchronously, the interaction is resonant; under these conditions, half the electrons in a monoenergetic beam decelerate, but half accelerate. Those that begin to accelerate continue to accelerate, and can reach extremely high energies over laboratory distances. In the limit of large energies, (15) can be inverted to find the asymptotic form for γ as a function of z

$$\gamma \approx \left[\left(\frac{eE_0}{mc^2}\right)^2\left(\frac{\lambda}{2\pi}\right)\left(\frac{eB_0}{mc^2}\right)^2\right]^{1/3} z^{2/3}, \tag{16}$$

where $\lambda_\gamma = 2\pi c/\omega_\gamma$ is the wavelength of the laser light, and (5) with $\Delta\omega = 0$ has been used to write ε in terms of B_0 and λ_γ. To maximize $\gamma(z)$, we should maximize B_0 and choose the laser to maximize the product $\lambda_\gamma E_0^2$. As technology progresses, higher laboratory magnetic fields, and more powerful, longer-wavelength lasers will make an accelerator based on these principles quite attractive.

An additional constraint on the parameters, not embodied in (17), is that the electron must remain in the

[2] Note that energy is exchanged in the absence of a static magnetic field. The laser could be used alone to accelerate particles, but the energy transfer is small

[3] The electric field strength E_0 is related to the laser power P through the beam diameter d: $P/c = (E_0 d/4)^2$. In the example in the text, a beam diameter of 0.5 cm (or greater) will remain substantially constant over the Rayleigh range of 10 m

laser beam if acceleration is to continue. This implies first that the laser pulse must be sufficiently long that the radiation does not pass completely over the electron before the end of the designated interaction region. In the example considered above, a 10^{-11} s laser pulse will remain coupled to the electrons over the 10 m length. Second, the diameter of the electron's spiral trajectory must not become greater than the diameter of the laser beam. In the asymptotic limit, $d = 2\sqrt{x^2 + y^2}$ grows as $\gamma^{1/2}$. In our example, $d_{max} \sim 0.2$ cm, so the laser beam diameter is determined instead by the Rayleigh range. In the above example, electrons injected with $\gamma_0 = 50$ spiral through a few hundred helical cycles while being accelerated. We assume that during this acceleration the electron beam evolution is not influenced by collisions: since the injected beam is relativistic, the effects of Coulomb interactions are quite small (and can, of course, be made as small as desired by reducing the beam density). To maintain the optimum acceleration ($\Delta\omega \approx 0$) in a practical machine, the inhomogeneities in the magnet and laser fields must be small enough that they do not cause the relative phase of $\boldsymbol{\beta}$ and $\mathbf{E}_\perp$ to evolve significantly ($\ll \pi$). This implies that, for our example, $\delta B/B_0$ should be less than ~ 0.1 %, and the optical wave should be coherent over ~ 1000 wavelengths. These are not stringent constraints.

The calculation presented here is also applicable to certain situations outside the laboratory. For example, our results could describe the interaction of whistlers (very low frequency waves in the magnetosphere) with the charged particle spiralling in the earth's magnetic field. This mechanism has been proposed as a means of precipitating electrons from the radiation belts [3]. Further, it has recently been shown [4] that free electron laser action can be sustained in a uniform magnetic field. If coherent radiation is produced, for example, in the magnetic fields associated with pulsars or quasars, this acceleration mechanism could operate over astrophysical distances.

References

1. R. B. Palmer: J. Appl. Phys. 43, 3014 (1972)
2. R. Kompfner, M. Chowdorow: Stanford University (preprint) (1977)
3. Umran Inan: Ph. D. Thesis, Stanford University (1977)
4. S. K. Ride, W. B. Colson: Appl. Phys. 20, 41–50 (1979)

HEPL Report
858

SPONTANEOUS EMISSION
IN
A FREE ELECTRON LASER

S. K. Ride, Johnson Space Center
Houston, Texas 77058

and

W. B. Colson,[‡] Space Physics, Rice University

[‡]Supported by NASA Grant NSG-7490

ABSTRACT

The modes of a free electron laser evolve from the spontaneous radiation emitted by relativistic electrons travelling in "small pitch angle" helical orbits in a magnetic field. The details of free electron laser operation depend on the angular and spectral characteristics of the emission spectrum, and laser gain is proportional to the slope of the spontaneous emission line.

We first obtain an exact, fully relativistic expression for the radiation emitted by a charge travelling in a finite helical trajectory (the finite length of the trajectory determines the spectral line width). We then examine the specific case of spontaneous emission in a free electron laser where the narrow radiation cone continually excites a detector on-axis at infinity. The result is a spectrum of sharp, well-separated harmonics, at frequencies that depend critically on the observation angle. We discuss the spectrum for electrons guided by (1) a periodic, transverse magnetic field, and (2) a uniform, longitudinal magnetic field, and show that a knowledge of the spontaneous spectrum, and its dependence on the field parameters, could be exploited to tune the laser, or induce gain in the higher harmonics.

I. Introduction

In a free electron laser,[1,2,3] highly relativistic electrons are guided in helical orbits and forced to emit spontaneous radiation. The laser mode grows from the spontaneous emission "noise" because this radiation acts back on the spiralling electrons to stimulate further emission. The properties of spontaneous emission are obviously crucial to laser operation. Since these lasers employ electron beams (produced by modern high energy accelerators or storage rings) which are nearly monoenergetic and have small angular divergence, the detailed spectral properties of the narrow radiation cone are not washed out. If the laser is to realize its full potential, these spontaneous emission features must be understood and utilized.

Work on the problem of spontaneous emission by a charge in periodic motion dates back to 1912, when Schott[4] derived the spectrum of radiation produced by charged particles in relativistic and non-relativistic circular orbits. These results were re-derived and extended by Schwinger,[5] and have been discussed more recently by Takakura[6] who also considered particles in helical motion.[7] The type of radiation analyzed in this work has been discussed by Epstein[8] in connection with astrophysical objects. In 1951, Motz[9] (and, more recently, Kincaid[10]) showed how helical motion can be harnessed as a laboratory radiation source, and Colson[3] related the process to the free electron laser.

In the present paper, we first obtain the exact, fully relativistic description of the spectral characteristics and angular distribution of the radiation emitted by a classical charged particle in a finite helical orbit. The finite extent of the trajectory is an important consideration,

and has not been included in previous works. We relate this general result to limiting cases derived elsewhere, then focus on radiation emitted by the highly relativistic electrons in a free electron laser as they spiral through their small pitch angle trajectories.

The resulting radiation, an interesting composite of two well-known limiting cases (emission into a single frequency by non-relativistic circular motion, and emission of a broad synchrotron spectrum by relativistic circular motion), is emitted into a few narrow, well-separated harmonics at multiples of the fundamental emission frequency. The details of the discrete spectrum depend crucially on the observation angle; and several "harmonics" may be observed at a single frequency by varying the observation angle slightly. Radiation into a small detector can therefore be continuously tuned over a wide frequency range by simply changing its angular location.

The properties of the spontaneous radiation can be used to good advantage in the operation of a free electron laser. For example, the oscillator mode could be changed by storing and amplifying radiation emitted slightly off-axis. This could allow continuous tuning of the frequency over a small range, or operation at significantly shorter wavelengths by inducing gain in the higher harmonics. Furthermore, it has been shown (both theoretically and experimentally[11]) that free electron laser gain is proportional to the slope of the spontaneous emission spectral line. It is the finite length of the trajectory, the number of oscillations the charge undergoes, that determines the spontaneous emission line shape; this feature is essential if the spontaneous and stimulated emission processes are to be related.

II. General Expression

In this section we calculate the intensity distribution of the radiation produced by a charged particle travelling in a helical orbit. Motion in a helix of radius a, with angular frequency b, is described by the equation

$$\vec{r} = \left(a \sin(bt+\alpha),\ a \cos(bt+\alpha),\ \beta_z c t\right) + (x_0, y_0, z_0) \tag{1}$$

This is a general expression, and assumes no particular form for the fields producing the motion; in particular, this motion could be produced by a uniform magnetic field, a spatially periodic magnetic field (as in the existing free electron laser at Stanford[3]), or a time-varying electric field. In (1) (x_0, y_0, z_0) is the initial position of the charge, $\beta_{z0}C$ its velocity along the z-axis (a constant if we neglect the effects of radiation losses).[+]

If the trajectory of the charge is known, the Lienard-Wieckert potentials provide a complete description of the resulting radiation fields (neglecting radiation reaction). The intensity distribution, in the radiation zone is

$$\frac{d^2I(\omega)}{d\Omega\, d\omega} = \frac{e^2\omega^2}{4\pi^2 c}\left|\int_{-\infty}^{\infty} \hat{n} \times (\hat{n} \times \vec{\beta})\, e^{i\omega\left(t - \frac{\hat{n}\cdot\vec{r}}{c}\right)} dt\right|^2 \tag{2}$$

where $d^2I/d\Omega\, d\omega$ is the energy radiated per unit solid angle ($d\Omega$) per unit frequency ($d\omega$), $\vec{\beta}c = d\vec{r}/dt$ is the velocity of the radiating charge, and $\hat{n}$ is the direction to the observer. Although the explicit dependence on the charge's acceleration has been removed by partial integration, there is no radiation if the velocity is constant; the integration should be performed over the time interval during which the charge accelerates.

The integral in (2) determines the character of the radiation emitted by

---

[+] In the free electron laser operating at Stanford, the spontaneous power emitted amounts to only 10^{-8} of the charge's total energy.

a charge in a particular trajectory. It is possible to make substantial progress toward a solution without reference to a specific particle trajectory. First, notice that the radiation can be decomposed into two linearly polarized components. Taking the scalar product of the vector integral with each of two unit polarization vectors enables us to calculate the intensity distribution of radiation with these polarizations. This decomposition not only yields information on the polarization of the radiation, but also greatly reduces the computational complexity of the problem.

We choose the polarization vectors to be $\hat{\theta}$ (θ measured from the + z-axis) and $\hat{\varphi}$ (φ measured from the + x -axis), the unit vectors transverse to $\hat{n}$. Writing the vector integral (2) in terms of components along $\hat{n}, \hat{\theta}$, and $\hat{\varphi}$, and using vector identities which relate the members of this right-handed triad,

$$\frac{d^2I}{d\Omega\, d\omega} = \frac{e^2\omega^2}{4\pi^2 c}\left|\hat{\theta}\int_{-\infty}^{\infty}(-\hat{\theta}\cdot\vec{\beta})\, e^{i\omega\left(t-\frac{\hat{n}\cdot\vec{r}}{c}\right)}dt + \hat{\varphi}\int_{-\infty}^{\infty}(-\hat{\varphi}\cdot\vec{\beta})\, e^{i\omega\left(t-\frac{\hat{n}\cdot\vec{r}}{c}\right)}dt\right|^2 \tag{3}$$

The absense of a component along $\hat{n}$ reflects the fact that the radiation fields are transverse. Equation (3) can be rewritten as

$$\frac{d^2I}{d\Omega\, d\omega} = \frac{d^2I_\theta}{d\Omega\, d\omega} + \frac{d^2I_\varphi}{d\Omega\, d\omega} \tag{4}$$

where I_θ and I_φ are the intensities of radiation polarized along $\hat{\theta}$ and $\hat{\varphi}$, respectively. Writing these explicitly in terms of the observation angles

$$\frac{d^2I_\theta}{d\Omega\, d\omega} = \frac{e^2\omega^2}{4\pi^2 c}\left|-\cos\theta\cos\varphi\int_{-\infty}^{\infty}\beta_x\, e^{i\omega\left(t-\frac{\hat{n}\cdot\vec{r}}{c}\right)}dt - \cos\theta\sin\varphi\int_{-\infty}^{\infty}\beta_y\, e^{i\omega\left(t-\frac{\hat{n}\cdot\vec{r}}{c}\right)}dt + \sin\theta\int_{-\infty}^{\infty}\beta_z\, e^{i\omega\left(t-\frac{\hat{n}\cdot\vec{r}}{c}\right)}dt\right|^2$$

$$\frac{d^2I_\varphi}{d\Omega\, d\omega} = \frac{e^2\omega^2}{4\pi^2 c}\left|\sin\varphi\int_{-\infty}^{\infty}\beta_x\, e^{i\omega\left(t-\frac{\hat{n}\cdot\vec{r}}{c}\right)}dt - \cos\varphi\int_{-\infty}^{\infty}\beta_y\, e^{i\omega\left(t-\frac{\hat{n}\cdot\vec{r}}{c}\right)}dt\right|^2 \tag{5}$$

To this point we have made no assumptions about the trajectory.

To obtain the radiation emitted by a charge in a helical orbit, substitute the trajectory, (1), into (5). The transverse velocities, β_x and β_y, are trigonometric functions of time, and $\beta_z = \beta_{zo}$ is a constant. The

periodic nature of the motion enables us to write the limits of integration in terms of the number of oscillations, N, that the charge travels through (if the charge accelerates from $t = -\infty$ to $t = \infty$, N is infinite). It is N which determines the width of the spontaneous emission line.

To evaluate the integrals in (5), use the Bessel function identity

$$e^{i x \cos\delta} = \sum_{n'=-\infty}^{\infty} J_{n'}(x)\, e^{i n' \delta}\, e^{i n' \pi/2} \tag{6}$$

This extracts the time dependence from the arguments of the trigonometric functions, and leaves us with the following integrals to perform:

$$A = \sum_{n'=-\infty}^{\infty} A' J_{n'}(\zeta)\, e^{i n'(\alpha+\varphi-\pi)} \int_{-N\pi}^{N\pi} \beta_{z0}\, e^{i(b'/b+n')\nu}\, d\nu$$

$$= \sum_{n'=-\infty}^{\infty} 2A'\beta_{z0} J_{n'}(\zeta)\, e^{i n'(\alpha+\varphi-\pi)}\, \frac{\sin\left[(b'/b+n')N\pi\right]}{(b'/b+n')} \tag{7a}$$

$$S = \sum_{n'=-\infty}^{\infty} A' J_{n'}(\zeta) e^{i n'(\alpha+\varphi-\pi)} \frac{ab}{2ic}\left[-\int_{-N\pi}^{N\pi} e^{i\left(\frac{b'}{b}+n'+1\right)\nu + i\alpha} d\nu + \int_{-N\pi}^{N\pi} e^{i\left(\frac{b'}{b}+n'-1\right)\nu - i\alpha} d\nu\right] \tag{7b}$$

$$= \sum_{n'=-\infty}^{\infty} A' J_{n'}(\zeta) e^{i n'(\alpha+\varphi-\pi)} \frac{ab}{ic}\left[-\frac{e^{i\alpha}\sin N\pi\left(\frac{b'}{b}+n'+1\right)}{\left(\frac{b'}{b}+n'+1\right)} + \frac{e^{-i\alpha}\sin N\pi\left(\frac{b'}{b}+n'-1\right)}{\left(\frac{b'}{b}+n'-1\right)}\right]$$

and,

$$C = \sum_{n'=-\infty}^{\infty} A' J_{n'}(\zeta) e^{i n'(\alpha+\varphi-\pi)} \frac{ab}{c}\left[\frac{e^{i\alpha}\sin N\pi\left(\frac{b'}{b}+n'+1\right)}{\left(\frac{b'}{b}+n'+1\right)} + \frac{e^{-i\alpha}\sin N\pi\left(\frac{b'}{b}+n'-1\right)}{\left(\frac{b'}{b}+n'-1\right)}\right] \tag{7c}$$

where $A' \equiv \exp\left[-\frac{i\omega}{c}(x_0 \sin\theta\cos\varphi + y_0 \sin\theta\sin\varphi + z_0\cos\theta)\right]$ is a phase and depends on the initial conditions, $J_{n'}(\zeta)$ is a Bessel function of order n' and argument $\zeta = (\omega a/c)\sin\theta$, $b' = \omega(1-\beta_{z_0}\cos\theta)$, and the integration variable is now $\nu \equiv bt$.

To put these results into a more physical form, we re-sum the series to collect the contributions to the intensity at a given frequency. We introduce Kronecker deltas in a new index, h, and rewrite equations (7) as,

$$A = 2\beta_{z_0} A' \sum_{h=-\infty}^{\infty} \frac{\sin\left[N\pi\left(\frac{b'}{b}-h\right)\right]}{\left(\frac{b'}{b}-h\right)} e^{-ih(\alpha+\varphi-\pi)}(-1)^h J_h(\zeta) \qquad (8a)$$

$$S = \frac{iab}{c} A' \sum_{h=-\infty}^{\infty} \frac{\sin\left[N\pi\left(\frac{b'}{b}-h\right)\right]}{\left(\frac{b'}{b}-h\right)} e^{-ih(\alpha+\varphi-\pi)}\left[e^{-i(\varphi-\pi)}(-1)^{h+1} J_{h+1}(\zeta) - e^{i(\varphi-\pi)}(-1)^{h-1} J_{h-1}(\zeta)\right] \qquad (8b)$$

$$C = \frac{ab}{c} A' \sum_{h=-\infty}^{\infty} \frac{\sin\left[N\pi\left(\frac{b'}{b}-h\right)\right]}{\left(\frac{b'}{b}-h\right)} e^{-ih(\alpha+\varphi-\pi)}\left[e^{-i(\varphi-\pi)}(-1)^{h+1} J_{h+1}(\zeta) + e^{i(\varphi-\pi)}(-1)^{h-1} J_{h-1}(\zeta)\right] \qquad (8c)$$

In terms of A, S and C, the intensity distributions are,

$$\frac{d^2I_\theta}{d\Omega\, d\omega} = \frac{e^2\omega^2}{4\pi^2 c b^2}\left[\cos^2\theta\cos^2\varphi\, C^*C + \cos^2\theta\sin^2\varphi\, S^*S + \sin^2\theta A^*A + \cos^2\theta\sin\varphi\cos\varphi(C^*S+S^*C) - \sin\theta\cos\theta\cos\varphi(A^*C+C^*A) - \sin\theta\cos\theta\sin\varphi(A^*S+S^*A)\right] \qquad (9)$$

$$\frac{d^2I_\varphi}{d\Omega\, d\omega} = \frac{e^2\omega^2}{4\pi^2 c b^2}\left[\sin^2\varphi\, C^*C + \cos^2\varphi\, S^*S - \sin\varphi\cos\varphi(C^*S+S^*C)\right]$$

When A, S, C, and their complex conjugates, A*, S*, and C*, are substituted into (9), these expressions exactly describe the radiation emitted into the radiation zone by a charge oscillating through N periods of a helical trajectory.

Equations (9), though exact, are unwieldly. Although the overall phase disappears (A*A = 1), the intensity distributions depend explicitly on N, θ, φ

and ω , as well as the parameters of the trajectory, through products of infinite sums of Bessel functions. We have evaluated the expressions numerically to study the intensity, polarization, and harmonic structure of the radiation as a function of both frequency and observation angle. Figure 1 shows the intensity distribution, as a function of θ and ω , for a particular choice of initial parameters. This particular case is appropriate to the radiation emitted by the relativistic electrons in the free electron laser, and will be discussed in detail later. Before addressing the detailed properties of the radiation, we will make some approximations which enable us to proceed further analytically, and reduce (9) to a more transparent result. The computer results, generated from (9), can be used to verify the validity of our approximations in the regimes of interest.

In particular, we will first investigate the role of the parameter N, the number of oscillations the charge goes through, and determine when the large N limit is appropriate. As noted above, the intensity distributions involve products of infinite sums of Bessel functions through the factors A*A, S*A, etc. Each term in each sum over h contains a factor

$$\frac{\sin\left[N\pi\left(\frac{b'}{b}-h\right)\right]}{\left(\frac{b'}{b}-h\right)} \equiv \sigma(h) \tag{10}$$

We define

$$\begin{Bmatrix} A \\ S \\ C \end{Bmatrix} = \sum_{h=-\infty}^{\infty} \sigma(h) \begin{Bmatrix} a(h) \\ s(h) \\ c(h) \end{Bmatrix} \tag{11}$$

and rewrite the intensity distribution displaying the double sums,

$$\frac{d^2 I_\varphi}{d\Omega\, d\omega} = \frac{e^2\omega^2}{4\pi^2 c\, b^2} \sum_{h=-\infty}^{\infty} \sum_{h'=-\infty}^{\infty} \sigma(h)\,\sigma(h')\, f_\varphi(h,h') \tag{12}$$

where f_φ is related to the bracketed terms in (9):

$$f_\varphi(h,h') = \sin^2\varphi\, c^*(h)c(h') + \cos^2\varphi\, c^*(h)c(h') - \sin\varphi\cos\varphi\left[c^*(h)s(h') + s^*(h')c(h)\right].$$

$\frac{d^2 I_\theta}{d\Omega\, d\omega}$ can be written in a similar way. The double sum in (12) can formally be rewritten as an infinite series of single sums

$$\mathcal{I} = \sum_{h=-\infty}^{\infty} \sigma(h)\sigma(h) f_\varphi(h,h) + \sum_{h=-\infty}^{\infty} \sigma(h)\sigma(h+1) f_\varphi(h,h+1) + \sum_{h=-\infty}^{\infty} \sigma(h)\sigma(h+2) f_\varphi(h,h+2) + \cdots \quad (13)$$

The size of each term depends on the overlap of the functions $\sigma(h)$ and $\sigma(h')$. This is clearly a maximum for $h = h'$, and decreases rapidly as $\Delta h \equiv |h-h'|$ increases. $\mathcal{I}$ can therefore be thought of as a perturbation series, with Δh the parameter which determines the "order." To evaluate the relative sizes of the terms note that $\sigma(h')$ peaks at a frequency $\omega \approx b h'(1-\beta_{z0}\cos\theta)$ and has width $\approx 1/N$. For relativistic motion nearly along the z-axis, the separation between $\sigma(h)$ and $\sigma(h')$, for the lower harmonics ($<N^{th}$), is much greater than the $1/N$ width. Even for small N, the overlap is small, and is negligible for $N \gtrsim 10$. Note that $N\to\infty$, the sum reduces exactly to

$$\mathcal{I} = \sum_{h=-\infty}^{\infty} \sigma(h)\sigma(h) f_\varphi(h,h) \quad (14)$$

The first order correction, for finite N, is just the second term in (13). Further, since $\sigma^2(h)$ is a sharply peaked function for large N, the harmonic frequencies are centered on $(b'/b - h)=0$; the argument can never vanish for $h<0$ (since ω must be positive), therefore the sum can be taken over positive values of h.

In the approximation (14),

$$\frac{d^2I_\varphi}{d\Omega\, d\omega} = \frac{e^2\omega^2}{4\pi^2 c\, b^2} \frac{\sin^2\left[N\pi\left(\frac{\omega}{b}(1-\beta_{z0}\cos\theta)-h\right)\right]}{\left(\frac{\omega}{b}(1-\beta_{z0}\cos\theta)-h\right)^2} \left[2\beta_{z0}\sin\theta\, J_h(s) + \frac{ab}{c}\cos\theta\left(J_{h+1}(s)+J_{h-1}(s)\right)\right]^2 \quad (15)$$

$$\frac{d^2I_\varphi}{d\Omega\, d\omega} = \frac{e^2\omega^2}{4\pi^2 c\, b^2} \frac{\sin^2\left[N\pi\left(\frac{\omega}{b}(1-\beta_{z0}\cos\theta)-h\right)\right]}{\left(\frac{\omega}{b}(1-\beta_{z0}\cos\theta)-h\right)^2} \left(\frac{ab}{c}\right)^2\left[J_{h+1}^2(s)+J_{h-1}^2(s)-2J_{h-1}(s)J_{h+1}(s)\right]$$

These results are independent of φ. The exact answer (9) does not have azimuthal symmetry because the trajectory has a finite extent: a

"beginning" and an "end."

III. Limiting Cases and Previous Results

It is easier to pick out the features of the spectrum from (15). First, if $\beta_\perp = 0$ (the particle moves with uniform velocity $\beta_{z0}c$), there is no radiation. Second, the on-axis result reduces to

$$\left.\frac{d^2I}{d\Omega\, d\omega}\right|_{\theta=0} = \frac{e^2\omega^2}{4\pi^2 c\, b^2}\sum_{h=1}^{\infty}\frac{\sin^2\left[N\pi\left(\frac{\omega}{b}(1-\beta_{z0})-h\right)\right]}{\left[\frac{\omega}{b}(1-\beta_{z0})-h\right]^2}\left(\frac{2a^2b^2}{c^2}\right)\left(J_{h+1}^2(0)+J_{h-1}^2(0)\right) \tag{16}$$

Both polarizations contribute equally (circular polarization) as would be expected from the symmetry of the orbit. Since all Bessel functions except J_0 vanish at zero, only h=1 contributes to the sum: all "harmonics" vanish on-axis, and there is radiation only in the fundamental. The frequency, $\omega = b/(1-\beta_{z0})$, selected by the delta-function is easily understood: cyclotron motion produces radiation at harmonics of the orbital frequency b; since the particle is also moving along the Z-axis, this frequency is Doppler-shifted to the value above.

We can, of course, recover the cyclotron spectrum from (15) simply by letting $\beta_{z0} = 0$. In this limit,

$$\left.\frac{d^2I}{d\Omega\, d\omega}\right|_{\beta_{z0}=0} = \frac{e^2\omega^2}{4\pi^2 c\, b^2}\sum_{h=1}^{\infty}\frac{\sin^2 N\pi\left(\frac{\omega}{b}-h\right)}{\left(\frac{\omega}{b}-h\right)^2}\left[\frac{a^2b^2}{c^2}(1+\cos^2\theta)\left(J_{h+1}^2\left(\frac{hab}{c}\sin\theta\right)+J_{h-1}^2\left(\frac{hab}{c}\sin\theta\right)\right)\right. \tag{17}$$
$$\left. -2\frac{ab}{c}\sin^2\theta\, J_{h+1}\left(\frac{hab}{c}\sin\theta\right)J_{h-1}\left(\frac{hab}{c}\sin\theta\right)\right]$$

As $N\to\infty$, the line shape approaches that of a delta-function and we obtain, after some manipulation of Bessel functions, the power (per cycle) emitted by a charge in circular motion into a particular harmonic[9,12]

$$\frac{dP}{d\Omega} = \frac{e^2h^2}{2\pi c}\left(\frac{ab}{c}\right)^2\left[\frac{\cot^2\theta}{(ab/c)^2}J_h^2\left(\frac{hab}{c}\sin\theta\right)+J_h'\left(\frac{hab}{c}\sin\theta\right)\right] \tag{18}$$

Returning to (15), we can evaluate the expression for $\theta = \pi/2$, an observer in the plane of the circular motion:

$$\left.\frac{d^2I}{d\Omega\, d\omega}\right|_{\theta=\pi/2} = \frac{e^2\omega^2}{4\pi^2 c b^2}\left(\frac{ab}{c}\right)^2 \sum_{h=1}^{\infty} \frac{\sin^2 N\pi\left(\frac{\omega}{b}-h\right)}{\left(\frac{\omega}{b}-h\right)^2}\left[J_{h+1}\left(\frac{\omega a}{c}\right) - J_{h-1}\left(\frac{\omega a}{c}\right)\right]^2 \qquad (19)$$

In the non-relativistic limit, ab/c << 1, and we can expand the Bessel functions to obtain the result that radiation is emitted primarily at the particle's orbital frequency, $\omega = b$. For extreme relativistic motion, ab/c $\approx$ 1, and the argument of the Bessel functions is no longer small. We therefore expect radiation into the high harmonics. Further, since the width of the lines is $\sim 1/N$, harmonics with $h \geq N$ will overlap and produce the broad, "continuous" spectrum normally associated with synchroton radiation.

IV. Application to the Free Electron Laser

We now turn to the specific limiting case of interest in this work: that which applies to the operation of free electron lasers. The laser mode grows from spontaneous emission radiated by the relativistic electrons. The intensity of the spontaneous emission which will contribute to a particular oscillator mode is found by integrating (9) over the angle and frequency which define that mode:

$$I = \iint_{mode} \frac{d^2I}{d\Omega\, d\omega}\, d\Omega\, d\omega \tag{20}$$

The expression for $d^2I/d\Omega d\omega$ can be simplified when we make the appropriate approximations. The electrons are injected in such a way that their motion along the axis of the helix is highly relativistic while their motion transverse to the axis is not: $\beta_{z0} \approx 1$, and $\beta_{\perp 0} = \frac{ab}{c} \ll 1$. Because of these conditions, the radiation cone (with angular width $\sim \gamma^{-1}$) is directed nearly along the axis of the helix. Assume γ is large; the pitch angle of the helical motion will be less than the width of the radiation cone if:

$$\left(\frac{ab}{c}\right)^2 < (1-\beta_{z0}) \approx \frac{1}{2\gamma_{z0}^2} \tag{21}$$

where $\gamma_{z0}^{-2} \equiv 1-\beta_{z0}^2$

If this condition is met (as it is, for example, in the free electron laser at Stanford), a detector placed on-axis at infinity receives radiation continuously. Assuming that the electron oscillates through many cycles in the magnetic field, this detector is able to resolve the Doppler-shifted frequency of the motion.[+] The line shape and angular dependence of radiation

[+] This distinguishes the radiation produced in this process from normal synchrotron radiation, in which the radiation cone rotates through 2π at the fundamental particle motion frequency (the "search-light" effect).

are both involved in the $\sin^2 x/x^2$ factor in (15). This factor is essentially a δ-function for $N \geq 20$, so the spectrum consists of sharp spikes. The on-axis ($\theta = 0$) spectrum contains only a sharp spike at $\omega = b/(1-\beta_{z_0})$. There is no radiation in the higher harmonics (the argument of the Bessel functions vanishes at $\theta = 0$; J_1, corresponding to fundamental, is the only contributer to the spectrum).

As the detector at infinity is moved slightly off-axis it records a different spectrum. Since the radiation cone wobbles about $\theta = 0$ as the electron spirals down the magnet, the detector samples (in a periodic manner) different regions of the cone. Off-axis the sampling is asymmetric (radiation from some parts of the orbit is sampled more often than that from others) and harmonics appear in the spectrum. The harmonic frequencies are given by

$$\omega_h = \frac{hb}{(1-\beta_{z_0}\cos\theta)} \approx \frac{2bh\,\gamma_{z_0}^2}{1+(\gamma_{z_0}\theta)^2} \qquad (22)$$

(the approximate relation is true for γ large and $\beta_{z_0} \approx 1$).

For a given detector location (a specific θ), the spectrum will consist of a series of spikes at the frequencies in (22) corresponding to h = (1, 2, 3, ...). As the angle is changed, the spectrum is changed. Although the radiation is emitted primarily into angles $\theta \leq \gamma_{z_0}^{-1}$, even slight excursions off-axis produce significant changes in the frequency. For example, the frequency of the "fundamental" (h=1) goes down by a factor of 2 from $\theta = 0$ to $\theta = \gamma_{z_0}^{-1}$. This dependence of emission frequency on angle for the first ten harmonics is shown in figure 2.

The fundamental is found at the locus of points satisfying (22) for h = 1, the first harmonic appears at the curve generated for h = 2, and so on. If we were to plot a third dimension, $d^2I/d\Omega d\omega$, coming out of figure 2, each value of h would correspond to a thin (width ~ 1/N) "curtain" of radiation. These curtains are sketched in figure 3.

We now examine the intensity of the radiaiton emitted into each harmonic (the "height" of each curtain); this is a function of the observation angle, and will change if the parameters of the electron trajectory are changed.

The amount of radiation emitted at a given frequency and angle is weighted by the Bessel function $J(\zeta)$ in (15). Using (22) at the emission spikes, and the small angle approximation (valid in this regime),

$$\zeta = 2\gamma h \left(\frac{ab}{c}\right) \frac{\theta \gamma_{z0}}{1+(\gamma_{z0}\theta)^2} \tag{23}$$

From (2) we know that ζ is less than unity. When it is very small, $J_{h=1}$ is the main contributor to the infinite sum in (15) and emission (at all angles) is primarily into the fundamental. This is illustrated in figure 4(a): the higher harmonics are small. Note again that the frequency of the "fundamental" (the radiation associated with h = 1) changes with angle. When ζ is near unity, (figure 4(b)) the ratio β_{z0}/β_{z0} is higher, the oscillation is more pronounced, and emission into the harmonics therfore becomes more important. The overall scale of figure 4 (the height of the "curtains") depends, of course, on the electron's acceleration. As either b (the oscillation frequency) or a (the orbital radius) increases, the intensity increases. The total instantaneous power can be computed exactly using the relation

$$P = \frac{2}{3} \frac{e^2 \gamma^6}{c} \left[\dot{\vec{\beta}}^2 - (\vec{\beta} \times \dot{\vec{\beta}})^2 \right] \tag{24}$$

For a charge in a helical orbit, (1),

$$P = \frac{2}{3} \left(\frac{e^2\gamma^6}{c}\right)\left(\frac{a^2b^4}{c^2}\right)\left[(1-\beta_{z0}^2) - \frac{a^2b^2}{c^2}\cos^2(2(bt+\alpha))\right] \tag{25}$$

Our results, to this point, have been formulated in terms of the parameters of a helical trajectory; we have made no reference to the fields which produce that trajectory. We now consider two particular field configurations which guide particles in helical paths, and could be used in free electron laser design: a periodic transverse magnetic field, and a uniform longitudinal magnetic field.

1) Periodic Transverse Field. This is the field configuration employed in the Stanford free electron laser. The relativistic electrons are injected nearly along the symmetry axis (z-axis)

of a field $\vec{B} = B_0(\cos \frac{\omega_0 z}{c}, \sin \frac{\omega_0 z}{c}, 0)$, which is periodic in z (with wavelength $\lambda_0 = 2\pi c/\omega_0$), and has strength B_0 (in the Stanford laser, $\lambda_0 = 3.2$ cm, $B_0 = 2.4 \times 10^3$ Gauss). The electrons follow the helical paths of (1) with

$$a = \frac{\omega_B c}{\omega_0^2 \beta_{z0}}, \qquad b = \omega_0 \beta_{z0} \tag{26}$$

where $\omega_B \equiv eB_0/\gamma mc$, and $\beta_{z0} c$ is the electron's initial z-velocity.

2) Uniform Longitudinal Field. It has recently been shown[13] that laser action could be sustained in a magnetic field of the form $\vec{B} = B_0(0,0,1)$. Again, relativistic electrons injected nearly along the z-axis will follow helical trajectories; in this case, the orbit parameters are

$$a = \frac{\beta_{\perp 0} c}{\omega_B}, \qquad b = \omega_B \tag{27}$$

where again $\omega_B = eB_0/\gamma mc$, and $\beta_{\perp 0} c$ is the electron's initial transverse velocity.

With (26), (27), and the results of this and the previous sections, we can immediately describe the spontaneous emission of a particular free electron laser in terms of its magnetic field structure. The frequency of the radiation is, of course, determined by the Doppler-shifted frequency of the particle's motion:

Periodic Field	Longitudinal Field
$\omega_h = \frac{h \beta_{z0} \omega_0}{(1 - \beta_{z0} \cos\theta)}$	$\omega_h = \frac{h \omega_B}{(1 - \beta_{z0} \cos\theta)}$

(28)

In the periodic field, the field strength has no affect on the emission frequencies--those are determined by the periodicity of the field. In the longitudinal field, however, the emission frequencies can be "tuned" by changing the field strength. The two lasers would operate at quite different frequencies for a given electron injection scheme and a given field strength, B_0. In the Stanford machine, electrons are injected with $\gamma \approx 50$, and emit on-axis radiation into the fundamental mode at a wavelength of ~ 10 microns; those same electrons injected into a longitudinal

field of comparable strength ($\sim 2.4 \times 10^3$ gauss) would radiate at ~ 500 microns (at $\theta = 0$, h = 1).

The intensity of the radiation, and the relative importance of the harmonics, depend on the parameter ab/c. In the helical-field free electron laser, $ab/c = \omega_s/\omega_o$. This suggests that a larger fraction of the radiation is emitted into the harmonics if either the period of the imposed magnetic field, or the strength of the field, is increased. In the longitudinal field, $ab/c = \beta_{\perp o}$: the combination of the electron's energy and injection angle determine the intensity (indirectly, since $\beta_{\perp o}$ determines N, the number of oscillations over a fixed length), and the relative importance of harmonics (since $\beta_{\perp o}$ controls the wobbling of the radiation cone in detector plane).

Either of the above lasers is continuously tunable: the operating frequency can be changed by changing the electron energy or the periodicity of the field (in a periodic field) or the field strength (in a longitudinal field). It is also possible to tune the laser by adjusting the mirrors of the cavity to store and amplify radiation emitted into some small, off-axis angle θ . Selecting θ selects a frequency. This may be an advantage for lasers operating in storage rings, where the detection angle can be altered more easily than the electron energy.

The off-axis radiation may enable us to extend the operating range of free electron lasers to shorter wavelengths. At all angles except $\theta = 0$, there is emission into many discrete, well-separated harmonics. It should be possible to induce laser gain in these higher harmonics[3], and therefore operate the laser at much higher frequencies without altering the field structure.

V. Discussion

We have derived the spectral and spatial characteristics of the spontaneous radiation emitted by a charge in a helical trajectory of finite length. The charge could be guided through this orbit by any one of several field configurations: a longitudinal magnetic field, a periodic transverse magnetic field, a periodic (in time, or in one space dimension) electric field, or a circularly polarized light wave. Our exact analytic result, (9), is formulated in terms of the parameters of a helical trajectory; writing these parameters in terms of the fields producing the motion immediately yields the spontaneous emission in as a function of the fields.

The character of the radiation depends crucially on the pitch angle of the particle trajectory. If the pitch angle is large ($\beta_{\perp_0}/\beta_{\parallel_0} > 1$), the radiation cone of a relativistic charge sweeps through the detector, and the harmonics cannot be resolved: the result is a broad, synchrotron-like spectrum. As the pitch angle decreases, the radiation cone deviates less and less from the forward direction, and harmonics characteristic of periodic motion can be resolved. If $\beta_{\perp_0} \leq 1/\gamma$, a detector near $\theta = 0$ is always illuminated by some part of the radiation cone; the spectrum it sees consists of sharp, well-separated harmonics, at frequencies which depend critically on the observation angle. This particular limiting case describes the spontaneous emission from a free electron laser.

The radiation produced by the electrons as they spiral in the fields of a free electron laser cavity is funadamental to the laser's operation. It is stored in the cavity, and can therefore act back on the electrons, stimulating further radiation and resulting in laser action. In a future paper, we will include the spontaneous emission "noise" in the laser evolution equations. In this paper we were able to derive the spectral line

shape, which relates the stimulated emission rate to the spontaneous emission rate, because to get (15) we integrated over a finite number of oscillations. The free electron laser gain is proportional to the slope of this spectral line.

If the features of spontaneous emission are understood, they can be used to great advantage in free electron laser technology. For example, since the free electron laser employs an overmoded optical cavity, the laser modes are not determined by cavity modes, but by the spontaneous emission modes. It should be possible to make use of the off-axis properties of the radiation to tune the laser, either by amplifying the off-axis radiation into the fundamental modes, or by stimulating gain in the higher harmonics. Harmonic gain should extend the operating range of free electron lasers to considerably shorter wavelengths.

An understanding of the spontaneous emission process is important to an understanding of the stimulated (laser) process in free electron devices. It is also possible to run this argument in reverse: stimulated radiation (from an external laser beam) could be used to probe the intricacies of the spontaneous emission spectrum. If the laser were tuned to the appropriate frequency, it would stimulate further emission from the radiating electron beam; the "appropriate frequency" is a function of angle and "harmonic," as discussed above. The spontaneous modes could be mapped by slowly sweeping the external laser beam through angle and frequency, providing a means to study the angular and spectral characteristics of the spontaneous spectrum experimentally.

REFERENCES

1. J. M. J. Madey: J. Appl. Phys. 42, 1906 (1971).
2. W. B. Colson: Phys. Lett. 59A, 187 (1976).
3. W. B. Colson: Ph.D. Thesis, "Free Electron Laser Theory," Stanford University (1977).
4. G. A. Schott: Electromagnetic Radiation (London, Cambridge University Press, 1912).
5. J. Schwinger: Phys. Rev. 75, 1912 (1949).
6. T. Takakura: Astr. of Japan, 12, 325 (1960).
7. T. Takakura: Astr. S. of Japan, 12, 352 (1960).
8. R. I. Epstein: Stanford University Institute for Plasma Research Report No. 435, March 1973.
9. H. Motz: J. Appl. Phys. 22, 527 (1951).
10. B. Kincaid: J. Appl Phys. 48, 2684 (1977).
11. J. M. J. Madey: High Energy Physics Lab Report No. 823, Stanford University, June 1978.
12. J. D. Jackson: Classical Electrodynamics (John Wiley & Sons, Inc.) 1975.
13. S. K. Ride, W. B. Colson: to be published in J. Appl. Phys.

Figure 1 - The intensity distribution, $d^2I/d\Omega\, d\omega$, is plotted vs. observation angle, θ , for values of ω ranging from $.5\,\omega_f$ to $2.0\,\omega_f$ ($\omega_f = b/(1-\beta_{z_0})$) is the fundamental frequency at $\theta = 0$). This was calculated from equation (9), with 10 elements of the sum, for N=20, a = 5×10^{-3} cm and b = 6×10^{10} radians/sec.

Figure 2 - The emission frequencies of the first 10 "harmonics" (h = 1, 2, ... 10) are plotted as a function of the observation angle in units of $\omega_f = b/(1-\beta_{z_0})$, the frequency of the fundamental (h = 1) at $\theta = 0$. We assume the charge is spiralling in a helix with $\beta_{z_0} = .9998$, the value attained by electrons in the Stanford free electron laser.

Figure 3 - This three dimensional sketch shows the dependence of the radiated intensity, $d^2I/d\Omega\, d\omega$, as a function of frequency and angle. The thin "curtains" correspond to the harmonics for h = 1, 2, and 3, and have width ~1/N. Note that only the fundamental (h = 1) contributes to the spectrum on-axis.

Figure 4 - We again plot $d^2I/d\Omega\, d\omega$ vs. observation angle for values of ω ranging from $.5\,\omega_f$ to $2.0\,\omega_f$ ($\omega_f = b/(1-\beta_{z_0})$) for (a) N = 20, a = 5 x 10^{-3}cm, b = 6 x 10^{10} rad/sec (this is identical to figure 1, and is reproduced here for the purposes of comparison) and (b) N = 20, a = 5 x 10^{-3}cm, b = 9 x 10^{10}rad/sec. As ab/c is increased (as it is by 50% from (a) to (b)), the overall intensity increases, and a larger fraction of the radiation is emitted into the harmonics.

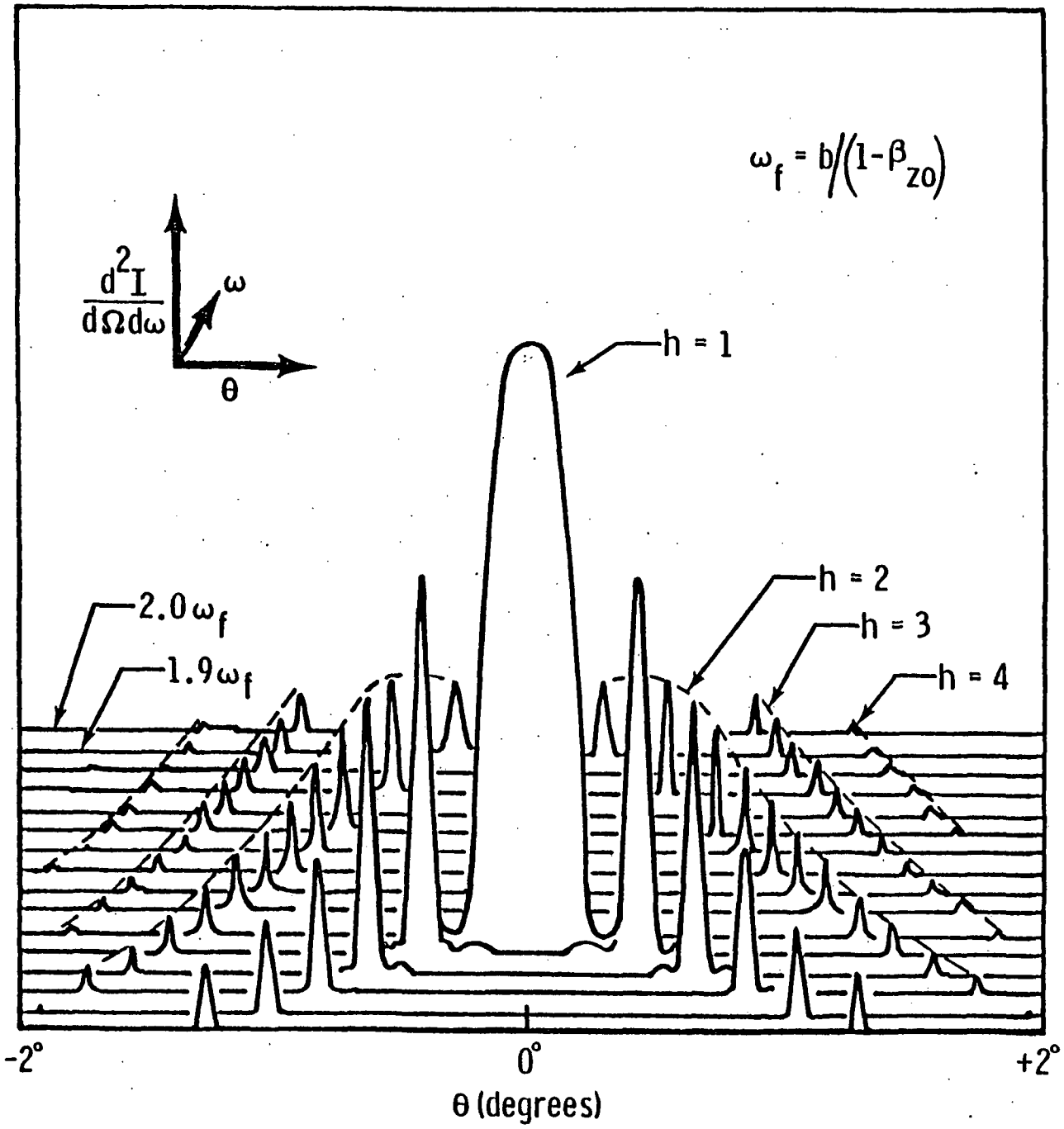
$\omega_f = b/(1-\beta_{zo})$
$\frac{d^2I}{d\Omega d\omega}$
ω
θ
h = 1
h = 2
h = 3
h = 4
$2.0\omega_f$
$1.9\omega_f$
-2°
0°
+2°
θ (degrees)

Figure 1

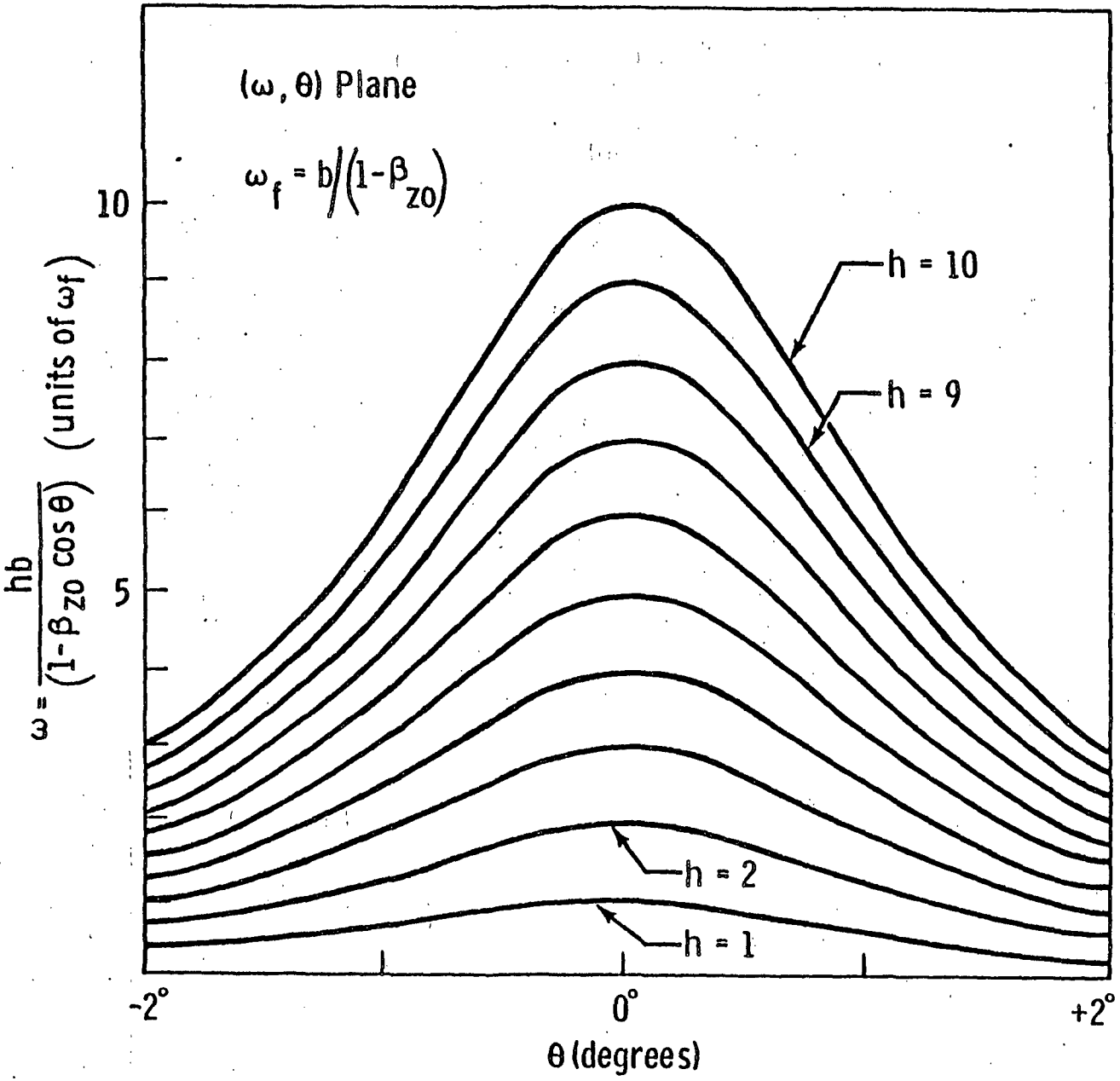
(ω, θ) Plane
$\omega_f = b/(1-\beta_{zo})$
10
5
$\omega = \frac{hb}{(1-\beta_{zo}\cos\theta)}$ (units of ω_f)
h = 10
h = 9
h = 2
h = 1
-2°
0°
+2°
θ (degrees)

Figure 2

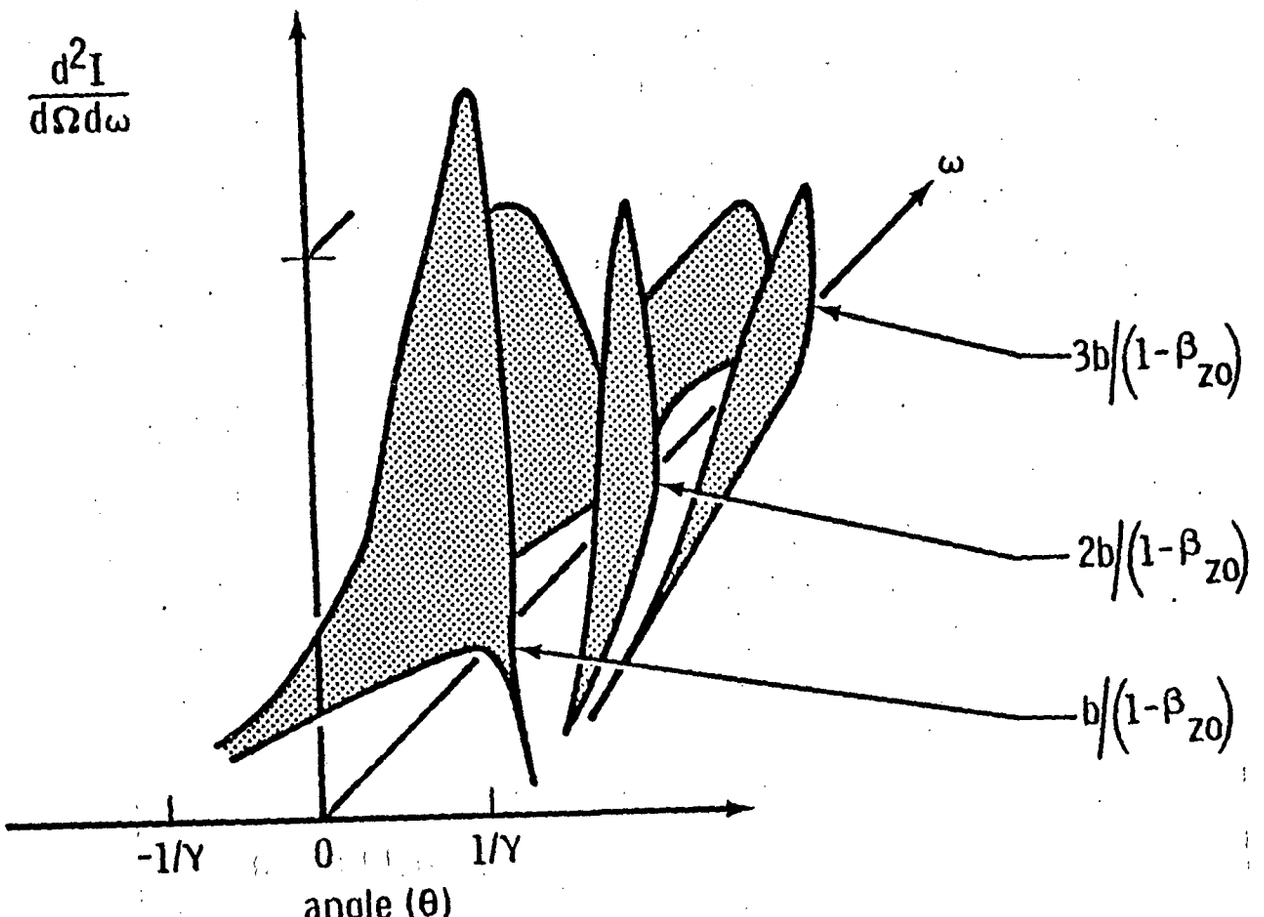

Figure 3

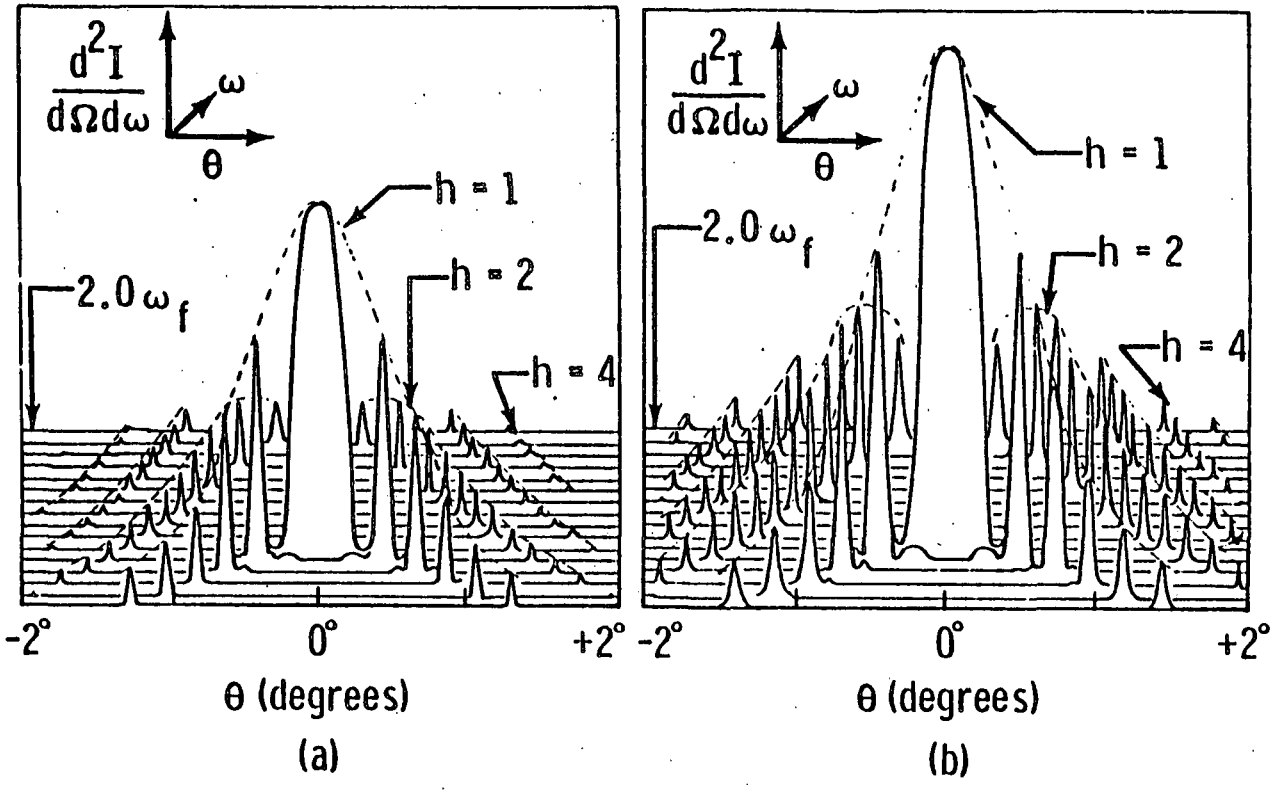

Figure 4

Space Solar Power Review, Vol. 1, pp. 145–154, 1980
Printed in the USA.

0191-9067/80/010145-10$2.00/0

THE PHOTOKLYSTRON

JOHN W. FREEMAN, SEDGWICK SIMONS
WILLIAM B. COLSON*, FRANZ R. BROTZEN†
and JEFF HESTER

Department of Space Physics and Astronomy
and Space Solar Power Research Program
*Center for Space Physics and
Space Solar Power Reserach Program
†Department of Mechanical Engineering and Material Science
Rice University
Houston, Texas 77001, U.S.A.

Abstract — This paper discusses a new device which oscillates at radio frequencies when illuminated by light. It was originally conceived as a reflex klystron with the thermionic electron source replaced by a photoemitter. In practice, the photoklystron‡ has been found to have different properties from what might be expected by simply scaling a reflex klystron to lower electron energies and oscillation frequencies. These include electron energy exchange with the rf field on multiple oscillations and plasma effects. The device can be made to "self-oscillate;" that is, no external accelerating bias voltage is necessary. The energy to sustain oscillation is derived solely from the photoelectrons. An electrical efficiency of 1% has been demonstrated for the first test model photoklystron. An ultimate efficiency of 10% appears possible. A solar power satellite configured with photoklystrons might be weight and cost competitive with solar cell designs.

INTRODUCTION

The Solar Power Satellite is basically a system for converting broadband, incoherent electromagnetic radiation (sunlight) into narrowband, coherent, ultra-high frequency electromagnetic radiation. In the conventional SPS concept this is accomplished by the conversion of sunlight to dc high voltage electricity which is then converted to microwaves via an array of high power klystrons. A solid state system is also being studied in which the solar cells and microwave amplifiers are an integral module.

It occurred to us that some increase in efficiency might be possible if photoelectrons could be used to generate the rf directly, possibly overcoming bandgap energy limitations inherent in solar cells (1).

The reflex klystron converts a monoenergetic electron beam to rf by passing the beam through a pair of grids on which an rf signal already exists. The rf field velocity modulates the electrons so that, upon reflection by a repelling electrode, the electrons may be bunched together instead of randomly distributed in their return arrival times at the grids. If the return arrival time of the bunch corresponds to a point in time at which the field between the grids is of such a polarity as to decelerate the electrons, the electrons give up some of their kinetic energy to the electric field thus

‡Patent applied for.

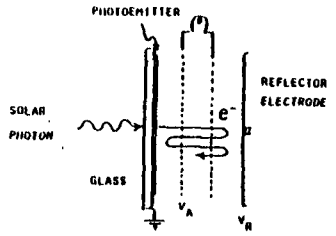

Fig. 1. Schematic diagram of a photoklystron.

reinforcing the oscillations in a tuned LC circuit (2). The time average of the electron energy imparted to the rf field is nonzero and positive because the electrons have been bunched.

If reflex klystron theory could be scaled to very low electron energies, a few eV, and if a spread in energies comparable to that expected from a photoemitter could be accommodated, it seemed possible that the photoelectron kinetic energy could be used to drive oscillations. If we chose the appropriate frequency for oscillation it appeared that conventional phototube photoemitters could provide sufficient photocurrent to sustain oscillations. To demonstrate that the concept was sound we had custom manufactured a proof-of-concept test model. Fig. 1 is a schematic of this device. The photoemitter is a standard S-4, CsSb photocathode deposited on a glass window. The two grids are 0.8 cm apart and separated 1 cm from the photocathode and reflector electrode. The grids are coupled by an air core inductor. Fig. 2 is a photograph of the test photoklystron.

II. TEST RESULTS

The initial tests were conducted with a small accelerating bias voltage on the grids, positive relative to the photocathode. We found no trouble obtaining a variety of modes of oscillations in the frequency range from 8 to about 240 MHz. To our surprise, most of these modes (combinations of accelerating and reflection bias voltages) did not correspond to what would be expected from reflex klystron theory. For example, we found that the photoklystron would oscillate with the reflection voltage less than the accelerating voltage. Fig. 3 is a mode chart showing the unconventional modes.

Throughout these tests a small tungsten microscope lamp, producing about 10 mW of light at the photocathode, was used. With no tuned antenna but with the inductor serving as a poor magnetic antenna, harmonics of the rf signal are detectable with a small transistor radio several meters away. Oscilloscope and rf voltmeter measurements indicate that the oscillations are strong and start spontaneously. A search coil pickup has been used to measure the output power under a 50 Ω load. The measured electrical efficiency is about 1%. Using an rf voltmeter, the output voltages for the strongest modes are about 2.0 V rms. An overall efficiency (including light energy input) for this particular tube is not very meaningful since the photocathode has been damaged and its quantum efficiency is now less than 1%. However, assuming an

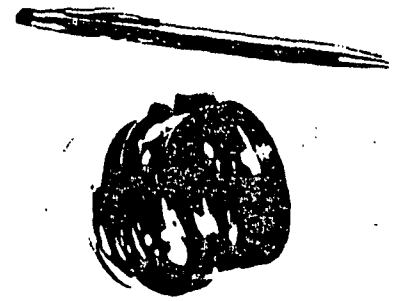

Fig. 2. Photograph of the test model photoklystron.

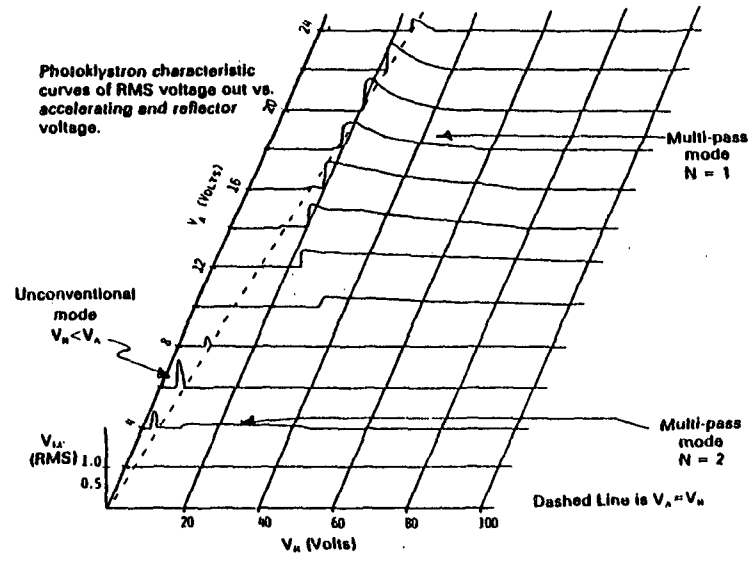

Fig. 3. Photoklystron test results showing actual modes.

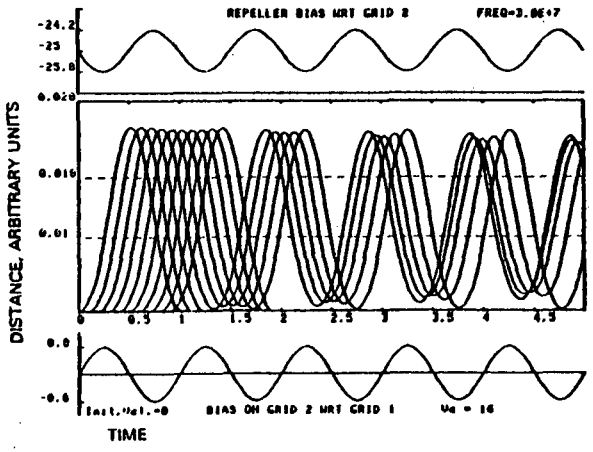

Fig. 4. An Applegate diagram for the photoklystron showing electron energy loss to the rf field over successive cycles. This is a plot of electron distance from the photocathode vs time for 10 electrons which leave the photocathode at equal time intervals and with 0 initial energy.

ultimate quantum efficiency of 25%, we estimate an overall efficiency of about 10% under AMO solar illumination. Furthermore, we wish to emphasize that this is the first photoklystron ever built and no attempt has been made to optimize the design.

III. THEORETICAL ANALYSIS

Since the strongest modes were those not attributable to conventional reflex klystron theory, we initiated a program of computer simulation to attempt to understand these modes. This computer code models the instantaneous electric field within the photoklystron and plots the resulting electron trajectories vs time. Based on this, we found a set of allowed conditions under which electrons leaving the photocathode at certain times and with certain energies can undergo multiple oscillations between the grids losing energy to the rf electric field all the while. Some electrons eventually fall out of phase with the rf field, however, after about five such oscillations 90% of these electrons have hit the grids. Figure 4 illustrates such trajectory calculations.

It is evident from these trajectory calculations that a selection process takes place. Electrons which take energy from the rf field on the first pass are quickly eliminated by collision with the cathode. The remaining electrons transfer a portion of their kinetic energy to the rf field over a period of several cycles.

The heart of our present photoklystron theory is the condition that the "favorable" electrons stay in phase with the rf field. To illustrate how this is possible, we calculate the total time required for an electron to perform a single cycle. We define an electron cycle as the sum of the times required for two grid crossings and the two turnaround times. We then set the period of an electron cycle equal to an integral number of rf periods. We have:

$$\frac{n}{f} = \frac{2m\delta v}{eV_a} + \frac{2d}{v} + \frac{2m\epsilon v}{eV_r} \qquad (1)$$

where

n=integer	e=the fundamental charge
f=frequency	m=electron mass
v=velocity	d=grid separation
V_a=accelerating voltage	δ=cathode to first grid distance
V_r=reflecting voltage	ϵ=second grid to reflector distance

This equation contains two assumptions:

(i) The rf field has negligible effect on the electron velocity on a single pass.

(ii) No electron–electron interactions occur.

From Eq. (1) we can gain some insight as to how the electrons can stay approximately in phase. As the electron velocity decreases so that the transit time between grids increases, the turnaround times decrease. Figure 5 represents a numerical solution of Eq. (1). We can see that for large v the curve becomes linear and the slope can be made small by careful choice of electrode separation distances and operating conditions. For example, a factor of two change in electron energy from 20 to 10 eV leads to less than a 20% phase shift between the rf field and the electron cycle.

If we assume that the electrons derive all their velocity from the accelerating field, Eq. (1) predicts modes. Examples of these modes are shown in Fig. 6. Note the excellent qualitative agreement between the location of the predicted modes shown in Fig. 6 and the observed modes in Fig. 3.

IV. SELF-OSCILLATION

Our first tests to understand the operation of the photoklystron were in the biased

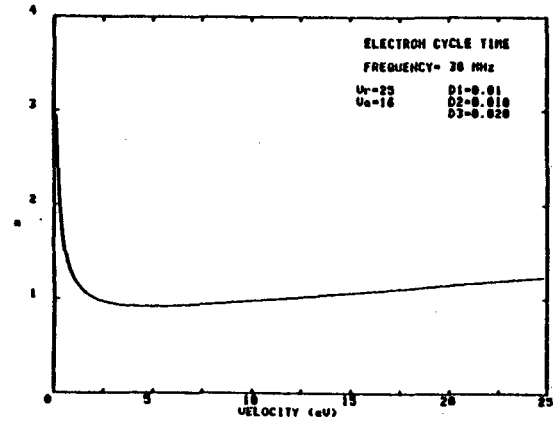

Fig. 5. Numerical solution to Eq. (1) at F=30 MHz. D1, D2 and D3 are parameters representing the grid, photocathode and reflector electrode spacing.

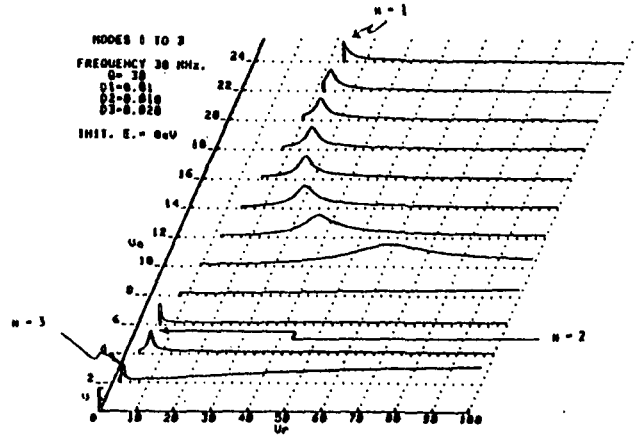

Fig. 6. Theoretical mode chart based on Eq. (1). Compare this with the actual test results shown in Fig. 3. The output amplitude is in arbitrary units.

mode, i.e. with an accelerating bias voltage on the grids used to boost the photoelectron energy by several electron volts. Our photoemitter has a quantum yield which peaks in the visible and uses a standard glass window. With our tungsten lamp, the measured photoelectron energy spectrum peaks at about 0.5 eV. After investigating the general properties of this photoklystron we began to investigate ways to lower the minimum accelerating bias voltage for which oscillations could be obtained in hopes that we could reach the point where oscillation could be sustained by the kinetic energy from photoemission alone, about 0.5 eV. The required accelerating voltge or electron energy can be lowered by lowering the resonant frequency. In our test model, the capacitance is that of the two parallel grids and is fixed. The inductor, however, is outside the vacuum seal and can be adjusted to a low or high inductance.

We found that at a frequency of 5.2 MHz our test model photoklystron will oscillate using only photoemission electron kinetic energy, that is, no external electron acceleration bias voltage is required. Switching from a tungsten lamp to a xenon lamp (a good solar spectrum approximation) greatly increases the rf output amplitude even though the CsSb photocathode material employed does not have a strong blue light response. Photoelectron kinetic energy is thus shown to be important in enhancing the oscillation amplitude. A small negative bias voltage is still required on the reflector electrode, however, since the reflector draws no current there is no energy drain on this bias supply. It may be possible to provide this bias voltage by tapping off a portion of the rf output and rectifying it. A voltage supply would be necessary to initiate oscillations but could be then removed.

We suspect but have not yet confirmed that space charge effects near the photoemitter play a role in shaping the photoelectron spectrum to a peaked spectrum suitable for interaction with the rf field (Cooke, D. private communication, 1979). A cloud of very low energy photoelectrons close to the photoemitter may repel other very low energy photoelectrons thus chopping off the low energy portion of the spectrum. Colson (private communication, 1979) has shown that a peaked spectrum

is essential for net positive energy exchange with the rf field. A negative space charge cloud near the photocathode may also provide the repelling voltage necessary for multiple oscillations in the self-oscillation mode. The self-oscillation mode cannot be fully understood in terms of the simplified analysis represented by Eq. (1). A fully self-consistent model including space charge is required.

V. THE PROSPECT FOR HIGHER FREQUENCIES

The present test model photoklystron with an 8 mm grid separation self-oscillates at about 5 MHz or lower, and in the biased mode, it has been operated at up to 240 MHz. Somewhat higher frequency oscillations are presumably possible by winding smaller inductors. To make the leap to ultra-high or microwave frequencies with the grid type device would require changes in the grid separation distance. From Eq. (1) we see that microwave frequency operation requires a substantial reduction in grid separation distance. One design with a grid separation of 0.5 mm was run on the computer and found to provide oscillations at 2.45 GHz, however, the parasitic capacitance of the grids at this distance is prohibitively high. Clearly the discreet elements must be replaced by a resonant cavity at these frequencies. This appears possible, however, additional research is necessary to determine if cavities with such narrow gaps are practical.

VI. ADDITIONAL RESEARCH

A problem found in some previous efforts to utilize photoelectric free electron devices for dc solar energy conversion has been the low quantum yield (3). The problem is that thick photocathodes which provide a high photon interaction probability leave a long escape path for the photoelectron. Negative electron affinity photoemitters have been tested which have quantum yields approaching 50% over a substantial portion of the visible spectrum, however, they are carefully prepared crystal surfaces. To solve the problem of low quantum yield, a photoklystron design may be possible which allows more than one photoemission surface to contribute to the electron beam. It has been found that oscillation modes exist in which the reflector electrode voltage is the same as the photocathode voltage relative to the grids. In this case, the electric fields are fully symmetric about a plane halfway between the grids. The reflector electrode can now be a photoemitter and contribute an independent stream of photoelectrons generated by photons which pass through the front photoemitter. Moreover, if the reflector electrode photoemitter is backed by a mirror, still unused photons traverse the tube backwards and can further liberate photoelectrons. In this way, it may be possible to design a photoklystron with a very high effective quantum yield.

An additional area for future research is the determination of an optimum photoemitter combining high quantum yield, stability and low cost. In order to maximize the effectiveness of the conversion device, photoemissive materials must be used which possess the lowest possible work function. A systematic search for stable and economical materials is presently underway. At this time, certain interstitial transition-metal compounds coated with alkali metals and their oxides are being tested for their photoemissive properties.

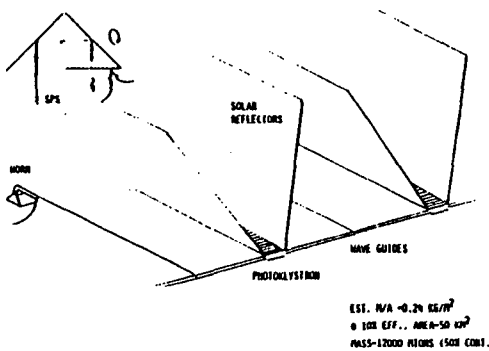

Fig. 7. A sketch showing a possible photoklystron SPS array configuration. The photoklystrons generate a rf wave which travels along the wave guide and emerges from the horn. The inset in the upper left hand corner shows the total satellite. The secondary mirror and photoklystron array rotate to follow the earth.

VII. PHOTOKLYSTRON APPLICATIONS

In the SPS application of the photoklystron, the entire solar array becomes the rf radiating surface. Instead of a cluster of high power klystrons we invision a large array of low power photoklystrons. This system lends itself to modular construction with radiating units being added as needed. This could reduce the high initial capitol cost for a given system. Moreover, the lower radiation energy density would reduce the hazard for astroworkers and make possible the addition of new modules without shutdown of the entire system.

To be competitive with a solar cell/klystron system (including bus bar and slip-ring), efficiencies for the photoklystron of about 12% will have to be demonstrated. Based on our present estimate of about 10% and the fact that reflex klystron efficiencies higher than this have been achieved, it appears possible to reach the 12% figure.

In order to obtain a mass per unit area estimate of an SPS configured with photoklystrons, we have developed a hypothetical design using resonant cavities and solar reflectors to concentrate sunlight on the photocathode surfaces. In this design, each photoklystron excites the center of a resonant cavity which forms a wave guide with adjacent resonant cavities. A traveling wave then moves down a line of adjacent photoklystrons. Since the resonant cavity/wave guide occupies more cross-sectional area than the photocathode surface, solar reflectors placed sunward of the resonant cavity/wave guide concentrate sunlight onto the photocathode surface. A concentration ratio of 3 is used. The resonant cavity/wave guide walls are made of aluminized 1/2 mil Kapton as are the solar reflectors. The photocathode consists of photoemissive material vapor deposited on a 1/2 mil Kapton (or similar uv transparent material) substrate. Wire grids are used at the resonant cavity gap. The reflector electrode is again an aluminized Kapton sheet. The resonant cavity/wave guide may be formed by separating the two sheets of aluminized Kapton by dielectric spacers or honeycomb material and drawing the sheets together into contact at the edge. Figure 7 is a sketch of this design.

The mass per unit area of the photoklystron area of such a configuration is estimated to be about 0.2 kg/m^2. The resonant cavity/wave guide reflector area is estimated at 0.25 kg/m^2.

For a CR3 satellite whose combined photoklystron and radiation efficiency are 10%, and which is required to radiate 6.75 GW (5 GW rectenna output), the required photoklystron area is 16.6 km^2 and the resonant cavity/wave guide reflector area is 33.3 km^2, for a total of 50 km^2. The resulting masses are 3.2×10^6 kg and 8.3×10^6 kg for the photoklystron and resonant cavity/wave guide reflector areas respectively. The total mass is 11.5×10^6 kg. This compares very favorably with the 13.8×10^6 kg and 27.6×10^6 kg for the GaAlAs Cr2 and silicon CR1 NASA/DOE reference system solar array masses (4), especially since an additional 13.5×10^6 kg must be added to the solar cell configuration weights for the klystron antenna array and slipring. In this photoklystron array weight estimate, no weight has been added explicitly for antennas, phase control, primary or secondary mirrors, or structure. However, an overall 50% contingency factor has been added to cover these items. It is expected that the antenna would be an integral part of the wave guide, probably periodic slots or horns, and would therefore add negligible weight. The overall satellite configuration could be similar to that proposed for the solid state sandwich system proposed by Rockwell International (5) with a primary and secondary mirror turning the solar flux through 90° and then onto the planar photoklystron configuration with rf radiating out the opposite side. See Fig. 7.

This mass and area estimate naively assumes that photoklystrons can be designed which will self-oscillate at the requisite frequency and efficiency. If it should turn out that bias voltages are required, these could be provided by interspersing solar cells among the photocathode surfaces in the trough. The solar cells would thus feed nearby photoklystrons and the modular nature of the concept would be preserved. The ratio of solar cell to photocathode area would depend on how much of the energy to drive the photoklystrons had to be derived from the bias voltages.

Aside from the application to the solar power satellite, the photoklystron may have other uses in space and on the earth. Communication satellites and telemetry transmitters for satellites and space probes have a need for highly reliable rf sources.

A great advantage of the photoklystron is its simplicity and hence reliability. It is a rf oscillator with only passive elements. Further, we expect low cost per unit area relative to solid state energy conversion devices because the photoemitter is vapor deposited. In space applications where large areas of photoklystrons are required, it may be possible to manufacture the photoklystron in space and dispense with vacuum encapsulation.

We expect the photoklystron to be relatively insensitive to degradation from charged particle radiation due to the thinness of the photoemitter.

Potential ground based applications of the photoklystron include direct production of power for microwave transmission lines and use in large scale drying operations such as drying lumber, grain or tobacco. When operated in the biased mode, the output frequency is sensitive to the accelerating bias voltage so the device may be used as a voltage controlled oscillator or alternatively as a simple precision voltage measuring device. It might also be used as a transmitting light sensor for alarm systems or to decode laser or fiber optic transmissions through rf amplifiers.

Acknowledgements — We acknowledge helpful discussions with Dr. William Wilson and Mr. David Cooke. This work has been supported by a grant from the Brown Foundation of Houston, Texas. The Editor wishes to thank Gordon Woodcock and Dr. Owen Garriott for their assistance in reviewing this paper.

REFERENCES

1. J.W. Freeman, W.B. Colson and Sedgwick Simons, New Methods of Conversion of Solar Energy to r.f. or Laser Power, 4th Princeton Conference on Space Manufacturing, May 1979.
2. J.J. Hamilton, *Reflex Klystron*, Chapter 3, MacMillan, New York, 1959.
3. Wm.P. Gilbreath and Kenneth W. Billman, A Search for Space Energy Alternatives, Radiation Energy Conversion in Space. Kenneth W. Billman, Ed. *Progress in Astronautics and Aeronautics*, Vol. 61, Amer. Inst. of Aeron. and Astron. 1978.
4. DOE/ER-0023, Satellite Power System Concept Development and Evaluation Program: Reference System Report, 1978.
5. G.M. Hanley, Rockwell Satellite Power System (SPS) Concept Definition Studies, *Space Solar Power Rev.* 1, 1980.

Appl. Phys. 22, 219–225 (1980)

Applied Physics

Energy Transfer in Constant Period Free-Electron Lasers

W. B. Colson

Space Physics Department, Rice University, Houston, TX 77001, USA

S. B. Segall

KMS Fusion, Inc., Ann Arbor, MI 48104, USA

Received 13 September 1979/ Accepted 18 January 1980

Abstract. A simple single particle model of a free-electron laser (FEL) amplifier has been used in a computer simulation to determine the maximum fractional conversion of electron kinetic energy to laser energy. The simulation results can be represented by a single universal curve. A simple scaling relationship for the length of the optimized constant period helix together with the universal curve permit one to predict maximum fractional energy conversion for any set of values of initial electron energy, initial laser intensity, magnetic field amplitude, and magnet period.

PACS: 42.55

In a free-electron laser a fraction of the energy in a relativistic electron beam is converted into coherent short wavelength radiation as both travel together through a periodic field which we will assume to be a static magnetic field. This laser is continuously tunable to short wavelengths and promises to be a powerful efficient radiation source. We are studying the free-electron laser as a potential fusion reactor driver [1, 2]. For this application we require short wavelength radiation ($\lesssim 1\,\mu m$), and high beam currents. To protect the focusing optics in a high-power laser system the cross sectional area of the laser beam at the focusing elements must be large. The cross sectional area of the electron beam must be matched to that of the optical beam in the laser amplifier, so that electron beam diameters of the order of centimeters may be needed. The period of a magnetic amplifier that can accomodate such a beam must be at least several centimeters to a few tens of centimeters. To obtain short wavelength light with large magnet periods, electron energies of several hundred MeV are required.

The existing technologies best suited for high current beams at high energy are induction linacs [3] and storage rings [4]. Both of these devices can produce beams with very low energy spread ($\Delta E/E \lesssim 10^{-3}$). The storage ring has the additional advantage, that the electrons may be repetively passed through an accelerator section which replaces the energy converted to radiation. The maximum peak current obtainable from these devices is about 10 kA for an induction linac and a few kA for a storage ring. For the laser wavelengths and electron energies and densities being considered, the interaction of individual electrons with the magnet and laser fields is the dominant effect.

Microscopic distortion of the electron density, or bunching, on the scale of an optical wavelength does produce longitudinal electric fields of the order of $2\pi\varrho\lambda_r$, where ϱ is the electron charge density and λ_r is the radiation wavelength. The effect of these microscopic fields on the highly relativistic electrons has been calculated and is small for the parameter range studied here. Electrostatic effects are therefore neglected in this paper.

Several previous studies of the FEL have already been made. Both experimental and theoretical work has been carried out at Stanford University [5–8]. Theoretical analyses of the FEL have been carried out using the Maxwell-Boltzmann equations [9–11] and

0340-3793/80/0022/0219/$01.40

the Vlasov equation [12, 13]. For this paper we describe the FEL by numerically solving the single particle Lorentz force equations in the combined magnet and laser fields. The goal of the study is to determine the maximum fraction of the electron beam energy that can be converted to radiation energy on a single pass through a constant period helical magnet. The electrons enter in a monoenergetic, uniform beam and the laser light is taken to be monochromatic with a self-consistency determined amplitude.

1. Basic Equations of the Single-Particle Model

The basic equations used in the single-particle model of the FEL are the Lorentz force equations which govern the electron trajectories. These are given in Gaussian units by [14]

$$\frac{d}{dt}(\gamma\boldsymbol{\beta})=\frac{e}{mc}[\mathbf{E}_r+\boldsymbol{\beta}\times(\mathbf{B}_r+\mathbf{B}_m)], \tag{1}$$

and

$$\frac{d\gamma}{dt}=\frac{e}{mc}\boldsymbol{\beta}\cdot\mathbf{E}_r, \tag{2}$$

where

$$\gamma^{-2}=1-\boldsymbol{\beta}\cdot\boldsymbol{\beta}. \tag{3}$$

Here $\boldsymbol{\beta}$ is the electron velocity divided by the speed of light c, γ is the ratio of electron energy to electron rest mass energy mc^2, $\mathbf{E}_r$ and $\mathbf{B}_r$ are the electric and magnetic fields of the electromagnetic wave, $\mathbf{B}_m$ is the magnetic field of the laser amplifier, and e is the charge of an electron. Equations (1) and (2) are a set of four equations, any three of which suffice to describe the interaction.

The static magnetic field is taken to be of the form $\mathbf{B}_m=B_m(\cos k_m z, \sin k_m z, 0)$, where $k_m=2\pi/\lambda_m$ and λ_m is the magnetic period. This is an excellent approximation for the magnetic field near the axis of a helical wiggler magnet as has been shown theoretically and experimentally [15]. The electric and magnetic fields of the laser beam are given by

$$\mathbf{E}_r=E_r(t)(\cos\chi, -\sin\chi, 0)$$
$$\mathbf{B}_r=B_r(t)(\sin\chi, \cos\chi, 0), \tag{4}$$

where $\chi=k_r z-\omega_r t+\phi$, $\lambda_r=2\pi/k_r=2\pi c/\omega_r$ is the optical wavelength, and ϕ is the optical phase.

Since all the fields are assumed to be transverse it is convenient to rewrite (1) through (3) in terms of axial and transverse components

$$\frac{d}{dt}(\gamma\boldsymbol{\beta}_\perp)=\frac{e}{mc}[\mathbf{E}_r+\boldsymbol{\beta}_z\times(\mathbf{B}_r+\mathbf{B}_m)], \tag{5}$$

$$\frac{d}{dt}(\gamma\boldsymbol{\beta}_z)=\frac{e}{mc}[\boldsymbol{\beta}_\perp\times(\mathbf{B}_r+\mathbf{B}_m)], \tag{6}$$

$$\frac{d\gamma}{dt}=\frac{e}{mc}\mathbf{E}_r\cdot\boldsymbol{\beta}_\perp, \tag{7}$$

and

$$\gamma^{-2}=1-\beta_\perp^2-\beta_z^2. \tag{8}$$

Because $\boldsymbol{\beta}_z\times\mathbf{B}_r=-\beta_z\mathbf{E}_r$, (5) becomes

$$\frac{d}{dt}(\gamma\boldsymbol{\beta}_\perp)=\frac{e}{mc}[\mathbf{E}_r(1-\beta_z)+\boldsymbol{\beta}_z\times\mathbf{B}_m]. \tag{9}$$

For the cases we are considering, $\beta_z B_m \gg E_r(t)(1-\beta_z)$, so that we can neglect the first term on the right-hand side in (9) giving

$$\frac{d}{dt}(\gamma\boldsymbol{\beta}_\perp)\approx\frac{e}{mc}\boldsymbol{\beta}_z\times\mathbf{B}_m. \tag{10}$$

Using the transformation $dt=dz/\beta_z c$, (10) can be easily integrated. Limiting ourselves to the case for which B_m and k_m are constants we obtain,

$$\boldsymbol{\beta}_\perp=\frac{e\mathbf{B}_m}{\gamma mc^2 k_m}+\text{const}. \tag{11}$$

We will assume that the electrons start out in perfect helical orbits, so that the constant of integration in (11) equals zero.

Defining

$$\alpha\equiv\frac{eB_m}{mc^2 k_m}, \tag{12}$$

the magnitude of $\boldsymbol{\beta}_\perp$ is given by

$$\beta_\perp=\frac{|\alpha|}{\gamma}. \tag{13}$$

From Eqs. (8) and (13) we obtain

$$\frac{(1+\alpha^2)}{\gamma^2}=1-\beta_z^2. \tag{14}$$

Differentiating and taking the limit $\beta_z\approx 1$ we obtain,

$$\frac{d\beta_z}{dt}=\frac{(1+\alpha^2)}{\gamma^3}\frac{d\gamma}{dt}=\frac{(1+\alpha^2)}{\gamma^3}\frac{e}{mc}\mathbf{E}_r\cdot\boldsymbol{\beta}_\perp$$
$$=\frac{\alpha(1+\alpha^2)}{\gamma^4}\frac{e}{mc}E_r(t)\cos\Psi, \tag{15}$$

where

$$\Psi=(k_m+k_r)z-\omega_r t+\phi. \tag{16}$$

Equation (15) can be put into the form of the pendulum equation in the low-gain limit [8].

An electron is said to be in resonance with the electromagnetic wave when the electron moves a dis-

tance of one magnet period during the time one wavelength of light passes over it.
When this is the case

$$\lambda_R = \lambda_m \frac{(1-\beta_z)}{\beta_z} \approx \frac{\lambda_m}{2\gamma^2}(1+\alpha^2), \tag{17}$$

where λ_R is the wavelength at resonance.
The position of an electron in the electron beam can be written in the form

$$z(t) = \beta_{0z} ct + z'(t), \tag{18}$$

where β_{0z} is the initial electron axial velocity. Using (18) we can write (16) as

$$\begin{aligned}\Psi &= (k_r + k_m) z' + \Delta\Omega t + \phi \\ &\approx k_r z' + \Delta\Omega t + \phi,\end{aligned} \tag{19}$$

where

$$\Delta\Omega \equiv (k_m + k_r)\beta_{0z} c - \omega_r. \tag{20}$$

From (20) we obtain

$$\frac{\Delta\Omega}{1-\beta_{0z}} = \omega_R - \omega_r, \tag{21}$$

where ω_R is the resonance frequency for electrons moving with the initial electron velocity.
The relative angle Ψ between $\mathbf{E}_r$ and $\boldsymbol{\beta}_\perp$ determines whether an electron loses or gains energy. From (19) we see that at any instant of time this angle varies by 2π radians over a distance of one wavelength of light and, therefore, sections of an electron beam λ_r in length will evolve identically in time provided the electron and laser beams are initially uniform. Electrons in a region where $\cos\Psi$ is positive will be decelerated and electrons in a region where $\cos\Psi$ is negative will be accelerated. This produces bunching of the electron beam on a scale of the wavelength of the laser light. If $\omega_r = \omega_R$ there will be no explicit time dependence in the phase factor Ψ, and the electrons will bunch symmetrically around the position $\Psi = -\pi/2$. For convenience we define a new angle $\theta = \Psi - \pi/2$ for which $\sin\theta = -\cos\Psi$. Bunching at resonance then occurs around $\theta = \pi$ (Fig. 1). Net transfer of energy to the laser field as a result of the bunching process will be zero at the resonance energy and there will be no laser gain.
If $\omega_r \neq \omega_R$ then θ will be explicitly dependent on time, the function $\sin\theta$ will shift relative to a reference frame moving with the initial electron velocity, and the electron density distribution will no longer be symmetric about $\theta = \pi$. If $\Delta\Omega$ is positive, the shift of the function $\sin\theta$ in the reference frame moving with the initial electron velocity will cause more electrons to lose energy than gain energy (Fig. 2). This produces amplification of the electromagnetic wave. If $\Delta\Omega$ were

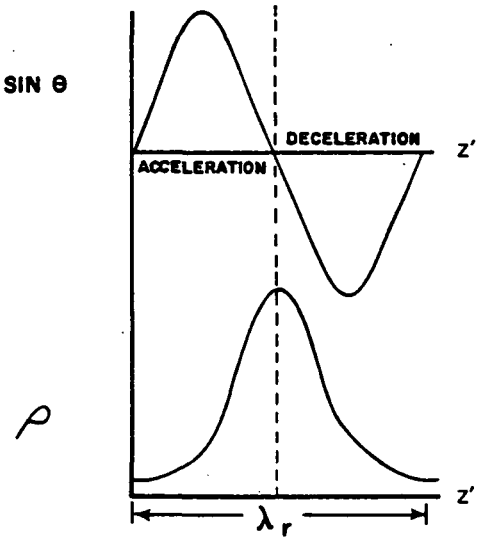

Fig. 1. Phase factor of the axial force on the electrons, $\sin\theta$, and electron density ϱ, as a function of position over a distance equal to one wavelength of light when the mean electron energy equals the resonance energy

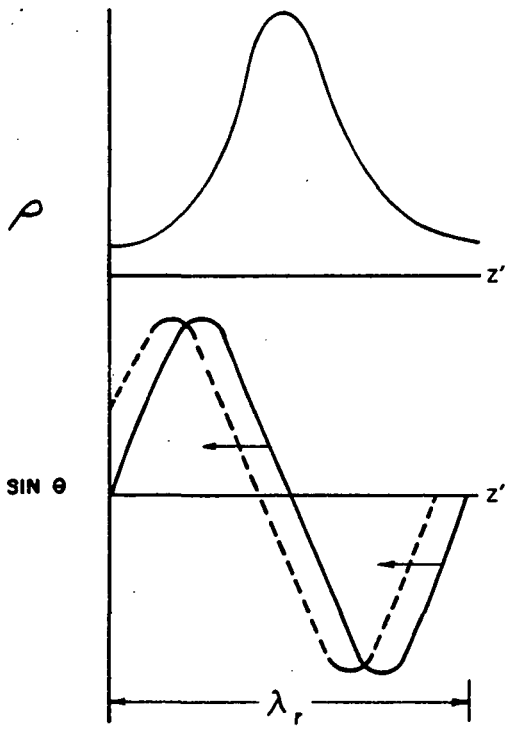

Fig. 2. For $\omega_r \neq \omega_R$ the phase factor $\sin\theta$ shifts with time relative to the position of the electron bunch. For the phase shift shown in this figure $\omega_r < \omega_R$

negative more electrons would be accelerated than decelerated, and the laser beam would give up energy to the electrons.
It is assumed that energy lost or gained by the electrons is transferred to or from the laser field. This

holds as long as the laser has a fixed frequency and resembles a single-mode plane-wave, which is usually the case. If the electron and optical beams are assumed to occupy the same volume, the condition for energy conservation can be written

$$\frac{[E_r^2(t)-E_r^2(0)]}{4\pi}dV=\varrho\gamma_0 mc^2\,dV-\sum_{i=1}^{N_e}\gamma_i(t)\,mc^2, \tag{22}$$

where $\gamma_0 mc^2$ is the initial electron energy, ϱ is the initial uniform electron density, dV is the volume element in the beam, and the sum is taken over all electrons in the volume element.

2. An Upper Bound on Energy Extraction

Using the basic equations derived in the previous section we can obtain an upper limit on the fraction of the electron energy that can be converted to laser energy in a single pass through a constant period helical wiggler magnet. Using the fact that $\varrho dV=N_e$ we can rewrite (22) in the form

$$E_r^2(t)=4\pi\varrho\gamma_0 mc^2\left(\frac{E_r^2(0)/4\pi}{\varrho\gamma_0 mc^2}+\frac{N_e\gamma_0-\Sigma\gamma_i(t)}{N_e\gamma_0}\right)$$
$$=4\pi\varrho\gamma_0 mc^2(s+\eta), \tag{23}$$

where

$$s\equiv\frac{E_r^2(0)/4\pi}{\varrho\gamma_0 mc^2} \tag{24}$$

is the initial ratio of field energy density to electron energy density and

$$\eta\equiv\frac{N_e\gamma_0-\Sigma\gamma_i(t)}{N_e\gamma_0}=\frac{-1}{N_e}\sum_{i=1}^{N_e}\frac{\Delta\gamma_i}{\gamma_0} \tag{25}$$

is the fraction of the initial electron energy that has been converted to laser energy at time t. Substituting (11) into (7) we have

$$\frac{d\gamma}{dt}=\left(\frac{e^2B_m\lambda_m}{2\pi m^2c^3\gamma}\right)E_r(t)\cos\Psi. \tag{26}$$

The expression for $E_r(t)$ in (23) is now substituted into (26) to give

$$\gamma d\gamma=\left(\frac{e^2B_m\lambda_m}{m^2c^3 2\pi}\right)(4\pi\varrho\gamma_0 mc^2)^{1/2}(s+\eta)^{1/2}\cos\Psi dt, \tag{27}$$

which describes the variation of electron energy with time for a single electron. Summing both sides of (27) over all electrons in the volume element dV and using $\gamma_i=\gamma_0+\Delta\gamma_i$ assuming $\gamma_0\gg\Delta\gamma_i$ we obtain

$$\gamma_0\sum_{i=1}^{N_e}d\gamma_i=\left(\frac{e^2B_m\lambda_m}{m^2c^3 2\pi}\right)(4\pi\varrho\gamma_0 mc^2)^{1/2}$$
$$\cdot(s+\eta)^{1/2}\sum_{i=1}^{N_e}\cos\Psi_i(t)dt. \tag{28}$$

Integrating over the length of the amplifier and utilizing the definition of η in (25) we obtain

$$\int_0^{\eta_f}\frac{d\eta}{(s+\eta)^{1/2}}=K\int_0^{N\lambda_m/c}\frac{(-1)}{N_e}\sum_{i=1}^{N_e}$$
$$\cdot\cos\Psi_i(t)\frac{dt}{N\lambda_m/c}. \tag{29}$$

Where η_f is the fractional energy conversion that has been attained at the output end of the amplifier, $N\lambda_m/c$ is the time required for the electrons to traverse the amplifier assuming $\beta_z\approx 1$, and

$$K\equiv\frac{e^2B_m\lambda_m^2NQ^{1/2}}{\pi^{1/2}(\gamma_0 mc^2)^{3/2}}. \tag{30}$$

The evolution of the phase angle Ψ_i is a complicated function of time which we are able to determine by calculating electron trajectories in a computer simulation. To obtain an upper limit for the fractional energy conversion η we assume that the electrons are perfectly bunched to provide maximum energy transfer to the electromagnetic field throughout the amplifier, so that $\cos\Psi_i$ always has the value -1. The integral on the right-hand side in (29) therefore has the value of unity. Performing the remaining integration in (29) we obtain

$$\frac{\eta_{\max}}{s}=\frac{K}{\sqrt{s}}+\frac{K^2}{4s}, \tag{31}$$

where $\eta_{\max}$ is the upper limit on fractional energy extraction. Equation (31) is a simple expression with only two variables, η/s and $K/\sqrt{s}$, which provides an upper limit for the performance of all constant λ_m, constant B_m amplifiers free electron laser. From conservation of energy it can be shown that $\eta/s=\Delta I/I_0=(I_f-I_0)/I_0$, where $I_0=E_r^2(0)c/4\pi$ is the input laser intensity and I_f is the output intensity.

3. Computer Simulations

A computer code has been written incorporating the basic equations of Sect. 1 which simulates the passage of an electron beam through an FEL amplifier. Using the computer code it is possible to calculate the value of the fractional energy conversion η for any given set of initial conditions. A segment of the electron beam one radiation wavelength long is followed through the amplifier. The beam is represented by an array of discrete charges initially positioned at equal intervals within a laser wavelength. At each time step the change in the electron energy, velocity, and position are calculated and the amplitude of the laser field is updated. Periodic boundary conditions are used. The electrons are assumed to be initially monoenergetic

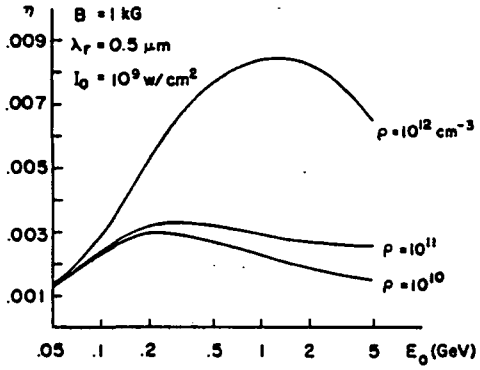

Fig. 3. Maximum single-pass fractional energy conversion, η, as a function of initial electron energy E_0 for a helical magnetic amplifier. Curves are shown for three values of the electron density ϱ

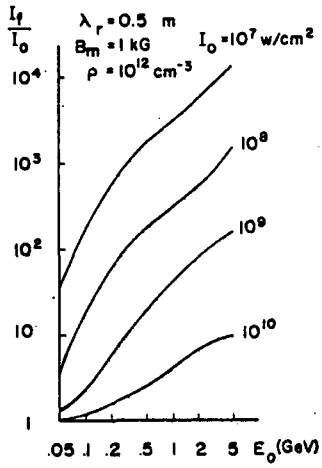

Fig. 4. Ratio of output laser intensity I_f to input intensity I_0 as a function of initial electron energy E_0 for several values of the input intensity and an electron density of $10^{12}\,\mathrm{cm}^{-3}$

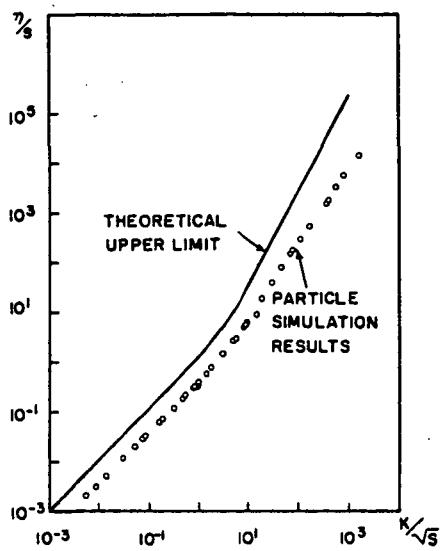

Fig. 5. Maximum single-pass fractional energy conversion for constant period helical amplifier. Data points are computer simulation results, and the solid line is the analytically derived upper limit given by (31)

and the laser beam traveling with the electrons is assumed to be monochromatic with frequency ω_r.

To find the conditions under which the greatest fractional energy conversion can be obtained for a given magnet period λ_m, magnet field strength B_m, initial electron energy E_0, and input laser intensity I_0, a laser frequency is chosen that differs from the resonance frequency ω_R by an amount $\Delta\omega$. For this frequency, $\omega_r = \omega_R - \Delta\omega$, electrons were permitted to progress down the amplifier until net transfer of energy to the laser field decreased to zero. This was done for a range of values of $\Delta\omega$. The laser frequency ω_r for which laser gain was a maximum was then assumed to be the frequency of the light propagating in the amplifier and the maximum fractional energy conversion was taken to be the maximum value for this frequency. The length of the amplifier was taken to be the length for which greatest fractional energy conversion was obtained and, therefore, varied as a function of initial electron energy E_0 and input intensity I_0. The computer simulation was used to find peak single-pass fractional energy conversion values for a range of values of initial electron energy, input laser intensity, and electron density. Calculations were made for a range of values of the laser frequency and magnetic field strength.

Figure 3 shows peak fractional energy conversion as a function of electron energy for three values of the electron density for an input laser intensity of $10^9\,\mathrm{W/cm}^2$, laser wavelength of 0.5 μm, and magnetic field of 1 kG. Fractional energy conversion is significantly higher at $\varrho = 10^{12}\,\mathrm{cm}^{-3}$ than at the lower densities. At this density small changes in electron energy produce large changes in laser intensity along the amplifier. As the laser intensity increases the magnitude of the forces that accelerate or decelerate the electrons increases resulting in greater fractional energy conversion. At lower densities the change in laser intensity as a result of energy transfer is lower, and a smaller fraction of the electron energy is converted to photon energy. For sufficiently low densities, fractional energy conversion will be essentially independent of electron density.

The ratio of output intensity I_f to input intensity I_0 for a range of input intensities at an electron density of $10^{12}\,\mathrm{cm}^{-3}$ is shown in Fig. 4. It can be seen from Fig. 4 that over a large range of electron energies the ratio of optimized output intensity to input intensity varies approximately inversely with input intensity, so that fractional energy conversion varies little with input intensity. However, the amplifier length required to

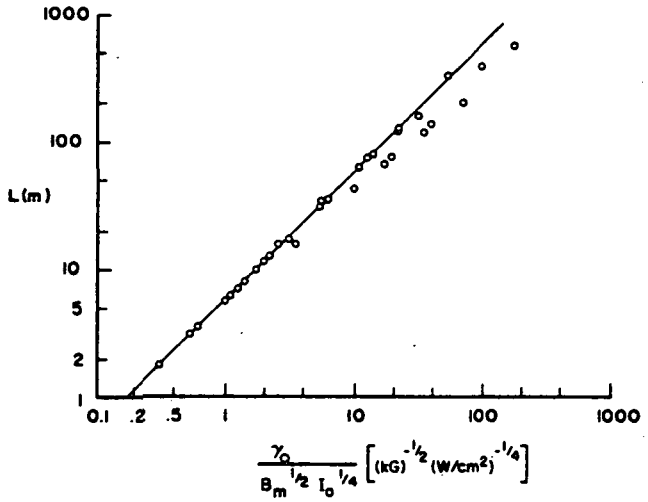

Fig. 6. Amplifier length at maximum gain as a function of the scaling parameter $\gamma_0/B_m^{1/2}I_0^{1/4}$

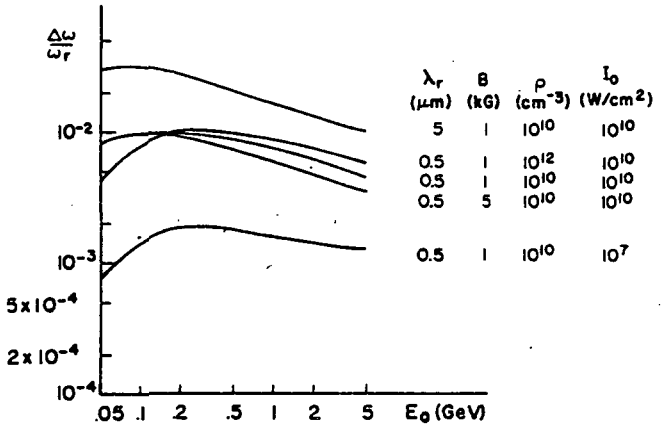

Fig. 7. Relative frequency difference at maximum gain as a function of initial electron energy for selected values of laser wavelength, amplifier magnetic field, electron density and initial laser intensity

obtain a given fractional energy conversion increases with decreasing input intensity.

In Fig. 5 data from the computer simulation are compared with the upper limit for η/s given by (31). The computed values are, as expected, always lower than the limiting value of the function η_{max}/s. All of the computed values for peak fractional energy conversion lie along a single curve in the $(\eta/s, K/\sqrt{s})$ parameter space. The data which are plotted cover a range of two orders of magnitude in electron energy (50 MeV to 5 GeV), three orders of magnitude in input laser power (10^7 to 10^{10} W/cm^2), and two orders of magnitude in electron density (10^{10} to 10^{12} cm^{-3}). They also cover a range of laser wavelengths from 0.5 to 15 μm and variations in magnetic field from 1 to 5 kG. We can fit an empirical curve to the simulation results. A function which fits this data is

$$\eta/s = 0.32\frac{K}{\sqrt{s}}\left[1+\frac{1}{4}\left(\frac{K}{\sqrt{s}}\right)^{2/3}\right]. \tag{32}$$

Equation (32) by itself is insufficient for determining peak fractional energy conversion η given a set of values γ_0, I_0, ϱ, B_m, and λ_m, since the number of periods in the magnet must be determined from the computer simulation for any particular set of conditions. An expression can be derived, however, which provides an upper limit for the length of the amplifier. This limit will be very close to the computed amplifier length when the laser gain is low. To obtain this upper limit we make the assumption that when the laser intensity is approximately constant in the amplifier (low gain), the evolution of the electron beam will be similar in all cases. Only the rate at which the distribution function evolves will be affected by the input parameters. The rate of evolution is determined by the magnitude of the axial acceleration. When the amplifier length has been optimized for maximum gain, electrons in the beam will move relative to each other a distance on the order of one wavelength of light. Let us assume that on the average the motion of the bunched electrons can be approximated by the formula

$$\lambda_r \approx 1/2 a_z t^2, \tag{33}$$

where a_z is the magnitude of the axial acceleration at the input end of the amplifier. From (15) we have

$$a_z = \left(\frac{4\pi}{c}\right)^{1/2}\frac{e}{m}\frac{(1+\alpha^2)\alpha}{\gamma^4}I_0^{1/2}. \tag{34}$$

The transit time across the amplifier is $t = L/c$. Using this and substituting (34) into (33) we obtain the scaling for L in terms of system parameters

$$L \propto \frac{(\lambda_r)^{1/2}}{a_z} \propto \frac{\gamma_0^2 \lambda_r^{1/2}}{[\alpha(1+\alpha^2)]^{1/2} I_0^{1/4}}. \tag{35}$$

Since $\lambda_r \approx \lambda_R$ we can use (17) in (35) to obtain

$$L \propto \frac{\gamma_0}{B_m^{1/2} I_0^{1/4}}. \tag{36}$$

In Fig. 6 the amplifier length, as determined from the computer simulation, is plotted as a function of $\gamma_0/(B_m^{1/2}I_0^{1/4})$. The straight line is a best fit to the low gain data. Because amplifier length is only weakly dependent on laser intensity calculated amplifier lengths were within 5% of the value given by the straight line for increases in laser intensity of up to a factor of 50. The data points which deviate from the straight line fit are high gain cases with I_f several hundred to over 10^4 times I_0. For these cases I_0 was not a good approximation to the average laser intensity in the amplifier.

The equation of the straight line in Fig. 6 is given by

$$L = 5.9\gamma_0 / B_m^{1/2} I_0^{1/4} \tag{37}$$

for B_m in kG and I_0 in W/cm^2. Equations (32) and (37) give the scaling for optimized constant period helical amplifiers in the low gain regime, and provide an upper limit for amplifier length and fractional energy conversion when laser gain is high.

The value of $\Delta\omega$ that is needed to maximize laser gain varies as a function of electron energy and density, laser intensity, laser frequency, and magnetic field. Typically values lie in the range between 10^{-3} and a few times 10^{-2} of the resonance frequency. Examples of the variation of $\Delta\omega/\omega$ as a function of energy for different values of electron density, magnetic field, and laser wavelength are shown in Fig. 7.

All of the computer simulations described above have been carried out for an initially monoenergetic electron beam. In practice the electron beam will always have some spread in energy which will tend to reduce laser gain. To prevent serious degradation of laser performance the initial energy spread should be less than the difference between the mean electron energy and the resonance energy. It can be shown by differentiating (17) that

$$(\omega_R - \omega_r)/\omega_r \approx 2(E_0 - E_R)/E_R\,, \tag{38}$$

where E_R is the resonant electron energy at the laser frequency. From the data of Fig. 7, we see that for an amplifier with a constant period helical magnetic field this energy spread is of the order of a few tenths of a percent of the resonance energy.

In conclusion, a simple model has been developed to predict the optimum performance of constant period free electron laser amplifiers with transverse helical magnetic fields. The model identifies the primary effects that can produce net laser gain in the single-particle regime, provides the scaling of fractional energy conversion with the various system parameters, and defines limits on the gain that can be obtained from constant period amplifiers.

Acknowledgements. The authors wish to acknowledge the computer programming assistance of Ralph Cover, Gary Catella, Larry Siebert, and H. Rodney Hiddleston. This work was supported by the U.S. Department of Energy under contract ED-78-C-08-1598.

References

1. S.B.Segall: KMSF Report No. KMSF-U698 (T) (February 1978)
2. S.B.Segall: KMSF Report No. KMSF-U892 (April 1979)
3. N.C.Christofilos, R.E.Hester, W.A.S.Lamp, D.D.Reagun, W.A.Sherwood, R.E.Wright: Rev. Sci. Instrum. **35**, 886 (1964)
4. J.R.Rees: IEEE Trans. Nucl. Sci. NS-**24**, 1836 (1977)
   G.A.Voss: IEEE Trans. Nucl. Sci. NS-**24**, 1842 (1977)
5. J.M.J.Madey: J. Appl. Phys. **42**, 1906 (1971)
6. L.R.Elias, W.M.Fairbank, J.M.J.Madey, H.A.Schwettman, T.I.Smith: Phys. Rev. Lett. **36**, 717 (1976)
7. D.A.G.Deacon, L.R.Elias, J.M.J.Madey, G.J.Ramian, H.A.Schwettman, T.I.Smith: Phys. Rev. Lett. **38**, 892 (1977)
8. W.B.Colson: In *Physics of Quantum Electronics*, Vol. 5, ed. by S.F.Jacobs, M.Sargent, and M.O.Scully (Addison Wesley, Reading, MA 1978)
9. F.A.Hopf, P.Meystre, M.O.Scully: Opt. Commun. **18**, 413 (1976)
10. F.A.Hopf, P.Meystre, M.O.Scully, W.H.Louisell: Phys. Rev. Lett. **37**, 1342 (1976)
11. H.A.Abawi, F.A.Hopf, P.Meystre: Phys. Rev. A**16**, 666 (1977)
12. N.M.Kroll, W.A.McMullin: Phys. Rev. A**17**, 300 (1978)
13. P.Sprangle, R.A.Smith, V.L.Granatstein: NRL Memorandum Report 3888 (1978)
14. J.D.Jackson: *Classical Electrodynamics* (Wiley, New York 1976)
15. L.R.Elias, J.M.Madey: Rev. Sci. Instrum. **50**, 1335 (1979)

THE NONLINEAR WAVE EQUATION FOR FREE ELECTRON LASERS DRIVEN BY SINGLE-PARTICLE CURRENTS ☆

W.B. COLSON [1]
Institute of Theoretical Physics, Department of Physics, Stanford University, Stanford, CA 94305, USA

and

S.K. RIDE
Johnson Space Center, Houston, TX 77058, USA

Received 7 August 1979
Revised manuscript received 14 November 1979

We develop a self-consistent, nonlinear description of the free electron laser using single-particle dynamics and Maxwell's wave equation. Microscopic electron bunching drives the amplitude and phase of the optical wave.

In a free electron laser [1], ultra-relativistic electrons travel through a static, periodic magnetic field, and oscillate to amplify coherent optical radiation ‡1. The electron trajectories are determined by both the helical magnet and the slowly evolving optical wave; the electron current drives Maxwell's equations, and in turn governs the evolution of the optical wave. We handle this nonlinear process by self-consistently coupling Maxwell's equations to the single-particle Lorentz force equations.

The single-particle formulation [4] provides a clear, intuitive description of the free electron laser, that accurately reproduces and extends the results obtained using more complex analyses (coupled Maxwell–Boltzmann equations [5], computer simulations [6], plasma dispersion relations [7], and quantum electrodynamics [8]). In previous applications of the single-particle approach, energy conservation was invoked to relate the decreased electron beam energy to the amplified intensity of the optical wave. We go a step further, and employ the single-particle dynamics to determine the transverse current in Maxwell's equations. Coupling to Maxwell's equations enables us to describe the evolution of both the amplitude and phase of the optical wave; employing the single-particle dynamics enables us to obtain a self-consistent analytic solution.

1. Optical wave evolution. Maxwell's equations govern the evolution of a light wave in the presence of an electron current. The resulting wave equation is

$$(\nabla^2 - c^{-2}\partial^2/\partial t^2)A(x, t) = -(4\pi/c)\,J_\perp(x, t)\,, \qquad (1)$$

where A is the radiation vector potential, c is the speed of light, and $J_\perp$ is the transverse current density (cgs units). The electron trajectories will be determined self-consistently in the next section.

When the laser is "turned on", the optical wave grows from spontaneous emission to a large amplitude wave with a well-defined phase. After the coherent wave is established, its amplitude and phase can still evolve in time. To represent the laser optical wave during these stages of evolution, we choose a waveform:

☆ The results of this paper were presented at the Free Electron Laser workshops at Stanford University (March 1979) and at Los Alamos Scientific Laboratory (April 1979).

[1] Supported by NASA Grant NSG-7490.

‡1 Stanford university experiments have demonstrated both amplification [2], and laser oscillation [3].

$$A(x, t) = [\mathcal{E}(z, t)/k_r](\sin\psi, \cos\psi, 0)\,, \qquad (2)$$

where $\mathcal{E}(z, t)$ is the wave amplitude, and $\psi = k_r z - \omega_r t + \phi(z, t)$; the wave has frequency $\omega_r = k_r c$, and phase $\phi(z; t)$, and depends only on z and t. When the amplitude and phase of this wave are held fixed, eq. (2) describes a plane wave traveling in the z-direction. We take the amplitude and phase to evolve slowly over an optical wave length ($\dot{\mathcal{E}} \ll \omega_r \mathcal{E}$, etc.); faster evolution would diminish the coherence and monochromicity. The left-hand side of eq. (1) can be rewritten by inserting eq. (2), and neglecting terms containing two derivatives. The remaining terms are "fast" rotating vectors with "slow" coefficients. In order to establish true slowly varying equations, we project the wave equation onto two unit vectors, $\hat{\boldsymbol{\varepsilon}}_1 = (\cos\psi, -\sin\psi, 0)$ and $\hat{\boldsymbol{\varepsilon}}_2 = (\sin\psi, \cos\psi, 0)$, to get

$$\begin{aligned} &\partial\mathcal{E}/\partial z + c^{-1}\partial\mathcal{E}/\partial t = -(2\pi/c) J_\perp \cdot \hat{\boldsymbol{\varepsilon}}_1\,, \\ &\mathcal{E}(\partial\phi/\partial z + c^{-1}\partial\phi/\partial t) = (2\pi/c) J_\perp \cdot \hat{\boldsymbol{\varepsilon}}_2\,. \end{aligned} \qquad (3)$$

The second-order partial differential equation (1) has now been reduced to two first-order differential equations (3), one describing the evolution of the amplitude of the wave, the other describing the evolution of its phase. When there is no source current ($J_\perp = 0$), $\mathcal{E}$ and ϕ satisfy the free-space wave equation.

The waveform (2) contains no dependence on x and y; a proper description would give it some finite transverse dimension. In order to address the essential physics of the problem, we choose to avoid this complication by describing dynamics well within the optical wave (an appropriate "filling factor" could be introduced to handle the overlap between the optical mode and the electron beam [2,3]).

2. Single-particle current. The dynamics of electrons in the combined static and radiation fields are governed by the Lorentz force equations. A helical magnetic field of the form

$$B_m = B_0(\cos k_0 z, \sin k_0 z, 0) \qquad (4)$$

produces the optical polarization in eq. (2). B_0 is the field strength, and $\lambda_0 = 2\pi/k_0$ the wavelength of the helical magnet. The radiation electric and magnetic fields are obtained from the vector potential; inserting the static and radiation fields into the fully relativistic Lorentz force equations yields the "self-consistent pendulum" equation for an electron's motion within an optical wavelength [9]:

$$\ddot{\zeta} = \frac{4e^2 B_0 \mathcal{E}(z, t) k_0 [1 - \nu(t)/k_0 L]^2}{(1 + K^2) m^2 c^2 k_r} \times \cos(\zeta + \phi(z, t))\,, \qquad (5)$$

where $\zeta(t) = (K_r + k_0) z(t) - \omega_r t$, $\nu(t) = \dot{\zeta}(t) L/c$, L is the magnet length, $K = |e| B_0 \lambda_0/2\pi mc^2$, and e (m) is the electron charge (mass). ζ and ν describe the electron's microscopic bunching on an optical scale; its evolution depends crucially on the initial conditions $\zeta_0 \equiv \zeta(0) = (k_r + k_0) z_0$ and $\nu_0 \equiv \nu(0) = [\beta_0 k_0 c - \omega_r \times (1 - \beta_0)] L/c$, where z_0 and $\beta_0 c$ are the electron's initial position and z-velocity. Since γ is large, $k_r \gg k_0$ and ζ_0 is the initial electron phase within an optical wavelength. If an electron is injected such that $\nu_0 = 0$, then exactly one wavelength of light will pass over it as it passes through one wavelength of the magnet. ν_0 therefore measures an electron's deviation from this "resonant" condition, and will be termed the resonance parameter. $\nu(t)$ is related to the evolving electron energy $\gamma(t)mc^2$ through $\gamma^2 = \frac{1}{2}(1+K^2) k_r L/(k_0 L - \nu)$. In the low gain limit, $\mathcal{E}$ and ϕ are nearly constant, and for small energy extraction, $\nu \ll k_0 L$; in this case eq. (5) becomes the pendulum equation.

The self-consistent pendulum equation (5) correctly describes electron dynamics up through saturation. When the radiation field becomes large, the electron becomes trapped in closed orbits of the pendulum phase space. In the beam frame, the bunching electrons will have moved on the order of an optical wavelength ($\Delta\zeta \approx 1$); at this point gain stops, and the laser saturates.

For relativistic electrons, the transverse radiation force is very small so the electron's transverse velocity (and therefore the transverse current) is determined almost entirely by the static magnetic field. Solving for the velocity in the field (4) alone, and projecting the single-particle current onto our two unit vectors $\hat{\boldsymbol{\varepsilon}}_1$ and $\hat{\boldsymbol{\varepsilon}}_2$:

$$\begin{aligned} J_{\perp i} \cdot \hat{\boldsymbol{\varepsilon}}_1 &= \frac{e^2 B_0 \lambda_0}{2\pi\gamma mc} \cos(\zeta + \phi)\delta^{(3)}(\boldsymbol{x} - \boldsymbol{r}_i(t))\,, \\ J_{\perp i} \cdot \hat{\boldsymbol{\varepsilon}}_2 &= \frac{e^2 B_0 \lambda_0}{2\pi\gamma mc} \sin(\zeta + \phi)\delta^{(3)}(\boldsymbol{x} - \boldsymbol{r}_i(t))\,, \end{aligned} \qquad (6)$$

where $\boldsymbol{r}_i(t)$ denotes the location of the ith particle at time t. Note that the sinusoidal factors depend on the

"Page missing from available version"

pg 381

H. Al-Abawi, F.A. Hopf and P. Meystre, Phys. Rev. A16 (1977) 666;
P. Sprangle, C.-M. Tang, W.M. Manheimer and R.A. Smith, Naval Research Lab Memorandum Report 4033 and 4034.
[6] T. Kwan, J.M. Dawson and T. Lin, Phys. Fluids 20 (1977) 581.
[7] N.M. Kroll and W.A. McMullin, Phys. Rev. 17A (1978) 300.
[8] W.B. Colson, Phys. Lett. 59A (1976) 187; Free electron laser theory, Ph.D. Thesis, Stanford Univ. (1977).
[9] W.B. Colson, Phys. Lett. 64A (1977) 190; Physics of quantum electronics, Vol. 5 eds. S. Jacobs, M. Sargent and M. Scully (Addison-Wesley, 1978) Ch. 4.
[10] W.B. Colson and S.K. Ride, Physics of quantum electronics, Vol. 7, eds. S. Jacobs, H. Pilloff, M. Sargent, M. Scully and R. Spitzer (Addison-Wesley, 1980).
[11] W.B. Colson, W.H. Louisell, J.F. Lam and C.D. Cantrell, Tenth IQEC (Atlanta, 1978);
R. Peccei and W. Colson, to be published.
[12] J.M.J. Madey, private communication; Final Technical Report to ERDA: Contracts EY 76-S-03-0326 PA 48 and PA 49 (1977).
[13] H. Haken, Synergetics (Springer, 1977);
V. DeGiogio and M.O. Scully, Phys. Rev. 2A (1979) 1170.

THE NONLINEAR WAVE EQUATION FOR FREE ELECTRON LASERS DRIVEN BY SINGLE-PARTICLE CURRENTS ☆

W.B. COLSON [1]
Institute of Theoretical Physics, Department of Physics, Stanford University, Stanford, CA 94305, USA

and

S.K. RIDE
Johnson Space Center, Houston, TX 77058, USA

Received 7 August 1979
Revised manuscript received 14 November 1979

We develop a self-consistent, nonlinear description of the free electron laser using single-particle dynamics and Maxwell's wave equation. Microscopic electron bunching drives the amplitude and phase of the optical wave.

In a free electron laser [1], ultra-relativistic electrons travel through a static, periodic magnetic field, and oscillate to amplify coherent optical radiation ‡1. The electron trajectories are determined by both the helical magnet and the slowly evolving optical wave; the electron current drives Maxwell's equations, and in turn governs the evolution of the optical wave. We handle this nonlinear process by self-consistently coupling Maxwell's equations to the single-particle Lorentz force equations.

The single-particle formulation [4] provides a clear, intuitive description of the free electron laser, that accurately reproduces and extends the results obtained using more complex analyses (coupled Maxwell–Boltzmann equations [5], computer simulations [6], plasma dispersion relations [7], and quantum electrodynamics [8]). In previous applications of the single-particle approach, energy conservation was invoked to relate the decreased electron beam energy to the amplified intensity of the optical wave. We go a step further, and employ the single-particle dynamics to determine the transverse current in Maxwell's equations. Coupling to Maxwell's equations enables us to describe the evolution of both the amplitude and phase of the optical wave; employing the single-particle dynamics enables us to obtain a self-consistent analytic solution.

1. Optical wave evolution. Maxwell's equations govern the evolution of a light wave in the presence of an electron current. The resulting wave equation is

$$(\nabla^2 - c^{-2}\partial^2/\partial t^2)A(x, t) = -(4\pi/c)\, J_\perp(x, t)\,, \qquad (1)$$

where A is the radiation vector potential, c is the speed of light, and $J_\perp$ is the transverse current density (cgs units). The electron trajectories will be determined self-consistently in the next section.

When the laser is "turned on", the optical wave grows from spontaneous emission to a large amplitude wave with a well-defined phase. After the coherent wave is established, its amplitude and phase can still evolve in time. To represent the laser optical wave during these stages of evolution, we choose a waveform:

☆ The results of this paper were presented at the Free Electron Laser workshops at Stanford University (March 1979) and at Los Alamos Scientific Laboratory (April 1979).

[1] Supported by NASA Grant NSG-7490.

‡1 Stanford university experiments have demonstrated both amplification [2], and laser oscillation [3].

Physics of Quantum Electronics, Vol. 7, p. 377
(Addison-Wesley Publishing Co., 1980), S. Jacobs, H. Pilloff,
M. Sargent, M. Scully, and R. Spitzer, eds.

The Free Electron Laser: Maxwell's Equations Driven by Single-Particle Currents

W. B. Colson and S. K. Ride

1. INTRODUCTION

In a free electron laser [1], ultra-relativistic electrons travel through a static, periodic magnetic field, and oscillate to amplify coherent optical radiation. The electron trajectories are determined by both the helical magnet and the slowly evolving optical wave; the electron current, the source term in Maxwell's equations, in turn governs the evolution of the optical wave. This non-linear process can be explored by self-consistently coupling Maxwell's equations to the single-particle Lorentz force equations.

The single-particle formulation [2] provides a clear, intuitive description of the free electron laser, and accurately reproduces results obtained using considerably more complex analyses (coupled Maxwell-Boltzmann equations [3], computer simulations [4], plasma dispersion relations [5], and quantum electrodynamics [6]). In previous applications of the single-particle approach, energy conservation was invoked to relate the decreased electron beam energy to the amplified

intensity of the optical wave. In this chapter, the formulation is taken a step further; the single-particle dynamics are used to determine the transverse current in Maxwell's equations [7]. This procedure produces immediate analytical benefits: Maxwell's equations describe the evolution of both the amplitude and phase of the optical wave; the single-particle dynamics describe the self-consistent electron evolution in phase space.

A free electron laser can operate as an amplifer [8], or as an oscillator [9]. In the first case, the electron beam amplifies an existing wave during a single pass through the interaction region. In the second case, a resonator is formed by placing mirrors at either end of the interaction region (see Figure 1); the radiation stored in the cavity bounces between the mirrors, and fresh electrons are either supplied continuously, or injected to overlap the rebounding optical pulse. The laser field grows on each pass, and becomes large. The equations developed in the next section will be used to describe laser evolution over a single pass (this is the timescale relevant to the electron beam evolution), but will also be used to describe the laser oscillator, following the evolution of the optical pulse (toward a steady state) over many passes.

In the later sections of this chapter, the coupled equations, and the phase space diagrams they generate, are applied to several aspects of free electron laser operation. How is laser gain affected if the electron beam has some angular divergence or energy spread? What are the qualitative and quantitative effects of ultra-short pulses? And, in particular, do experimental results show evidence of these effects?

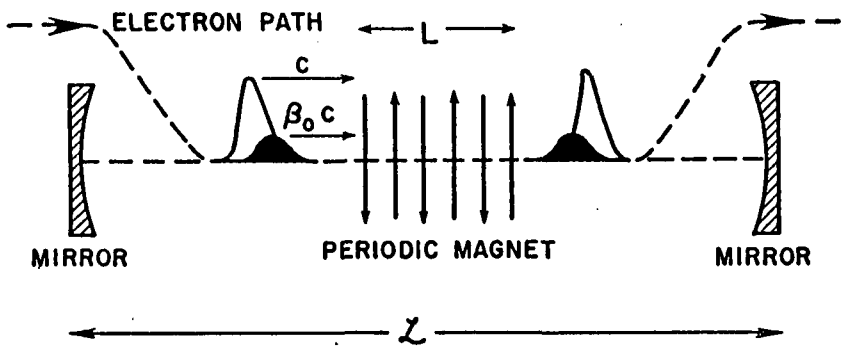

OPTICAL RESONATOR

Figure 1. The electron pulse is injected into the resonator with velocity $\beta_0 c$, and travels through the periodic magnetic field with the optical pulse. The electron pulse is removed after a single pass, the enhanced optical pulse is stored in the cavity. The parameters of the Stanford free electron laser are summarized in the table.

B_0 = 2.4 kgauss

λ_0 = 3.2 cm

N = 160

L = 5.2 m

λ_r = 3.4 microns

mode area = 0.096 cm^2

$\mathcal{L}$ = 12 m

power loss per pass = 3.5%

γ = 84.524

peak current = 0.66 amps

electron pulse length = 0.13 cm

beam cross section = 0.0079 cm^2

The results dealing with initial pulse shapes and "imperfect" initial conditions must be obtained numerically. It is possible, however, to make significant progress analytically, and attain results valid in the strong-field regime. The single-pass result can be incorporated in the laser rate equations to describe the operation of an laser oscillator analytically throughout its evolution to saturation.

2. MAXWELL'S EQUATIONS

Maxwell's equations govern the evolution of a light wave in the presence of an electron current. The resulting wave equation is

$$\left(\vec{\nabla}^2 - \frac{1}{c^2}\frac{\partial^2}{\partial t^2}\right)\vec{A}(\vec{x},t) = -\frac{4\pi}{c}\,\vec{J}_\perp(\vec{x},t) \qquad (1)$$

where $\vec{A}$ is the radiation vector potential, c is the speed of light, and $\vec{J}_\perp$ is the transverse current density (cgs units). When the laser is "turned on", the optical wave grows from spontaneous emission to a large amplitude wave with a well-defined phase. After the coherent wave is established, its amplitude and phase can still evolve in time. The following waveform was chosen to represent the laser optical wave during these stages of evolution:

$$\vec{A}(\vec{x},t) = \frac{\mathcal{E}(z,t)}{k_r}\left(\sin\psi, \cos\psi, 0\right) \qquad (2)$$

where $\mathcal{E}(z,t)$ is the wave amplitude, and $\psi = k_r z - \omega_r t + \phi(z,t)$; the wave has frequency $\omega_r = k_r c$, and phase $\phi(z,t)$, and depends only on z and t. When the amplitude and phase of this wave are held fixed, (2) describes a plane wave traveling in the z-direction.

The amplitude and phase of the wave evolve slowly over an optical wavelength ($\dot{\mathcal{E}} \ll \omega_r \mathcal{E}$, etc,); a faster evolution would diminish the coherence and monochromicity of the radiation. The left-hand side of (1) can therefore be rewritten by inserting (2), and neglecting terms containing two derivatives. The remaining terms are "fast rotating

vectors with "slow" coefficients. Equations which are truly slowly-varying can be constructed by projecting the wave equation onto two unit vectors, $\hat{\epsilon}_1 = (\cos\psi, -\sin\psi, 0)$ and $\hat{\epsilon}_2 = (\sin\psi, \cos\psi, 0)$, to get

$$\left(\frac{\partial \mathcal{E}}{\partial z} + \frac{1}{c}\frac{\partial \mathcal{E}}{\partial t}\right) = -\frac{2\pi}{c}\,\vec{J}_\perp \cdot \hat{\epsilon}_1$$
$$\mathcal{E}\left(\frac{\partial \phi}{\partial z} + \frac{1}{c}\frac{\partial \phi}{\partial t}\right) = \frac{2\pi}{c}\,\vec{J}_\perp \cdot \hat{\epsilon}_2 \quad . \qquad (3)$$

The second-order partial differential equation (1) has now been reduced to two first-order differential equations (3); one describing the evolution of the amplitude of the wave, the other describing the evolution of its phase. When there is no source current ($\vec{J}_\perp = 0$), $\mathcal{E}$ and ϕ satisfy the free-space wave equation.

The waveform (2) contains no dependence on x and y; a proper description would give it some finite transverse dimension. In order to address the essential physics of the problem, we choose to avoid this complication by describing dynamics well within the optical wave (an appropriate "filling factor" is included in the definition of the electron density to handle the overlap between the optical mode and the electron beam [1]).

The dynamics of electrons in the combined static and radiation fields are governed by the Lorentz force equations. A helical magnetic field of the form

$$\vec{B}_m = B_0\left(\cos k_0 z, \sin k_0 z, 0\right) \qquad (4)$$

produces the optical polarization in (2). B_o is the field strength, $\lambda_o = 2\pi/k_o$ the wavelength, and $L = N\lambda_o$ the length of the helical magnet. The radiation electric and magnetic fields are obtained from the vector potential; inserting the static and radiation fields into the fully relativistic Lorentz force equations yields the "pendulum" equation for an electron's motion within an optical wavelength [10]:

$$\ddot{\zeta} = \left(\frac{2e^2 B_o \mathcal{E}(z,t)}{\gamma^2 m^2 c^2}\right) \cos\left(\zeta + \phi(z,t)\right) \qquad (5)$$

where $\zeta(t) = \mu ct/L + \zeta_o + k_p \Delta z(t)$, $\zeta_o = k_p z_o$ is the initial electron phase within optical wavelength, $z(t) = z_o + \beta_o ct + \Delta z(t)$ is its position along magnet axis, $\beta_o c$ is its initial velocity along the z-axis. If the electron is injected with a velocity $\beta_o c$ such that $\mu = (L/c)[\beta_o k_o c - \omega_p(1-\beta_o)] = 0$, exactly one wavelength of light will pass over the electron as it passes through one wavelength of the periodic magnet. μ, determined by the initial conditions, therefore measures an electron's deviation from this "resonant" condition, and will be termed the resonance parameter. Equation (5) is the self-consistent, non-linear equation for a electron's microscopic position; $\nu(t) = \dot{\zeta}(t)L/c$ is the electron's microscopic velocity. "Perfect injection" into helical orbits has been assumed. As the electron energy changes, $\Delta z(t)$ describes bunching on the optical scale. If the electrons are relativistic, as they are in a free electron laser, $k_p >> k_o$. The electron energy, $\gamma(t)mc$, can be updated to evolve with ν, but in most cases this leads

to minor corrections (in the Stanford laser, an electron's energy changes by less than ~0.1% on a single pass).

The pendulum equation correctly describes the electron dynamics through laser saturation. When the radiation field becomes large, an electron becomes "trapped" in the closed orbit region of the pendulum phase space. In the beam frame, the bunching electrons will have moved on the order of an optical wavelength ($k_p \Delta z \sim 1$); at this point gain stops, and the laser saturates.

For relativistic electrons, the transverse radiation force is very small, so the electron's transverse velocity (and therefore the transverse current) is determined almost entirely by the static magnetic field. Solving for the electron velocity in the field (4) alone, and projecting the single-particle current onto the two unit vectors $\hat{\epsilon}_1$ and $\hat{\epsilon}_2$:

$$\vec{J}_{\perp i} \cdot \hat{\epsilon}_1 = \frac{e^2 B_o \lambda_o}{2\pi\gamma mc} \cos(\zeta + \phi)\, \delta^{(3)}(\vec{x} - \vec{r}_i(t))$$
$$\vec{J}_{\perp i} \cdot \hat{\epsilon}_2 = \frac{e^2 B_o \lambda_o}{2\pi\gamma mc} \sin(\zeta + \phi)\, \delta^{(3)}(\vec{x} - \vec{r}_i(t)) \qquad (6)$$

where $\vec{r}_i(t)$ denotes the location of the ith particle at time t. Note that the sinusoidal factors depend on the longitudinal position of the electrons through ζ, the solution to the pendulum equation.

The total beam current is the sum of all single-particle currents. The electrons can be labelled by their initial positions and velocities (or, equivalently, resonance parameters); this definition is unique, and rigorously defines the electron beam current (Jean's theorem). In

experimental situations, the electron pulse is large compared to an optical wavelength, so on a microscopic scale the electrons are initially spread uniformly over each wavelength of light. Although bunching occurs within an optical wavelength, it does not affect the average density in any macroscopic section of the beam. Similarly, although the energy spread of the injected electron beam would generally not be large enough to result in distortion of the pulse as it travels down the magnet, it may be large enough to result in a significant spread in resonance parameters. Neither the bunching mechanism nor an initial velocity spread alter the macroscopic electron pulse shape, and it travels undistorted through the interaction region. Microscopically, however, an electron's resonance parameter μ and initial position witin a wavelength of light ζ_0 (i.e., its initial coordinates in the pendulum phase space) are crucial in determining the result of its interaction with the wave. The beam current density in a volume dV (which is large compared to an optical wavelength, but small compared to the pulse length) is found by averaging over μ and ζ_0, then weighting this result by the macroscopic particle density $\rho(z)$ within that volume element. Combining (5) and (6), and indicating the appropriate microscopic averages by $\langle\rangle_\mu$ and $\langle\rangle_{\zeta_0}$ the coupled Maxwell and Lorentz force equations become:

$$\left(\frac{\partial \mathcal{E}}{\partial z} + \frac{1}{c}\frac{\partial \mathcal{E}}{\partial t}\right) = -\frac{e^2 B_0 \lambda_0}{\gamma m c^2}\rho(z-\beta_0 ct)\langle\langle \cos(\zeta+\phi)\rangle_{\zeta_0}\rangle_\mu$$

$$\mathcal{E}\left(\frac{\partial \phi}{\partial z} + \frac{1}{c}\frac{\partial \phi}{\partial t}\right) = \frac{e^2 B_0 \lambda_0}{\gamma m c^2}\rho(z-\beta_0 ct)\langle\langle \sin(\zeta+\phi)\rangle_{\zeta_0}\rangle_\mu \qquad (7)$$

where $\rho(z-\beta_0 ct)$ is the density of the travelling electron pulse at position z.

In their general form, the non-linear equations (5) and (7) are valid for low-gain and high-gain systems, in weak or strong optical fields, and describe the evolution of an arbitrary electron pulse, and the amplitude and phase (and therefore structure and spectrum) of the optical pulse. The remainder of this chapter is dedicated to exploring the content of these equations, both numerically and analytically.

3. ELECTRON PHASE SPACE EVOLUTION

The physics contained in equations (5) and (7) can be understood by appealing to the electron phase space diagrams. Consider the microscopic current within a small volume of the beam. If the coefficient $\Omega L/c = (2B_0\epsilon)^{1/2} eL/\gamma mc^2$ in (5) were truly constant, the electron phase space would be exactly that of a single pendulum, as shown in Figure 2.

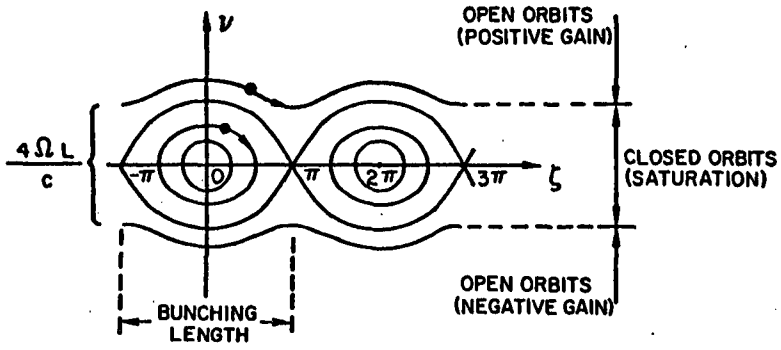

Figure 2. The pendulum phase space ($\zeta(t)$, $\nu(t)$) is periodic in the optical wavelength which defines the bunching length. Electrons evolve along their paths in either the open or closed orbit regions. The optical field strength ϵ determines the height of the closed orbit region $4\Omega L/c$.

Two sample electrons are included in the figure; each electron's initial conditions determine the evolution of its "velocity" $\nu(t) = \dot{\zeta}(t)L/c$ and "position" $\zeta(t)$, and therefore constrain it to follow a particular path in phase space. The height of the "closed-orbit region", $4\Omega L/c$, is determined by the optical field strength, and is important in determining the character of electron evolution and hence the laser gain process.

Equations (5) and (7) indicate that an electron's evolution is not governed by the exact pendulum equation, but by a "self-consistent" pendulum equation; at any instant in time, however, an electron's motion can be determined from the pendulum phase space defined by the value of $4\Omega L/c$ and ϕ at that instant. The phase space picture therefore remains a valuable tool in understanding beam evolution. Figures 3-6 show the evolution of a monoenergetic beam with the parameters of Stanford's laser (Figure 1) in terms of the phase space of an "evolving pendulum". Since the electrons in a pulse are spread uniformly over an optical wavelength, and the pendulum phase space is periodic in the optical wavelength; it is only necessary, then, to consider a sample of electrons distributed uniformly over one optical wavelength.

In low gain, weak-field lasers, electron evolution can be described quite accurately by the exact pendulum phase space; this is evident in Figure 3. All electrons are injected with $\mu = 2.6$, the maximum gain point in weak fields. With the optical power only 5×10^3 W/cm^2, all electrons fall in the open orbit region. The beam acquires an energy spread, and some bunching can be detected. The gain equation and electron distributions have previously been derived in this regime by expanding the pendulum equation in the field strength [10]; in section 6,

we solve Maxwell's equations analytically in this same regime.

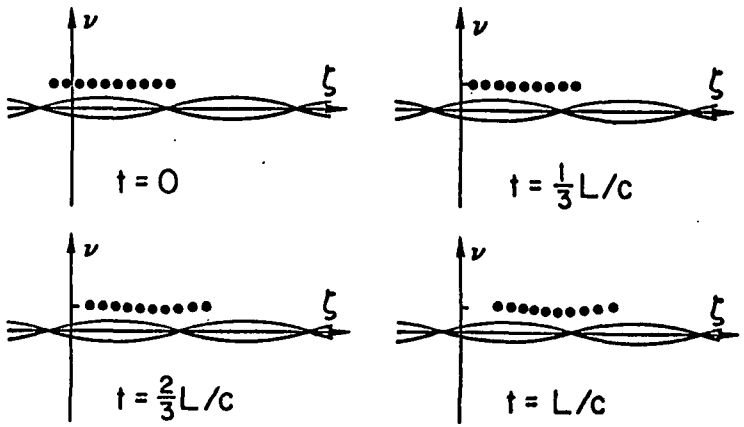

Figure 3. In weak optical fields (power = 5×10^3 W/cm^2), electrons evolve in the open-orbit region and acquire a small spread in energy.

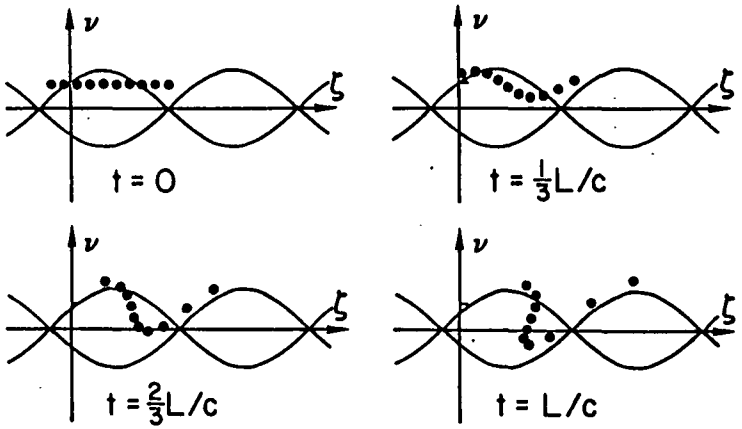

Figure 4. In stronger fields (power = 10^6 W/cm^2) Ω is larger; bunching becomes evident at the end of the laser.

In Figure 4, the optical field is stronger (10^6 W/cm^2); the closed-orbit region has expanded, and now contains some of the electrons. The energy spread is larger, and bunching is more evident.

In Figure 5, the field is larger enough (5×10^6 W/cm^2) that saturation begins to occur:

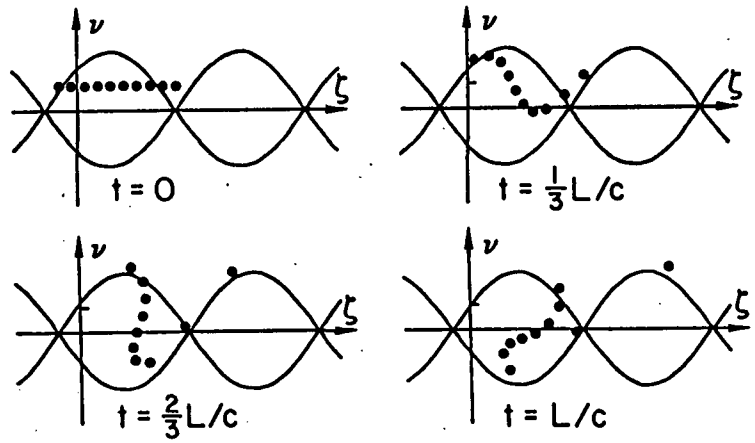

Figure 5. Saturation occurs when the fields become so strong (power = 5×10^6 W/cm^2) that nearly all electrons are "trapped" in the closed-orbit region.

electrons gain and lose energy in a nearly symmetric way, and the gain (originally ~15%) has dropped to ~5%. When the laser oscillator reaches the point that gain per pass = loss per pass, it runs in a steady state.

Each of these figures are derived from the self-consistent equations, so the phase is also allowed to evolve. As it evolves, the separatrix (the path which separates the closed and open orbit regimes) shifts. For low gain the shift is slight, and is barely perceptible in Figure 3 through 5. However, this effect is larger if taking into account the laser cavity mode. In the Stanford laser, radiation is stored in an over-moded resonant cavity, 12 m long. Although the mode geometry causes only a small change in the field's amplitude along the laser, it results in a significant change the phase of the wave. In Figure 6, the effect of the cavity is included. The separatrix clearly shifts with the phase; the qualitative behavior of the electrons remains the same, but there are slight quantitative differences.

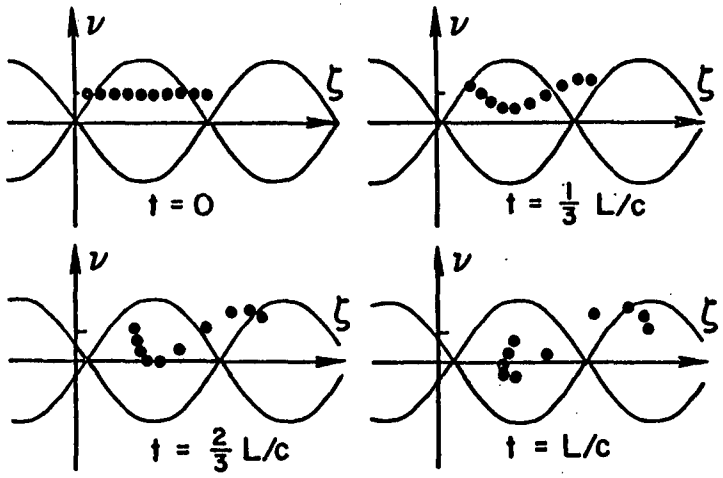

Figure 6. Now a finite length resonator ($\mathcal{L}$ = 12 meters) is included; the major effect is a shift in the phase of the optical wave along the magnet length. This is evident as a shift in the pendulum separatrix at each point in time (compare to Figure 4).

4. GAIN DEPRESSION

The phase space diagrams of the previous section show how the gain of a monoenergetic beam depends on its resonance parameter, and on the field strength. The electrons in a beam populate the horizontal ζ(position)-axis of an element of phase space uniformly, and Figures 4-6 show that the history of an individual electron depends critically on its location along that axis. This section addresses population of the vertical axis as well. A range of resonance parameters results from a range of z-velocities, μ's. A perfectly injected, monoenergetic electron beam is characterized by a single resonance parameter; any realistic beam, however, will enter the laser with a range of μ's. The electron beam powering Stanford's free electron laser is supplied by a superconducting linear accelerator with excellent beam quality; measurements indicated a fractional energy spread of only ~0.05%, and an emittance (angular divergence at a given beam diameter) of ~0.06 mm-mrad over 1 mm. This beam can be characterized by a single μ. Other electron sources, which may power future free electron lasers, are capable of supplying higher average currents, but with lower beam quality; the fractional energy-spread and the emittance may be a factor of ten to hundred higher, and in some recirculation schemes (storage rings, for example) the beam quality may deteriorate with time. It is clearly important to evaluate the effects of these factors on laser performance. The "gain depression" which occurs if the beam quality is low has been explored for weak fields [11,12], and also for high density beams (in which collective effects are important, and the single pass

gain is very large [4,5]).

The equations of section 2 allow an exploration of this phenomenon in strong, as well as weak, optical fields. Extenstion to strong-fields is important for free electron laser oscillators, which operate in this regime.

A weight function, $f(\mu)$ can be introduced to populate the velocity dimension of phase space and appropriately reflect the range of μ's. The gain which results is then an average gain $\langle g \rangle = \int_{-\infty}^{\infty} f(\mu)g(\mu)d\mu$. A wide distribution will tend to yield a small $\langle g \rangle$, depressed gain, since $g(\mu)$ is anti-symmetric. The distribution in μ (centered at μ_o) which results from an initial distribution in electron energies, is defined as $f_E(\mu, \mu_o)$; the distribution in μ (positioned at μ_o) which results from a distribution in injection angles, is defined at $f_\theta(\mu, \mu_o)$.

If the gain is low, the gain curve in weak fields is anti-symmetric, and peaks at a resonance parameter $\mu = 2.6$ (i.e., if the parameters of the system are chosen such that $\mu = 2.6$, the laser will operate at maximum gain). In weak fields, gain has been shown to be proportional to the slope of the spontaneous emission line, $\sin^2(\mu/2)/(\mu/2)^2$ [10]; if the field strengths are increased, the gain curve is altered. The effect is examined for parameters of a low gain laser similar to Stanford's: $B_o = 2\times10^3$ gauss, $\lambda_o = 5$ cm, $\gamma = 100$, $N = 200$, and $\lambda_r = 2\times10^{-4}$ cm (these parameters lead to ~10% gain). Figure 7 shows a family of gain curves, derived for this system, in increasingly strong optical fields. The peak of the gain curve decreases, and shifts to higher μ, as stronger optical fields ($B_o\ell \gtrsim 0.85(\gamma mc^2/eL)^{1/2}$) are imposed.

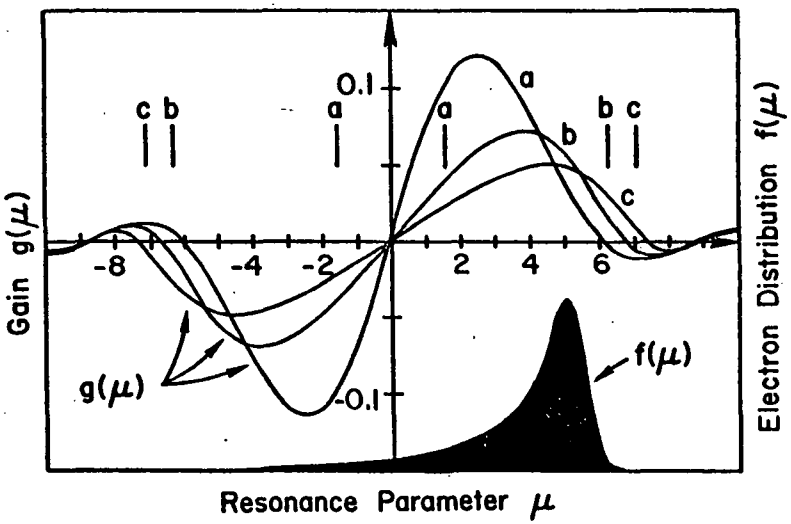

Figure 7. In weak optical fields (curve a, power = 5×10^3 W/cm^2), $g(\mu)$ is anti-symmetric and peaks at $\mu = 2.6$; the width of the closed-orbit region is shown. At stronger fields (curve b, power = 10^6 W/cm^2), the closed-orbit region is wider than the gain region. Saturation occurs when the fields are sufficiently strong (curve c, power = 2×10^6 W/cm^2) to significantly reduced gain. The maximum available gain occurs at $\mu \cong 4$ (in b) and 4.5 (in c). Inserted is an electron distribution distorted by an energy spread and imperfect injection.

In higher gain lasers (up to ~100% gain has been examined with this approach) the positive gain "bump" begins to swell, while the absorption region shrinks. An energy spread and angular spread have similar effects on the average gain; in fact, a single distribution function, which takes

into account both the angular and energy distribution, can be found from f_E and f_θ:

$$f(\mu,\mu_o) = \int_{-\infty}^{\mu_o} f_E(\mu',\mu_o)\, f_\theta(\mu,\mu')\, d\mu' \qquad (8)$$

A typical distribution, with both an energy spread and angular spread is shown in Figure 7. It is clear that the location and size of the distribution, relative to the gain curve, are crucial in determining the average gain.

Electron Energy Distribution. The strong-field results will be obtained numerically from (5) and (7). It is possible, however, to derive the weak-field average gain analytically in the low-gain limit [11,12]. Assuming the spontaneous emission line-shape to be gaussian introduces negligible error, but simplifies the analysis considerably. The gain, proportional to the slope of the line-shape, is then $g \propto \mu e^{-\mu^2/\sigma^2}$, where σ should be chosen so that the peaks of the approximate gain curve occur at the correct values of μ ($\sigma = 2.6\sqrt{2}$).

Consider a beam with a range of energies $\delta\gamma$. The range of resonance parameters is related to the fractional energy spread in a simple way, $\delta\gamma/\gamma \approx \Delta\mu/4\pi N$. Taking $f_E(\mu)$ to be a normalized gaussian centered at $\mu_o = 2.6$, with a 1/e half-width of $\Delta\mu$, the average gain is

$$\langle g\rangle_E = (8.55)\left(e^4 B_o^2 \rho\lambda_o\right)\left(\frac{N\lambda_o}{\gamma mc^2}\right)^3 \frac{\mu_o \exp\left[-\mu_o^2/(\sigma^2+\Delta\mu^2)\right]}{(\sigma^2+\Delta\mu^2)^{3/2}} \qquad (9)$$

The constant of proportionality has been determined by comparing $\langle g\rangle_E$ for $\mu_o = 2.6$ and $\Delta\mu = 0$ to the correct maximum gain [10].

On resonance, $\mu_o = 0$, $\langle g\rangle_E$ is zero regardless of $\Delta\mu$; if $\Delta\mu \ll \sigma$, the weak-field, low gain formula result (for a gaussian line-shape) is recovered. If the beam quality is "poor", so that $\Delta\mu \gg \sigma$, (9) shows that the maximum possible gain decreases as $\Delta\mu^{-2}$. The characteristic spread is $\Delta\mu_c \approx \sigma$. Note that the maximum average gain occurs for $\mu_o = \sqrt{(\sigma^2+\Delta\mu^2)/2}$. As the beam quality decreases ($\Delta\mu$ increases), it becomes beneficial to move the mean resonance parameter μ_o, further away from resonance, toward larger μ: a less severe penalty is incurred (the gain depression is less), if $f_E(\mu)$ is shifted to the right (to overlap zero gain regions) instead of being allowed to overlap negative gain regions. Gain begins to deteriorate when the spread in resonance parameters is larger than the characteristic width of the positive gain region in phase space ($\Delta\mu \gtrsim \sigma$).

Gain depression in the strong-field regime must be calculated using numerical techniques. Each appropriately populated "bin" in the electron phase space ($\mathcal{P}$, ν) is allowed to evolve and drive Maxwell's equations ((5) and (7) are solved self-consistently). The resulting gain depression, as a function of the initial energy spread of the electron beam is shown in Figure 8 for lasers of different optical power levels. The uppermost curve is for weak optical fields, and agrees with the analytic result (9). For stronger fields, the average gain is depressed even if $\Delta\mu = 0$; further depression occurs as $\Delta\mu$ increases. Each curve in Figure 8(a) is plotted assuming the laser is turned on with $\mu_o = 2.6$ (the value which gives maximum gain in weak fields); Figure 7, however, shows that in strong fields this μ_o is no longer the optimum resonance parameter. In Figure 8(b), each curve is plotted with μ_o equal to the value that gives maximum gain for the particular field strength.

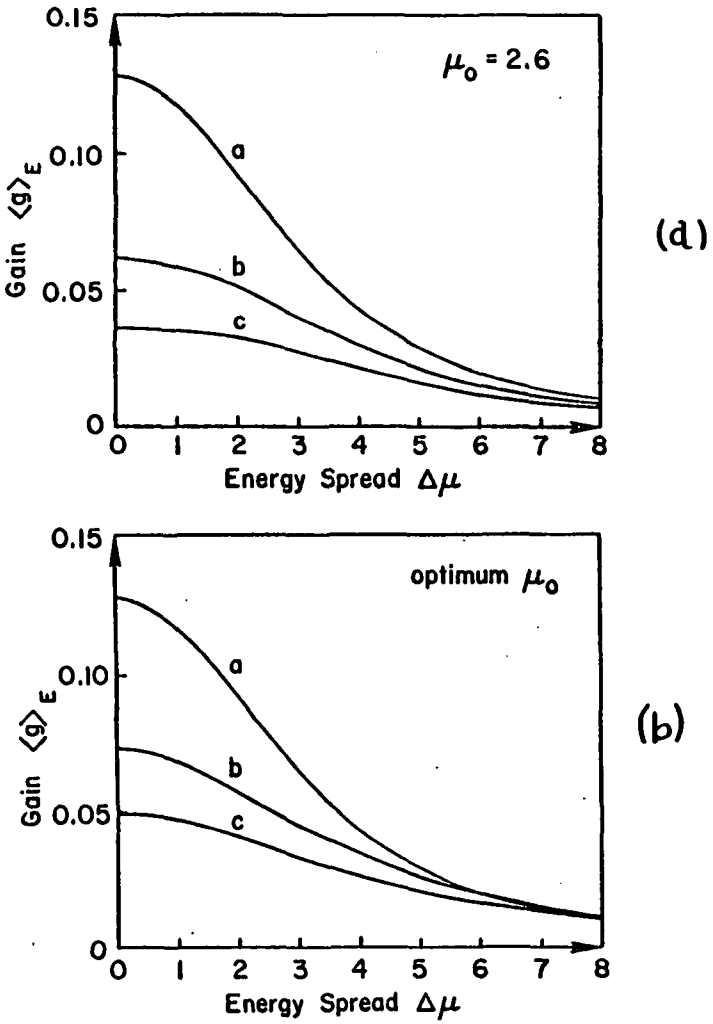

Figure 8. If the electron beam has an initial energy distribution, laser gain is depressed. The curves show the gain as a function of energy spread $\Delta\mu = 4\pi N \delta\gamma/\gamma$ for the three power levels in Figure 7: in 8(a), with $\mu_o = 2.6$; in 8(b), with μ_o chosen optimally for each power level parameter.

All curves decrease with $\Delta\mu$ in qualitatively the same way as in Figure 8(a). Note that the characteristic spread $\Delta\mu_c \approx 4$ causes approximately a factor of two decrease in gain for strong or weak fields, but $\Delta\mu_c$ is somewhat larger for higher power levels (this roughly agrees with the analytic result above).

Electron Beam Angular Spread. All electron beams have a finite emittance, so not all the electrons in a beam can be injected into perfect helical orbits. Physically, a poorly injected electron will drift off-axis and fall behind "perfectly injected" electrons with the same initial energy and z-velocity. A small angular misalignment θ, translates directly into an altered resonance parameter: $\mu \to \mu_o + \delta\mu$, where

$$\delta\mu = -4\pi N \gamma^2 \theta^2/(1+K^2) \tag{10}$$

and $K = eB_o\lambda_o/2\pi mc^2$. For typical parameters, an angular spread of a few tenths of a milliradian gives a unit shift in $\delta\mu$.

A finite-emittance electron beam contains a distribution of θ's; we take this distribution to be gaussian centered about $\theta = 0$, with characteristic angular spread $\Delta\theta$. The distribution of μ's populated by (10) is not gaussian, because $\delta\mu$ is quadratic in θ:

$$f_\theta(\mu,\mu_o) = \begin{cases} \exp\left[-(\mu_o-\mu)/a\right]/\left(\pi a(\mu_o-\mu)^{1/2}\right) & \mu < \mu_o \\ 0 & \mu > \mu_o \end{cases} \tag{11}$$

where $a = 4\pi N \gamma^2 \Delta\theta^2/(1+K^2)$ and f_θ has been normalized. This distribution has a spike at $\mu = \mu_o$ (corresponding to $\theta = 0$), and is zero above (since imperfect injection can only lower the resonance parameter). Figure 7 shows a composite $f(\mu)$, which combines the effects of a gaussian energy spread and this asymmetric angular spread.

The gain depression in weak and strong fields, determined numerically from (5) and (7) for $\mu_o = 2.6$, is shown in Figure 9(a); in each case the average gain peaks at $\Delta\theta = 0$ (no angular spread) and decreases substantially for an angular spread of only 2 milliradians. In Figure 9(b), the laser is started at its optimum resonance parameter for that power level. Remarkably, we find that if the laser is operating in the saturated regime (strong field), and at the optimum resonance parameter, there is comparatively little penalty for these angular spreads. If we compare the strong-field gain curve in Figure 7 to the shape of f_θ, the reason becomes clear: increasing $\Delta\theta$ produces a distribution which can expand and fill the positive region in the gain curve without much gain depression; no negative or zero gain regions are populated. In fact, given a beam with some angular spread, the gain can be larger for strong fields than for weak.

The free electron laser experimentalist (who is given an electron beam of fixed emittance), may find it beneficial to accept a larger angular spread in order to obtain a smaller electron beam diameter. The increased beam density will yield higher gain, while the angular spread will cause only modest depression in the strong-field regime if the resonance parameter is optimized.

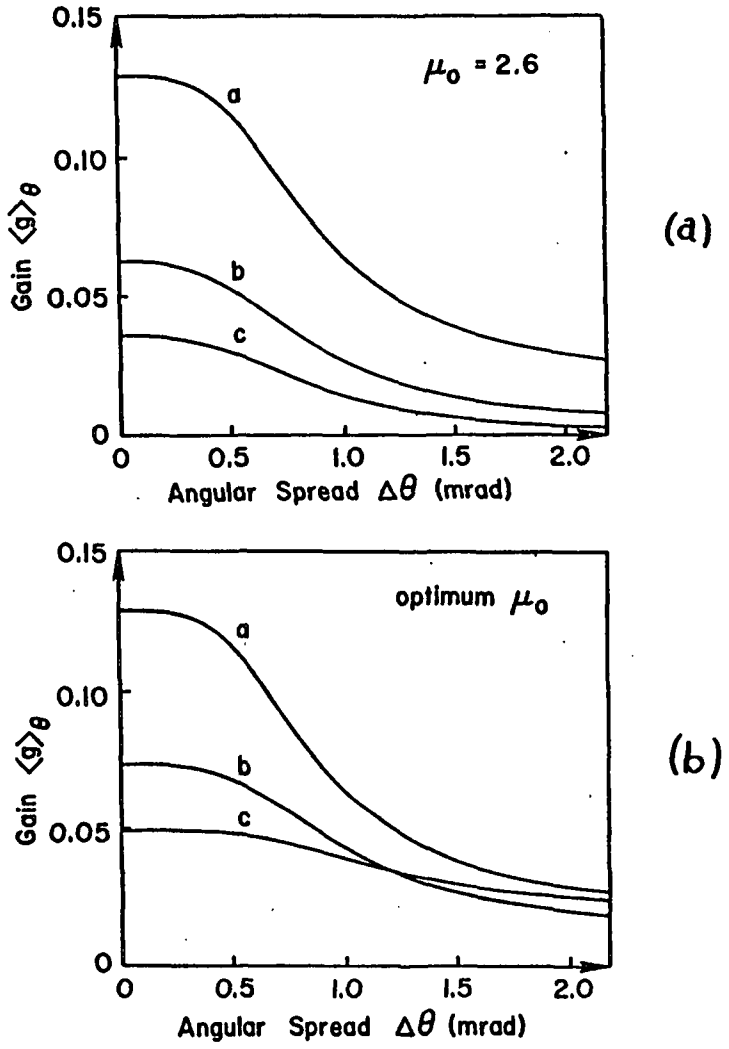

Figure 9. If the electron beam has an intial angular spread, $\Delta\theta$, laser gain is depressed. The curves show gain as a function of $\Delta\theta$ for the three power levels in Figure 7: in 9(a), with $\mu_o = 2.6$, in 9(b), with μ_o chosen optimally for each power level.

5. ULTRA-SHORT PULSE PROPAGATION

To this date, the free electron laser at Stanford University is the only such device to have demonstrated amplification and oscillation. Detailed comparison between experimental results and theoretical predictions have been difficult because analyses have assumed long optical and electron pulses, while the experimental device produces ultra-short pulses. The system of equations, (5) and (7), can be solved iteratively, step-by-step along the laser, and take into account the spatial structure of both the optical and electron pulses.

The behavior of the free electron laser is, in fact, modified by short-pulse effects [13]. The shape of the optical pulse, its Fourier transform (which shows the laser line shift), and the optical pulse "slippage", are all sensitive to the pulse length. This is not particularly surprising, since each of these depends on the overlap between the optical pulse and the electron beam--which for ultra-short pulses is continually changing. In Stanford's system, for example, as the short ($\sim$ 1 mm) pulses travel together down the 5.2 m magnet (Figure 1), the optical pulse gradually passes part of the way over the electron pulse. Each section of the optical pulse sees a varying electron density; similarly, each section of the electron pulse sees a varying optical field. The evolution is therefore quite complex.

In the working laser oscillator, the optical pulse remains in the resonator, bouncing between mirrors at either end. On each roung-trip 3.5% of the pulse's power is lost at the mirrors. To maintain the pulse, a fresh electron beam is injected every cycle, and timed to overlap the

rebounding optical pulse. The evolution of a low amplitude, coherent wave, can be followed through many hundreds of cycles in the resonator; the parameters chosen are those in Figure 1, so the results of this section can be compared directly to Stanford results.

Optical Pulse Slippage. One might think that to "synchronize" each electron pulse with the rebounding optical pulse (to have it overlap the optical pulse in the same way on each pass), the electrons should be injected every $2\mathcal{L}/c$ seconds ($\mathcal{L}$ is the resonator length). But while $2\mathcal{L}/c$ is the bounce time of a photon, it is not the bounce time of the centroid of the optical pulse. The physics: since there is more gain at the end of a free electron laser than at the beginning [10], the trailing edge of an ultra-short optical pulse experiences more amplification than its leading edge. The net effect is that the centroid of the optical pulse passes over the electrons at a speed less than $c(1-\beta_o)$, and would therefore intercept the next electron pulse later than the expected $2\mathcal{L}/c$. If the experimenter does not compensate for this effect, the optical pulse centroid will continually "slip" back, and after many passes will no longer adequately overlap the electron pulse; when this occurs, the absorption per pass exceeds the gain, and the equilibrium oscillator power is zero.

In the Standford experiment, the resonator length was varied until maximum steady-state power was achieved. The experimenters found that the power was sensitive to changes on the order of microns, but did not measure the absolute length of the cavity. It is now clear that the resonator must have been slightly shortened (by $\Delta\mathcal{L} \sim$ microns), to

decrease the $2\mathcal{L}/c$ bounce time, and compensate for the optical pulse "slippage". Figure 10 shows the steady-state power as a function of cavity length; our results agree well with the "detuning curve" found experimentally [14].

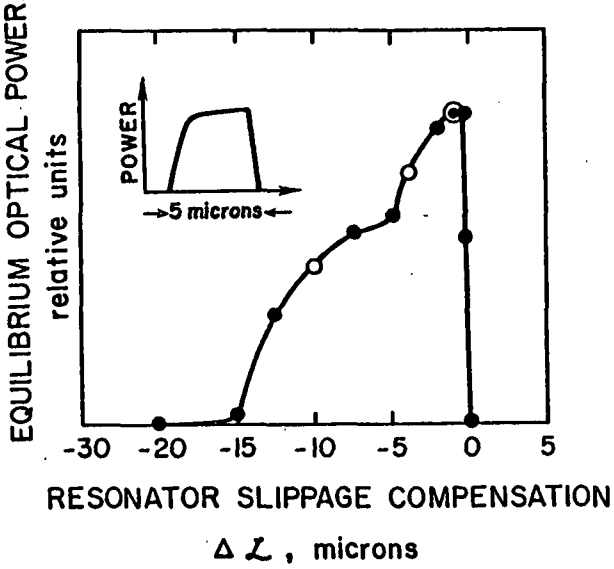

Figure 10. The length of the resonator must be "tuned" to compensate for optical pulse "slippage". The steady-state power is a sensitive function of the length. The inset shows Stanford's experimental "detuning curve", which is similar to the theoretical curve, but only 5 microns wide.

Optical Pulse Structure. Once the cavity has been properly adjusted, the ultra-short pulse in a free electron laser can evolve to, and operate in, a steady state. In Figure 11 we show a predicted optical pulse in the Stanford laser; after ~600 passes the pulse evolution slows considerably

and has nearly reached a steady state. The Stanford group has not yet had the opportunity to measure the structure of the optical pulse; when the measurement is performed, it will be an excellent test of the predictive powers of this analytic technique. Various pulse shapes are possible depending on the cavity length; often a large peak is followed by a smaller bump.

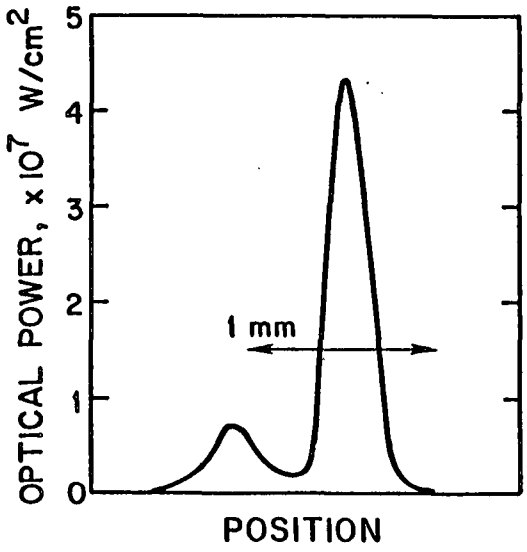

Figure 11. After 600 passes, with $\Delta\mathcal{L}$ = -0.5 microns, the optical pulse has grown to ~3×10^{7} W/cm^2. It can evolve through various shapes which depend on $\Delta\mathcal{L}$; multiple peaks can occur as can single wider shapes. The multiple peak spacing is ~0.8 mm.

The multiple peak structure in Figure 11 does, however, explain an observed feature of the power spectrum. The peaks (~0.8 mm apart) would

correspond to approximately a 60 GHz modulation in the laser line shape. The Stanford experiments do report a 60 GHz modulation. This can be interpreted as indirect evidence for multiple peak structure.

The spatial Fourier transform of the steady-state optical pulse yields the laser power spectrum shown in Figure 12. A low amplitude pulse starts at maximum weak-field gain ($\mu = 2.6$); after many passes the pulse amplitude grows large and the power spectrum shifts to $\mu_f \approx 4$ for maximum strong-field gain (see Fig. 7). The structural cause for the shift is a linear phase change along the pulse profile so that $\phi \approx \delta kz$ where $\delta k/k_r \approx -0.0015$; the resonance parameter is shifted by $\delta\mu = -2\pi N \delta k/k_r = +1.5$.

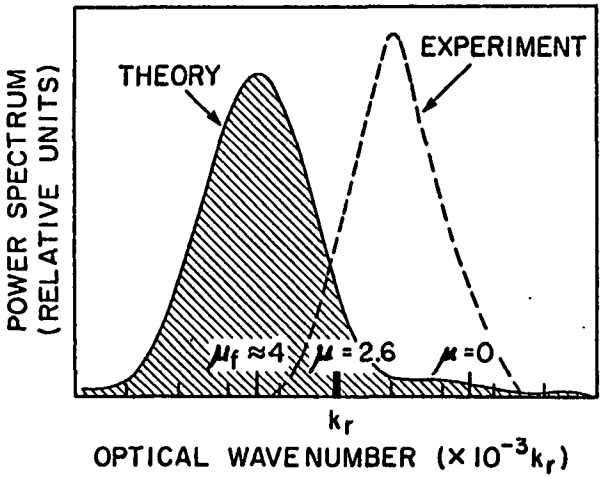

Figure 12. The power spectrum is obtained by taking the spatial Fourier transform of the pulse.

The theoretical width and shape of the power spectrum is in excellent agreement with experiment, but the reported laser line appears to be shifted towards resonance ($\mu = 0$) as determined by comparison with the spontaneous emission line-center. A possible cause for this discrepancy is a slight

misalignment of the detector from the magnet axis during the spontaneous emission measurement. This alignment is so delicate that $\theta \approx 0.0007$ radians would shift the spontaneous line-center up by $\delta\mu = 2\pi N\gamma^2\theta^2/(1+K^2) = 2.5$ and make the laser line appear to be shifted towards resonance by the amount shown. Note that there is no other determination of resonance in the Stanford experiment and such a misalignment can only cause the laser line to appear shifted towards resonance.

No matter how the laser pulse grows, $\beta_z (\approx 1)$ remains nearly constant for all electrons and the electron pulse retains its shape. On

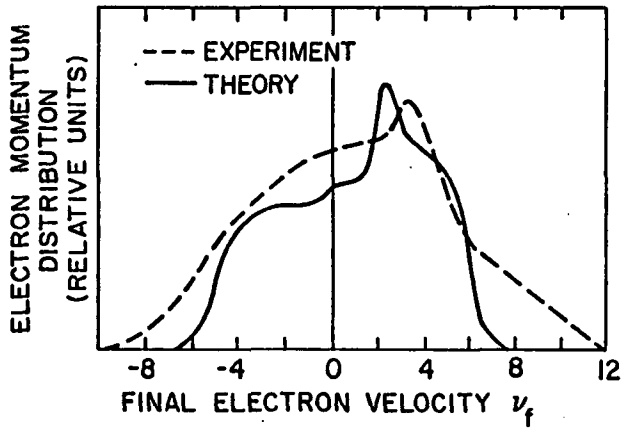

Figure 13. As the steady-state optical pulse passes over the monoenergetic electron beam, an energy distribution results: $\nu_f = L[\beta_f k_o - (1-\beta_f)k_r]$.

each pass all electrons are injected with the same energy, but as they respond to the local optical field a small microscopic energy change alters the resonance parameter. Figure 13 shows the resultant energy distribution within the electron pulse envelope; experimental agreement is consistent with the resolution of the spectrometers.

6. ANALYTIC STRONG-FIELD TECHNIQUES

The results presented to this point have been derived numerically from the self-consistent coupled equations. It is possible, however, to make progress analytically in the limit of low gain and long pulses**. Wave dynamics depends only on the average phase shifts $\langle \cos(\zeta^*) \rangle_{\zeta_0}$ and $\langle \sin(\zeta^*) \rangle_{\zeta_0}$ (where $\zeta^* = \zeta + \phi$). These phase averages cannot be performed analytically since the solutions to the full pendulum equation (5) are elliptic integrals. In the low gain limit, however, ζ^* can be written as an expansion in powers of ε: $\zeta^* = \zeta^{*(0)} + \zeta^{*(1)} + \zeta^{*(2)} + \ldots$, where the superscript indicates the power of ε ($\zeta^{*(1)}$ is proportional to ε, etc.). We expand $\langle \cos(\zeta^*) \rangle_{\zeta_0}$, then perform a partial resummation of important terms. This can be diagrammed in the following way:

$$\langle \cos(\zeta^*) \rangle_{\zeta_0} = \langle 1 \rangle_{\zeta_0} - \left\langle \frac{1}{2!} \left(\underline{\underline{\zeta^{*(0)}}} + \underline{\underline{\zeta^{*(1)}}} + \zeta^{*(2)} + \ldots \right)^2 \right\rangle_{\zeta_0}$$

$$+ \left\langle \frac{1}{4!} \left(\underline{\underline{\zeta^{*(0)}}} + \underline{\underline{\zeta^{*(1)}}} + \zeta^{*(2)} + \ldots \right)^4 \right\rangle_{\zeta_0} + \ldots \qquad (12)$$

$$\approx \left\langle \cos\left(\underline{\underline{\zeta^{*(0)}}} + \underline{\underline{\zeta^{*(1)}}} \right) \right\rangle_{\zeta_0}$$

where the resummation retains the underlined terms, $\underline{\underline{\zeta^{*(0)}}}$ and $\underline{\underline{\zeta^{*(1)}}}$, to all powers in ε. We do the same for $\langle \sin(\zeta^*) \rangle_{\zeta_0}$. A selective summation which retains only $\zeta^{*(0)}$ vanishes when averaged over initial

---

**A monoenergetic, perfectly injected beam, a good approximation for the Stanford laser, is again assumed.

phases. If $\zeta^{*(1)}$ is retained as well, the net average current can be non-zero, and will drive the wave's evolution. We will see that this resummation, rather than a straight-forward expansion in powers of ε, is necessary to retain the essential features of the strong-field effect.

The quantity $(\zeta^{*(0)} + \zeta^{*(1)})$ is obtained by expanding the full pendulum equation, (5), to order ε, and integrating twice with respect to time. Inserting the result into (12), and performing the average over initial positions within the optical wave,

$$\left\langle \cos\left(\zeta^{*(0)} + \zeta^{*(1)} \right) \right\rangle_{\zeta_0} =$$

$$\left(-\sin \Delta\omega t + \Delta\omega t \cos \Delta\omega t \right) \frac{J_1\left(f(\Delta\omega t)\, b\varepsilon \right)}{\sqrt{2}\, f(\Delta\omega t)} \qquad (13)$$

$$\left\langle \sin\left(\zeta^{*(0)} + \zeta^{*(1)} \right) \right\rangle_{\zeta_0} =$$

$$\left(-1 + \cos \Delta\omega t + \Delta\omega t \sin \Delta\omega t \right) \frac{J_1\left(f(\Delta\omega t)\, b\varepsilon \right)}{\sqrt{2}\, f(\Delta\omega t)}$$

where $b^2 = 8e^4 B_0^2 / (\gamma mc\, \Delta\omega)^4$, $f(\Delta\omega t) \equiv (1 + (\Delta\omega t)^2/2 - \cos \Delta\omega t - \Delta\omega t \sin \Delta\omega t)$, and $\Delta\omega = \mu c/L$. In this low gain case, the microscopic average is independent of ϕ, and the only dependence on the fields is in the argument of the Bessel function. Further, the functional form (13) is non-analytic in the coupling constant, e, and therefore could not be obtained to any finite order in perturbation theory.

Summing an infinite class of diagrams, then performing the microscopic average, yields a result which describes the growth of the wave to saturation. When the amplitude is small, (9) is proportional to ε, so the field's growth rate is proportional to its amplitude. As the field grows, problems with the expansion might be expected: the

argument of the Bessel function contains the same expansion parameter used to calculate the electron single-particle currents; the results are consistent (the Bessel function description is applicable) only so long as this parameter does not grow too large. Fortunately, before this parameter becomes too large, the Bessel function approaches its first zero--the growth rate decreases, and the laser begins to saturate. In other words, the result remains consistent with the perturbation expansion of the pendulum equation, and is therefore a reliable description of laser behavior through saturation.

Further analytic progress can be made, and the essential physics retained, if the Bessel function is approximated by the first two terms in its expansion: $J_1(x) \approx (x/2)(1-x^2/8+\ldots)$. Since the expanded form has the same functional dependence as J_1 up to its first zero, this formulation still allows a description of the laser through saturation.

The differential equations, (7), can be simplified by choosing to follow the evolution of a single point ($\zeta = z - ct$) within the optical pulse as it travels down the magnet. The amplitude and phase of this portion of the wave evolve in time according to

$$\frac{d\mathcal{E}_\zeta}{dt} = \frac{e^4 B_0^2 \lambda_0}{(\gamma mc)^3 \Delta\omega^2}\rho(\zeta-(1-\beta_0)ct)\mathcal{E}_\zeta\left(\sin\Delta\omega t - \Delta\omega t\cos\Delta\omega t\right) S(\Delta\omega t)$$

$$\frac{d\phi_\zeta}{dt} = \frac{e^4 B_0^2 \lambda_0}{(\gamma mc)^3 \Delta\omega^2}\rho(\zeta-(1-\beta_0)ct)\left(-1+\cos\Delta\omega t + \Delta\omega t\sin\Delta\omega t\right) S(\Delta\omega t) \qquad (14)$$

where $S(\Delta\omega t) = [1-(b\,\mathcal{E}_\zeta f(\Delta\omega t))/8]$ is called the "saturation function".

If the field is small, $S \approx 1$, and (14) reduces to the weak field gain equation. As the field grows, $S \to 0$, and evolution stops. An important point is that $S(\Delta\omega)$ is a function of the laser frequency, and has no nodes: for any ω_r, $S(\omega_r)$ will saturate at some value of $\mathcal{E}$.* These equations therefore can describe the evolution of the amplitude and phase through saturation.

*Previous perturbative approaches, with no resummation of terms, give divergent results [15], and cannot describe laser saturation.

7. LASER OSCILLATOR EVOLUTION: A PHASE TRANSITION

In a laser oscillator the optical wave grows slightly during each pass, and requires many passes to achieve saturation. Its growth, $d\mathcal{E}$, over a number of round-trips, dn (which is >1, but small compared to the characteristic evolution time of the wave), is $\delta\mathcal{E}\,dn$, where $\delta\mathcal{E}$ is the growth per pass. $\delta\mathcal{E}$ will have contributions from two sources: the wave will grow or decay as a result of its interaction with electron pulse; it will also decay due to losses inherent in the optical cavity. The fractional power lost on each round-trip is modelled by the resonator Q. The growth due to the wave's interaction with the electron beam is found by integrating (14) over the interaction time, t = 0 to t = L/c, on a single pass. In the low gain limit, $\mathcal{E}$ and ϕ change very little over this timescale, and can therefore be taken outside the time integrals on the right-hand side. Performing the resulting integrals produces terms proportional to $\mathcal{E}$ and $\mathcal{E}^3$, with constant coefficients. The long term behavior of $\mathcal{E}$ and ϕ are described by the following equations:

$$\frac{d\mathcal{E}}{dn} = \alpha\mathcal{E} - \beta\mathcal{E}^3$$
$$\frac{d\phi}{dn} = \alpha' - \beta'\mathcal{E}^2 \qquad (15)$$

where n is the number of round-trips of the optical pulse in the resonator, and we have assumed that the pulse is long enough that every point z evolves in the same way (we therefore drop the subscript z). The coefficients are

$$\alpha = \frac{2e^4B_o^2\lambda_o\rho L^3}{(\gamma mc^2\mu)^3}\left(1-\cos\mu-\frac{\mu}{2}\sin\mu\right)-\frac{1}{2Q}$$

$$\alpha' = \frac{2e^4B_o^2\lambda_o\rho L^3}{(\gamma mc^2\mu)^3}\left(\sin\mu-\frac{\mu}{2}(1+\cos\mu)\right)$$

$$\beta = \frac{2e^8B_o^4\lambda_o\rho L^7}{(\gamma mc^2\mu)^7}\left(\frac{\mu}{2}(6-\mu^2)\sin\mu+2(1-\mu^2)\cos\mu\right.$$
$$\left.+\frac{3}{4}\mu\sin 2\mu+\frac{1}{4}\left(\frac{5}{2}-\mu^2\right)\cos 2\mu-\frac{21}{8}\right) \qquad (16)$$

$$\beta' = \frac{2e^8B_o^4\lambda_o\rho L^7}{(\gamma mc^2\mu)^7}\left(-\frac{\mu}{2}\left(3+\frac{2}{3}\mu^2\right)+2\mu^2\sin\mu\right.$$
$$\left.+\mu\left(2-\mu^2/2\right)\cos\mu+\left(\frac{\mu^2}{4}-\frac{5}{8}\right)\sin 2\mu+\frac{3}{4}\mu\cos 2\mu\right)$$

Note that 2α is the gain per pass, and is identical to the gain coefficient derived by other techniques [10]; Q^{-1} is the fractional power loss per pass.

These differential equations can be solved for the amplitude and phase of the wave:

$$\mathcal{E}^2(n) = \mathcal{E}_o^2 e^{2\alpha n}\Big/\left(1+\frac{\beta\mathcal{E}_o^2}{\alpha}e^{2\alpha n}\right) \qquad (17)$$

$$\phi(n) = \phi_o+\alpha' n-\frac{\beta'}{2\beta}\ln\left(1+\frac{\beta\mathcal{E}_o^2}{\alpha}e^{2\alpha n}\right)$$

where $\mathcal{E}_o$ and ϕ_o are the initial amplitude and phase at t = 0, and it is assumed that the laser starts far from saturation, $\mathcal{E}_o^2 << \alpha/\beta$. The square of the amplitude is related to the power in the wave, $2\mathcal{E}^2 c/8\pi$, plotted in Figure 14.

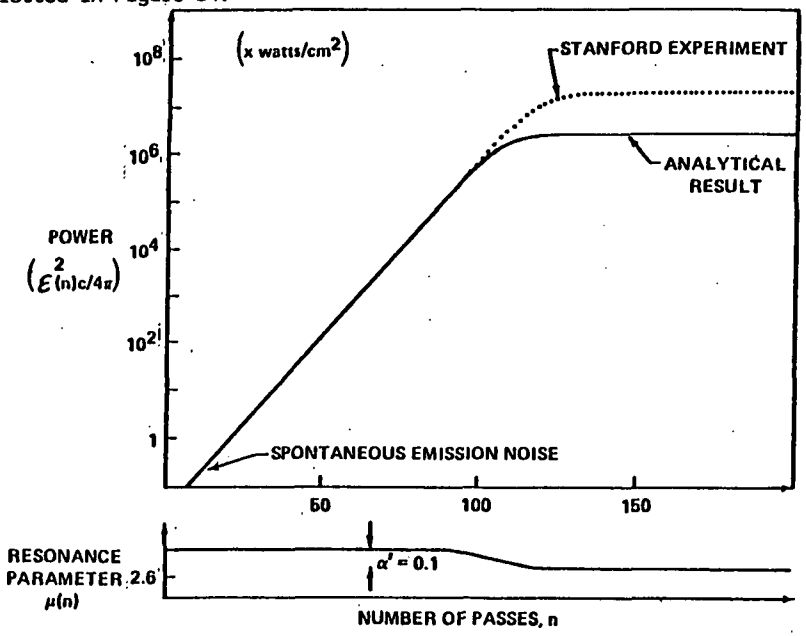

Figure 14. Laser power grows exponentially from noise to saturation. The laser frequency shifts during amplification, and again near saturation.

In the early stages of evolution, the power grows exponentially in time, and the phase shifts linearly in time. Near saturation, $e^{2\alpha n} \gg 1$, and the power asymptotically approaches the constant value $\alpha c/4\pi\beta$. The phase changes linearly in time, as before, but now the coefficient of the

linear growth is different: $\phi - \phi_o = (\alpha' - \alpha\beta'/\beta)n$.

In the laser oscillator, $\mathcal{E}$ and ω_f are not externally prepared, but evolve in a manner determined by the system parameters: ρ, B_o, λ_o, γ, N. The changing phase can again be interpreted as an evolving laser frequency, and a correspondingly evolving resonance parameter, μ. The definition of μ, and the form of the optical wave, imply $\mu(n) = \mu(0) + \partial\phi(n)/\partial n\,|_{\mu=\mu(0)}$. The conditions $\dot{\mathcal{E}} = \dot{\phi} = 0$ define the stationary points of the system (determined by $\mathcal{E}^2 = \alpha/\beta$, $\alpha'\beta = \beta'\alpha$). In general, the rate at which ϕ evolves is determined by α' and/or α; since they are roughly the same magnitude as the gain in the system, the shift in $\mu(0)$ is small (only 2% of its initial value of 2.6 at maximum gain). During oscillator growth, the resonance parameter is shifted away from resonance; after saturation it moves back towards resonance. The net shift is small and positive. Note that this result, for a long pulse, is much smaller and opposite to that for the ultra-short pulses.

The theoretical growth rate, power at saturation, and frequency shift are shown in Figure 14 where we plot (17) for the set of physical parameters appropriate to the Stanford free electron laser.

This formulation is important for the physical insight it provides into free electron laser operation. Equation (15) can be rewritten in the form $\dot{\mathcal{E}} = -\partial\mathcal{F}(\mathcal{E})/\partial\mathcal{E}$, where $\mathcal{F}(\mathcal{E}) = -\alpha\mathcal{E}^2/2 + \beta\mathcal{E}^4/4$. The dynamic equation for the amplitude of the laser field is then desribed by the overdamped motion of the coordinate $\mathcal{E}$ in the generalized potential $\mathcal{F}(\mathcal{E}$.. This potential has the form shown in Figure 15. It is evident from the graph that the behavior of $\mathcal{E}$ depends critically on the sign of α. If $\alpha < 0$, the losses in the system exceed the gain, and the

steady-state amplitude of the field is zero. Now suppose the electron current density, $\rho\beta_o c$, were slowly increased.

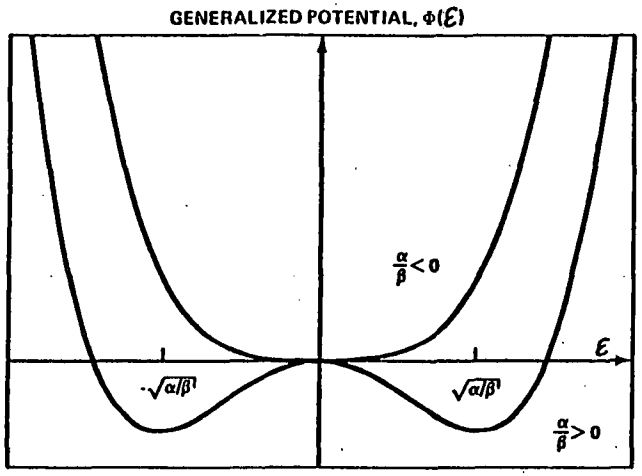

Figure 15. If the electron current is raised above threshold, the generalized potential $\Phi(\mathcal{E})$ changes shape; fluctuations drive the field from zero to the new steady-state minima $\pm(\alpha/\beta)^{1/2}$.

As long as $\alpha < 0$, this has no effect on the only stable point of the system: $\mathcal{E} = 0$. At some critical value of the current, the value for which $\mathcal{E} = 0$ is now an unstable point, and fluctuations will drive the system to a new steady-state configuration, $\mathcal{E} = (\alpha/\beta)^{1/2}$.

The potential $\Phi(\mathcal{E})$ has the same form as the thermodynamic potentials which describe ferroelectricity, ferromagnetism (in the Ginzburg-Landau formulation), superconductivity, and laser action in

atomic lasers [16]. Each of these phenomena can be described by a mean-field theory, with the result that the system (described by a potential of the form Φ above) changes from a disordered state to an ordered state when an external parameter attains some critical value. The low-gain analysis of the free electron laser presented above is also a self-consistent, mean-field theory: each electron is influenced by the radiation fields produced by the other electrons. $\mathcal{E}$ can be identified as the "order parameter" of the system, analogous, for example, to the magnetization in a ferromagnet. If the optical field strength is small, there are only a few photons, and the laser phase is disordered; if $\mathcal{E}$ is large (the system has "lased"), the optical wave becomes ordered and coherent. The free electron laser is a system which undergoes a second-order phase transition.

8. DISCUSSION

The single particle analysis of the free electron laser has proven to be a valuable description of laser performance. If the single particle currents are coupled to Maxwell's equations (section 2) the resulting set of self-consistent, non-linear equations describe the evolution of the electron beam and the amplitude and phase of the laser field. The two keys to the formulation of section 2 were (a) the slowly varying amplitude and phase approximation, an approximation commonly applied to laser systems, and (b) the distinction between microscopic and macroscopic scales, which distinguishes the microscopic bunching from the macroscopic pulse progagation.

The coupled equations lend themselves to numerical analysis, and such analysis is instructive for both experimenters and theorists. The analysis of gain depression, for example, directs the experimenter to run his laser far off-resonance for poorer quality electron beams (the electron distribution function should be "moved" to populate zero-gain regions instead of the negative-gain region just below resonance). The fact that the fractional gain depression is largely independent of the gain makes these results quite general.

The capabilities of this new theoretical approach become apparent when its predictions for the ultra-short pulse free electron laser are compared to the experimental data. The optical pulse evolution, determined simply and accurately, agrees well with observations. This moves free electron laser theory into a new regime, making it a tool which can be used to explain detailed experimental observations.

Although the coupled equations are easily solved numerically, it is instructive to investigate them analytically. A selective summation (involving terms to all orders in $\mathcal{E}$) can be performed to obtain non-divergent analytic results which capture the physics of the processes occuring in the closed-orbit regions of the pendulum phase-space. When these results are incorporated in a set of laser rate equations, the laser oscillator can be followed analytically through saturation. This description correlates well with numerical analyses, but can only describe evolution of long pulses. Its real value comes from the insight it yields into the physics of the free electron laser: the form of the equations reveals that this laser, like an atomic laser, is a self-ordering, many-body system which undergoes a second-order phase transition.

We are grateful for the support (of W. B. C.) by NASA Grant NSG-7490.

REFERENCES

1. J. M. J. Madey, J. Appl. Phys. 42, 1906 (1971).
2. W. B. Colson, Phys. Lett. 64A, 190 (1977); A. Bambini and A. Renieri, Nuovo Cimento 21B, 339 (1978); V. N. Baier and A. I. Milstein, Phys. Lett. 65A, 310 (1978).
3. R. A. Hopf, P. Meystre, M. O. Scully and W. H. Louisell, Opt. Comm. 18, 413 (1976); F. A. Hopf, P. Meystre, M. O. Scully and W. H. Louisell, Phys. Rev. lett. 37, 1342 (1976); H. Al-Abawi, F. A. Hopf and P. Meystre, Phys. Rev. A. 16, 666 (1977); P. Sprangle, Cha-Mei Tang, W. M. Manheimer, and R. A. Smith, Naval Research Lab memorandum Report 4033 and 4034.
4. T. Kwan, J. M. Dawson, T. Lin, Phys. of Fluids 20, 581 (1977).
5. N. M. Kroll and W. A. McMullin, Physical Review 71A, 300 (1978).
6. W. B. Colson, Phys. Lett. 59), 187 (1976); W. B. Colson, Free Electron Laser Theory, Ph.D. Thesis, Stanford University (1977).
7. W. B. Colson and S. K. Ride, "The Free Electron Laser: Maxwell's Equations Driven by Single-Particle Currents", accepted by Physics Letters A.
8. L. R. Elias, W. M. Fairbank, J. M. J. Madey, H. A. Schwettman, and T. I. Smith, Phys. Rev. Lett. 36, 717, (1976); Physics Today, February (1976) p. 17.
9. D. A. G. Deacon, L. R. Elias, J. M. J. Madey, G. J. Ramian, H. A. Schwettman, and T. I. Smith, Phys. Rev. Lett. 38, 892 (1977); Scientific American, June, 63 (1977).

10. W. B. Colson, Phys. Lett. 64A, 190 (1977); W. B. Colson, Physics of Quantum Electronics Vol. 5, Chapter 4 (Addison-Wesley Publishing Co. 1978) ed. S. Jacobs, M. Sargent, and M. Scully.
11. C. Brau, Los Alamos Scientific Lab, to be published.
12. J. M. J. Madey, "Effect of Energy-Spread and Beam-Emittance on the Gain Profile in the Small Signal, Low-Gain, Single-Paritcle Limit", to be published.
13. H. Al-Abawi, F. A. Hopf, G. T. Moore, and M. O. Scully, Optics Comm. 30, 235 (1979); G. Dattoli and A. Renieri, to be published.
14. J. M. J. Madey, Final Technical Report to ERDA: Contracts EY 76-S-03-0326 PA 48 and PA 49 (1977).
15. W. B. Colson, W. H. Louisell, J. F. Lam, and C. D. Cantrell, Tenth IQUE in Atlanta (1978); R. Peccei and W. B. Colson, to be published.
16. H. Haken, Synergetics, Springer-Verlag (1977); V. Degiorgio and M. O. Scully, Phys. Rev. 2A, 1170 (1979).

From: FREE ELECTRON LASERS
Edited by S. Martellucci and Arthur N. Chester
(Plenum Publishing Corporation, 1983)

FREE ELECTRON LASER WAVE AND PARTICLE DYNAMICS

William B. Colson

Quantum Institute
University of California Santa Barbara
Santa Barbara, CA 93106

INTRODUCTION

In a free electron laser, a beam of relativistic electrons passes through a static periodic magnetic field to amplify a superimposed coherent optical wave (Figure 1). Here, the lasing process has been reduced to its most fundamental form and is manifestly classical in nature. This point is at the root of many of the free electron lasers potential advantages over conventional atomic lasers; many properties of atomic lasers such as efficiency, are limited by quantum mechanics. This new laser is free from the bonds constraining atomic lasers to a particular wavelength and therefore is continuously tunable. The optical cavity contains only light, radiating electrons and the magnetic field so that intense optical fields may propagate without the degrading non-linear effects (self-focussing, etc.) of denser media. The advanced technology of high-energy electron accelerators and storage rings promises efficient recirculation of the beam energy.

The earliest coherent radiation sources, radar and microwave electron tubes, used classical non-relativistic electron beams to amplify long wavelength radiation (10 cm to 0.1 cm). These devices satisfied a wide range of applications with hundreds of varied designs, but it was not possible to generate shorter wavelengths until the early sixties when atomic and molecular lasers were developed. A necessary technical advance at the time was the replacement of "closed" microwave cavities with "open" optical resonators. J.M.J. Madey's conception[1] of the free electron laser in 1971 showed how relativistic electrons and "open" resonators could extend the advantages of electron tubes to the optical regime.

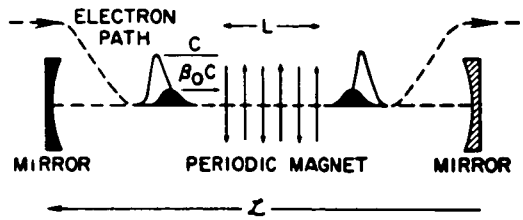

Fig. 1. Successive electron pulses travel through the periodic magnet with z-velocity $\beta_0 C$; the optical pulse is amplified as it slowly passes over oscillating electrons.

Madey and his collaborators at Stanford University demonstrated free electron laser amplification[2] in 1976 and laser oscillation in 1977. In the oscillator experiments, a nearly monoenergetic 43 MeV electron beam from a superconducting linear accelerator was passed through a 5.2 m long helical magnet with a field strength of B = 2.4 kGauss and wavelength $\lambda_0 = 3.2$ cm. Short 4 picosecond electron pulses of 1 amp peak current produced 2×10^7 W/cm^2 peak optical power at $\lambda = 3.4$ μ wavelength with circular polarization.

The fundamental physics of free electron lasers is now well understood; several theoretical viewpoints adequately describe its behavior. Semi-classical quantum theory, or quantum electrodynamics,[1,4-6] explains the laser action as stimulated Compton back-scattering of the virtual photons in the periodic magnet, or equivalently, as stimulated magnetic Bremsstrahlung. In this view, the finite length magnet and the resulting electron kinematics allow stimulated emission to exceed absorption. Viewed classically,[7] the electron beam is a cold relativistic plasma;[8-10] dispersion relations from the Boltzmann equation can properly characterize the evolution of the electron distribution in the optical wave. The most fruitful and widely used theory calculates the dynamics of individual electrons[11-13] as they are affected by the fields in the laser cavity; the total transverse current then drives Maxwell's non-linear wave equation.[14] Reference 15 and this volume review most of the current theoretical and experimental work on the free electron lasers.

In the next section we develop the equations governing wave and electron dynamics. The electron phase-space, and the optical wave evolution are each examined separately. Finally, the short pulse problem of Stanford's laser is reviewed.

Formalism

In the FEL oscillator, mirrors are placed at each end of the interaction region to store radiation; fresh electrons are either supplied continuously or injected to overlap the rebounding optical pulse. As electrons enter the laser cavity, they are acted on by the static magnetic field, and the oscillating electric and magnetic components of the nearly free optical plane-wave; interparticle Coulomb forces are small for the high energy, low density beam of the Stanford experiment. The magnet guides an electron through N periodic oscillations as it travels the length of the magnet ($L=N\lambda_o$) with z-velocity $\beta_z c(\beta_z \sim 1)$; the small transverse accelerations produce a small amount of spontaneous radiation carrying the polarization of the magnet geometry: circular polarization for a helical magnet, linear polarization for alternating poles. The emission is confined to within an angle $\approx \frac{1}{2\gamma}$ (γmc^2 is the electron energy) about the forward motion, and within a narrow ($\approx \frac{1}{2N}$) spectral line-width about the fundamental $\lambda=\lambda_o(1-\beta_z)\approx\lambda_o(1+\kappa^2)/2\gamma^2$ for $\gamma>>1$ and $\kappa=eB\lambda_o/2\pi mc^2$ where $e=|e|$ and m are the electron charge magnitude and mass, B is magnetic field strength, c is the speed of light. If $\kappa\lesssim 1$, as is usually the case, there will be a small amount of emission into a few well-separated higher harmonics. The Stanford experiment gives typical values for these parameters, and has demonstrated the tunable characteristic of the laser frequency by varying the accelerator energy. In future machines the tunable wavelength range is estimated to be about a decade; this is primarily determined by the dynamic range of the electron source.

The radiation from multiple passes of the electron beam is stored in the resonant cavity. Maxwell's wave equation governs the evolution of a light wave in the presence of an electron current:

$$\left(\vec{\nabla}^2 - \frac{1}{c^2}\frac{\partial^2}{\partial t^2}\right)\vec{A}(\vec{x},t) = -\frac{4\pi}{c}\vec{J}_\perp(\vec{x},t) \qquad (1)$$

where $\vec{A}$ is the radiation vector potential, and $\vec{J}_\perp$ is the transverse current density (cgs units). When the laser is "turned on", the optical wave grows from spontaneous emission to a large amplitude wave with a well-defined phase. After the coherent wave is established, its amplitude and phase can still evolve in time. The following waveform was chosen to represent the laser optical wave during these stages of evolution:

$$\vec{A}(\vec{x},t) = \frac{E(z,t)}{k}\,(\sin(kz-\omega t+\phi(z,t)),\ \cos(kz-\omega t+\phi(z,t)),0) \quad (2)$$

where $E(z,t)$ is the wave amplitude; the carrier frequency is $\omega=kc$, and the phase is $\phi(z,t)$. When the amplitude and phase of this wave are held fixed, (2) describes a plane wave traveling in the z-direction.

The waveform (2) contains no dependence on x and y; a proper description would give it some finite transverse dimension. In order to address the essential physics of the problem, we choose to avoid this complication by describing dynamics well within the optical wave (an appropriate "filling factor" is included in the definition of the electron density to handle the overlap between the optical mode and the electron beam[1]).

The dynamics of electrons in the combined static and radiation fields are governed by the Lorentz force equations. A helical magnetic field of the form

$$\vec{B}_{mag} = B(\cos k_o z,\ \sin k_o z, 0) \quad (3)$$

produces the optical polarization in (2) and $\lambda_o=2\pi/k_o$ is the magnet wavelength. The radiation electric and magnetic fields are obtained from the vector potential using the slowly varying amplitude and phase approximation explained below. When both of these fields are inserted into the transverse components of the relativistic Lorentz force equations, their contributions nearly cancel in comparison to the magnet (2): $\beta_z B>>(1-\beta_z)E$ when $\beta_z\approx 1$. If injecting perfectly, the large scale, or macroscopic, helical motion is then $\vec{\beta}=\beta_o\hat{z}+\vec{\beta}_\perp$ where $\vec{\beta}_\perp=-|e|\vec{B}_{mag}/\gamma mc^2k_o$. This motion alone appears uninteresting, but it allows efficient energy exchange with the purely transverse radiation field (2) if near "resonance": $\beta_o k_o\approx k(1-\beta_o)$.

Substituting $\vec{\beta}_\perp$ into the fourth component of the Lorentz force we have

$$\frac{d\gamma}{dt} = \frac{e\kappa E}{\gamma mc}\cos(\zeta+\phi) \quad (4)$$

and

$$\frac{d\zeta}{dt} \equiv \frac{\nu c}{L} = c(\beta_z k_o - k(1-\beta_z)) \quad (5)$$

where $\gamma^2=(1+\kappa^2)/(1-\beta_z^2)$, and $\zeta\equiv(k+k_o)z-\omega t$ is the electrons phase within an optical wavelength. If an electron has a velocity such that $\nu=0$, then exactly one wavelength of light is passing over the electron as it travels through one magnet wavelength.

$\nu_o \equiv \nu(t=0)$ is determined from initial conditions and is called the resonance parameter. E and ϕ are to be interpreted as the local radiation field and phase in the superimposed macroscopic (covering several optical wavelengths) part of the optical beam; the phase-space coordinates (ζ,ν) describe the evolution of electrons on a microscopic scale ($\lesssim\lambda$). The coordinates (ζ,γ) may also be used since $\nu \approx 4\pi N(\gamma-\gamma_R)/\gamma_R$ near resonance where $\gamma_R^2 = k(1+\kappa^2)/2k_o$ $(\gamma>>1)$. The number of periods N is usually large, a few hundred, so that small changes in γ give large changes in ν. This point means that, in general, fractional changes in γ are small during a single pass through the laser, and to a good approximation (4) and (5) become

$$\ddot{\zeta} = \left(\frac{2e^2 B E}{(\gamma_o mc)^2}\right)\cos(\zeta+\phi) = \left(\frac{\Omega c}{L}\right)^2 \cos(\zeta+\phi) \qquad (6)$$

where $\gamma_o mc^2$ is the initial electron energy, and $k \approx (1+\kappa^2)k_o/2\gamma_o^2$ has been used. 4Ω is the height of the closed orbit separatrix in the dimensionless pendulum phase-space.

Electron dynamics (6) have now been put into a form where we see that the fundamental phase-space is that of the simple pendulum. While exact for low gain, where E and ϕ are nearly constant, the pendulum phase-space is only slightly modified when more complicated effects are self-consistently included. It therefore has been and remains a valuable tool for experiments and theorists.

The optical wave evolves on a slower time scale than do individual electrons. The changes in E and ϕ then act back to slightly alter the phase-space paths guiding electrons. The amplitude and phase of the wave evolve slowly over an optical wavelength ($\dot{E} << \omega_T E$, etc.); a faster evolution would diminish the coherence and monochromicity of the radiation. The left-hand side of (1) can therefore be rewritten by inserting (2), and neglecting terms containing two derivatives, either spatial, temporal, or both. The remaining terms are "fast" rotating vectors with "slow" coefficients. Equations which are truly slowly-varying can be constructed by projecting the wave equation onto two unit vectors, $\hat{\varepsilon}_1=(\cos\psi,-\sin\psi,0)$ and $\hat{\varepsilon}_2=(\sin\psi,\cos\psi,0)$ to get

$$\left(\frac{\partial E}{\partial z} + \frac{1}{c}\frac{\partial E}{\partial t}\right) = -\frac{2\pi}{c}\vec{J}_\perp \cdot \hat{\varepsilon}_1$$

$$E\left(\frac{\partial \phi}{\partial z} + \frac{1}{c}\frac{\partial \phi}{\partial t}\right) = \frac{2\pi}{c}\vec{J}_\perp \cdot \hat{\varepsilon}_2. \qquad (7)$$

The second-order partial differential equation (1) has now been reduced to two first-order differential equations (7); one describing the evolution of the amplitude of the wave, the other describing the evolution of its phase. When there is no source current ($\vec{J}_\perp=0$), E and ϕ satisfy the free-space wave equation.

For relativistic electrons, the transverse radiation force is very small, so the electron's transverse velocity (and therefore the transverse current) is determined almost entirely by the static magnetic field. We project the single-particle currents, $e\vec{\beta}_\perp c$, onto the two unit vectors $\hat{\epsilon}_1$ and $\hat{\epsilon}_2$.

The total beam current is the sum of all single-particle currents. The electrons can be labelled by their initial positions and velocities (or, equivalently, resonance parameters); this definition is unique, and rigorously defines the electron beam current (Jean's theorem). In experimental situations, the electron pulse is large compared to an optical wavelength, so on a microscopic scale the electrons are initially spread uniformly over each wavelength of light. Although particle redistribution (bunching) does occur within an optical wavelength, it does not affect the average density in any macroscopic section of the beam several wavelengths long. Similarly, although the energy spread of the injected electron beam would generally not be large enough to result in distortion of the pulse as it travels down the magnet, it may be large enough to result in a significant spread in resonance parameters. On a macroscopic scale neither the bunching mechanism nor an initial velocity spread alter the macroscopic electron pulse shape, and it travels undistorted through the interaction region. Microscopically, however, an electron's resonance parameter, ν_o and initial position within a wavelength of light ζ_o (i.e., its coordinates in the pendulum phase-space) are crucial in determining the result of its interaction with the wave. The beam current density in a volume dV (which is large compared to an optical wavelength, but small compared to the pulse size) is found by averaging over ν_o and ζ_o, then weighting this result by the macroscopic particle density $\rho(z)$ within that volume element. Indicating the appropriate microscopic average by $\langle\ \rangle$ the equation becomes

$$\left(\frac{\partial E}{\partial z}+\frac{1}{c}\frac{\partial E}{\partial t}\right) = -2\pi e\kappa\ \rho(z-\beta_o ct)\left\langle\frac{\cos(\zeta+\phi)}{\gamma}\right\rangle \tag{8}$$

$$E\left(\frac{\partial \phi}{\partial z}+\frac{1}{c}\frac{\partial \phi}{\partial t}\right) = 2\pi e\kappa\ \rho(z-\beta_o ct)\left\langle\frac{\sin(\zeta+\phi)}{\gamma}\right\rangle \tag{9}$$

where $\rho(z-\beta_o ct)$ is the density of the traveling electron pulse. Within the slowly varying amplitude and phase approximation, macroscopic sections of the electron beam (those covering several

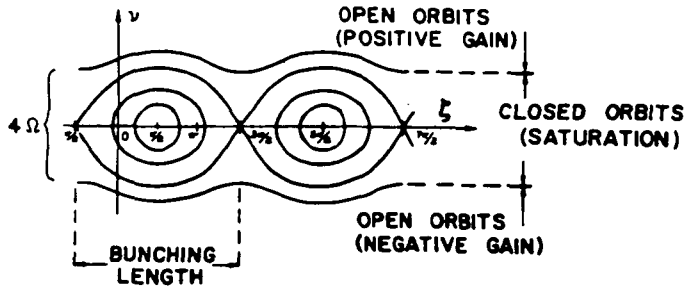

Fig. 2. The pendulum phase-space $(\zeta(t),\nu(t))$ is periodic in the optical wavelength which defines the bunching length. Electrons evolve along their paths in either the open or closed orbit regions. The optical field strength E determines the height of the closed orbit region 4Ω.

optical wavelengths) can be accurately represented in the periodic pendulum phase-space by a single section of phase-space λ long. Equations (8) and (9) are coupled through the pendulum equation (6), or the more general equations (4) and (5). In more complicated magnet structures, the electron equations (4) and (5) may be altered, but the wavelength equations (8) and (9) retain a similar form.

In their general form, the non-linear equations (8) and (9) are valid for low-gain and high-gain systems, in weak or strong optical fields. They describe the evolution for an arbitrary electron pulse shape, and the resulting amplitude and phase (and therefore the structure and spectrum) of the optical pulse. The remainder of this work explores the content of these equations.

ELECTRON PHASE SPACE EVOLUTION

The electron physics can be understood by appealing to the electron phase-space diagrams. Consider the microscopic current within a small volume of the beam. If the pendulum equation coefficient $\Omega=(2B_0E)^{\frac{1}{2}}eL/\gamma mc^2$ were truly constant, the electron phase-space would be exactly that of a single pendulum, as shown in Figure 2. Two sample electrons are included in the figure;

each electron's initial conditions determine the evolution of its "velocity" $\nu(t)=\dot{\zeta}(t)L/c$ and "position" $\zeta(t)$, and therefore constrain it to follow a particular path in phase-space. The height of the "closed-orbit region", 4Ω, is determined by the optical field strength, and is important in determining the character of electron evolution and hence the laser gain process. A large Ω "traps" a large area of the phase-space in closed orbit paths.

The fully coupled equations indicate that an electron's evolution is not governed by the exact pendulum equation, but by a "self-consistent" pendulum equation; at any instant in time, however, an electron's motion can be determined from the pendulum phase-space defined by the values of Ω and ϕ at that instant. The phase-space picture therefore remains a valuable tool in understanding beam evolution. Figures 3-5[16] show the self-consistent evolution of a monoenergetic beam with the approximate parameters of Stanford's laser (except that the optical pulse is assumed to be long and the optical cavity mode structure has not been included). The electrons phase-space paths are almost indistinguishable from pendulum paths; the self-consistent separatrix is included for reference. Since the electrons are spread uniformly over an optical wavelength, and the pendulum phase-space is periodic in the optical wavelength; it is only necessary, then, to consider a sample of electrons distributed uniformly over one optical wavelength.

In Figure 3, all electrons are injected with $\nu_o=2.6$ for maximum gain in weak fields.[11] With the optical power only 10^5 W/cm^2, all electrons fall in the open orbit region. The beam acquires a small energy spread, and some bunching about $\zeta=\pi$ can be detected. The gain equation and electron distributions have previously been derived in this regime by expanding the pendulum equation in powers of E.[11]

In Figure 4, the initial optical field is stronger (10^6 W/cm^2); the closed-orbit region has expanded, and now contains some of the electrons. The energy spread is larger, and bunching is more evident. Note that in both Figures 3 and 4 the $\zeta=\pi$ is overpopulated at the end of the laser to amplify E in (8).

In Figure 5, the field is large enough (10^7 W/cm^2) that saturation begins to occur: electrons gain and lose energy in a nearly symmetric way, and the gain (originally $\sim$15%) has dropped to $\sim$5%. When the laser oscillator reaches the point where gain per pass equals the loss per pass, it runs in a steady state. Note here that the $\zeta=\pi$ phase is overpopulated before the end of the laser! The electrons become spread again at the end of the laser and do not efficiently drive the wave. In the Stanford experiment, only a small fraction ($\approx\nu_o/4\pi N\approx 0.1\%$) of the electron beam energy

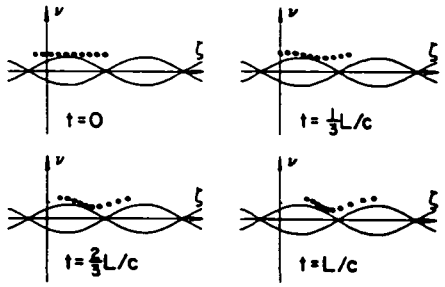

Fig. 3. In weak optical fields (power=10^5 W/cm^2), electrons evolve in the open-orbit region and acquire a small spread in energy.

is extracted at saturation.

The character of the gain process is analogous to the energy exchanged between two weakly coupled pendula (the optical wave and electron beam). For very short times, little energy can be transfrred, and for very long times, the exchange averages to zero. But for the appropriate finite time, defined by ν_o in our case, energy flows in one direction only, giving a net transfer to the optical wave. Note that the energy density in a relativistic electron beam can be quite large; any reasonable fraction that can be transferred to an optical wave produces a sizable laser field.

Electron dynamics may also be derived from a self-consistent pendulum potential; $V(\zeta)=-(\Omega c/L)^2\sin(\zeta+\phi)$ and $\ddot{\zeta}=-V'(\zeta)$ give (6). The potential changes slowly and self-consistently with Ω and ϕ coupled to the wave equations. From this viewpoint, when electrons enter at the resonant velocity $c\lambda_o/(\lambda_o+\lambda)$, they are initially stationary on the $V(\zeta)$-surface ($\nu_o=0$); an equal number of particles "roll" ahead and back exchanging equal amounts of energy with the optical wave. There is no gain in this case. If electrons enter at a slightly higher velocity, then all electrons are initially "rolling" along the ζ-axis of the corregated V-surface. For optimum

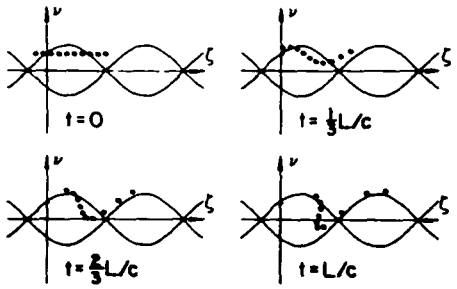

Fig. 4. In stronger fields (power=10^6 W/cm^2) Ω is larger; bunching becomes evident at the end of the laser.

gain conditions the "rolling" is slow; none will "roll" past more than one crest during the interaction time, and the electron beam will then lose energy to the optical wave. This is the gain mechanism. During amplification the initially monoenergetic, uniform beam becomes bunched at the optical wavelength and spread in energy; the fractional energy spread is $\delta\gamma/\gamma \approx \Omega/\pi N$ for weak fields and $\approx 1/4N$ at saturation. Maximum gain for weak fields occurs when the "rolling" velocity is $v_o=2.6$. Absorption is predicted and observed for $v_o \lesssim 0$. For typical parameters, each ampere of beam current within the optical mode cross section gives a few percent gain; one to one-hundred amps of peak current can be provided by accelerators or storage rings. The useful energy range is roughly ten to several hundred MeV; this spans a range of wavelengths from submillimeter to x-rays. Higher energies (with the best feasible magnets) result in very low gain.

After many passes of the electron beam, the intracavity optical amplitude becomes large, $V(\zeta)$ becomes large, and saturation occurs. When $\Omega \gtrsim 2.6$, there is no value of v_o which can prevent the nearly symmetric falling of particles into the potential troughs, the electrons become "trapped," and gain decreases. In future experiments, the deep troughs may be put to an advantage, increasing the energy

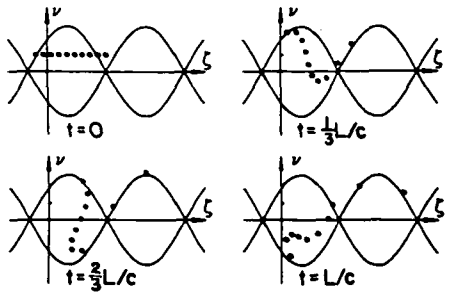

Fig. 5. Saturation occurs when the fields become so strong (power= 10^7 W/cm^2) that nearly all electrons are "trapped" in the closed-orbit region.

extracted from the electron beam and extending the laser performance. At large field strengths, electrons are trapped in the beginning stages of the magnet; the magnet (called a "tapered wiggler") is designed with a slowly decreasing wavelength so the guiding phase-space paths move down. Computer simulations show that about half the electrons remain trapped in the deep decelerating "buckets" with ≈10% (possibly 50%) energy extraction. This is the same mechanism (in reverse) used in linear accelerators; in fact, a periodic magnet with a slowly increasing wavelength and a powerful laser pulse may be used as a particle accelerator. The possibility of modified magnet geometries is an important flexibility in free electron laser design; in an atomic laser, this would correspond to altering the atomic structure, seen by an excited electron, during the emission process.

Optical Wave Evolution

After concentrating on electron dynamics, we now consider the result wave evolution. In a small section within long pulses, we can take ρ, E, and ϕ to be spatially uniform in z. Furthermore, assume

small electron energy extraction ($\gamma \approx \gamma_o$) and low gain so that the pendulum equation is valid. The phase averages are difficult to perform, since the solutions to the full pendulum equation ζ are elliptic integrals. The averages start at zero since the phases are uniformly populated, but the electrons response to the wave leads to non-zero values. In weak optical fields, the pendulum equation and averages may be expanded to first-order in E and the integrals performed; this gives a maximum gain $G_{max} = 0.27 e^4 B^2 \rho \lambda_o (L/\gamma_o mc^2)^3$ when $\nu_o = 2.6$.

In reference 15 (Colson and Ride, Chapter 13) an approximate solution was found for these phase averages with higher order E-dependence included. On each pass through the magnet, E and ϕ are nearly constant; they evolve on a slower time-scale than the electrons. A more appropriate time-scale for light is the evolution over many passes. The light will bounce between the mirrors many times, and if electrons are continuously supplied (or injected in pulses to overlap the optical pulse), it will grow during each pass until saturation. Its growth, dE, over a number of round-trips, dn (which is $\gtrsim 1$, but small compared to the characteristic evolution time), is $\delta E dn$, where δE is the growth per pass. δE will have contributions from two sources: the electron beam interaction, and the inherent losses of the optical cavity. The net growth over a single pass is found by integrating (8) and (9) from t=0 to t=L/c. E and ϕ change very little over this time-scale and the resulting integrals produce terms proportional to E and E^3 with constant coefficients. The long term behavior of E and ϕ are described by

$$\frac{dE}{dn} = \alpha E - \beta E^3$$
$$\frac{d\phi}{dn} = \alpha' - \beta' E^2 \qquad (10)$$

where n is the number of round-trips of the light in the resonator (pulses must be long enough so that every part of the pulse evolves in the same way) and the lowest order coefficients are

$$\alpha = \frac{2e^4 B^2 \lambda_o L^3 \rho}{(\gamma_o mc^2 \nu_o)^3} (1 - \cos \nu_o - \tfrac{1}{2}\nu_o \sin \nu_o) - \frac{1}{2Q}$$
$$\alpha' = \frac{2e^4 B^2 \lambda_o L^3 \rho}{(\gamma_o mc^2 \nu_o)^3} (\sin \nu_o - \tfrac{1}{2}\nu_o (1 + \cos \nu_o)) \qquad (11)$$

Note that 2α is the gain per pass and is identical with the gain coefficient derived using energy conservation;[11] Q^{-1} is the fractional power loss per pass. α and α' are exact in the weak-field, low-gain limit and are therefore fundamental results for the free electron laser. The coefficients β and β' are lengthy expressions not presented here; they are written out in reference 15. Furthermore, they are less fundamental since they are dependent on the specific higher order approximation scheme. Both α and β are antisymmetric functions of ν_o centered about resonance ($\nu_o=0$), but they are not exactly the same shape. Both α' and β' are symmetric functions of ν_o and also differ in detailed shape. β and β' are proportional to $[(2e^8B^4\lambda_o L^7\rho)/(\gamma_o mc^2\nu_o)^7]$ times a function of ν_o.

The differential equations (10) can be solved for the amplitude and phase of the wave after any pass n.

$$E^2(n) = E_o^2 e^{2\alpha n}\left(1+\frac{\beta E_o^2}{\alpha}e^{2\alpha n}\right)^{-1}$$

$$\phi(n) = \phi_o + \alpha' n - \frac{\beta'}{2\beta}\ln\left(1+\frac{\beta E_o^2}{\alpha}e^{2\alpha n}\right) \qquad (12)$$

where E_o and ϕ_o are the initial amplitude and phase and it is assumed that the laser starts far from saturation, $E_o^2 << \alpha/\beta$. The phase initially accumulates as $\alpha' n$; then after saturation (when $e^{2\alpha n} >> 1$) $\phi(n) \rightarrow (\alpha' - \alpha\beta'/\beta)n$. In the early stages of evolution, the power grows exponentially then asymptotically approaches the constant value $\alpha c/4\pi\beta$.

In the laser E and λ are not externally prepared, but evolve as determined by the system parameters: ρ, B, λ_o, γ_o, N and Q. We chose $\rho = 1.9\times10^9$ cm^{-3}, B=2.4 kGauss, λ_o=3.2 cm, γ_o=85, N=160, and Q^{-1}=0.35 to describe the Stanford laser.[2] The changing phase $\phi(n)$ is to be interpreted as an evolving laser frequency $\omega = 2\pi c/\lambda$ which slowly changes the resonance parameter ν. From the definition of ν and the form of the optical wave (2), we identify $\nu(n) = \nu_o + \partial\nu(n)/\partial n\big|_{\nu=\nu_o}$. The shift in ν is small (only 2% of its initial value of 2.6 for maximum gain). We previously neglected this shift in the low gain limit; here we see that this was justified. During growth the shift is away from resonance (and the maximum gain point at 2.6); after saturation ν moves nearly back to the maximum gain point.

The formulation above enables us to describe the onset of free electron laser operation as a second-order phase transition. Equation (10) may be rewritten in the form $\dot{E} = -\partial\Phi(E)/\partial E$, where $\Phi(E) = -\alpha E^2/2 + \beta E^4/4$. The dynamic equation for the amplitude of the laser field is then described by the overdamped motion of the coordinate E

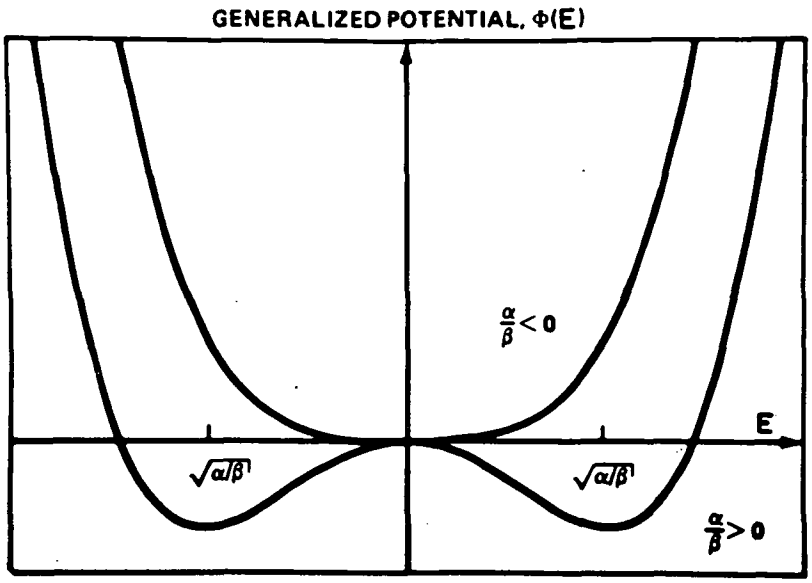

Fig. 6. If the electron current is raised above threshold, the generalized potential $\Phi(E)$ changes shape; fluctuations drive the field from zero to the new steady-state minima $\pm(\alpha/\beta)^{\frac{1}{2}}$.

in the generalized potential $\Phi(E)$. It is evident in Figure 6 that the behavior of E depends critically on the sign of α. If $\alpha<0$, losses in the system exceed the gain, and the field amplitude fluctuates near zero. At the critical current density $\rho\beta_o c$ (for which $\alpha=0$) the laser reaches threshold; for greater currents the potential takes on a different form and fluctuations cause evolution to a new steady-state configuration at $E^2=\alpha/\beta$. It is important we found that $\nu(n)\approx\nu_o$ for all n so that only the amplitude evolution needs to be followed in developing $\Phi(E)$; therefore, β and β' need only be accurate near $\nu\approx\nu_o=2.6$ (as they are), the maximum gain point in weak fields.

The potential $\Phi(E)$ has the same form as the thermodynamic potentials which describe ferroelectricity, ferromagnetism (in the Ginzburg-Landau formulation), superconductivity, and laser action in atomic lasers.[17] Each of these phenomena can be described by a mean-field theory, with the result that the system changes from a disordered state to an ordered state when an external parameter attains some critical value. This low-gain analysis of the free electron laser is also a self-consistent mean-field theory. The "order parameter" is E (analogous, for example, to the magnetization in a ferromagnet). If E is small, the photon density ($E^2/4\pi\hbar k_r c$) is small, and the laser phase ϕ has no long range order. If the system has "lased", E^2 goes to its large value of α/β; the laser phase becomes ordered over many optical wavelengths (the coherence length) producing a classical electromagnetic wave. The role of spontaneous emission has been included in a quantum mechanical description of this same evolution.[5]

Short Pulse Evolution

Now that the electron and wave evolution has been explored for long uniform beams, we consider the short pulse dynamics. The system of equations (6), (8) and (9) can be solved to take into account the spatial structure of both the optical and electron pulses. The behavior of the free electron laser is, in fact, modified by short-pulse effects.[18] The shape of the optical pulse, its Fourier transform (which shows a laser line shift), and the optical pulse "slippage" over the slightly slower electrons, are all sensitive to the pulse length. This is not particularly surprising, since each of these depends on the overlap between the optical pulse and the electron beam--which for short pulses is continually changing. In Stanford's system, for example, as the short ($\sim$1 mm) pulses travel together down the 5.2 m magnet (Figure 1), the optical pulse gradually passes part of the way (.5 mm) over the electron pulse. Each section of the optical pulse sees a varying electron density; similarly, each section of the electron pulse sees a varying optical field. The evolution is therefore quite complex.

In the Stanford laser, radiation is stored in an over-moded resonant cavity, $\mathcal{L}$ =12 m long. The mode geometry causes a small change in the field's amplitude along the laser, and a more significant change in the phase of the wave. The self-consistent separatrix shifts with the phase ($\Delta\phi/\text{pass} \approx \pi/4$), but the qualitative behavior of the electrons remains the same. The undriven wave's amplitude and phase vary as they propagate along the laser magnet axis. E varies in proportion to $(1+(2z-L)^2/\mathcal{L}^2)^{-\frac{1}{2}}$ and the optical phase changes by $-\tan^{-1}((2z-L)/\mathcal{L})$. These undriven changes in the wave are included at each step in the systems evolution. This mode

also changes the coupling in (8) and (9) and is included by introducing a "filling factor" $F(z)=F_o/(1+(2z-L)^2/\ell^2)$ which multiplies ρ everywhere. F is the ratio of the electron beam area to the optical mode area and equals $F_o=.082$ at $z=L/2$.

In the working laser oscillator, the optical pulse remains in the resonator, bouncing between mirrors at either end. On each round-trip 3.5% of the pulse's power is lost at the mirrors. To maintain the pulse, a fresh electron beam with fixed gaussian shape is injected every cycle, and timed to overlap the rebounding optical pulse. The evolution of a low amplitude, coherent wave, can be followed through many hundreds to a thousand cycles in the resonator.

It would appear that to "synchronize" each electron pulse with the rebounding optical pulse (to have it overlap the optical pulse in the same way on each pass), the electrons should be injected every $2\ell/c$ seconds. But while $2\ell/c$ is the bounce time of a photon, it is not the bounce time of the centroid of the optical pulse. Since there is more gain at the end of a free electron laser than at the beginning,[11] the trailing edge of an ultra-short optical pulse experiences more amplification than its leading edge. The net effect is that the centroid of the optical pulse passes over the electrons at a speed less than $c(1-\beta_o)$, and would therefore intercept the next electron pulse later than the expected $2\ell/c$. If the experimenter does not compensate for this effect, the optical pulse centroid will continually move back, and after many passes will no longer adequately overlap the electron pulse; when this occurs, the absorption per pass exceeds the gain, and the equilibrium oscillator power is zero.

In the Stanford experiment, the resonator length was varied until maximum steady-state power was achieved. The experimenters found that the power was sensitive to changes on the order of microns, but did not know the absolute length of the cavity within microns. We can now infer that the resonator must have been slightly shortened by $\Delta\ell$, to decrease the $2\ell/c$ bounce-time, and compensate for the slower speed of the optical pulse. Figure 7 shows the steady-state power as a function of $\Delta\ell$. Our result is in fair agreement with the curve found experimentally, but is wider for the precise parameters reported.[19] One of the less well-known experimental quantities is the electron pulse length (a factor of two uncertainty), which could clearly have a serious effect on the slippage curve width. The average current is actually well-known, so that uncertainties in the electron pulse length translate into uncertainties in ρ and therefore, gain. We have seen numerically that larger gain widens the curve in Figure 7 (50% gain/pass and 10% loss/pass make the curve $\approx$30 microns wide) so that less gain from a slightly longer electron pulse could conceivably give closer agreement to experiment. At this point, however, there are too many uncertainties to meaningfully

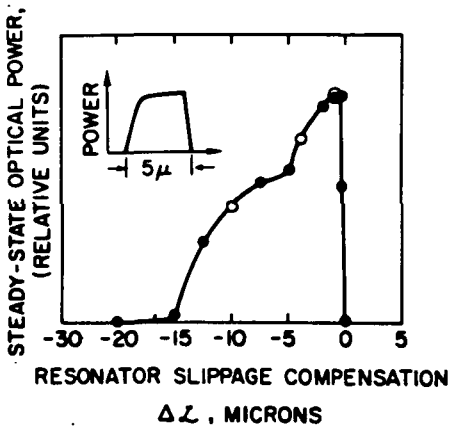

Fig. 7. The length of the resonator must be adjusted to compensate for reshaping of the optical pulse. The steady-state power is a sensitive function of the length, $\Delta\mathcal{L}$. The inset shows Stanford's experimental curve, which is similar to the theoretical curve, but not as wide.

pursue better agreement; future experiments will improve this situation.

Once the cavity has been properly adjusted, the free electron laser can evolve to, and operate in, a steady state. In Figure 8 are shown two optical pulses evolving in the Stanford laser; after several hundred passes the pulse evolution slows considerably to a steady state. The multiple peaked structure is typical of short pulses with small slippage compensation $\Delta\mathcal{L}$ ($\lesssim$2 microns); in this case the optical pulse "rides" near the middle of the electron pulse. If $\Delta\mathcal{L}$ is larger ($\gtrsim$2 microns), the optical pulse is longer with no structure and "rides" near the front of the electron pulse. The Stanford group has not yet had the opportunity to measure the structure of the optical pulse; when the measurement is performed,

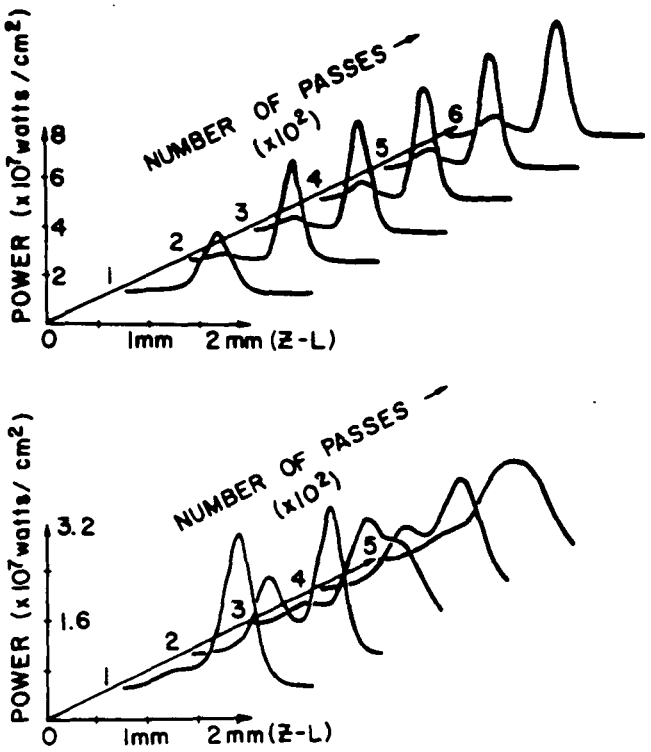

Fig. 8. In (a), the laser runs with small $\Delta\mathcal{L}$ (=½ micron) to steady-state, and in (b) the laser runs with larger $\Delta\mathcal{L}$ (= 2 micron).

it will be a good test of the predictive powers of this analytic technique.

The multiple peak structure in Figure 8 does, however, explain an observed feature of the power spectrum. The peaks (∿0.8 mm apart) would correspond to approximately a 60 GHz modulation in the laser line; the Stanford experiments do report a clear 60 GHz modulation which is indirect evidence for this multiple peak structure.

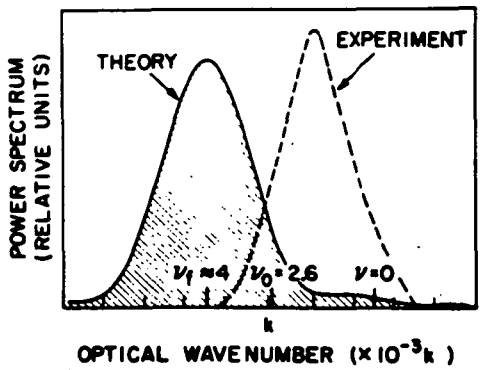

Fig. 9. The power spectrum dP/dk (laser lines) is obtained by taking the spatial Fourier transform of the pulse. The steady-state line-center is calculated to move from $k_r(\nu_o=2.6)$ to $\nu_f \approx 4$ (largely independent of $\Delta\mathcal{L}$), the resonance parameter for maximum strong-field gain. We suggest that the experimental line-center is placed too close to resonance ($\nu=0$) due to detector misalignment (by $\Theta \approx 0.0007$ radians) during the spontaneous emission measurement.

Furthermore, as $\Delta\mathcal{L}$ is increased, the modulation is observed to disappear and the power spectrum narrows; each feature is predicted by the theory here.

The spatial Fourier transform of a steady-state optical pulse yields the laser power spectrum dP(k)/dk as shown in Figure 9. A low amplitude pulse should start at $\nu_o=2.6$, the resonance parameter for maximum weak-field gain; this determines the carrier wavenumber k. After many passes the pulse amplitude becomes large and the power spectrum shifts to $\nu_f \approx 4$, the resonance parameter for maximum strong-field gain.[15] The structural cause for the shift is a linear phase change along most of the pulse profile so that $\varphi \approx \delta kz$ where $\delta k/k \approx -0.0015$; the resonance parameter as observed in a detector outside the laser cavity is then shifted by $\delta\nu = -2\pi N \delta k/k = 1.5$.

The theoretical width and shape of the power spectrum are in excellent agreement with experiment,[20] but the experimental laser line appears to be shifted towards resonance as determined by comparison with the spontaneous emission line-center. A possible cause for this discrepancy is a slight misalignment of the detector from the magnet axis during the spontaneous emission measurement.[21] This alignment is so delicate that $\Theta \approx 0.0007$ radians (well within the relativistic emission cone of angular width $\gamma^{-1} \approx 10^{-2}$ radians) would shift the spontaneous emission line-center up by $\delta\nu \approx 2.5$ (since $\delta\nu = 2\pi N\gamma^2\theta^2/(1+\kappa^2)$) and make the laser line appear to be shifted towards resonance by the amount shown in Figure 9. Note that there is no other determination of resonance in the Stanford experiment and such a misalignment can only cause the laser to appear shifted towards resonance as found.

No matter how the laser pulse grows, for electrons $\beta_z (\approx 1)$ remains nearly constant and the electron pulse retains its shape. On each pass all electrons are injected with the same energy, but as they respond to the local optical field a small microscopic energy change alters their resonance parameter. In reference 15 the resultant energy distribution is shown; experimental agreement is consistent with the resolution of the spectrometers.[19] For small $\Delta\mathcal{L}$, the fraction energy spread is $\Omega/\pi N$. We found that large $\Delta\mathcal{L}$ produces anamolously small electron distributions by about a factor of two. The electron moves out of the back of the optical pulse prematurely on each pass since the pulse is "riding" on the front of the electron pulse. This early decoupling fails to spread electron energies the expected amount.

The author wishes to acknowledge support by NASA Grant NSG-7490 and many helpful discussions with S.K. Ride, J.M.J. Madey, and J. Eckstein and the numerical assistance of K. Lind and R. Zarnowski.

REFERENCES

1. J.M.J. Madey, J. Appl. Phys. 42, 1906 (1971).
2. L.R. Elias, W.M. Fairbank, J.M.J. Madey, H.A. Schwettman, T.I. Smith, Phys. Rev. Lett. 36, 717 (1976); reported in Physics Today, p. 17, February (1976).
3. D.A.G. Deacon, L.R. Elias, J.M.J. Madey, G.J. Ramian, H.A. Schwettman, T.I. Smith, Phys. Rev. Lett. 38, 892 (1977); reported in Scientific American, p. 63, June (1977).
4. R.H. Pantell, G. Soncini, and H.E. Puthoff, IEEE J. Quantum Electronics 4, 905 (1968).
5. W.B. Colson, Phys. Lett. 59A, 187 (1976); W.B. Colson, Ph.D. Thesis, Stanford University (1977).
6. W. Becker and H. Mitter, Z. Physik B35, 399 (1979).
7. F.A. Hopf, P. Meystre, M.O. Scully and W.H. Louisell, Phys. Rev. Lett. 37, 1342 (1976).

8. N.M. Kroll and W.A. McMullin, Phys. Rev. 17A, 300 (1978).
9. T. Kwan, J.M. Dawson and T. Lin, Phys. of Fluids 20, 581 (1977).
10. P. Sprangle, Cha-Mei Tang, W.M. Manheimer and R.A. Smith, Naval Research Lab memorandum Report 4033 and 4034.
11. W.B. Colson, Phys. Lett. 64A, 190 (1977); W.B. Colson, "Physics of Quantum Electronics Vol. 5, Chapter 4," ed. S. Jacobs, M. Sargent, and M. Scully, Addison-Wesley Publishing Co., (1978).
12. A. Bambini and A. Renieri, Nuovo Cimento 21 , 399 (1978).
13. V.N. Baier and A.I. Milstein, Phys. Lett. 65A, 319 (1978).
14. W. Colson and S.K. Ride, Phys. Lett. 79A, 379 (1980).
15. "Physics of Quantum Electronics, Vol. 7", Ed. S. Jacobs, H. Pilloff, M. Sargent III, M. Scully and R. Spitzer, Addison-Wesley Publishing Co., (1980).
16. Similar figures in reference 15 (Colson and Ride, Chapter 13) do not have the separatrix properly positioned along the ζ-axis.
17. H. Haken, Synergetics, Springer-Verlag, (1977); V. de Giorgio and M.O. Scully, Phys. Rev. 2A, 1170 (1979).
18. F.A. Hopf, T.G. Kuper, G.T. Moore, and M.O. Scully, Physics of Quantum Electronics Vol. 7, Chapter 3", ed. S. Jacobs, H. Pilloff, M. Sargent III, M. Scully and R. Spitzer, Addison-Wesley Publishing Co., (1980).
19. J.M.J. Madey, Final Technical Report to ERDA, Contract EY 76-S-03-0326 PA 48 and PA 49 (1977).
20. In reference 15 (Colson and Ride, Chapter 13), the theoretical laser line was improperly presented as overlapping the experimental line; this was due to a numerical mistake in evaluating the Fourier transform of $\phi(z)$.
21. J.M.J. Madey, Private Communication.

1981 McGraw-Hill Yearbook of Science and Technology, page 218.

Free Electron Lasers

W. B. Colson

Quantum Institute and Department of Physics

University of California

Santa Barbara, California 93106

In a free electron laser, a beam of relativistic electrons passes through a static periodic magnetic field to amplify a superimposed coherent optical wave. Such a laser is free from the bonds constraining atomic lasers to a particular wavelength and therefore is continuously tunable. The optical cavity contains only light, radiating electrons, and the magnetic field so that intense optical fields may propagate without the degrading non-linear effects (self-focusing, etc.) of denser media. The advanced technology of high-energy electron accelerators and storage rings promises efficient recirculation of the beam energy. Here, the lasing process has been reduced to its most fundamental form and is manifestly classical in nature. This point is at the root of many of the free electron lasers potential advantages over conventional atomic lasers; many properties of atomic lasers, such as efficiency, are limited by quantum mechanics.

The earliest coherent radiation sources, radar and microwave electron tubes, used classical non-relativistic electron beams to amplify long wavelength radiation (10 cm to 0.1 cm). These devices satisfied a wide range of applications with hundreds of varied designs, but is was not possible to generate shorter wavelengths until the early sixties when atomic and molecular lasers were

developed. A necessary technical advance at that time was the replacement of "closed" microwave cavities with "open" optical resonators. J. M. J. Madey's conception of the free electron laser in 1971 showed how relativistic electrons and "open" resonators could extend the advantages of electron tubes to the optical regime.

Madey and his collaborators at Stanford University demonstrated free electron laser amplification in 1976 and laser oscillation in 1977. In the oscillator experiments (Fig. 1), a nearly monoenergetic 43 MeV electron beam from a superconducting linear accelerator was passed through a 5.2 m long helical magnet with a field strength of B_0 = 2.4 kG and wavelength λ_0 = 3.2 cm. Short 4 picosecond electron pulses of ~1A peak current produced 2000 kW peak optical power at $\lambda = 3.4\mu$ wavelength with circular polarization.

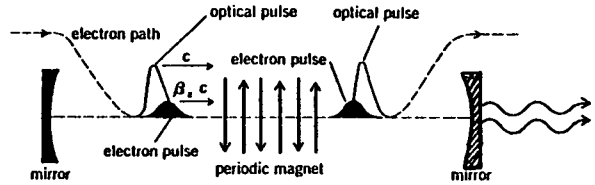

Figure 1. In the oscillator configuration, the electrons are guided into the transverse periodic magnetic field with velocity $\beta_z c$; the stored optical pulse slowly passes over them and stimulated emission occurs. The electrons are removed after each pass, and the enhanced optical pulse is stored between the mirrors of the resonant cavity. A partially-transmitting mirror allows useful coherent radiation to escape.

The fundamental physics of free electron lasers is now well understood; several theoretical viewpoints adequately describe its behavior. Semi-classical quantum theory, or quantum electrodynamics, explains the laser action as stimulated Compton back-scattering of the virtual photons in the periodic magnet, or equivalently, as stimulated magnetic Bremsstrahlung. In this view, the finite length magnet and the resulting electron kinematics allow stimulated emission to exceed absorption. Viewed classically, the electron beam is a cold

relativistic plasma; dispersion relations from the Boltzmann equation can properly characterize the evolution of the electron distribution in the optical wave. The most fruitful and widely used theory calculates the dynamics of individual electrons as they are affected by the fields in the laser cavity; the total transverse current then drives Maxwell's non-linear wave equation.

To simplify the discussion, only the essential physics of the Stanford oscillator experiment are explained. Mirrors are placed at each end of the interaction region to store radiation; fresh electrons are either supplied continuously or injected to overlap the rebounding optical pulse. As electrons enter the laser cavity, they are acted on by the static magnetic field, and the oscillating electric and magnetic components of the nearly free optical plane-wave; interparticle Coulomb forces are small for the high energy, low density beam of the Stanford experiment. The magnet guides an electron through N periodic oscillations as it travels the length of the magnet $L = N\lambda_0$ with z-velocity $\beta_z c$ ($\beta_z \approx 1$); the small transverse accelerations produce a small amount of spontaneous radiation carrying the polarization of the magnet geometry: circular polarization for a helical magnet, linear polarization for alternating poles. The emission is confined to within an angle $\approx 1/2\gamma$ (γmc^2 is the electron energy) about the forward motion, and within a narrow ($\approx 1/2N$) spectral line-width about the fundamental $\lambda = \lambda_0 (1 - \beta_z) \approx \lambda_0(1 + K^2)/2\gamma^2$ for $\gamma \gg 1$ and $K = eB_0\gamma_0 / 2\pi mc^2$ where e and m are the electron charge and mass, c is the speed of light. If $K \leq 1$, as is usually the case, there will be a small amount of emission into a few well-separated higher harmonics. The Stanford experiment gives typical values for these parameters, and has demonstrated the tunable characteristic of the laser frequency by varying the accelerator energy. In future machines the tunable wavelength range is estimated to be about a decade; this is primarily determined by the dynamic range of the electron source.

The radiation from multiple passes of the electron mass is stored in the resonant cavity. The magnet alone does no work on electrons (neglecting spontaneous emission), but does give a small transverse velocity, $\vec{\beta}_t$. The radiation fields alone have no significant effect on either the electron trajectory or energy, since the forces due to the optical electric and magnetic fields nearly cancel. In combination, the magnetic field guides electrons through a transverse path so that the radiation electric field $\vec{E}$ can do work on an electron according to $\dot{\gamma} = (e/mc)\vec{\beta}_t \cdot \vec{E}$. The fundamental emission frequency is such that one wavelength of light passes over an electron as it passes through one magnet wavelength; therefore, the transverse velocity $\vec{\beta}_t$ retains its orientation relative to $\vec{E}$ over many magnet periods and the energy exchange persists in the same direction. The direction of energy flow ($\dot{\gamma}$ being positive or negative) is determined by the electron's phase $\zeta = 2\pi[(\lambda^{-1}+\lambda_0^{-1})z(t)-\lambda^{-1}ct]$ within sections of the electron beam, each an optical wavelength long. Evolution of electrons in the ζ-coordinate space (the "resonant frame") is slow and simple; for low gain, ζ is approximately governed by the pendulum equation $\ddot{\zeta} = \Omega^2\cos(\zeta + \varphi)$ where $\Omega^2 = 2e^2B_0E/(\gamma mc)^2$ and φ is the optical phase.

Since any practical electron beam is many optical wavelengths long, the potential $V(\zeta) = -\Omega^2 \sin(\zeta + \varphi)$ is uniformly populated with electrons along the ζ-axis. If electrons enter at the resonant velocity $c\lambda_0/(\lambda_0 + \lambda)$, they are initially stationary on the $V(\zeta)$-surface ($\dot{\zeta}(0) = 0$); an equal number of particles "roll" ahead and back exchanging equal amounts of energy with the optical wave. There is no gain in this case. If electrons enter at a slightly higher velocity, then all electrons are initially "rolling" along the ζ-axis of the corrugated V-surface. For optimum gain conditions the "rolling" is slow; none will "roll" past more than one crest during the interaction time, and the electron beam will then lose energy to the optical wave (Fig. 2). This is the gain mechanism. During

amplification the initially monoenergetic, uniform beam becomes bunched at the optical wavelength and spread in energy; the fractional energy spread is $\delta\gamma/\gamma \approx \Omega L/\pi Nc$ for weak fields and $\approx 1/2N$ at saturation. Maximum gain for weak fields is $G_{max} = 0.27e^4 B_0^2 \rho \lambda_0 (L/\gamma mc^2)^3$ when the "rolling" velocity is $\dot{\zeta}(0) = 2.6c/L$, and the beam density is ρ. Absorption is predicted and observed for $\dot{\zeta}(0)L/c \leq 0$. For typical parameters, each ampere of beam current within the optical mode cross section gives a few percent gain; one to one hundred amperes of peak current can be provided by accelerators or storage rings. The useful energy range is roughly ten to several hundred MeV; this spans a range of wavelengths from submillimeter to x-rays. Higher energies (with the best feasible magnets) result in very low gain.

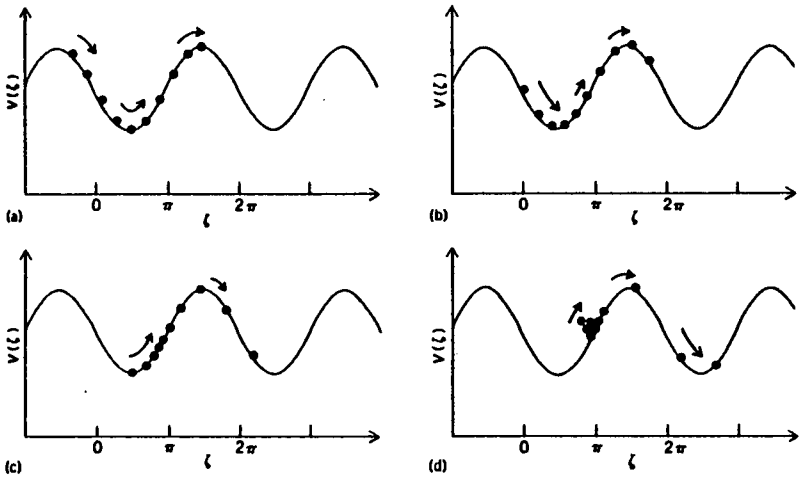

Figure 2. In the resonant beam frame, sample electrons (spanning one optical wavelength) evolve in the potential $V(\zeta)$. Maximum gain is achieved by initially "rolling" particles along the ζ-axis. The peaks in $V(\zeta)$ cause spatial bunching and decelerate the particles so that they give up their energy to the optical beam; an energy spread results. (The potential $V(\zeta)$ shown here actually grows in amplitude and shifts in phase self-consistently, and almost imperceptibly, according to Maxwell's wave equation; this shows the simple pendulum to be an accurate concept.)

The character of the gain process is analogous to the energy exchanged between two weakly coupled pendula (the optical wave and electron beam). For very short times, little energy can be transferred, and for very long times, the exchange averages to zero. But for the appropriate finite time, defined by $\dot{\zeta}(0)L/c$ in our case, energy flows in one direction only, giving a net transfer to the optical wave. Note that the energy density in a relativistic electron beam can be quite large; any reasonable fraction that can be transferred to an optical wave produces a sizable laser field.

After many passes of the electron beam the intercavity optical amplitude becomes large, $V(\zeta)$ is large, and saturation occurs. When $\Omega L/c \geq 2.6$, there is no value of $\dot{\zeta}(0)$ which can prevent the nearly symmetric falling of particles into the potential troughs, the electrons become "trapped," and gain decreases. As the gain decreases to equal the cavity loses, the laser runs in steady-state. In the Stanford experiment, only a small fraction ($\approx 1/2N \approx 1/2\%$) of the beam energy is extracted prior to saturation.

In future experiments, the deep troughs may be put to an advantage, increasing the energy extracted from the electron beam and extending the laser performance. At large field strengths, electrons are trapped in the beginning stages of the magnet; the magnet (called a "tapered wiggler") is designed with a slowly decreasing wavelength so $V(\zeta)$ moves to the left in the resonant frame. Computer simulations show that about half the electrons remain trapped in the deep decelerating "buckets" with ≈10% (to possibly 50%) energy extraction. This is the same mechanism used in linear accelerators; in fact, a periodic magnet with a slowly increasing wavelength and a powerful laser pulse may be used as a particle accelerator. The possibility of modified magnet geometries is an important flexibility in free electron laser design; in an atomic laser, this would correspond to altering the atomic structure, seen by an excited electron, during

the emission process.

For high density, low energy electron beams (where $\rho/\gamma^3 \gtrsim 10^2$ times Stanford's parameters), interparticle Coulomb forces can influence a particle's motion in competition with $V(\zeta)$. The gain process is then collective; many electrons oscillate together due to spatial beam instabilities and amplification is non-linear in the current. Still, relativistic electrons are necessary to reach short wavelengths and electron bunching is the key to gain; the emitted wavelength is generally related to the system parameters through dispersion relations containing the electron density. Groups at Columbia and TRW have demonstrated free electron maser action in the collective regime with moderate energy beams ($\gamma \leq 2.4$).

At present, free electron laser development is in its infancy; only the Stanford laser has operated in the short wavelength regime. Several experiments are now underway in the U.S. and Europe and many new designs are being considered. The necessity of high current, high energy electron beams appears to dictate that, for the near future at least, free electron lasers will be large machines; but, these facilities will be unique in that they are continuously tunable with high average power and high efficiency. Some basic configurations currently under investigation are diagramed in Fig. 3. A specific single-pass arrangement (3(a)) uses an induction linac (50 MeV and 2 kAmps peak current) as the electron source for a "tapered wiggler" magnet; collective effects are important for this beam. With high energy extraction, an impressive optical pulse (50 GW) is developed; the degraded electron pulse would then be discarded.

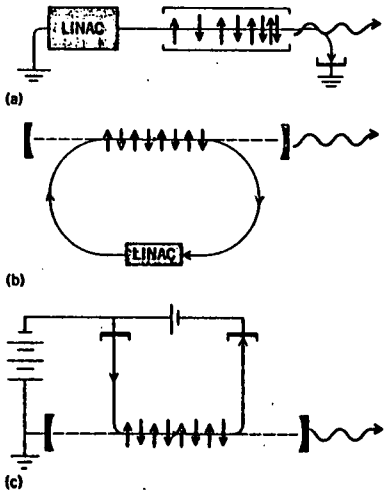

Figure 3. Some basic free electron laser systems.

With less energy extraction, the electron beam quality can be maintained and recirculated in a storage ring (3(b)); the electron energy lost per pass is replaced with an RF linac in the ring. However, even small beam degradation per pass can build up over many cycles until synchrotron radiation damping eventually allows steady-state operation; analysis predicts that the available laser power will then be only a small fraction ($\approx 1/2N$) of the synchrotron power. Several possible "cures" for this "ailment" are described in the references and now it appears that the laser output can greatly exceed the necessary synchrotron damping. One method alters the periodic magnetic structure to diminish the beam degradation; in another, the magnet structure is specifically designed to operate with an energy broadened electron beam; and another method recycles the beam energy without recycling the electrons. Electrostatic accelerators can also be used efficiently with lower energy beams ($\gamma \leq 10$). The electron current ($\approx$10A) and energy can be recovered by electrostatic deceleration of the beam after a pass through the laser (3(c)).

Several conceptual designs indicate 20% (to possibly 50%) "wall-plug"

efficiency is possible; the greatest losses coming from bending magnets and power supplies. It is the classical and relativistic nature of the electron beam which, in principle, allows efficient flow of energy into the electrons and then the optical wave. Efficient free electron lasers with an average optical output from 10 kW (at $\lambda > 10\mu$) to MW (at $\lambda \approx 1\mu$) are proposed.

A review of all the proposed free electron laser schemes with their advantages and disadvantages is lengthy. The above ideas just give the "flavor" of the research. Scientific, industrial, and military applications look promising. Solid-state, atomic, and chemical spectroscopy can reach wavelengths not previously accessible. The military needs powerful far-reaching beams for communications, radar, and weapons; in particular, space applications require high efficiency. Industrial photochemical processing looks promising in that free electron laser light appears relatively inexpensive. Judging from the more mature technologies, electron masers and atomic lasers, several free electron laser configurations will be required to satisfy differing needs; there won't be just one free electron laser.

BIBLIOGRAPHY:

J. M. J. Madey, J. Appl. Phys. **42**, 1906-1913 (1971).

D. A. G. Deacon et. al., Phys. Rev. Lett., **38**, 892-894 (1977).

W. B. Colson, "Free Electron Laser Theory," Ph.D. Thesis, Stanford University (1977).

W. B. Colson, *Physics of Quantum Electronics*, vol. 4 (1978) and vol. 7 (1980), (Addison-Wesley Publishing Co.).

Free-electron lasers operating in higher harmonics

W. B. Colson
Quantum Institute, University of California, Santa Barbara, California 93106
(Received 24 February 1981)

The nonlinear wave equation and self-consistent pendulum equation are used to generalize free-electron-laser operation to higher harmonics; this can significantly extend their tunable range to shorter wavelengths.

INTRODUCTION

In a free-electron laser, a beam of relativistic electrons travels through a static periodic magnetic field and oscillates to amplify coherent optical radiation with the same polarization as the magnet.[1] While the laser radiation causes spatial "bunching" on the optical wavelength scale,[2] the large-scale electron trajectories are primarily determined by the magnet. Several theoretical approaches have been used to describe the free-electron laser, and Ref. 3 compiles many of these techniques. The picture of single-particle electron currents driving the nonlinear optical wave equation[4] provides a clear, intuitive description of both electron and wave dynamics; we use this view to analyze the feasibility of operating free-electron lasers at selected frequencies which are odd multiples of the fundamental $3\omega, 5\omega, \ldots$.

Theory and experiment have been primarily applied to free-electron lasers using helical magnets, but many proposed experiments will use linearly polarized magnets, which are magnets with alternating poles. A small periodic longitudinal motion of electrons in the linear magnet causes spontaneous emission and gain in the higher harmonics; this has been proposed as a method of extending their tunable range.[5] Backscattering into higher harmonics has also been described (Ref. 3, Chap. 32, Vol. 7), but this process does not involve gain. Recently,[6] harmonic gain has been calculated for the low-gain case, but an incorrect result is presented; also, we are told of a quantum-mechanical contribution to the topic.[7] We derive a complete nonlinear, self-consistent wave equation for the laser field and show how the coupling between the electrons and light is altered in a nontrivial way. A useful notation allows simple scaling arguments to compare operation in any selected harmonic.

NONLINEAR WAVE EQUATION

General solutions to the electron motion in a purely transverse, periodic magnetic field $\vec{B} = B(0, \sin k_0 z, 0)$ with wavelength $\lambda_0 = 2\pi/k_0$ are difficult; but the physical situation of interest occurs when $\beta_z \approx 1 >> \beta_x, \beta_y$. An electron's path through the magnet is nearly sinusoidal with oscillation amplitude $K/\gamma_0 k_0$, where $K = eB\lambda_0/2\pi mc^2$, $e = |e|$ is the electron charge, m is the electron mass, and $\gamma_0 mc^2$ is the initial electron energy; smaller longitudinal oscillations of amplitude $K^2/8\gamma_0^2 k_0$ cause spontaneous emission and gain into a few higher harmonics.[8]

Calculation of the detailed properties of spontaneous radiation is straightforward using standard classical techniques.[5] In a long magnet ($N = L/\lambda_0 \approx 10^2$), emission is sharply peaked at well-separated harmonics

$$f\omega = 2\pi cf/(1-\beta_0)\lambda_0 \approx 2\gamma_0^2 fk_0 c/(1+\tfrac{1}{2}K^2)$$

in the forward direction, where $\beta_0 c$ is the electron's z velocity; the spectral width is $\sim 1/2N$. Far away from the linearly polarized magnet the element of optical energy received in the fth harmonic per unit solid angle, $d\Omega$, in the forward direction per unit frequency interval, $d(f\omega)$, is

$$\frac{dW_f}{d\Omega\, d(f\omega)} = \left|\frac{eN\gamma_0 f}{1+\frac{1}{2}K^2}\right|^2 \frac{\mathfrak{K}_f^2(\xi)}{c} , \qquad (1)$$

$$f = 1, 3, 5, 7, \ldots ,$$

where

$$\mathfrak{K}_f(\xi) = K(-1)^{(f-1)/2}[J_{(f-1)/2}(f\xi) - J_{(f+1)/2}(f\xi)] ,$$

$$\xi = K^2/4(1+\tfrac{1}{2}K^2) .$$

The radiation is stored in a resonant cavity which we take to be selective to only one of the harmonics. In order to describe stimulated emission, we must calculate the feedback of the light wave on the electron current using Maxwell's nonlinear wave equation. The detailed derivation of the wave equation is presented elsewhere.[9] The optical wave amplitude $E(t)$ and phase $\phi(t)$ slowly evolve into a coherent laser beam.

Relativistic electrons in both $\vec{B}$ and the radiation fields are governed by the Lorentz force equations. The electron motion contains factors which oscillate periodically each magnet wavelength, but we actually

want to describe the slow evolution about these periodic oscillations. This is accomplished by averaging the motion over each magnet wavelength.[6] It is then convenient to define a slowly evolving dimensionless velocity $\nu(t) \equiv L[(k+k_0)\bar{\beta}_z(t) - k]$ using the wave number of the fundamental $k = \omega/c$, and the averaged electron z velocity $c\bar{\beta}_z$. The initial velocity $\nu_0 \equiv \nu(0)$ is called the "resonance parameter"; when $\nu = 0$, exactly one wavelength of light passes over an electron as it passes through one period of the magnet and the coupling between light and electrons is maximized. The dimensionless phase is $\zeta(t) \equiv [(k+k_0)\bar{z}(t) - \omega t]$, where $\bar{z}(t) \equiv \int_0^t c\bar{\beta}_z(t')\,dt'$; note that $\dot{\zeta} \equiv d\zeta/d\tau = \nu$, where $\tau \equiv tc/L$. ζ describes electron dynamics on the optical wavelength scale. The total beam current is the sum of all single-particle currents which we label by initial positions ζ_0 (spread uniformly) and velocities ν_0; we average over sample electrons $\langle\ \rangle$, then weight this result by the macroscopic particle density ρ_0. Furthermore, we note that in long, periodic magnets, the fractional changes in γ are always small [$\lesssim (2N)^{-1}$].

The coupled wave and electron equations are, respectively,

$$\dot{a} = -r\langle e^{-if\zeta}\rangle, \quad f\ddot{\zeta} = \tfrac{1}{2}|a|\cos(f\zeta+\phi)\ , \qquad (2)$$

where $|a| \equiv 4\pi Nef\mathcal{K}_f(\xi)LE/\gamma_0^2 mc^2$, and $r \equiv 8\pi^2 Nef\mathcal{K}_f^2(\xi)L^2\rho_0/\gamma_0^3 mc^2$, and $a = |a|e^{i\phi}$. The second equation is recognized as the self-consistent pendulum equation. The Bessel functions $\mathcal{K}_f(\xi)$ express the reduced coupling between electrons and light resulting from the time electrons spend in periodic longitudinal motion (instead of transferring energy to the optical wave). A helical magnet has $\mathcal{K}_f(\xi) \to K$ throughout (2) and $\frac{1}{2}|a| \to |a|$ in the pendulum equation. Since the pendulum equation is periodic in $f\zeta$, we only need to explore one 2π section of phase space; with the transformation $(\zeta, \nu) \to (f\zeta, f\nu)$ the pendulum phase space can be transformed into the same phase space of the fundamental ($f = 1$). The separatrix $\nu_s^2 = 2|a| \times [1+\sin(\zeta_s+\phi)]$ is a slowly evolving function of $|a|$ and ϕ which guides electrons into bunches about the $\zeta \approx \pi$ phase; this drives the wave equation and is the gain mechanism.[2,3]

It is instructive to solve (2) for weak fields and low gain. We expand the pendulum equation in weak fields ($|a| \ll 1$) and insert ζ into the wave equation. The resulting gain g (the fractional increase in wave energy $|a|^2$) and phase shift $\Delta\phi$ describe the evolution of the optical wave:

$$\frac{g}{r} = \frac{1}{2}\frac{d}{dx}\left[\frac{\cos x - 1}{x^2}\right]_{x=f\nu_0}, \qquad \frac{\Delta\phi}{r} = \frac{1}{4}\frac{d}{dx}\left[\frac{\sin x - x}{x^2}\right]_{x=f\nu_0}. \qquad (3)$$

These are fundamental results, and the effects of stronger fields and higher gain are best described as deviations from these expressions. The maximum weak-field gain occurs at $f\nu_0 = 2.6056$ and the maximum gain is $g = 0.06752r$; the gain curve is symmetric in $f\nu_0$ and $\Delta\phi$ is antisymmetric. For large r, a large optical phase shift causes the gain curve to distort and become more symmetric about $\nu_0 = 0$. In strong fields ($|a| \gg 1$), electrons become trapped, the gain curve becomes broader in ν_0, and decreases in height; this is the saturation mechanism.

HARMONICS

We now examine Eqs. (2) with particular attention paid to the possibility of operating in higher harmonics ($f = 3, 5, 7, \ldots$). Several points are explored separately:

(1) The optical wavelength in higher harmonics is given by $\lambda_0(1+\frac{1}{2}K^2)/2\gamma_0^2 f$; the tunable range can now be adjusted by f as well as K and γ.

(2) The weak-field, low-gain expression (3) gives us a good indication of many of the scaling results. Maximum gain occurs closer to resonance in higher harmonics than in the fundamental; $\nu_0^{\max} = 2.6056/f$. This creates a stiff requirement for the electron beam energy and angular spreads since their initial range in ν_0's must avoid the negative-gain region of the gain curve.

(3) Since the natural energy spread of the electron beam must fit into the narrower gain curve, we must have $\delta\nu_0 \lesssim \pi/f$. In terms of a real fractional energy spread this becomes $\delta\gamma/\gamma \lesssim 1/4Nf$ where N is the number of magnet periods.

(4) For an initial angular spread, there is the similar restriction in f since a change in electron angle also changes ν_0 through $\bar{\beta}_z$. The requirement is $\Delta\theta^2 \lesssim (1+\frac{1}{2}K^2)/2N\gamma^2 f$.

These restrictions on the energy spread $\delta\gamma/\gamma$ and the angular spread $\Delta\theta$ are the most serious problems.

(5) The gain in a free-electron laser is decreased in higher harmonics due to the factor $f\mathcal{K}_f^2$ in r. See Fig. 1. Gain decreases rapidly in f, but the decrease can be diminished using higher values of K. Practical values[10] can reach $K \approx 10$, but $K \approx 2$–4 seems to be adequate to reach higher harmonics.

(6) After a pass through the laser, the final electron energy spread is given by $\delta\gamma/\gamma \approx |a|/8\pi Nf$ in weak fields, and $\delta\gamma/\gamma \approx 1/4Nf$ in strong fields. These results may be important for recirculating electron beams in a storage ring[6] or Van de Graaff.[11]

(7) The laser saturates when $|a| \gtrsim 2\pi$; this gives the final optical-field strength. The optical power at saturation actually increases in the higher harmonics in proportion to $(f\mathcal{K}_f)^{-2}$.

(8) At shorter wavelengths, the optical-mode area in the resonator tends to decrease. The mode area at

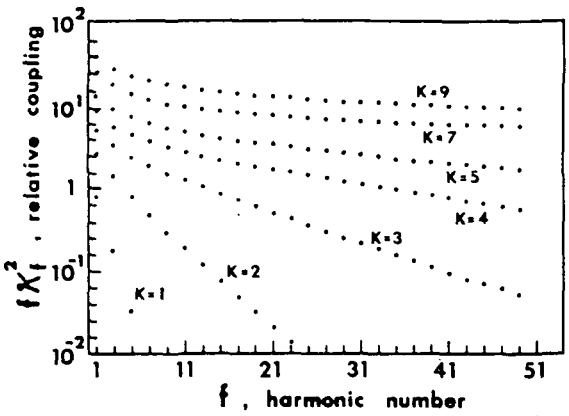

FIG. 1. Gain r is proportional to the new coupling factor fx_f^2 in linearly polarized magnets. In higher harmonics $f=3, 5, 7, \ldots$ the coupling decreases rapidly unless K is large.

the optical beam waist is $\pi w_0^2 = z_0\lambda/f$, where $2z_0$ is the confocal mirror spacing. As the harmonic number increases, the resonator should be adjusted so that the overlap with the electron beam cross section is maximized. With $f=10$, for example, one could decrease the beam waist w_0 by 2.15 and increase z_0 by 2.15. If the increase in f is shared between w_0^2 and z_0^{-1}, the optical cavity for higher harmonics can be made reasonable.

CONCLUSION

The use of free-electron lasers in higher harmonics is promising; a fixed facility then has a much broader tunable range by another factor of $f \sim 10$ or 20. The major limitation seems to be in the electron beam quality (as usual); the necessary energy and angular spreads decrease with f. A shorter magnet length L may relieve this restriction somewhat. The gain also decreases in higher harmonics, but if $K \approx 2-4$ this penalty does not seem too severe. Van de Graaff free-electron lasers[11] tend to have high gain (larger r because of lower γ_0) and excellent beam quality, but produce long wavelengths ~ 200 μm; higher harmonics may help to reach shorter wavelengths (~ 10 μm) without changing γ_0. Storage rings also have excellent beam quality, but not such large gain (smaller r because of higher γ_0). Even so, with sufficiently high K, higher harmonics could, in principle, extend these free-electron lasers to new shorter wavelengths in the uv and towards x rays. For instance, when γ is increased to achieve an 11-fold decrease in optical wavelength, the normal-gain process ($r \sim \gamma_0^{-3}$ and $\lambda \sim \gamma_0^{-2}$) drops by a factor of 36 (decreasing λ_0 is worse). But, if the $f=11$th harmonic is used with $K=5$, then only a factor of 2.5 in gain is lost; comparisons of higher harmonics are even more dramatic, but the excess beam quality necessary is less likely.

ACKNOWLEDGMENTS

The author wishes to acknowledge helpful discussions with Dr. J. M. J. Madey and Dr. P. Michelson. This research was supported by NASA Grant No. NAG 2-48, NATO Collaborative Grant No. 1876, and Air Force Grant No. AFOSR-81-0061.

[1]J. M. J. Madey, J. Appl. Phys. 42, 1906 (1971).
[2]W. B. Colson, Phys. Lett. 64A, 190 (1977).
[3]*Physics of Quantum Electronics*, edited by S. Jacobs *et al.* (Addison-Wesley, Reading, Mass., 1980), Vols. 5 and 7.
[4]W. B. Colson and S. K. Ride, Phys. Lett. 76A, 379 (1980).
[5]W. B. Colson, Ph.D. thesis (Stanford University, 1977), available from University Microfilms International, Ann Arbor, Mich., publication No. 78-02,145 (unpublished).
[6]J. M. J. Madey and R. C. Taber, Chap. 30, Vol. 7, Ref. 3.
[7]W. Becker, Z. Phys. B (in press).
[8]W. B. Colson, Phys. Lett. 59A, 187 (1976).
[9]W. B. Colson IEEE J. Quantum Electron. (in press).
[10]L. R. Elias and J. M. J. Madey, Rev. Sci. Instrum. 50, 1335 (1979).
[11]L. R. Elias, Phys. Rev. Lett. 42, 977 (1979).

The Nonlinear Wave Equation for Higher Harmonics in Free-Electron Lasers

WILLIAM B. COLSON

Abstract—The nonlinear wave equation and self-consistent pendulum equation are generalized to describe free-electron laser operation in higher harmonics; this can significantly extend their tunable range to shorter wavelengths. The dynamics of the laser field's amplitude and phase are explored for a wide range of parameters using families of normalized gain curves applicable to both the fundamental and harmonics. The electron phase-space displays the fundamental physics driving the wave, and we use this picture to distinguish between the effects of high gain and Coulomb forces.

Introduction

In a free-electron laser, relativistic electrons travel through a static periodic magnetic field and oscillate to amplify coherent optical radiation with the same polarization as the magnet [1]-[3]. The electron trajectories are primarily determined by the magnet, but the laser radiation causes "bunching" on the optical wavelength scale and leads to gain [4]-[6]. Several theoretical approaches have been used to describe the free-electron laser; [7] gives a good description of many of these techniques. While the first analyses used quantum mechanics [1] and quantum electrodynamics [8]-[10], classical methods have been shown to be clear and accurate [4]-[7], [11]-[21]. The coupled Maxwell-Boltzmann equations have been developed into quasi-Bloch equations to enhance the laser physics perspective [14], while plasma dispersion relations [15]-[17] and computer simulations [18], [19] emphasize the role of interparticle Coulomb forces and collective effects. The picture of single-particle currents driving Maxwell's nonlinear wave equation is a mixture of these views and provides a clear, intuitive description of both electron and wave dynamics [7], [20], [21].

In the past, theory and experiment have been primarily applied to free-electron lasers using helical magnets, but most proposed experiments will use linearly polarized magnets: a magnet with alternating poles. In this paper, the wave equation technique is applied to linearly polarized magnets and the possible use of higher harmonics. Although the basic operation of the free-electron laser in either polarization magnet remains essentially the same, a periodic longitudinal motion of electrons in the linear magnet causes spontaneous emission and gain in higher harmonics of the optical field; this has been proposed as a method to extend their tunable range [9]. In a recent work [22] the electron trajectories in linearly polarized magnets and the gain in higher harmonics were calculated; we extend the method developed there to derive a complete nonlinear, self-consistent wave equation for the laser field and electrons. We show how the coupling between the electrons and light is altered in a nontrivial way. We then consider some examples of high gain and low gain in both weak and strong optical fields. A useful notation is proposed which reduces the system parameters and meaningfully relates the remaining variables to the self-consistent pendulum phase-space evolution. A simple extension of the theory includes Coulomb forces [23] within the single-particle viewpoint, and we show that these forces are not usually significant except for very high gains. A distinction is made between the effects of high gain (with an accompanying optical phase shift) and the effects of Coulomb forces.

Manuscript received January 2, 1981; revised April 6, 1981. This work was supported in part by NASA Grant NAS 2-48, NATO Collaborative Grant 1876, and Air Force Office of Scientific Research Grant AFOSR-81-0061.

The author is with the Quantum Institute, University of California, Santa Barbara, CA 93106.

Simple Magnet Trajectories and Radiation

The character of radiation from a free-electron laser is ultimately determined by electron trajectories in the periodic magnet structure. If radiation losses and radiation feedback are neglected, electron motion in an external magnetic field $\vec{B}_m$ is governed by the Lorentz force:

$$\frac{d(\gamma\vec{\beta})}{dt} = -\frac{e}{mc}(\vec{\beta}\times\vec{B}_m) \tag{1}$$

where $e = |e|$, m, and $c\vec{\beta}$ are, respectively, the electron charge, mass, and velocity, $\gamma^{-2} \equiv 1 - \vec{\beta}\cdot\vec{\beta}$, and c is the speed of light. The electron energy γmc^2 in a magnetic field is a constant of motion so that $\gamma = \gamma_0$, the initial gamma. Introduce a purely transverse, periodic magnetic field

$$\vec{B}_m = iBe^{ik_0 z}(\hat{z}\times\vec{a}) \tag{2}$$

with maximum strength B, wavelength $\lambda_0 = 2\pi/k_0$, and polarization vector $\vec{a}$. The transverse polarization vector ($\vec{a}\cdot\hat{z} = 0$) can describe various polarizations:

$$\vec{a} = \begin{cases} (0,-1,0) & x \text{ linearly polarized magnet} \\ (1,0,0) & y \text{ linearly polarized magnet} \\ (-1,i,0) & \text{left circularly polarized magnet} \\ (1,i,0) & \text{right circularly polarized magnet.} \end{cases}$$

This representation of $\vec{B}_m$ is only accurate near the $\hat{z}$-axis and it is assumed that electrons only sample fields near that axis; farther off-axis, the transverse field lines bend to satisfy Maxwell's equations.

General solutions are difficult, even for specific choices of $\vec{a}$, but the physical situation of interest here is $\beta_z \approx 1 \gg \beta_x$,

0018-9197/81/0800-1417$00.75

β_y. Since the deflection from uniform motion is proportional to the magnetic field strength, a perturbation in powers of the field is suggested:

$$\vec{r}(t) = \beta_0 ct\hat{z} + \frac{i\lambda_0}{2\pi}\left(\frac{K}{\gamma_0}\right)e^{i\omega_0 t}\vec{a} + \frac{i\lambda_0}{16\pi}\left(\frac{K}{\gamma_0}\right)^2 e^{i2\omega_0 t}\hat{z}(\vec{a}\cdot\vec{a}) + \cdots \quad (3)$$

where $\omega_0 = k_0 c$, $K = eB\lambda_0/2\pi mc^2$, and $\beta_0 c$ is the initial electron $\hat{z}$-velocity. For a circularly polarized magnet $\vec{a}\cdot\vec{a} = 0$ and the path is helical; in a linear magnet $\vec{a}\cdot\vec{a} = 1$, giving a sinusoidal path with slight longitudinal corrections.

Radiation from relativistic particles is confined to a forward cone of angular width $\sim\gamma_0^{-1}$. If transverse motion has a large amplitude (K/γ_0), the radiation cone will periodically deflect out of a detector placed on-axis at infinity (the "searchlight effect"). This will cause radiation from many harmonics to appear (up to $\sim\gamma_0^3$ times the fundamental) and produce a broad band of frequencies. The requirement for the cone to stay in the detector is $K \lesssim 1$; then the radiation will have sharp emission lines but still could have small contributions at well-separated harmonics.

In the magnetic fields considered here [24], accelerations are small ($K/\gamma_0 \ll 1$). Calculation of the detailed properties of radiation is straightforward using standard classical techniques [9], [25]. Electrons accelerate, and hence radiate, only within the length of the magnet $L = N\lambda_0$, so that the radiating time is L/c. For a long magnet (large N), resonant terms become sharply peaked about a spectrum of radiation frequencies ω satisfying

$$\omega = f\omega_0/(1 - \beta_0\cos\theta) \quad (4)$$

where θ is the observation angle away from $\hat{z}$, f is the harmonic number: $f = 1$ is the fundamental and $f = 2$ is the next harmonic, etc. A detector typically looks at each harmonic separately because they are separated by $\sim N$ times the linewidth.

Far away from a linearly polarized magnet, $\vec{a} = (0, -1, 0)$, the element of energy received dW, the per unit solid angle $d\Omega$, the per unit frequency interval $d\omega$, is

$$\frac{dW_f}{d\Omega d\omega} = \left(\frac{e^2}{4\pi^2 c}\right)\frac{\sin^2\left[\left(\frac{\omega}{\omega_0}(1-\beta_0\cos\theta) - f\right)N\pi\right]}{\left[\frac{\omega}{\omega_0}(1-\beta_0\cos\theta) - f\right]^2} \cdot \frac{f^2}{(1-\beta_0\cos\theta)^2}\left\{\sin^2\theta A_0^2 + \left(\frac{K}{\gamma_0}\right)\sin 2\theta\cos\phi A_0 A_1 + \left(\frac{K}{\gamma_0}\right)^2(1-\sin^2\theta\cos^2\theta)A_1^2 - \frac{1}{2}\left(\frac{K}{\gamma_0}\right)^2\sin^2\theta A_0 A_2\right\} \quad (5)$$

where

$$A_\alpha = \sum_{n,n'=-\infty}^{\infty} J_{-n}\left(\frac{fK\sin\theta\cos\phi}{\gamma_0(1-\beta_0\cos\theta)}\right)J_{-n'}\left(\frac{fK^2\cos\theta}{8\gamma_0^2(1-\beta_0\cos\theta)}\right)\cdot(\delta_{n+2n'+\alpha,f} + \delta_{n+2n'-\alpha,f}).$$

ϕ is measured away from $\hat{x}$ in the x-y plane and J_n is an nth ordinary Bessel function of the first kind. Since the line shape factor is narrow, the value for ω in (4) has been used throughout (5) except in the line shape itself. The complete spectrum is a sum over all harmonics f.

The expression in (5) is plotted in Fig. 1(a) for the first three harmonics of ω and θ; ϕ-dependence is small for large N. Each harmonic has an increasing number of lobes (f = number of lobes) within the forward cone $\theta < \gamma_0^{-1}$ and is centered about $\theta = 0$. There is some radiation into higher harmonics because $K = 0.72$ (the Stanford magnet [2]) is close to unity. If K is made smaller, the harmonics retain the same shape but decrease relative to the fundamental. N has been taken large enough ($N = 200$) so that emission about each harmonic can only occur in thin "sheets" or "curtains;" following these curtains gives a large frequency shift in each harmonic when θ covers the narrow range 0-γ_0^{-1}. At a fixed angle within this range, a sweep through ω would reach all harmonics. For fixed ω, the harmonics would be spaced at angles $\theta_f \approx \sqrt{f-1}/\gamma_0$ symmetric about $\theta = 0$. All this has been observed in the Orsay free-electron laser experiments [26].

The radiation spectrum for a circularly polarized magnet $\vec{a} = (-1, i, 0)$ is given below:

$$\frac{dW_f}{d\Omega d\omega} = \left(\frac{e^2}{4\pi^2 c}\right)\frac{\sin^2\left[\left(\frac{\omega}{\omega_0}(1-\beta_0\cos\theta) - f\right)N\pi\right]}{\left[\frac{\omega}{\omega_0}(1-\beta_0\cos\theta) - f\right]^2} \cdot \frac{f^2}{(1-\beta_0\cos\theta)^2}\left\{\sin^2\theta|A|^2 + \left(\frac{K}{\gamma_0}\right)^2(1-\sin^2\theta\sin^2\phi)|G|^2 + \left(\frac{K}{\gamma_0}\right)^2(1-\sin^2\theta\cos^2\phi)|S|^2 - \left(\frac{K}{\gamma_0}\right)(A^*G + G^*A)\sin\theta\cos\theta\sin\phi - \left(\frac{K}{\gamma_0}\right)(A^*S + S^*A)\sin\theta\cos\theta\cos\phi - \left(\frac{K}{\gamma_0}\right)^2(G^*S + S^*G)\sin^2\theta\sin\phi\cos\phi\right\} \quad (6)$$

where

$$A = \sum_{n,n'} J_n\left(\frac{fK\sin\theta\sin\phi}{\gamma_0(1-\beta_0\cos\theta)}\right)J_{n'}\left(\frac{fK\sin\theta\cos\phi}{\gamma_0(1-\beta_0\cos\theta)}\right)\cdot e^{in'\pi/2}(2\delta_{n-n',f})$$

$$S = \sum_{n,n'} J_n('')J_{n'}('')e^{in'\pi/2}\left(\frac{\delta_{n-n'-1,f} - \delta_{n-n'+1,f}}{i}\right)$$

$$G = \sum_{n,n'} J_n('')J_{n'}('')e^{in'\pi/2}(\delta_{n-n'-1,f} + \delta_{n-n'+1,f}).$$

The arguments of Bessel functions J_n and $J_{n'}$ in the expansions S and G are the same as occur in A. For a long magnet, the electron motion attains a large amount of azimuthal symmetry, making the ϕ-dependence unimportant as $N \to \infty$. An

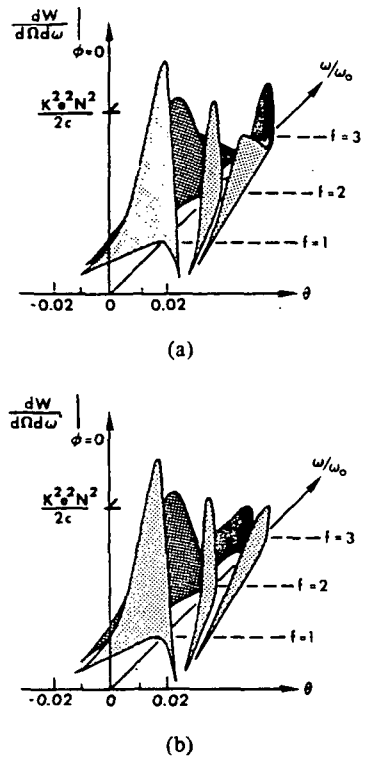

Fig. 1. The spontaneous emission is a sharp function of the observation angle θ and radiation frequency ω. In (a), a linearly polarized magnet radiates in the forward direction ($\theta = 0$) at odd harmonics f; while in (b), a helical magnet only radiates into $\theta \neq 0$ for $f > 1$. Both cases are for $K = 0.72$, $\gamma_0 = 100$.

addition theorem (Neumann's) for Bessel functions shows analytically that the ϕ-dependence may be removed from the arguments of the Bessel functions, and ϕ explicitly disappears as $N \to \infty$. As before, a complete spectrum would be a sum over all harmonics.

A plot of (6) is shown in Fig. 1(b). The fundamental line and first harmonic ($f = 1, 2$) are nearly the same shape as for the linear magnet, but each higher harmonic has only two symmetric lobes within the γ_0^{-1} radiation cone. On-axis, each harmonic occurs at $\omega \approx 2\gamma_0^2 f\omega_0$. In weak fields (6) gives twice the total forward power as from a linearly polarized magnet. This is because an electron in a circular magnet is experiencing maximum acceleration at all times in its trajectory.

In principle, there is the possibility of laser gain wherever there is nonzero spontaneous emission. In the exact forward direction, however, only the linear magnet radiates at $f = 3, 5, 7, \cdots$. It is for this case ($\theta = 0$) that we develop the nonlinear wave equation and examine stimulated emission. In the future, stimulated emission for $\theta \neq 0$ (in higher harmonics or the fundamental) is an interesting problem theoretically and experimentally.

Slow Optical Wave Evolution

Maxwell's wave equation governs the evolution of the light wave in the presence of an electron current. In the Coulomb (or transverse) gauge

$$\left(\vec{\nabla}^2 - \frac{1}{c^2}\frac{\partial^2}{\partial t^2}\right)\vec{A}(\vec{x}, t) = -\frac{4\pi}{c}\vec{J}_\perp(\vec{x}, t) \tag{7}$$

where $\vec{A}(\vec{x}, t)$ is the radiation vector potential and $\vec{J}_\perp(\vec{x}, t)$ is the transverse current density (CGS units). In order to describe stimulated emission, we must calculate the feedback of the light wave on the current; we must calculate the response of $\vec{J}_\perp(\vec{x}, t)$ to the presence of $\vec{A}(\vec{x}, t)$. When the laser is started, the optical wave grows from spontaneous emission to a large amplitude wave with a well-defined phase; after the coherent wave is established, its amplitude and phase can still evolve further. The following waveform is chosen to represent the laser optical wave during these stages of evolution:

$$\vec{A}(\vec{x}, t) = \frac{E(z, t)}{fk}(\sin(fkz - f\omega t + \phi(z, t)), 0, 0) \tag{8}$$

where $E(z, t)$ is the wave amplitude, f is the harmonic number so that $f\omega$ is the carrier frequency [note that ω was the frequency in (4)-(6); from now on it is $f\omega$], $\omega = kc$ is the fundamental, and the phase is $\phi(z, t)$. We imagine the laser is operating at selected frequency $f\omega$ and wavelength $\lambda/f = 2\pi/fk$. When the amplitude and phase of this waveform are held fixed, we have a plane wave traveling in the $\hat{z}$-direction. The polarization is chosen to match the spontaneous emission from a linearly polarized magnet $\vec{a} = (1, 0, 0)$.

The waveform above contains no dependence on x and y; a more complete description would give the wave some finite transverse dimension; we avoid this complication and describe only the essential physics of the problem in the longitudinal direction.

We now employ the slowly varying amplitude and phase approximation. The waveform above is inserted into the left-hand side of the wave equation; we assume that all terms containing two derivatives are small compared to terms containing fewer derivatives. The assumption of a slowly varying amplitude and phase anticipates long-range coherence and nearly monochromatic laser light; if the laser is well above threshold, this is a good assumption. The resulting wave equation now has only one component in the $\hat{x}$-direction:

$$\left(\frac{\partial E}{\partial z} + \frac{1}{c}\frac{\partial E}{\partial t}\right)\cos\alpha - E\left(\frac{\partial \phi}{\partial z} + \frac{1}{c}\frac{\partial \phi}{\partial t}\right)\sin\alpha = -\frac{2\pi}{c}J_{\perp x} \tag{9}$$

where $\alpha \equiv fkz - f\omega t + \phi$. The left-hand side is not yet slowly varying because of the "sin α" and "cos α" factors. Multiply (9) by cos α, then by sin α, to obtain two equations each with slow and fast factors:

$$\left(\frac{\partial E}{\partial z} + \frac{1}{c}\frac{\partial E}{\partial t}\right)(1 + \cos 2\alpha) - E\left(\frac{\partial \phi}{\partial z} + \frac{1}{c}\frac{\partial \phi}{\partial t}\right)\sin 2\alpha = -\frac{4\pi}{c}J_{\perp x}\cos\alpha$$

$$\left(\frac{\partial E}{\partial z} + \frac{1}{c}\frac{\partial E}{\partial t}\right)\sin 2\alpha - E\left(\frac{\partial \phi}{\partial z} + \frac{1}{c}\frac{\partial \phi}{\partial t}\right)(1 - \cos 2\alpha) = -\frac{4\pi}{c}J_{\perp x}\sin\alpha. \tag{10}$$

At any point in time, the fast factors on the left oscillate like $\cos(2fkz)$ over optical wavelengths. We therefore average over many optical wavelengths so that the fast factors are removed; we want (10) to describe the slow evolution of (E, ϕ) over many wavelengths. This gives

$$\frac{\partial \mathcal{E}}{\partial z} + \frac{1}{c}\frac{\partial \mathcal{E}}{\partial t} = -\frac{4\pi}{c}\overline{J_{\perp x}e^{i\alpha}} \tag{11}$$

where $\mathcal{E} = Ee^{i\phi}$ is the complex radiation field and $\overline{(\ )}$ implies an average over many optical wavelengths. The current $\overline{J_{\perp x} e^{i\alpha}}$ does not average to zero because both $J_{\perp x}$ and $e^{i\alpha}$ oscillate fast; when nearly resonant, we will see that the slow product drives the optical wave.

The wave equation now describes the dynamics of electrons and light over many optical wavelengths. Note that the last averaging step is not necessary for the helical magnet case [20]; the simpler algebra of the helical case is used in the "rotating wave" approximation of laser physics. However, the helical case is *so* simple (when $\theta = 0$) that there are no harmonics.

Single-Particle Dynamics

The dynamics of relativistic electrons in the combined static and radiation fields are governed by the Lorentz force equations:

$$\frac{d(\gamma\vec{\beta})}{dt} = -\frac{e}{mc}\left[\vec{E}_{op} + \vec{\beta} \times (\vec{B}_{op} + \vec{B}_m)\right]; \quad \frac{d\gamma}{dt} = -\frac{e}{mc}\vec{\beta}\cdot\vec{E} \tag{12}$$

where $\vec{E}_{op}$ and $\vec{B}_{op}$ are the optical wave's electric and magnetic fields obtained from $\vec{A}(\vec{x}, t)$ in (8) using the slowly varying amplitude and phase approximation. Now the electron energy γmc^2 will change in the presence of light-stimulated emission. Of these four equations only three are needed to completely solve the problem. We dispense with the z-component equation since $\gamma^{-2} = 1 - \vec{\beta}\cdot\vec{\beta}$ can relate the longitudinal and transverse motions. The static magnet is represented by

$$\vec{B}_m = B(0, \sin k_0 z, 0). \tag{13}$$

When $\gamma \gg 1$ the electric and magnetic optical fields nearly cancel in the transverse equation of motion; we neglect the transverse optical force compared to the transverse force of the static magnet: $E(1 - \beta_z) \ll \beta_z B_{op}$. This allows exact integration of the transverse equation and $\vec{\beta}_\perp = -(K/\gamma)(\cos k_0 z, 0, 0)$; perfect injection into long periodic orbits has been assumed and removes the constants of integration. The single-particle transverse current is now $-ec\vec{\beta}_\perp \delta^{(3)}(\vec{x} - \vec{r}_i(t))$ where $\vec{r}_i(t)$ is the trajectory of the ith electron. The total current is just the sum over all single-particle currents.

Insert $\vec{\beta}_\perp$ into the energy transfer equation to get

$$\frac{d\gamma}{dt} = \frac{eKE}{\gamma mc}\cos k_0 z \cos\alpha \tag{14}$$

and, using $\gamma^{-2} = 1 - \beta_\perp^2 - \beta_z^2$, we have

$$\beta_z = [1 - \gamma^{-2}(1 + \tfrac{1}{2}K^2 + \tfrac{1}{2}K^2 \cos 2k_0 z)]^{1/2}. \tag{15}$$

Changes in γ result in changes of β_z through (15); since $\gamma \gg 1$, it is quite accurate to use the expanded form of the square root.

All electron equations of motion contain factors which oscillate once per magnet wavelength; we actually want to describe the slow evolution about these periodic oscillations. Start by averaging (15) over one magnet wavelength to get $\bar{\beta}_z = 1 - \frac{1}{2}\bar{\gamma}^{-2}(1 + \frac{1}{2}K^2)$; now an average change in $\bar{\gamma}$ is related to an average change in $\bar{\beta}_z$. It is convenient to define a dimensionless velocity in terms of the magnet wavenumber k_0 and the wavenumber of the fundamental k:

$$\nu(t) \equiv L[(k + k_0)\bar{\beta}_z(t) - k]. \tag{16}$$

The initial dimensionless velocity of electrons $\nu_0 \equiv \nu(0)$ is crucial in determining the phase-space evolution. When $\nu = 0$, note that exactly one wavelength of light passes over the electrons as they pass through one period of the magnet; this gives the maximum coupling between light and electrons. If we integrate this dimensionless velocity in time, we get a dimensionless electron phase:

$$\zeta(t) \equiv (k + k_0)\bar{z}(t) - \omega t \tag{17}$$

where $\bar{z}(t) \equiv \int_0^t c\bar{\beta}_z(t')\,dt'$ and we have multiplied by c/L; note that $\dot{\zeta} \equiv d\zeta/d\tau = \nu$ where $\tau \equiv tc/L$. It is useful to think of ζ and ν as only measured at the end of every magnet wavelength; the fast periodic motion will factor out, leaving only the small change after each period. It is important to appreciate that ζ describes electron dynamics on the optical wavelength scale and that these spatial variations are typically much smaller than the magnet wavelength (by $\gamma^2 \sim 10^{-4}$).

We now recall the fast periodic factor and add it onto the slow motion:

$$z(t) \approx \bar{z}(t) - \frac{\lambda_0}{16\pi}\left(\frac{K}{\gamma}\right)^2 \sin 2\omega_0 t \approx \bar{z}(t) - \frac{\xi}{k}\sin 2\omega_0 t \tag{18}$$

where $\xi \equiv K^2/4(1 + \frac{1}{2}K^2)$. Within the argument of the fast factor $\sin 2\omega_0 t$, we have neglected small changes in ζ; this does not significantly alter the periodic motion through the magnet wavelengths since $\lambda \ll \lambda_0$. Also, the coefficient of the fast factor varies slightly with γ^{-2}, but for long magnets the maximum fractional change in γ is small ($\lesssim (2N)^{-1}$), so γ can be replaced by γ_0. In fact, since the electron energy never evolves far from resonance, we can also replace γ in (18) with the resonant energy $(k(1 + \frac{1}{2}K^2)/2k_0)^{1/2}$ to evaluate the constant coefficient ξ/k. Typically, $K \approx 1$ (and $\xi \approx 1/6$) so the fast, periodic longitudinal motion occurs on the optical wavelength scale and causes higher harmonics.

The energy transfer equation can now be written more explicitly in terms of fast and slow variables:

$$\frac{d\gamma}{dt} = \frac{eKE}{2\gamma mc}\left[\cos(f\zeta + \phi - (f-1)\omega_0 t - f\xi \sin(2\omega_0 t)) + \cos(f\zeta + \phi - (f+1)\omega_0 t - f\xi \sin(2\omega_0 t))\right]. \tag{19}$$

The factors $f \pm 1$ show how extra oscillations occur at each magnet wavelength in the higher harmonics; since ξ is not necessarily small, the fast terms cannot be expanded outside of the cosines to any finite order. Use the generating function to expand the sinusoidal terms in Bessel functions and average (19) over one magnet period to obtain

$$\frac{d\gamma}{d\tau} = \frac{eK_f(\xi)EL}{2\gamma mc^2}\cos(f\zeta + \phi) \tag{20}$$

where

$$K_f(\xi) \equiv K(-1)^{(f-1)/2}\left[J_{(f-1)/2}(f\xi) - J_{(f+1)/2}(f\xi)\right] \quad \text{for } f = 1, 3, 5 \cdots.$$

The cylindrical Bessel functions in $K_f(\xi)$ express a weighted coupling between electrons and light; the weighting is mea-

sured by f and ξ (or K) and is due to the time electrons spend in periodic longitudinal motion instead of transferring energy to the optical wave. A helical magnet has $K_f(\xi) \to 2K$ in (20). The result (20) has been derived by Madey [22] [except for some misprints in $K_f(\xi)$] and gain in the higher harmonics is found using energy conservation (which is only appropriate for low gain). We proceed now to the more general nonlinear wave equation.

The Nonlinear Wave Equation

The total beam current driving the wave equation is the sum of all single-particle currents. To evaluate the single-particle currents we use the same procedure as in (20). We follow the current in a small volume element: 1) much larger than an optical wavelength, 2) much smaller than the optical pulse length, and 3) very much smaller than the magnet wavelength. All electrons in the volume element experience the same fast motion together. When averaging $\overline{J_{\perp x} e^{i\alpha}}$ over a magnet period, we experience the same integrals as in (20); the electron current then becomes

$$\overline{J_{\perp x} e^{i\alpha}} = \frac{ec}{2} \sum_i \overline{\frac{K_f(\xi)}{\gamma}} e^{i(f\zeta+\phi)} \delta^{(3)}(\vec{x} - \vec{r}_i(t)). \tag{21}$$

In order to evaluate Σ_i we choose to label all electrons by their initial positions ζ_0 and velocities ν_0; this definition is unique and rigorously defines the electron beam current (Jean's theorem). The electrons are initially spread uniformly over each optical wavelength. Although particles become redistributed over each optical wavelength, this does not affect the average density in any macroscopic section of the beam several wavelengths long. The energy spread and emittance of the electron source are carefully chosen to give a minimal spread in resonance parameters ν_0. Therefore, on a macroscopic scale neither the bunching mechanism nor an initial velocity spread alter the macroscopic electron pulse shape and it travels undistorted through the interaction region. Microscopically, however, the electron's initial position within the wavelength of light and its resonance parameter (ζ_0, ν_0) are crucial in determining the result of its interaction with the wave. The beam current density in a volume element dV (which is large compared to an optical wavelength, but small compared to the pulse size and magnet wavelength) is found by averaging over sample electrons and then weighting this result by the macroscopic particle density $\rho(z)$ within dV. Indicating the appropriate microscopic average over (ζ_0, ν_0) by $\langle\ \rangle$, the current driven wave equation becomes

$$\frac{\partial \mathcal{E}}{\partial z} + \frac{1}{c} \frac{\partial \mathcal{E}}{\partial t} = -2\pi e K_f(\xi) \rho(z - \beta_0 ct) \left\langle \frac{e^{-if\zeta}}{\gamma} \right\rangle_{(z-\beta_0 ct)} \tag{22}$$

where $\rho(z - \beta_0 ct)$ is the density of the traveling electron pulse shape, and the average $\langle\ \rangle_{(z-\beta_0 ct)}$ flows along with a volume element of the electron pulse at speed $\beta_0 c$. The optical wave only slowly passes over the relativistic electrons at speed $c(1 - \beta_0) \approx c/2\gamma^2$; this situation is quite distinct from atomic lasers.

The complete system of (20) and (22) with (16) and (17) is now slowly varying. If we use $\bar{\beta}_z = 1 - \frac{1}{2}\gamma^{-2}(1 + \frac{1}{2}K^2)$ and (16) to eliminate γ on the left side of (20), we see that the electron dynamics are governed by the self-consistent pendulum [5]

$$\frac{d^2\zeta}{d\tau^2} = \left(\frac{2\pi e L N K_f(\xi) E}{\gamma^2 mc^2} \right) \cos(f\zeta + \phi). \tag{23}$$

It has been enlightening to consider the pendulum phase-space paths as guiding electrons, even as the paths themselves are being slowly changed by E and ϕ self-consistently [6], [27].

The coupled equations (22) and (23) [or (20)] are suitable for solving pulse propagation problems in the free-electron laser; we will not proceed with the pulse problem further, but note that the form of the wave equation is the same as for the helical magnet where several aspects of the problem have been solved [6].

We assume that $\rho(z) = \rho_0$ is uniform and study a simpler wave equation; $\partial/\partial z$ does not now occur in (22), or it can be removed by the method of characteristics. It is convenient to combine some constants in these equations so that we may study their properties systematically and comprehensively. For long, periodic magnets, it is useful to note that the changes in γ are always small $[\lesssim (2N)^{-1}]$. We replace γ throughout the wave and pendulum equations with either its initial value γ_0 or the resonant energy $(k(1 + \frac{1}{2}K^2)/2k_0)^{1/2}$ where $\nu = 0$; these choices are nearly equivalent and lead to no significant error. Define a new field strength as

$$|a| \equiv \left(\frac{2\pi N e f K_f(\xi) L E}{\gamma_0^2 mc^2} \right) \text{ and } r \equiv \left(\frac{4\pi^2 N e^2 f K_f^2(\xi) L^2 \rho_0}{\gamma_0^3 mc^2} \right). \tag{24}$$

Now the wave and pendulum equations can be written more compactly:

$$\dot{a} = -r\langle e^{-if\zeta} \rangle_{\nu_0}, \qquad \ddot{f\zeta} = |a| \cos(f\zeta + \phi) \tag{25}$$

where $\dot{(\ )} \equiv d(\ )/d\tau$ and $a = |a| e^{i\phi}$. We have assumed that the electron beam is initially monoenergetic and uniformly spread so that $\langle\ \rangle$ contains only one parameter ν_0, as written explicitly above. Not only have the number of parameters been reduced, but the values of these parameters give us an immediate "picture" of dynamics in the pendulum phase space.

To get a feel for the parameters $|a|$ and r in terms of physical variables, consider $N = 10^2$, the fundamental $f = 1$, $K_f = 1$ (for a magnet providing $B \approx 3 \times 10^3$ G and $\lambda_0 \approx 3$ cm), $L = 300$ cm, $\gamma_0 = 10^2$, $\rho_0 = 10^{10}$ cm^{-3} (a current density of 50 A/cm^2 usually over a 1 mm diameter beam), and $E = 200$ stat · V/cm (for a laser power of 10^8 W/cm^2); then $r \approx 1$ and $|a| \approx 10$. Such a laser would produce 3 μm radiation.

The meaning of $|a| \ll 1$ is that we have weak optical fields in the self-consistent pendulum equation; the closed orbit region has height $2|a|^{1/2}$ and is small. All electrons are in open orbits if $\nu_0 > 2|a|^{1/2}$, and some electrons are in closed orbits when $\nu_0 < 2|a|^{1/2}$. Significant energy transfer requires that ν_0 be not too far from resonance $|\nu_0| \lesssim 10$, so, when $|a| \gg 1$, the electrons become trapped in closed orbits and gain decreases. This is the saturation mechanism.

The parameter r determines the rate at which things happen, and is a measure of gain in this system. In fact, the maximum weak field, low gain [5] is just $g_{\max} = 0.13504r$. The result

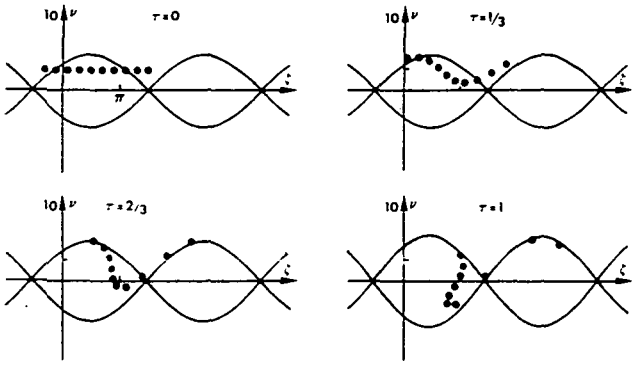

Fig. 2. The electron phase space shows beam evolution and bunching at optical wavelengths; the self-consistent separatrix serves as a guide to the optical wave evolution.

can be obtained by a simple expansion of (25) in powers of the field $|a| \ll 1$. The fractional gain in power is defined as $g \equiv (a/a_0)^2 - 1$ where a_0 is the initial field strength. If $r \approx 1$, we expect about 10 percent gain per pass through the laser (typical), and if r is larger the gain will be larger.

The coupled system of (25) contains $a = |a|e^{i\phi}$ and $f\zeta$ as three dynamical variables; their evolution during the time interval $0 < \tau < 1$ is governed by four independent parameters: $|a_0|$ and ϕ at $\tau = 0$, r, and ν_0. The initial optical phase ϕ is arbitrary, however, and we always start it at zero; this still leaves three parameters a_0, r, and ν_0. It has been stated [21] that an equivalent set of equations for the fundamental frequency contains only two parameters; this appears to be incorrect unless a_0 is taken to be arbitrarily small, as if started from noise. The phase space (ζ, ν) gives an excellent understanding of electron beam dynamics for a given set of parameters a_0, r, and ν_0. We only consider $f = 1$ now. Since the pendulum equation is periodic in ζ, we need only to look at one 2π section of phase space; this is only one optical wavelength of the electron beam. All other sections evolve in the same way. The beam can be represented by a few sample electrons uniformly spread along the ζ-axis and positioned at $\nu = \nu_0$ on the velocity (or energy) axis. See Fig. 2 at $\tau = 0$.

The "separatrix" equation is a locus of the phase-space points (ζ_s, ν_s) which separate the closed orbits from open orbits in the phase space:

$$\nu_s^2(\zeta_s) = 2|a|(1 + \sin(\zeta_s + \phi)). \tag{26}$$

Not only does the separatrix indicate the guiding phase-space paths, but the dynamics of the separation itself tells us about the optical wave through $|a|$ and ϕ. A shift in the separatrix indicates a shifting phase $\phi(\tau)$; growth of the separatrix height ($4|a|^{1/2}$ from peak to peak) indicates a change in the optical wave amplitude. Thus, in a single "picture"—the pendulum phase space with a self-consistent separatrix—we can exhibit the dynamics of all variables in the free-electron laser: (ζ_i, ν_i) for each electron and $(|a|, \phi)$ for the optical wave.

An example is shown in Fig. 2. Ten sample electrons start out at energy $\nu = \nu_0$ and are uniformly spread from $-\pi/2$ to $3\pi/2$, covering one 2π closed orbit section. With the independent parameters $a_0 = 5$, $r = 10$, and $\nu_0 = 2.6$, the ten electrons closely follow the paths indicated by the separatrix, even though it is only a guide. In this example, bunching about the π phase is clear; this is necessary for gain [see (25)]. An energy transfer is also clear, since electrons have moved down in phase space and lose energy to the optical wave. The resulting wave growth and accompanying phase shift are visible in the separatrix. A characteristic energy spread is seen to develop in the electron beam.

While Fig. 2 follows the evolution of slow coordinates, it is interesting to consider the fast, periodic motion of (18) in the same phase space. The fast term in (18) gives $\delta\zeta = -\xi \sin 2\omega_0 t$ and $\delta\nu = -4\pi N\xi \cos 2\omega_0 t$. For $N = 10^2$ and $K = 1 (\xi = 1/6)$, the vertical excursions of each particle to $\delta\nu \approx \pm 200$ are far off-scale; there are $N = 10^2$ such oscillations during $\tau = 0 \rightarrow 1$. Fortunately, this "blur" of fast motion closely follows (ζ, ν) which describes bunching and drives the wave equation.

Harmonics

Before examining the wave equation extensively, we discuss free-electron laser operation in a selected higher harmonic [28]. Note that f can only have odd values, since spontaneous emission is generated only in the odd harmonics when $\theta = 0$:

$$\left.\frac{dW}{d\Omega d(f\omega)}\right|_{\theta=0} = \left(\frac{eN\gamma_0 f}{1 + \frac{1}{2}K^2}\right)^2 \frac{K_f^2(\xi)}{c} \qquad f = 1, 3, 5 \cdots. \tag{27}$$

Recall that the gain r in higher harmonics is also directly proportional to $K_f^2(\zeta)$.

We have carefully written (25) to clarify the pendulum and wave evolution in higher harmonics. The dynamical variable $f\zeta$ evolves just like ζ alone in the fundamental. The occurrence of $f\zeta$ instead of ζ expresses that we are dealing with a new wavelength in the higher harmonics; the pendulum equation is still periodic in ζ, but the range of phases to consider is only $2\pi/f$. If we merely change the phase-space coordinate axes to $(f\zeta, f\nu)$, the phase-space dynamics in higher harmonics are the same as the fundamental.

However, the definitions of $|a|$ and r show how K_f modifies the real field and gain. In Fig. 3 we plot K_f as a function of K, for a range of the harmonics f. It is useful to view K_f as a coupling constant; it occurs in both the pendulum and wave equation. For fixed f, $K_f(\xi)$ is determined by the magnet design through $K = eB\lambda_0/2\pi mc^2$; $\xi \equiv K^2/4(1 + \frac{1}{2}K^2)$. For $K \ll 1$, the coupling constant decreases to zero for all harmonics f. At large K, $K_f \propto K$ with a slope determined by the Bessel functions; the coupling constant is positive for $f = 1, 5, 9$, etc., and negative for $3, 7, 11$, etc. But the wave and pendulum equations are invariant to the transformation $K_f \rightarrow -K_f$ and $\phi \rightarrow \phi + \pi$ (or $E \rightarrow -E$), so alternate harmonics merely produce a wave that is 180° out of phase with the other harmonics.

The practical possibility of extending free-electron laser operation to higher harmonics is important. A given electron source (storage ring, Van de Graaf, linac, etc.) may be "tunable" over a X3 range in γ; this gives a X10 range in laser wavelengths since $\lambda \sim \lambda_0/2\gamma^2$. The use of higher harmonics

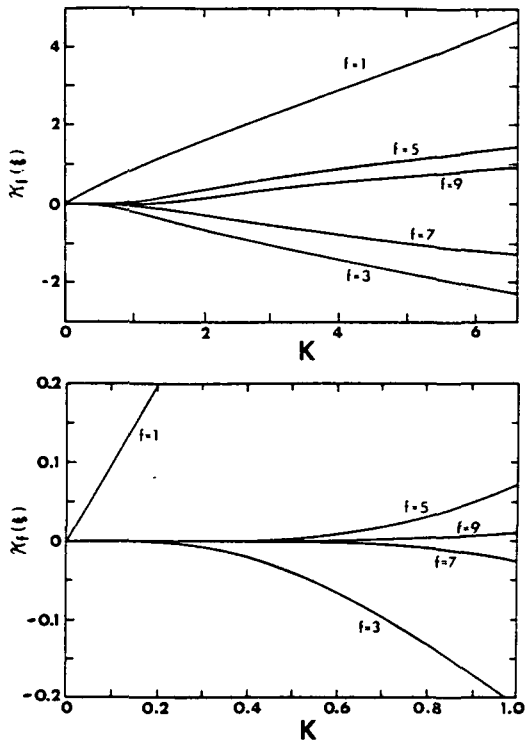

Fig. 3. The coupling constant $K_f(\xi)$ depends on the magnet design and the harmonic number f. Generally, the magnitude of K_f increases with K and decreases with f; for f even $K_f = 0$, and the odd harmonics alternate in sign.

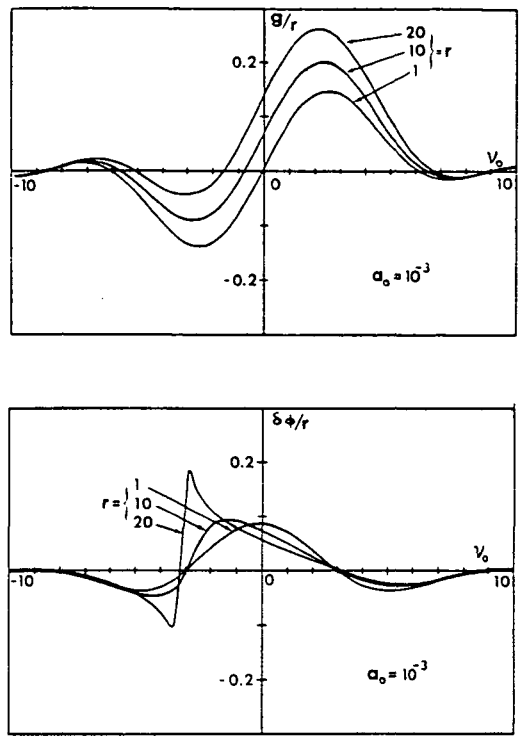

Fig. 4. The normalized change in the optical field amplitude $g/r = (a^2/a_0^2 - 1)/r$ and phase $\delta\phi/r$ as a function of the resonance parameter ν_0 form the gain curve. As r increases, g/r becomes more symmetric, and $\delta\phi/r$ becomes divergent for high absorption. The initial fields are weak: $a_0 = 10^{-3}$.

can extend the tunable range by another factor of 10 or 20! The limitation comes from the decrease in fK_f^2 gain for large f. If $K = 1$ and the experimentalist's gain is $\times 10^3$ above threshold, he could run in the $f = 9$th harmonic. With higher K values, say $K = 2 \to 10$, operation in the higher harmonics is more feasible. With $K = 6$, the penalty for using the $f = 9$th harmonic is only $\times 2$. This may be most important for low γ free-electron lasers [29], which tend to have large $r \sim 10^2$ (plenty of gain), but to produce long wavelengths $\lambda \sim 200\ \mu$m.

While the gain in higher harmonics is given by $g_f/g_{f=1} = fK_f^2$, the final saturation still occurs at $|a| \gtrsim 2\pi$; the optical power at saturation is given by $P_f/P_{f=1} = (K_1/fK_f)^2$.

Another interesting point that may be explored experimentally is the operation of the free-electron laser at several harmonics simultaneously, say $f = 1$ and 5 together. There is no difficulty in imagining that the electron beam could become bunched on multiple scales of the frequency, say λ and $\lambda/5$.

High and Low Gain, Weak and Strong Fields

We now turn to exploring the more general dynamics of the wave equation. Since the only explicit occurrence of f in (25) is $f\zeta$, and f can be removed by a coordinate transformation, we need not discuss higher harmonics specifically. These results also apply to the helical magnet; (25) can formally be converted to the helical case with the prescription 1): $K_f \to K$ and 2): $|a| \to 2|a|$ in the pendulum equation. It is useful to give the definitions a_0, r, and ν_0 in terms of the physical variables

$$a_0 = \frac{e^2 BE(0)L^2}{(\gamma_0 mc^2)^2}, \qquad r = \frac{e^4 B^2 \lambda_0 \rho_0 L^3}{(\gamma_0 mc^2)^3},$$

$$\nu_0 = L[(k + k_0)\beta_z(0) - k] \tag{28}$$

so that it is clear that each can be manipulated separately. We view a_0 as measuring the input laser field and r as the electron density or gain. For a fixed initial electron beam velocity $\beta_z(0)c$, we think of the resonance parameter ν_0 as a measure of various optical modes, or k's, that could be excited by the laser; the range of relevant resonance parameters is $|\nu_0| \lesssim 10$, since there is little energy exchange for $|\nu_0| \gtrsim 10$.

The changes in the optical wave during the evolution time $\tau = 0 \to 1$ are measured by $g \equiv a^2(1)/a^2(0) - 1$ and $\delta\phi \equiv \phi(1) - \phi(0) = \phi(1)$. These changes are a function of the resonance parameter ν_0, with a_0 and r as parameters. $g(\nu_0)$ is now known as the "gain curve;" we propose generalizing this name to include $\delta\phi(\nu_0)$. Furthermore, since r is roughly a measure of gain, it makes sense to plot a new "gain curve" measured in units of r: $g(\nu_0)/r$ and $\delta\phi(\nu_0)/r$. This definition also has the advantage of easily showing the effects of large and small gain on a single scale.

In Fig. 4 we see $g(\nu_0)/r$ and $\delta\phi(\nu_0)/r$ for small and large rates r with weak initial fields $a_0 = 10^{-3}$; we have simply integrated the nonlinear coupled equation (25). For small rates $r = 1$ and weak fields we have the well-known antisymmetric gain curve originally found in the first free-electron laser paper [1]. With higher gains $r = 10$ and 20, gain is somewhat underestimated by r alone and g becomes somewhat more symmetric about resonance. This distortion of the normally antisymmetric gain

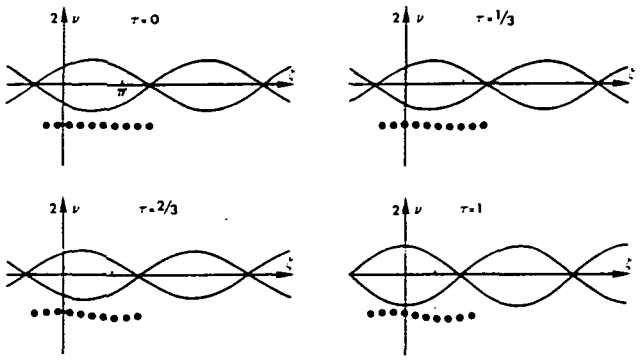

Fig. 5. In the case of large r, the optical wave can shift its phase to optimize the location of the electron bunch causing gain for $\nu_0 \lesssim 0$.

curve has been presented previously [30], but with the implication that the cause was collective Coulomb forces; we find here that the effect is merely due to high gain and the accompanying phase shift.

This can be understood by looking at $\delta\phi$. On resonance ($\nu_0 = 0$) we see the maximum phase shift and little gain. When gain r is large, that phase shift may be large since $\delta\phi \propto r/|a|$; in fact, the optical wave changes its phase so that the electron bunching is in the optimal position within the optical wavelength. In Fig. 5, for $r = 20$ and weak fields $a_0 = 0.1$, we look at $\nu_0 = -1$, which would typically give negative gain. The self-consistent separatrix shows that $\phi(\tau)$ increases to move the optical wave "under" the electron bunch that originally formed at $\sim\pi/2$; with $\delta\phi \sim \pi/2$, the phase-space arrangement has still overpopulated the π phase and drives the wave. Note that the optical phase shift $\phi(\tau)$ should be interpreted as a change in frequency of the optical wave; specifically, $\omega(\tau) = \omega + c\dot{\phi}/L$.

An interesting feature of $\delta\phi$ in Fig. 4 is its behavior around $\nu_0 \sim -\pi$; recall that $|a|$ is experiencing negative gain or absorption here. Furthermore, the phase shift crudely goes as $\delta\phi \sim r/|a|$. So when $|a| \to 0$, we should find a discontinuity and peculiar behavior in $\delta\phi$; $\phi(\tau)$ is of little consequence, however, when $|a| \approx 0$.

Fig. 6 represents gain curves for weak and strong fields $a_0 = 0.1$, 10, 15 in the low gain case $r = 1$. As the fields become stronger, all modes in the free-electron laser eventually saturate. An important feature of this process is that the point of maximum gain moves away from resonance; it starts at 2.6 in weak fields and moves to ~5 or 6. The accompanying phase shift also diminishes in stronger fields and becomes wider in ν_0.

The broadening of both g and $\delta\phi$ is due to the large closed orbit region in strong fields (proportional to $4|a|^{1/2}$), as shown by the large separatrix in Fig. 7. Something like $\delta\nu \sim |a|^{1/2}$ of the electron beam energy can be extracted in these deep optical "buckets" and this occurs over a wide range of resonance parameters. Saturation occurs because the optical power needed to achieve the deep buckets increases as $|a|^2$; eventually deep buckets must decrease gain.

For high gain and strong fields we see a more symmetric gain curve, and a decrease in all modes due to high fields. This is shown in Fig. 8 for $r = 10$ now and $a_0 = 0.1$, 10, and 15. These curves can give a better feeling for how the laser works

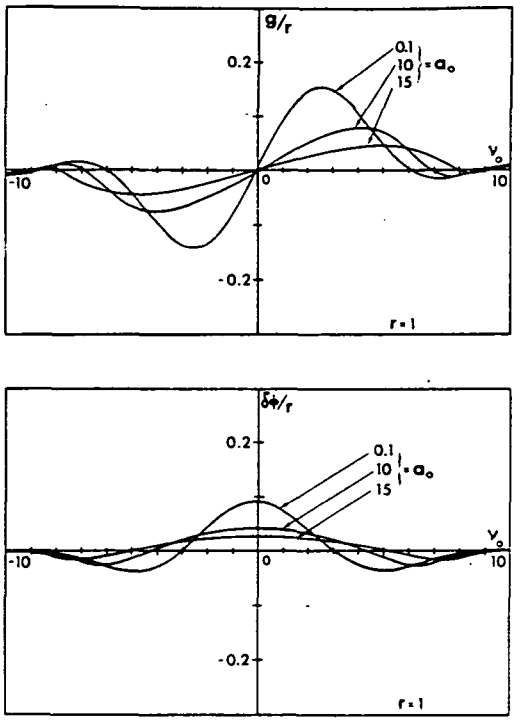

Fig. 6. The gain and phase shift decrease in strong optical fields; maximum gain occurs at larger ν_0.

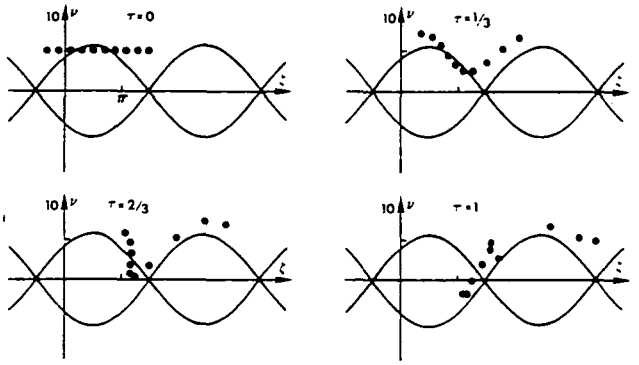

Fig. 7. At saturation, the self-consistent separatrix is too large ($4|a|^{1/2}$ peak-to-peak) and the electron bunch disperses at the end of the laser.

in a variety of situations; most of the important physics of the wave and pendulum equations has now been displayed.

Coulomb Forces

We have seen that the parameter r is proportional to the electron density and would be a measure of the importance of Coulomb forces. Within the single-particle philosophy, we should try to calculate the force on a given electron due to the presence of all the other electrons in the beam. A more traditional approach assumes a form for the plasma waves and solves the nonlinear Boltzmann equation [7]. We do not assume a form for $\rho(z)$ other than its periodicity [23].

Consider the situation where some bunching in the electron beam has already occurred; we calculate the Coulomb forces due to an arbitrary, but periodic, density variation in the electron beam. The electron beam is taken to be of infinite ex-

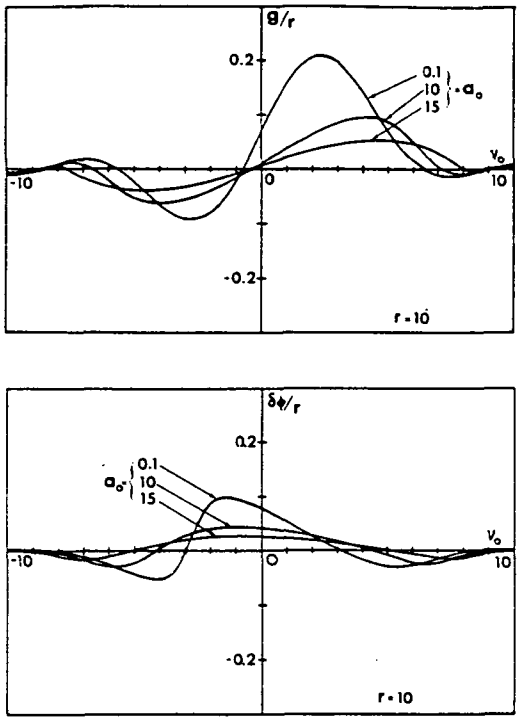

Fig. 8. The high gain and strong field effects in Figs. 4 and 6 merely combine to distort the weak field, low gain curve.

tent in all directions, as in the previous calculations. Poisson's equation $\vec{\nabla} \cdot \vec{E} = -4\pi e\rho$ in one dimension becomes

$$\frac{\partial E_z(z)}{\partial z} = -4\pi e\rho(z) = -4\pi e\rho(z + \lambda). \tag{29}$$

The one-dimensional Green's function for this operator is $G(z - z') = 2\pi[\theta(z - z') - \theta(z' - z)]$. In one dimension, a "point" source $\rho \sim \delta(z - z_0)$ is an infinite disk which exerts a force on a test charge independent of distance: $E_z \propto z/|z|$; our $\rho(z)$ is a periodic density of such disks.

The long range periodicity of $\rho(z)$ gives long-range periodicity to $E_z(z)$, and E_z can only respond to variations $\rho(z) - \rho_0$ in the electron density. Then

$$E_z(z) = -2\pi e\left(\int_{\infty}^{0} + \int_{0}^{z} - \int_{z}^{\lambda} - \int_{\lambda}^{\infty}\right)(\rho(z') - \rho_0)\,dz'. \tag{30}$$

The two infinite integrals contain no z-dependence and their infinite contributions must nearly cancel to leave a constant.

Since $\rho(z)$ is periodic, we should be able to solve the problem for just one section of the electron beam from $0 < z < \lambda$. The total charge for one section is conserved and is $\rho_0\lambda$; if not, the long-range periodicity would be spoiled. We can now write

$$E_z(z) = \text{constant} - 4\pi e\int_0^z (\rho(z') - \rho_0)\,dz'. \tag{31}$$

$E_z(z)$ also must be periodic and averaging E_z over a single wavelength must give zero; otherwise electrons would feel a net force to the left or right. Averaging (31) allows us to determine the unknown constant. The electric field in the longitudinal direction is now completely determined. To make contact with our previous notation, define $\zeta = kz$:

$$E_z(\zeta) = -4\pi e\rho_0\lambda\sigma(\zeta) \tag{32}$$

where

$$\sigma(\zeta) \equiv \int_0^{\zeta} \frac{\rho(\zeta')}{\rho_0}\frac{d\zeta'}{2\pi} - \frac{\zeta}{2\pi} + \frac{1}{2} - \int_0^{2\pi}\frac{d\zeta'}{2\pi}\int_0^{\zeta'}\frac{\rho(\zeta'')}{\rho_0}\frac{d\zeta''}{2\pi}.$$

The scale factor $4\pi e\rho_0\lambda$ measures the strength of Coulomb forces. $\sigma(\zeta)$ is of order unity and is easily evaluated numerically given the particle positions.

As an example, suppose all the charge is accumulated in one sharp disk $\rho(\zeta) = 2\pi\rho_0\delta(\zeta - \zeta_0)$; this is a perfectly bunched beam. The resulting field is

$$E_z(\zeta) = -4\pi e\rho_0\lambda\left(\frac{\zeta_0}{2\pi} - \frac{\zeta}{2\pi} \pm \frac{1}{2}\right) \quad \text{for} \quad \begin{pmatrix}\zeta > \zeta_0\\ \zeta < \zeta_0\end{pmatrix}. \tag{33}$$

This is merely the field from an infinite series of equally spaced disks.

We need to incorporate the new electrostatic Coulomb force in the electron equation of motion. The longitudinal Coulomb field does not occur in the transverse equations, so their solution $\vec{\beta}_\perp$ remains the same. The energy transfer equation, however, contains E_z and adds a term to the self-consistent pendulum equation. The coupled wave and pendulum equations are now

$$\ddot{f\zeta} = |a|\cos(f\zeta + \phi) - \left(\frac{r}{4N\xi}\right)\sigma(f\zeta) \tag{34}$$

$$\dot{a} = -r\langle e^{-if\zeta}\rangle_{\nu_0}$$

where N is the number of magnet periods, and $\xi = K^2/4(1 + \frac{1}{2}K^2)$. The coefficient can be written as the relativistic plasma frequency in dimensionless form: $r/4N\xi = 2\pi\Omega_p(1 + \frac{1}{2}K^2)$ where $\Omega_p^2 = \omega_p^2L^2/\gamma^3c^2$ and $\omega_p^2 = 4\pi e^2\rho_0/mc^2$ is the nonrelativistic plasma frequency. Note that both the optical wave $a(\tau)$ and plasma frequency Ω_p drive the wave equation through the pendulum equation; therefore, $\phi(\tau)$ and the optical frequency are affected by Ω_p.

When the beam is uniform, $\sigma(\zeta)$ is zero; nonzero Coulomb forces develop when the optical wave causes bunching. To estimate the maximum strength of Coulomb forces, set $\sigma(\zeta) \to 1$; to estimate their effect, ask whether an electron can be moved an appreciable fraction of an optical wavelength during a single pass through the laser. This requires that $r \gtrsim 16\pi N\xi \sim 10^3$. We see that Coulomb forces are negligible except for extremely high gains; most proposed free-electron lasers use $r < 10$. Our point here is not that Coulomb forces are always unimportant (although they are important in only a few cases), but that severe high-gain effects occur long before r reaches $16\pi N\xi$. Typically, only a tiny fraction of a plasma oscillation occurs during $\tau = 0 \to 1$ with typical values of r.

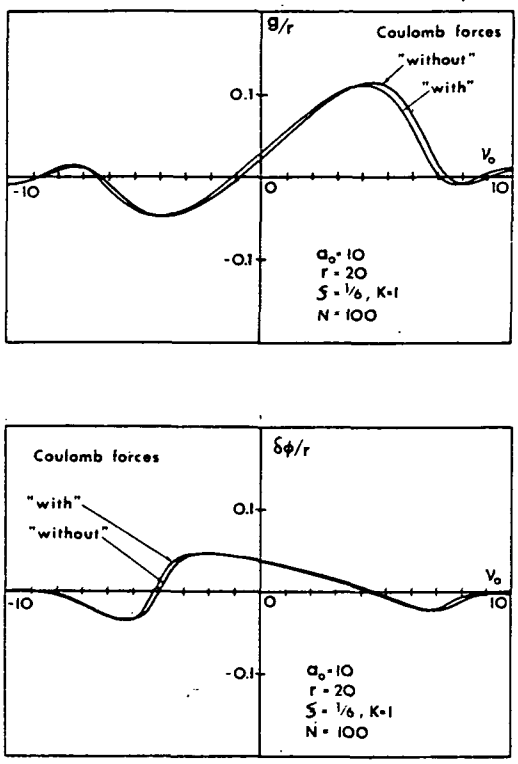

Fig. 9. Interelectron Coulomb forces only slightly distort the gain curve for the parameters explored in this paper.

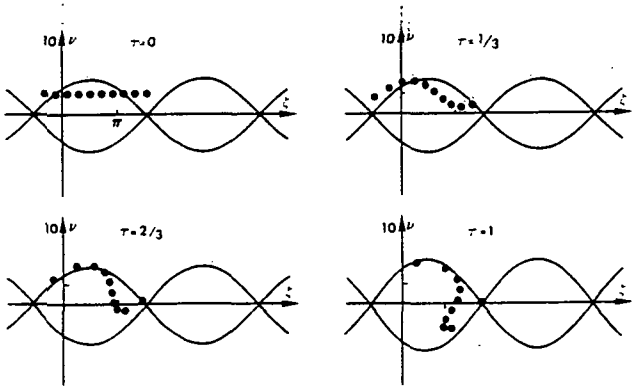

Fig. 10. With Coulomb forces included, we can compare the electron phase-space evolution to Fig. 2; there is little change. We have imposed periodic boundary conditions so that electrons stay in $-\pi/2 < \zeta < 3\pi/2$.

We reexamine the gain curve with the inclusion of Coulomb forces in Fig. 9. We chose $a_0 = 10$ to get good bunching and $r = 20$ for a large density; $N = 100$ and $\xi = 1/6$, $(K = 1)$, so that $r/4N\xi = 3$. We see that Coulomb forces play a minor role even when r is as large as 20; at the same time, high-gain effects are quite important. In Fig. 10 we compare the phase-space evolution of electrons (with Coulomb forces included) to a previous high-gain example $a_0 = 5$ and $r = 10$. The electron positions have a discernable effect on each other, but bunching occurs in much the same way. (Periodic boundary conditions restrict ζ to the interval $-\pi/2$-$3\pi/2$ so that $\rho(\zeta)$ can be determined.)

Acknowledgment

The author wishes to acknowledge helpful discussions with J.M.J. Madey, S. B. Segall, P. Michelson, L. R. Elias, and J. Galardo.

References

[1] J.M.J. Madey, "Stimulated emission of bremsstrahlung in a periodic magnetic field," *J. Appl. Phys.*, vol. 42, pp. 1906-1913, 1971.

[2] L. R. Elias, W. M. Fairbank, J.M.J. Madey, H. A. Schwettman, and T. I. Smith, "Observation of stimulated emission of radiation by relativistic electrons in a spatially periodic transverse magnetic field," *Phys. Rev. Lett.*, vol. 36, pp. 717-720, 1976.

[3] D.A.G. Deacon, L. R. Elias, J.M.J. Madey, G. J. Ramian, H. A. Schwettman, and T. I. Smith, "First operation of a free electron laser," *Phys. Rev. Lett.*, vol. 38, pp. 892-894, 1977.

[4] F. A. Hopf, P. Meystre, M. O. Scully, and W. H. Louisell, "Classical theory of a free electron laser," *Phys. Rev. Lett.*, vol. 37, pp. 1215-1218, 1976.

[5] W. B. Colson, "One-body electron dynamics in a free electron laser," *Phys. Lett.*, vol. 64A, pp. 190-192, 1977.

[6] —, "One-body analysis of free electron lasers," in *Physics of Quantum Electronics*, vol. 5, Jacobs *et al.*, Eds. Reading, MA: Addison-Wesley, 1978.

[7] *Physics of Quantum Electronics*, vols. 5 and 7, Jacobs *et al.*, Eds. Reading, MA: Addison-Wesley, 1980.

[8] W. Colson, "Theory of a free electron laser," *Phys. Lett.*, vol. 59A, pp. 187-190, 1976.

[9] —, "Free electron laser theory," Ph.D. dissertation, Stanford University, 1977, publication 78-02, 145, Univ. Microfilm Inst., Ann Arbor, MI.

[10] W. Becker and H. Mitter, "Quantum theory of a free electron laser," *Z. Physik*, vol. 35B, pp. 399-404, 1979.

[11] A. Bambini, A. Renieri, and S. Stenholm, "Classical theory of the free electron laser in a moving frame," *Phys. Rev.*, vol. 19A, pp. 2013-2025, 1979.

[12] V. N. Baier and A. I. Milstein, "On free electron laser theory," *Phys. Lett.*, vol. 65A, pp. 310-312, 1978.

[13] N. M. Kroll and W. A. McMullin, "Stimulated emission from relativistic electrons passing through a spatially periodic transverse magnetic field," *Phys. Rev.*, vol. 17A, pp. 300-308, 1978.

[14] H. Al-Abawi, F. A. Hopf, G. T. Moore, and M. O. Scully, "Coherent transients in the free-electron laser: Laser lethargy and coherence brightening," *Opt. Commun.*, vol. 30, pp. 235-238, 1979.

[15] P. Sprangle, C. Tang, and W. Manheimer, "Nonlinear formulation and efficiency enhancement of free electron lasers," *Phys. Rev. Lett.*, vol. 43, pp. 1932-1935, 1979.

[16] —, "General non-linear theory of free electron lasers and efficiency enhancement," in *Physics of Quantum Electronics*, vol. 7, Jacobs *et al.*, Eds. Reading, MA: Addison-Wesley, 1980, ch. 8.

[17] D. B. McDermott and T. C. Marshall, "The collective free electron laser," in *Physics of Quantum Electronics*, Jacobs *et al.*, Eds. Reading, MA: Addison-Wesley, 1980, ch. 18.

[18] T. Kwan, J. M. Dawson, and A. T. Lin, "Free electron laser," *Phys. Fluids*, vol. 20, pp. 581-588, 1977.

[19] A. T. Lin and J. M. Dawson, "High-efficiency free electron laser," *Phys. Rev. Lett.*, vol. 42, pp. 1670-1673, 1979.

[20] W. Colson and S. K. Ride, "The nonlinear wave equation for free electron lasers driven by single-particle currents," *Phys. Lett.*, vol. 76A, pp. 379-382, 1980.

[21] P. Sprangle and C. Tang, "Formulation of non-linear free electron laser dynamics with space charge effects and spatially varying wiggler," in *Proc. 4th Int. Conf. Infrared Millimeter Waves and Their Applications*, Miami Beach, FL, Dec. 10-15, 1979.

[22] J.M.J. Madey and R. C. Taber, "Equations of motion for a free-electron laser with a transverse gradient," in *Physics of Quantum Electronics*, vol. 7, Jacobs *et al.*, Eds. Reading, MA: Addison-Wesley, 1980, ch. 30.

[23] W. B. Colson and S. B. Segall, "Energy transfer in constant period free-electron lasers," *Appl. Phys.*, vol. 22, pp. 219-225, 1980.

[24] L. R. Elias and J.M.J. Madey, "Superconducting helically wound magnet for the free electron laser," *Rev. Sci. Instr.*, vol. 50, pp. 1335-1340, 1979.

[25] B. M. Kincaid, "A short period helical wiggler as an improved

source of synchrotron radiation," *J. Appl. Phys.*, vol. 48, pp. 2684-2690, 1977.

[26] C. Bazin, M. Billardon, D. Deacon, Y. Farge, J. M. Otega, J. Perot, Y. Petroff, and M. Velghe, "First results of a superconducting undulator on the ACO storage ring," in *International Summer School of Quantum Electronics*, A. Renieri and S. Martellucci, Eds. New York: Plenum, 1981.

[27] W. B. Colson, "Free electron laser wave and particle dynamics," in *International Summer School of Quantum Electronics*, A. Renieri and S. Martellucci, Eds. New York: Plenum, 1981.

[28] W. B. Colson, "Free electron lasers, operating in higher harmonics," *Phys. Rev. A*, to be published.

[29] L. R. Elias, "A high power, CW tunable, efficient, UV-visible and IR free electron laser using low energy electron beams," *Phys. Rev. Lett.*, vol. 42, pp. 977-979, 1979.

[30] M. Z. Caponi, J. Munch, and H. Boehmer, "Optimized operation of a free electron laser," in *Physics of Quantum Electronics*, Jacobs *et al.*, Eds. Reading, MA: Addison-Wesley, 1980, ch. 19.

William B. Colson was born in Washington, DC, on October 24, 1943. He received the B.S. and M.A. degrees from Wayne State University, Detroit, MI, and the Ph.D. degree from Stanford University, Stanford, CA, all in physics, in 1966, 1972, and 1977, respectively.

From 1966 to 1972 he was a Senior Physicist for the Bendix Research Laboratory, Southfield, IL. From 1978 to 1980 he was an Assistant Research Scientist at the Center for Space Physics, Rice University, Houston, TX, and an Acting Assistant Professor at Stanford University. He is presently an Associate Research Physicist at the Quantum Institute, University of California, Santa Barbara, where his research interests include optical pulse propagation in free-electron lasers and microwave electron tubes as phase transitions, quantum electrodynamics and quantum statistical properties of lasers, laser accelerators, solar cells with RF output, and astrophysical laser processes. He holds 8 patents.

Appl. Phys. B 29, 101–109 (1982)

Applied Physics B Photophysics and Laser Chemistry

Electron Dynamics in Free Electron Laser Resonator Modes

W. B. Colson*

Quantum Institute, University of California, Santa Barbara, CA 93106, USA

P. Elleaume**

C.E.N. Saclay, DPC/SPP/SP, F-91190 Gif-sur-Yvette Cedex, France, and LURE, Bâtiment 209C, Université de Paris-Sud, F-91405 Orsay Cedex, France

Received 8 April 1982/Accepted 25 June 1982

Abstract. We study the electron phase-space evolution and gain in free electron lasers whose short-wavelength radiation has Gaussian spherical wavefronts. Several free electron laser designs are considered: the undulator, the tapered wavelength undulator, and the optical klystron. We find that the gain spectrum is no longer proportional to the slope of the forward spontaneous emission spectrum, and we determine the design of the Gaussian mode which maximizes the energy extraction from the electron beam.

PACS: 42.50, 42.55, 52.60

Free electron lasers (FEL) use a beam of relativistic electrons passing through a static periodic magnetic field to amplify a co-propagating electromagnetic wave at optical frequencies [1]. A schematic of a free electron laser oscillator with the transverse dimensions exaggerated is shown in Fig. 1. In both the free electron laser amplifier [2] or oscillator [3], the electrons interact with Gaussian optical beams which are formed inside a spherical mirror optical resonator [4]. Our topic is to study the electron dynamics in the combined static magnetic field and the propagating Gaussian optical wave. The fundamental interaction can be described by the pendulum equation [5] which is parametrically modified during the laser interaction.

Much of the knowledge which has been developed about free electron lasers has assumed a plane-wave representation of the optical waves. A particular theorem which has found widespread use relates the slope of the spontaneous emission radiation spectrum to the shape of the laser gain spectrum [6]. However, this theorem is only valid for plane waves in the forward direction, and does not hold when the Gaussian beam of finite width is designed to maximize the electron energy extraction or nominal gain. The theorem originated from the quantum analysis of gain

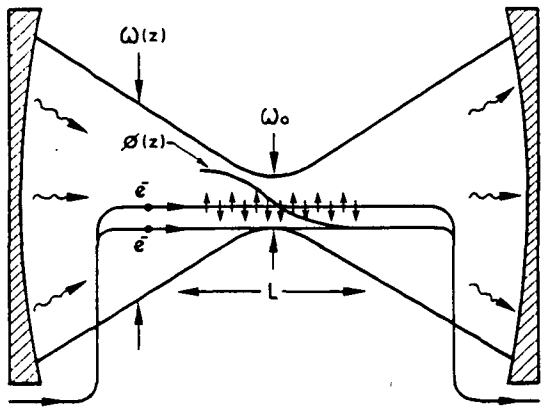

Fig. 1. A schematic of the free electron laser oscillator shows the Gaussian optical mode transverse size $w(z)$ expanding away from the waist w_0 centered in the static periodic magnet of length L. The optical phase $\phi(z)$ changes along L also. Two electron paths are shown: one on-axis at $r=0$ and one off-axis at $r>0$

* Supported by the Air Force Office of Scientific Research 81-0061, the Office of Naval Research N00014-81-K-0809, NASA NAG-2-48, and NATO Collaborative Grant No. 1876

** Supported partly by the Centre d'Etudes Nucléaires de Saclay, DPC/SPP/SP and DRET, Contract 81-131

0721-7269/82/0029/0101/$01.80

[1, 7, 8], where a slight difference in the kinematics of stimulated emission and absorption allows a Taylor expansion (and therefore derivative) of their respective probabilities. But the kinematic arguments are based on single-mode relationships and a realistic Gaussian beam contains a range of plane-wave states with a spread of angles which complicate the simple kinematic relations. In the plane wave limit there is vanishingly small gain.

Another theorem [6] relates the "second moment of the mean electron energy loss evaluated to first order in the optical field strength $\langle \delta\gamma^{(1)^2} mc^2 \rangle$" to the "mean energy loss evaluated to second order in the optical field strength $\langle \delta\gamma^{(2)} mc^2 \rangle$":

$$\langle \delta\gamma^{(2)} mc^2 \rangle = \tfrac{1}{2} \frac{\partial}{\partial \gamma} \langle \delta\gamma^{(1)^2} mc^2 \rangle ,$$

where γmc^2 is the electron energy. For all the magnet designs examined here, this theorem remains true. Recent papers and preprints [9, 10] have shown this theorem to have a broad range of validity.

The main topic of this paper is the electron evolution in Gaussian resonator modes. We restrict ourselves to low gain so that the wavefront of the Gaussian optical beam is not significantly distorted by the single-pass laser amplification. While the complete problem of coupled optical mode and electron evolution can be complicated, optical resonators can be made sufficiently selective of the laser runs in a single mode. We are attempting to illuminate one aspect of the problem without the complicating effects of the other. Our analysis pertains more precisely to single-pass amplifier measurements which are often used as preliminary tests in the development of free electron laser oscillators.

Three important kinds of FEL are explored. The fundamental magnet design is a long periodic undulator. A tapered wavelength undulator uses a long alternating magnet design with a slight increase in the wavelength along its lenth [11–13]. The tapered undulator is designed to extend the operating limit of the laser to higher powers, but introduces some loss of gain at low power. The last example is an optical klystron where the periodic magnet is split into two sections separated by a dispersive section [14, 15]. The optical klystron is designed to give high gain at low power, but with some loss of gain at high power.

1. Theory

The form of an electromagnetic wave $E(r, z)$ in a fundamental Gaussian mode [4] is

$$E(r,z) = \frac{E_0}{w(z)} \exp\left\{ \mathrm{i}[kz - \eta(z)] - r^2 \left(\frac{1}{w_0^2 w^2(z)} - \mathrm{i} \frac{k}{2R(z)} \right) \right\}, \tag{1}$$

where $w^2(z) = (1 + z^2/Z_0^2)$, $R(z) = z + Z_0^2/z$, $\eta(z) = \tan^{-1}(z/Z_0)$, $Z_0 = \pi w_0^2/\lambda$ is the Rayleigh length, w_0 is the mode waist at $z=0$, $k = 2\pi/\lambda$ is the carrier wavenumber, r and z are cylindrical coordinates, and E_0 is the electric field amplitude. Although we will only consider the lowest-order Gaussian modes, results can easily be extended to higher-order modes in the Gaussian-Laguerre form using the following prescription:

$$E_0 \mathrm{e}^{-r^2/w_0^2 w^2(z)} \to \frac{1}{\sqrt{1+\delta_{0,l}}} \frac{p!}{\pi(l+p)!} \left(\frac{\sqrt{2r}}{w_0 w(z)} \right)^l \cdot \mathrm{L}_p^l \left(\frac{2r^2}{w_0^2 w^2(z)} \right) \begin{pmatrix} \cos(l\theta) \\ \sin(l\theta) \end{pmatrix} E_0 , \tag{2}$$

$$\eta(z) \to (2p + l + 1)\eta(z) ,$$

where L_p^l are associated Laguerre polynomials, θ is the cylindrical coordinate angle, and l and p are integers labeling the mode [16].

In order to make better use of (1) it is convenient to shift the origin $z=0$ to the beginning of the laser magnet (Fig. 1). Define L as the magnet length and introduce $\tau = z/L$, $q = L/Z_0 = \lambda L/\pi w_0^2$. The new definitions mean that in (1) we now have

$$\begin{aligned} w^2(\tau) &= 1 + q^2(\tau - \tau_m)^2 , \\ \eta(\tau) &= \tan^{-1}[q(\tau - \tau_m)] , \\ R(\tau) &= L(\tau - \tau_m)[1 + q^{-2}(\tau - \tau_m)^{-2}] , \end{aligned} \tag{3}$$

where τ_m is the position of the Gaussian mode waist along the magnet length. We will take the mode to be centered ($\tau_m = 1/2$) throughout the rest of this paper since this point is near a broad maximum in gain. Writing the exponential in (1) in the form $\exp[\mathrm{i}(kz + \phi)]$ define

$$\phi(\tau) = -\tan^{-1}[q(\tau - 1/2)] + \frac{\varrho^2 q(\tau - 1/2)}{1 + q^2(\tau - 1/2)^2} , \tag{4}$$

where $\varrho = r/w_0$.

The simple undulator FEL has a helical magnetic field represented by $B(\cos k_0 z, \sin k_0 z, 0)$ where B is the magnetic field strength and $\lambda_0 = 2\pi/k_0$ is the magnet wavelength. If the electrons are perfectly injected near the magnet axis their helical motion is given by $\boldsymbol{\beta}_\perp = -(K/\gamma)(\cos k_0 z, \sin k_0 z, 0)$ where $\boldsymbol{\beta}_\perp c$ is the transverse velocity, $K = eB\lambda_0/2\pi mc^2$, and $e = |e|$ is the electron charge. We have assumed that the free electron laser has established a well-defined classical wave represented by (1). Furthermore, the wave has taken the form for a Gaussian beam through successive reflections from spherical resonator mirrors. We assume only the fundamental mode is present for simplicity. Generalizations from this work are straightforward.

In the presence of both the static magnetic field and the Gaussian optical wave, the electron energy changes according to $\dot{\gamma} = -e\boldsymbol{\beta}_\perp \cdot \mathbf{E}(r, z, t)/mc$ where $\mathbf{E}(r, z, t) = E(r, z)\hat{\varepsilon}\exp(-i\omega t)$, $\hat{\varepsilon} = -(1, i, 0)$ is the polarization vector, and $\omega = kc$ is the carrier frequency. The transverse motion of the electrons allows efficient energy exchange with the purely transverse radiation field (1). [We note that the transverse form (1) is approximate and provide justification for this approximation in Appendix A]. When the optical and magnet forces are nearly resonant, the resulting rate of energy exchange evolves slowly. The electron phase in the combined optical-magnet potential well is given by $\zeta(t) = (k + k_0)z(t) - \omega t$. When the number of magnet periods N is large, the resulting changes in γ are small and the electron equation of motion takes the form of the pendulum equation.

$$\ddot{\zeta} = \dot{v} = a(\tau)\cos[\zeta + \phi(\tau)], \tag{5}$$

where from now on $(\dot{}) = d()/d\tau$, $\tau = ct/L = z/L$ is the dimensionless interaction time, $v = \dot{\zeta} = L[(k + k_0)\beta_z - k]$ is the dimensionless electron velocity, $a(\tau) = a_0 \exp[-\varrho^2/w^2(\tau)]/w(\tau)$, and $a_0 = 4\pi NeKLE_0/\gamma^2 mc^2$ is the dimensionless optical wave amplitude. (In a linearly polarized magnet the coupling in a_0 is modified [17]: $K \to (K/2)[J_0(\xi) - J_1(\xi)]$ where $J_{0,1}$ are Bessel functions of the first kind and $\xi = K^2/4[1 + K^2/2]$.) The dimensionless time τ varies from 0 to 1 during one pass through the laser magnet of length $L = N\lambda_0$. The electron coordinates (ζ, v) follow pendulum phase space paths with parametrically changing amplitude $a(\tau)$ and phase $\phi(\tau)$. The separatix is given by curve $v_s^2 = 2a[1 + \sin(\zeta_s + \phi)]$ (Fig. 2). Each periodic section of phase space corresponds to the distance $\lambda\lambda_0/(\lambda_0 + \lambda) \approx \lambda$, the optical wavelength. The dimensionless electron velocity v measures the resonance between the optical wave and magnet forces. If $v = 0$, exactly one optical wavelength of light passes over an electron as it passes through one magnet wavelength and the forces are resonant. The initial value $v_0 = v(\tau = 0)$ is important in determining whether a monoenergetic electron beam "loses energy to" or "takes energy from" the optical wave, and therefore determines the gain. v_0 is called the "resonance parameter." When $Z_0 \to \infty$, then $w \to 1$, $q \to 0$ and $\phi \to 0$ and (5) is exactly the pendulum equation. The parameter $q = L/Z_0$ compares the length of the magnet L with the Rayleigh range Z_0. Significant changes in the Gaussian beam waist w and phase ϕ are measured by the size of q. Our problem is the more complicated electron evolution that occurs when $a(\tau)$ and $\phi(\tau)$ are parametrically altered because of the Gaussian optical beam with $q > 0$.

To illustrate some of the effects of the Gaussian beam, consider $q \ll 1$ so that we almost have plane waves.

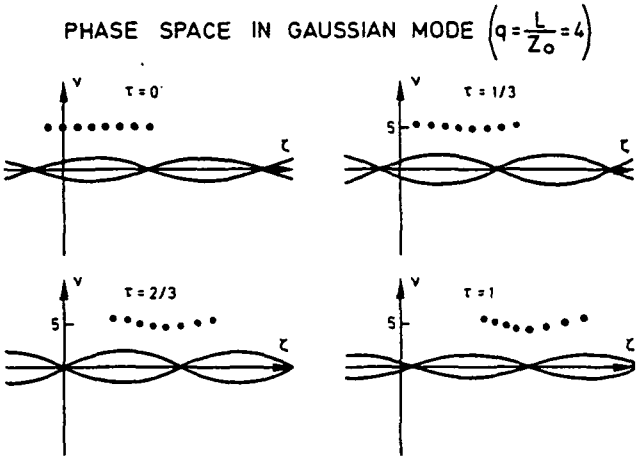

Fig. 2. The evolution ($\tau = 0 \to 1$) of ten sample electrons starts at $v_0 = 5$ in the (ζ, v) phase-space. The self-consistent separatrix $v_s(\zeta_s)$ acts as a guide to the distortion of phase-space paths caused by the optical mode structure. Increased fields cause an increase in the separatrix height $2a^{1/2}$, and the shifting phase $\phi(\tau)$ moves the separatrix along the ζ-axis. Spreading in v and bunching in the ζ-coordinate are visible at $\tau = 1$

With $q \ll 1$, $w = 1 + O(q^2)$ and $\phi = -q(1 - \varrho^2)(\tau - 1/2)$. Now consider weak optical fields $a_0 \ll 1$, so that we can make a perturbation expansion in powers of a_0. To lowest order $v^{(0)} = v_0$ and $\zeta^{(0)} = \zeta_0 + v_0\tau$. To first order in a_0

$$\ddot{\zeta}^{(1)} = \dot{v}^{(1)} = \underbrace{a_0 e^{-\varrho^2}}_{\text{new field}} \cos\{\underbrace{\zeta_0 + \tfrac{1}{2}q(1 - q^2)}_{\text{new phase}} + \underbrace{[v_0 - q(1 - \varrho^2)]}_{\text{new resonance parameter}}\tau\}. \tag{6}$$

The role of the non-planar Gaussian beam now becomes quite clear. The field strength or amplitude of the modified pendulum equation contains the exponential factor $e^{-\varrho^2}$ (where $\varrho = r/w_0$) which simply diminishes the field driving an off-axis electron. The electron also has a new initial phase but since the beam is uniformly spread over each optical wavelength the shift in each phase is inconsequential. The average energy loss is found by expanding to $v^{(2)}$ and averaging uniformly over the initial phases $0 < \zeta_0 < 2\pi$.

The interesting modification is the shifted resonance parameter $v_0 \to [v_0 - q(1 - \varrho^2)]$ which can cause a measurable change in the operation of the laser. The average loss $\langle v^{(2)} \rangle$ is maximum when $v_0^{max} = 2.6 + q(1 - \varrho^2)$ is shifted to a higher resonance parameter by the Gaussian beam with $q > 0$. If we assume this energy loss is the nominal gain in the wave energy, gain is proportional to $-\langle v^{(2)} \rangle/\pi w_0^2$ [5]. The factor πw_0^2 appears because the optical wave's energy is proportional to its transverse mode volume. In weak fields, the nominal gain spectrum $g(v_0)$ has the form $[1 - \cos v_0^* - v_0^*(\sin v_0^*)/2]/v_0^{*3}$ where $v_0^* = v_0 - q(1 - \varrho^2)$.

The point of zero gain, $\nu_0^*=0$, is now shifted away from the exact resonance by an amount $q(1-\varrho^2)$. This means, for instance, that a Gaussian mode storing radiation of frequency ω will not have its gain spectrum centered about the traditional value of resonance $\nu_0=0$. The reason is the shifting phase $\phi(\tau)=-q(1-\varrho^2)\cdot(\tau-1/2)$ of the Gaussian optical beam illustrated in Fig. 1. The effect occurs because the Gaussian beam mode is actually a superposition of plane waves.

In order to further illustrate the effects of Gaussian beams on electron dynamics, we can follow the evolution of sample electrons in phase space. The phase-space coordinates for each electron are (ζ_j, ν_j) in the phase space (ζ, ν). In Fig. 2 we show the evolution of ten sample electrons initially spread uniformly over one optical wavelength at the mode axis ($\varrho=0$) with $q=4$. We will show later that a mode with $q\approx 4$ maximizes the possible energy extraction from the electron beam. The electrons begin their evolution at $\tau=0$ at the energy $\nu_0=5$. The fields are weak ($a_0<\nu_0^2/4$) so that the separatix given by $\nu_s(\zeta_s)$ does not intercept any particle's path. As $\tau\to 1$ (the end of the laser) an energy spread is acquired, and we can see a small amount of bunching of the electrons. The separatrix is shown as a guide to the evolving phase-space paths. The distance between critical points is fixed at 2π as usual, but the height of the separatrix is $2(a_0/w)^{1/2}$ and visibly changes throughout the interaction. As the mode waist $w(\tau)$ decreases, the height of the separatrix increases. This effect is comparatively minor since the height of the separatrix is only proportional to $w^{-1/2}$. A much more important effect is the phase change $\phi(\tau)$. This causes the separatrix to shift to the right. Electrons must then start at a higher phase-space path (larger ν_0) to compensate. The case shown for $q=4$ requires $\nu_0=5$ instead of the usual $\nu_0=2.6$ to give nearly maximum energy loss.

For large q we cannot expand $w(\tau)$, but we can still expand the pendulum equation in weak fields a_0, integrate, and phase average to get the electron energy extraction or efficiency. The first-order phase-space coordinates are

$$\zeta^{(1)}(\tau)=\int_0^\tau d\tau' \int_0^{\tau'} d\tau'' a(\tau'')\cos[\zeta_0+\nu_0\tau''+\phi(\tau'')] \tag{7}$$

and $\nu^{(1)}(\tau)=\dot{\zeta}^{(1)}(\tau)$. The second-order $\nu^{(2)}$ is phase-averaged to give the net efficiency at the end of the laser magnet $\tau=1$.

$$\langle \nu^{(2)}\rangle = -\tfrac{1}{2}\int_0^1 d\tau \int_0^\tau d\tau' \int_0^{\tau'} d\tau'' a(\tau)a(\tau'') \cdot\sin[\nu_0(\tau-\tau'')+\phi(\tau)+\phi(\tau'')]. \tag{8}$$

This expression is compact but difficult to integrate analytically. The result is easy to integrate numerically, however, and will be done to all orders in the field a_0 in the next section. We first generalize the procedure to the more complicated magnet designs of the "tapered undulator" and "optical klystron".

The tapered undulator has a slow decrease in the magnet wavelength λ_0 along the magnet length [11, 13]. The electrons then experience a changing magnet wavenumber so that $\dot{k}_0(\tau)\neq 0$. In a strong field a_0, electrons can become trapped in the closed-orbit region of phase-space and experience a much larger energy loss than in the normal undulator. This free electron laser design works well at high power, but at the sacrifice of low power gain. The modified pendulum equation for the tapered undulator is

$$\ddot{\zeta}=\dot{\nu}=\delta+a(\tau)\cos[\zeta+\phi(\tau)], \tag{9}$$

where $\delta=\dot{k}_0(\tau)L$. We have again assumed that $\gamma\approx$ const; the fractional energy extraction can be small and still much bigger than the normal undulator. We also consider a special case of tapering where δ is constant. With this simplification, we retain the important features of a tapered undulator. The second-order efficiency is calculated just as for the undulator. The result is

$$\langle \nu^{(2)}\rangle = -\tfrac{1}{2}\int_0^1 d\tau \int_0^\tau d\tau' \int_0^{\tau'} d\tau'' a(\tau)a(\tau'') \cdot\sin[\nu_0(\tau-\tau'')+\tfrac{1}{2}\delta(\tau^2-\tau''^2)+\phi(\tau)+\phi(\tau'')]. \tag{10}$$

Setting $\delta=0$ we obtain the untapered result (8). The prescription for generalizing (8) to include tapering is $(\nu_0\tau)\to(\nu_0\tau+\frac{1}{2}\delta\tau^2)$.

In order to understand the equations of motion for the optical klystron free electron laser it is necessary to briefly discuss the dynamics of the dispersive element. The dispersive section separates the first and second half of the undulator magnet. The purpose of the dispersive section is to magnetically deflect electrons away from the beam axis so that they fall behind the propagating optical wave in an energy dependent manner. In this way, a small spread in energies created in the first undulator section can cause electron phase shifts to bunch electrons in the second undulator section. This allows high gain in weak fields, but results in low gain in moderately strong fields; the characteristics are just opposite to those of the tapered undulator.

We first choose a convenient representation for the magnetic field in the dispersive section. Define $\mathscr{K}(z)=(e/mc^2)\int_0^z B(z')dz'$ so $\mathscr{K}'(z)=eB(z)/mc^2$. With perfect injection, $\beta_\perp=\mathscr{K}/\gamma$ in the dispersive section. γ is constant in the dispersive section since the motion through

$B(z)$ is far from resonant with the optical wave. Since γmc^2 is constant, the transverse deflection causes $\beta_z c$ to decrease giving rise to a net shift $\Delta\zeta$ in the electron-optical phase at the end of the dispersive section with length d:

$$\Delta\zeta = d\left(k_0 - \frac{k}{2\gamma^2}\right) - \frac{k}{2\gamma^2}\int_0^d \mathscr{K}^2(z)dz \tag{11}$$

for large γ. The first term in (11) is the phase shift which would occur in the absence of the deflecting magnetic field (k_0 occurs because of the definition of ζ) and is less than the second term for a well designed dispersive section. For large γ we have $v \approx L[k_0 - k(1+K^2)/2\gamma^2]$ and v can replace γ which gives

$$\Delta\zeta = v\int_0^d \frac{[1+\mathscr{K}^2(z)]}{(1+K^2)}\frac{dz}{L} + k_0\left(d - \int_0^d \frac{[1+\mathscr{K}^2(z)]}{(1+K^2)}dz\right). \tag{12}$$

The second term is large ($\sim 10^3\pi$ typically) but is independent of the electron energy, or v. A slight adjustment in the design of $B(z)$ can make the second term equal to a multiple of 2π without seriously affecting the first term. Since the electron phase space is periodic in ζ with period 2π, the second term can be dropped in this special case leaving the simple form

$$\Delta\zeta = Dv, \quad \text{where} \quad D = \int_0^d \frac{[1+\mathscr{K}^2(z)]}{(1+K^2)}\frac{dz}{L}. \tag{13}$$

It is easy to show [15] that $D = N_d\lambda_0/L$ where N_d is the number of optical wavelengths from a plane wave which would pass over a resonant ($v=0$ calculated in the undulator) electron in the dispersive section. As an example we can take a specific design for the dispersive section. Let

$$B(z) = \begin{cases} B_0, & 0<z<d/4, \\ -B_0, & d/4<z<3d/4, \\ B_0, & 3d/4<z<d. \end{cases} \tag{14}$$

Note that $\int_0^d B(z)dz = 0$, and $\int_0^d \int_0^z B(z')dz'dz = 0$, so that there is no net transverse displacement, nor an angular displacement of the electron beam [15] in the dispersive section. The dispersive section is described by

$$D = \frac{d}{L(1+K^2)}\left[1 + \left(\frac{eB_0}{mc^2}\right)^2 \frac{d^2}{48}\right]. \tag{15}$$

A typical design ($L = 100$ cm, $d = 20$ cm, $B_0 = 6$ kilogauss, and $K = 1$) gives $D \approx 10$, so that a spread in $\delta v \sim \pi/D \approx 0.31$ caused by the weak optical fields $a_0 \sim \pi v_0/D \sim 0.8$ of the first klystron section can actually result in bunches in the second klystron section. A large D makes a small a_0 more able to bunch electrons.

We now calculate the average energy extraction from an electron beam in a klystron with a superimposed optical mode. The equations of motion are

$$\begin{aligned} \dot{v} &= a(\tau)[1 - \theta(\tau-\tau_1)\theta(\tau_2-\tau)]\cos[\zeta+\phi(\tau)], \\ \dot{\zeta} &= v[1 + D'\delta(\tau-\tau_2)] \end{aligned} \tag{16}$$

with $D' = D - (\tau_2 - \tau_1)$ and where $\theta(x) = \begin{cases} 1 \\ 0 \end{cases}$ for $x \gtrless 0$ and $\delta(x)$ is the Dirac δ-function. The second equation governs the evolution of the electron phase ζ which changes sharply at the end of the dispersive section at τ_2 when the electron enters the second stage of the klystron. The optical wave does not drive electrons from the time it leaves the first stage τ_1 to the time it enters the second stage τ_2.

To lowest order with no optical field present, the electron motion is given by

$$\begin{aligned} v^{(0)} &= v_0, \\ \zeta^{(0)} &= \zeta_0 + v_0\tau + D'v_0\theta(\tau-\tau_2). \end{aligned} \tag{17}$$

The second order efficiency is again obtained by a perturbation expansion:

$$\langle v^{(2)}\rangle = -\frac{a_0^2}{2}\int_0^1 d\tau \int_0^\tau d\tau' \int_0^{\tau'} d\tau'' \Psi(\tau)\Psi(\tau'')[1 + D'\delta(\tau'-\tau_2)] \cdot \sin[Z(\tau) - Z(\tau'')], \tag{18}$$

where

$$\Psi(\tau) \equiv \frac{e^{-\varrho^2/w^2(\tau)}}{w(\tau)}[1 - \theta(\tau-\tau_1)\theta(\tau_2-\tau)],$$

$$Z(\tau) \equiv v_0\tau + D'v_0\theta(\tau-\tau_2) + \phi(\tau).$$

Symmetric choices are (i) $\tau_1 = 1/3$ and $\tau_2 = 2/3$, or (ii) $\tau_1 = \tau_2 = 1/2$ representing a very small d with $D \neq 0$. In order to recover the results for the undulator from (18), let the dispersive displacement $D \to 0$ and let $\tau_{1,2} > 1$.

Note that (8), (10), and (18) assume an electron beam of infinitesimal width positioned at radius $\varrho = r/w_0 = 0$. A numerical integration over ϱ is necessary for wider beams.

2. Energy Extraction in Gaussian Optical Beams

We now examine how energy extraction, or the nominal gain, is modified by operating FEL's in realistic Gaussian beams. The deviation of the Gaussian mode from a plane-wave is measured by the parameter $q = L/Z_0 = L\lambda/\pi w_0^2$. If $q \ll 1$ the Gaussian mode is nearly a plane-wave. In this case the nominal gain spectrum $g(v_0) \propto -\langle v^{(2)}\rangle/\pi w_0^2 \propto -q\langle v^{(2)}\rangle$ has the same shape as those previously published for the undulator

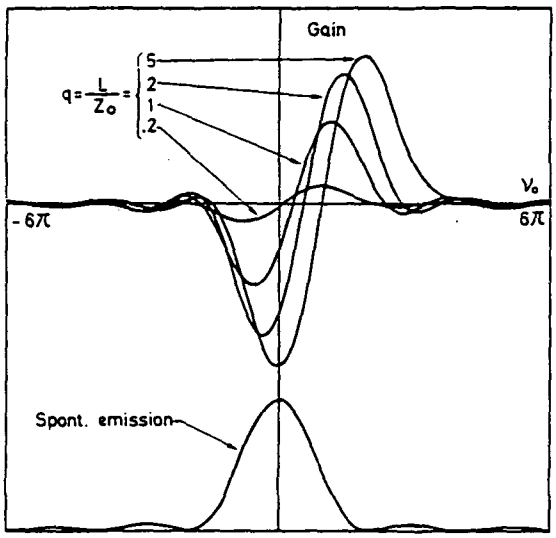

Fig. 3. The nominal undulator gain or energy extraction $g(\nu_0) \propto -q\langle \nu^{(2)} \rangle$ is plotted in relative units versus the resonance parameter ν_0 in weak fields for $q=0.2$, 1, 2, and 5. As q increases the peak gain increases and shifts to larger ν_0. The forward spontaneous power spectrum at each ν_0 is shown for reference. Note that $g(\nu_0)$ is not proportional to the slope of the forward spontaneous power

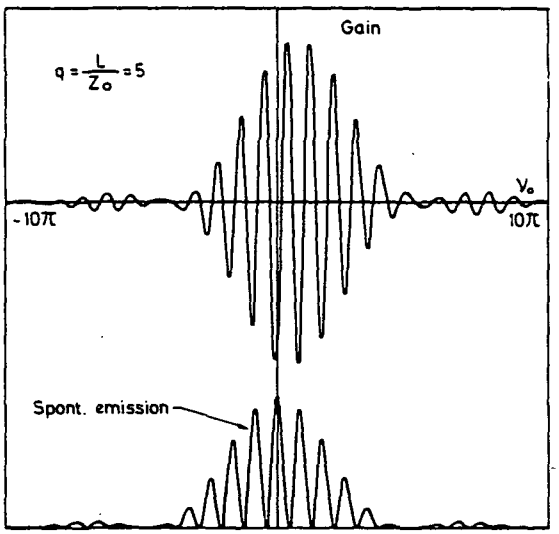

Fig. 4. The nominal optical klystron gain or energy extraction $g(\nu_0)$ is shown in relative units for $q=5$, $D=2$, $\tau_1=0.42$, and $\tau_2=0.58$ and is shifted away from resonance $\nu_0=0$ by the Gaussian beam. The forward spontaneous power is shown for reference

[5, 18], tapered undulator [11–13], and optical klystron [15]. We show here the modifications that occur in each gain spectrum $g(\nu_0)$ due to nonzero q. We find that the maximum gain increases with q up to $q \approx 3-5$. Thus, the Gaussian modes which are designed for maximum energy extraction actually lead to significant changes in the gain spectrum.

When $q \ll 1$, (8), (10), and (18) can be expanded in q and complicated analytical results are obtained. However, as $q \to 0$, $g(\nu_0) \to 0$; so the plane-wave design is poorly optimized and uninteresting. More realistic work for larger values of q requires numerical analysis. The equations of motion (5), (9), and (16) are therefore solved numerically in this section to present the gain spectra in weak fields a_0 for electron beams of infinitesimal width.

Figure 3 shows $g(\nu_0)$ in the simple undulator. Four gain curves are shown for different values of $q=0.2$, 1, 2, and 5. When $q=0.2$, the system behaves as if the laser were amplifying plane waves. $g(\nu_0)$ is nearly antisymmetric, and $g(\nu_0)$ peaks at $\nu_0 \approx 2.6$. However, when q is increased, $g(\nu_0)$ is shifted to higher ν_0 and peak gain increases. At even larger $q \to 5$ a distortion of the curve shape becomes evident; the absorption peak is slightly larger than the gain peak. At higher $q>5$ (not shown), the shifting continues, but peak gain decreases.

For reference, the shape of the forward spontaneous emission spectrum is shown in Fig. 3. Spontaneous emission power is shown as a function of ν_0 at a given wavenumber k. The spontaneous power for the undulator peaks at $\nu_0=0$ and is independent of q. As can be seen $g(\nu_0)$ is not proportional to the slope of the forward spontaneous power spectrum when $q \neq 0$ and therefore is not in agreement with the wide spread use theorem in [6].

We next move to the example of an optical klystron. Because of the complexity of $g(\nu_0)$ only the example $q=5$ is shown in Fig. 4 for the parameters $D=2$, $\tau_1=0.42$, and $\tau_2=0.58$. Again the gain spectrum is clearly shifted from the derivative of the forward spontaneous emission spectrum. Note that the amount of shift in the resonance parameter is about the same as for the undulator at the same $q=5$ (Fig. 3).

Our final example, Fig. 5, shows the tapered undulator gain spectrum for $q=0.2$, 1, 2, and 5. When $q=0.2$, the gain curve is located to the left of resonance $\nu_0=0$ and the overall gain is smaller than for the undulator. As q increases, the available peak gain increases significantly and the gain spectrum shifts towards resonance. There is also a distortion in the shape of $g(\nu_0)$ evident at $q=5$. Curves with $q>5$ distort further and decrease in peak gain.

In the FEL designs presented, we can search through ν_0 for the maximum available gain as a function of q. We seek to optimize $g(\nu_0)$ in the (ν_0, q) plane. Figure 6 plots the gain in relative units as a function of q^{-1} with ν_0 chosen for maximum $g(\nu_0)$. For q^{-1} large we have plane waves. It is well known that the tapered undulator has less gain than the undulator, and the optical klystron has more gain than either of them. With increasing q the Gaussian modes become more pronounced, and we see that the tapered undulator

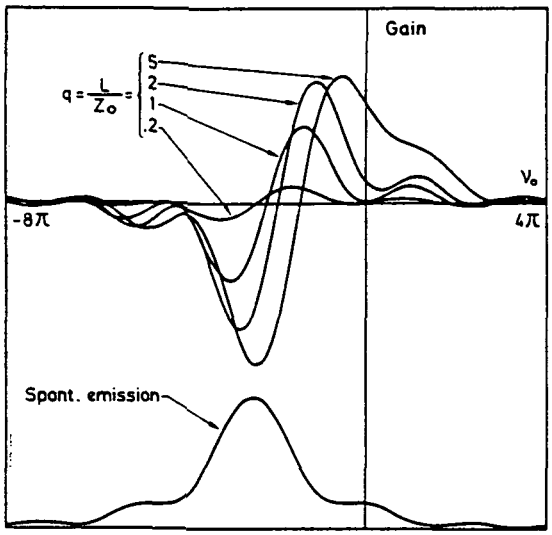

Fig. 5. The nominal gain or energy extraction $g(\nu_0)$ of a tapered undulator with $\delta=5\pi$ is shown in relative units for $q=0.2$, 1, 2, and 5. Peak gain is significantly increased and shifted to higher ν_0 when q increases. The forward spontaneous power is shown for reference

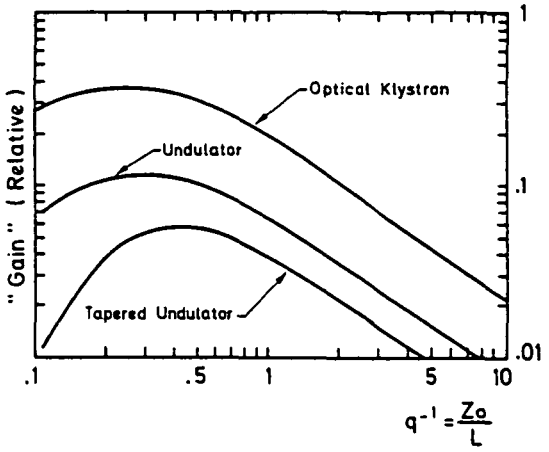

Fig. 6. The peak gain or energy extraction (in ν_0) is plotted in relative units versus q^{-1}. For small q (plane waves) the gain in each magnet design falls off like q. The highest gain design, the optical klystron, sustains high gain to quite large q and peaks at $q\approx 5$. The undulator gain peaks for $q\approx 3$, while the tapered undulator gain drops off after $q\approx 2.5$

gain first drops off sharply after $q\approx 2.5$. The undulator then drops off more slowly after $q\approx 3$, and the optical klystron sustains its broad maximum to $q\gtrsim 5$. Surprisingly, the peak gains in these quite different magnet designs are all near $q\approx 5=L/Z_0$. This figure can be useful to experimenters when chosing the optical resonator mode for their particular magnet design.

Figure 7 shows how gain can be affected by electrons entering the laser off-axis. Four gain curves are presented for $\varrho=r/w_0=0$, 0.4, 0.7, and 1 with $q=5$. As ϱ increases, the energy extraction decreases because electrons are moving outside the mode to weaker optical fields. In addition, the peak of the gain curve is shifted back towards resonance $\nu_0=0$. Electrons off-axis encounter smaller phase shifts than when on-axis. This trend was predicted in (6). The gain curve for a real beam with a transverse dimension will be the average over gain curves like those in Fig. 7. However, since electrons on-axis have the maximum gain, the resulting gain curve will have a shape close to the $\varrho=0$ case.

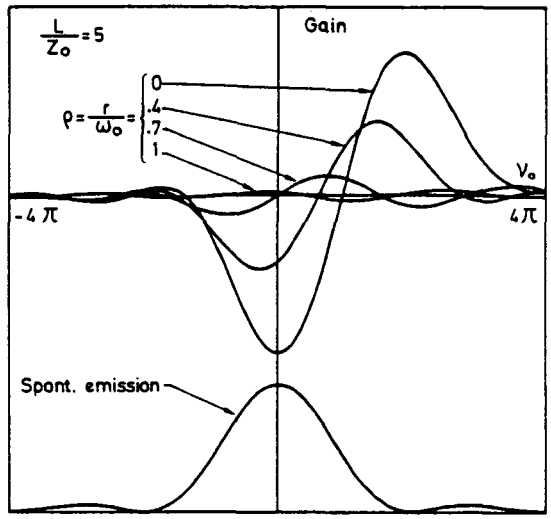

Fig. 7. The nominal undulator gain or energy extraction $g(\nu_0)$ shows the affects of injecting electrons off-axis at $\varrho=r/w_0=0$, 0.4, 0.7, and 1 for $q=5$. Gain decreases and is shifted back towards resonance $\nu_0=0$ as predicted by (6)

3. Experimental Implications

The results of this paper lead to many new features which can be experimentally observed. Gaussian optical modes will cause a shift in the gain spectrum $g(\nu_0)$ away from the derivative of the forward spontaneous emission spectrum. This is not the usual conclusion derived from a widely used theorem [6], and occurs because the Gaussian mode contains off-axis spectral components which alter the resonance condition. Experiments in Orsay will explore the undulator and klystron magnet designs, while groups at TRW, Math Sciences Northwest, and Los Alamos National Laboratory are planning to explore the tapered undulator design.

It might be noted that the shift in the weak-field gain away from the forward spontaneous power does not constitute a problem for FEL oscillator start-up. The characteristic range of angles in a Gaussian modes is $\delta\theta\approx\sqrt{q\lambda/2\pi L}$ which results in a characteristic shift in the resonance parameter by $\delta\nu\approx -4\pi N\gamma^2\delta\theta^2\approx -q$ in agreement with (6). Therefore, the shift in the gain curves of Fig. 3 through 5 is such that the off-axis

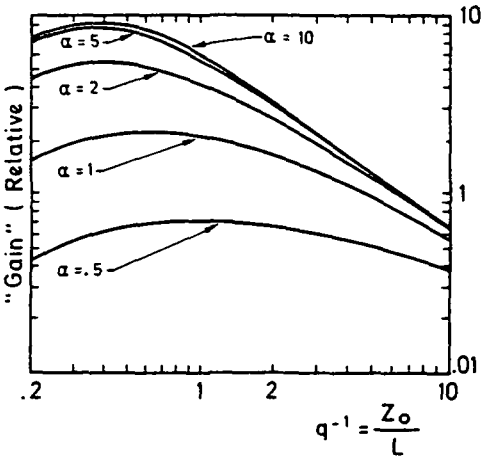

Fig. 8. The peak gain (in v_0) is plotted versus q^{-1} for $\alpha=0.5$, 1, 2, 5, and 10. As $\alpha=(w_0/\sigma)\sqrt{q/2}$ increases, characterizing narrower electron beams of width σ, gain increases until $\alpha\approx 5$. For $\alpha\gtrsim 5$, the beam is a filament. The best available gain occurs at smaller q when $\alpha(\sigma)$ decreases; larger electron beams work better in wider modes

plane-wave components of a rapidly diverging Gaussian beam (large q) experience gains comparable to the plane-wave components of a slowly diverging beam (small q).

The reasoning presented here gives a procedure for designing FEL cavities. As we have shown, for an on-axis electron $\varrho=0$, there is a value of q that gives maximum gain (Fig. 7). This value of q can be selected by proper choice of the mirror's radius of curvature and spacing. An estimate of the best q has been made by calculating the minimum cavity mode cross-section averaged over the whole undulator length [19, 20]. It was found that the best overlap with the electron beam occurred for q equal to $2\sqrt{3}$; close to our numerical optimum of $q\approx 3$ for an undulator. However, the actual optimum q depends on the magnet design and on the transverse size of the electron beam. Suppose the electron beam is perfectly aligned along the cavity mode and has a Gaussian shape with transverse standard deviation σ. Define the dimensionless parameter $\alpha=\sqrt{\lambda L/2\pi\sigma^2}=(w_0/\sigma)\sqrt{q/2}$. Figure 8 plots the gain in relative units as a function of q^{-1} with v_0 chosen for maximum gain $\{g(q,\alpha)\}$ and for $\alpha=0.5$, 1, 2, 5, and 10 ({ } is now averaging over the transverse electron positions). As α decreases (that is as the beam size increases) the maximum gain occurs for a smaller q and the maximum becomes broad.

In the gain calculation the overlap of the electron and light beams can be taken into account by defining a filling factor $F(\sigma)=1/(w_0^2+4\sigma^2)$ such that the maximum final gain $\{g(q=0,\alpha(\sigma))\}\propto F(\sigma)g(q=0,\sigma=0)$. This filling factor $F(\sigma)$ agrees with our calculation when $q\ll 1$, but for $q\gtrsim 1$ there is a correction $f(q,\alpha)$:

$$\{g(q,\alpha(\sigma))\}\propto F(\sigma)f(q,\alpha(\sigma))g(q=0,\sigma=0). \tag{19}$$

Values of $f(q,\alpha)$ for an undulator are given in Table 1 below.

The shift of the gain curve calculated for the Orsay experiment with the superconducting undulator [19] was too small to be seen; however this is not expected to be the case in the new series of experiments, where the following parameters are applicable: $\sigma\sim 0.3$ mm, $\lambda\sim 0.5\,\mu$m, $L\sim 1.3$ m, $\lambda_0\sim 8$ cm, $\gamma mc^2\sim 240$ MeV.

Therefore with $\alpha\sim 1$ Fig. 8 shows maximum gain occurs for $q^{-1}\approx 0.6$. For a 5.5 m distance between mirrors (1/4th the storage ring perimeter) we get an optimum cavity mode for a mirror radius of curvature $R_c\sim 3$ m. This value is a larger than $R_c=2.8$ m giving $q\sim 2\sqrt{3}$ and has the advantage of leaving the cavity more stable [4] (the stability limit being $R_c=2.75$ m). At this optimal cavity mode $f(q^{-1}=0.6,\alpha=1)=0.89$. The gain curve is shifted to the higher electron energies by $\delta\gamma mc^2\sim\gamma mc^2\lambda_0 q/4\pi L\cong 1.8$ MeV. Equivalently the wavelength for maximum gain is increased by $\delta\lambda/\lambda\approx\lambda_0 q/2\pi L\approx 0.016$. This shift is easy to measure since it is going to correspond to a one period shift of the fine structure in the gain curve of the optical klystron with $D\sim 4$.

Finally it is to be noticed that we only predicted the gain curve changes for colinear electron and photon beams. Misaligned beams add further modifications which can further reduce gain.

Table 1. New filling factor $f(q,\alpha(\sigma))$ with $\alpha=(w_0/\sigma)\sqrt{q/2}$

	$\alpha=10$	$\alpha=5$	$\alpha=3$	$\alpha=2$	$\alpha=1$	$\alpha=0.5$	$\alpha=0.3$	$\alpha=0.1$
$q^{-1}=100$	1.00	1.00	1.00	1.00	1.00	1.00	1.00	1.00
$q^{-1}=10$	1.00	1.00	1.00	1.00	1.00	1.00	1.00	1.00
$q^{-1}=5$	1.00	1.00	1.00	1.00	1.00	1.00	1.00	1.00
$q^{-1}=3$	0.99	0.99	0.99	0.99	0.99	0.99	0.99	0.99
$q^{-1}=2$	0.97	0.98	0.98	0.98	0.98	0.99	0.99	0.99
$q^{-1}=1$	0.87	0.88	0.90	0.91	0.94	0.95	0.96	0.96
$q^{-1}=0.8$	0.83	0.84	0.86	0.89	0.93	0.94	0.94	0.94
$q^{-1}=0.6$	0.74	0.76	0.80	0.84	0.89	0.90	0.90	0.90
$q^{-1}=0.4$	0.55	0.59	0.65	0.72	0.79	0.80	0.81	0.80
$q^{-1}=0.3$	0.41	0.46	0.54	0.62	0.70	0.71	0.71	0.70

Appendix

Neglecting the Longitudinal Electric Field in Gaussian Beams

In the derivation of Gaussian resonator modes it is assumed that the amplitude and phase of the optical wave are slowly variyng along the length of the cavity axis and that the electromagnetic wave is purely transverse. At the same time the optical wave is not traveling precisely along the cavity axis, but expands outward from the waist to the mirrors. The modes actually violate Maxwell's equations since a small longitudinal component of the field is neglected. The question arises as to the work done on electrons by the actual longitudinal electric field of Gaussian modes.

In order to estimate the longitudinal electric field we use $\nabla \cdot \mathbf{E} = 0$. In this estimate let $E_y = 0$ and assume $q = L/Z_0$ is small. Then the transverse field component

$$E_\perp \approx E_0 e^{ikz} e^{-r^2/w_0^2} \tag{20}$$

and the longitudinal field is

$$E_{\|} = \frac{4E_0 e^{ikz}}{kw_0} \frac{r e^{-r^2/w_0^2}}{w_0}. \tag{21}$$

We find the work done on an electron in the whole undulator is non-resonant and is given by

$$\Delta\gamma_{\|} mc^2 = e E_0 \lambda_0 \left(\frac{r e^{-r^2/w_0^2}}{\pi Z_0}\right). \tag{22}$$

This energy change has been previously neglected. It is relevant to compare $\Delta\gamma_{\|}$ to the work done by the transverse fields $\Delta\gamma_\perp$ in the Gaussian modes. In this case the interaction is resonant and the ratio is

$$\frac{\Delta\gamma_{\|}}{\Delta\gamma_\perp} = \frac{\gamma r e^{-r^2/w_0^2}}{\pi K N Z_0}. \tag{23}$$

Typically $\gamma/\pi KN \sim 1$, but $r/Z_0 \ll 1$ for electrons in the Gaussian cavity. Therefore, the longitudinal optical field is always negligible compared to the transverse field in FEL.

Acknowledgements. The authors are grateful to D. A. G. Deacon, J. M. J. Madey, R. Freedman, and Y. Petroff for many helpful discussions.

References

1. J.M.J. Madey: J. Appl. Phys. **42**, 1906 (1971)
2. L.R. Elias, W.M. Fairbank, J.M.J. Madey, H.A. Schwettman, T.I. Smith: Phys. Rev. Lett. **36**, 717 (1976)
3. D.A.G. Deacon, L.R. Elias, J.M.J. Madey, G.J. Ramian, H.A. Schwettman, T.I. Smith: Phys. Rev. Lett. **38**, 892 (1977)
4. A. Yariv: *Quantum Electronics* (Wiley, New York 1975) Chaps. 6 and 7
5. W.B. Colson: Phys. Lett. A**64**, 190 (1977)
6. J.M.J. Madey: Nuovo Cimento B**50**, 64 (1979)
7. W.B. Colson: Phys. Lett. A**59**, 187 (1976)
8. W.B. Colson: Ph. D. Dissertation, Stanford University 1977
9. N.M. Kroll: In *Physics of Quantum Electronics*, Vol. 8 (Addison-Wesley, Reading, MA 1982) Chap. 12
10. N.A. Vinokurov: Preprint, INP 81–02, Novosibirsk (1981)
11. J.M.J. Madey: U.S. Patent No. 3,822,410 (1974)
12. P. Sprangle, C.M. Tang, W.M. Manheimer: Phys. Rev. Lett. **43**, 1932 (1979)
13. N.M. Kroll, P.L. Morton, M.N. Rosenbluth: IEEE J. QE-**17**, 1436 (1981)
14. N.A. Vinokurov, A.N. Skrinsky: Preprint INP 77–59, Novosibirsk (1977)
15. P. Elleaume: In *Physics of Quantum Electronics*, Vol. 8 (Addison-Wesley, Reading, MA 1982) Chap. 5
16. A.E. Siegman: *An Introduction to Lasers and Masers* (McGraw-Hill, New York 1971) p. 330
17. W.B. Colson: IEEE J. QE-**17**, 1417 (1981)
18. W.B. Colson: In *Physics of Quantum Electronics*, Vol. 5 (Addison-Wesley, Reading, MA 1978) Chap. 4
19. D.A.G. Deacon, L.R. Elias, J.M.J. Madey, H.A. Schwettman, T.I. Smith: Proc. Society of Photo-Optical Instrumentation Engineers **181**, 89 (1977)
20. R. Barbini, G. Vigrola: Internal report LNF-80/12(R) Frascati (Rome)

published in Phys. Quantum Electronics, 8-9 (Addison-Wesley, 1982) eds. Jacobs, Moore, Pilloff, Sargent III, Scully and Spitzer.

OPTICAL PULSE EVOLUTION IN THE STANFORD FREE ELECTRON LASER AND IN A TAPERED WIGGLER

W.B. Colson
University of California

INTRODUCTION

The Stanford free electron laser oscillator[1-3] is driven by a series of electron pulses from a high quality super-conducting linac. The electrons pass through a transverse and nearly periodic magnetic field, a "wiggler", to oscillate and amplify a superimposed optical pulse. See Fig. 1. The rebounding optical pulse must be closely synchronized with the succession of electron pulses from the accelerator, and can take on a surprising range of structures depending on the precise degree of synchronism. Small adjustments in desynchronism can make the optical pulse either much shorter or longer than the electron pulse, and

can cause significant subpulse structure. In the first part of this chapter, the oscillator start-up from low level incoherent fields is discussed. In the next section, the effects of desynchronism on coherent pulse propagation are presented and compared with the recent Stanford experiments. In the last part, the same pulse propagation effects are studied for a magnet design with a tapered wavelength in which electrons are trapped in the ponderomotive potential.

There is a good deal of theory on free electron lasers and the tapered wavelength wiggler. Recent collections of research papers cover the most important topics.[4,5] Specific work on short pulse propagation started with the original experiments,[1,2] and was followed shortly after with the quasi-Bloch theoretical description of "lethargy."[6] Later, the multimode Hamiltonian picture of pulse dynamics was developed.[7] Concurrently, the single-particle electron model[8] was coupled to Maxwell's non-linear wave equation.[9] This last-named approach has proven to be a clear and accurate method in both weak and strong optical fields.[10,11] The wave-particle equations are reduced to contain only four independent parameters to allow scaling to other free electron laser systems. Improved theoretical and experimental techniques have brought excellent agreement between them. All predicted qualitative trends[11] have been confirmed by experiment, and quantitative agreement is as good as can be meaningfully ascertained from the available measurements. These trends characterize how the laser power spectrum, pulse shape, and electron velocity distribution all depend on the electron-optical pulse desynchronism. Limit cycle behavior and complicated pulse structure are presented.

The tapered wiggler pulse problem explored here shows similar trends. The growth from weak fields is shown not to

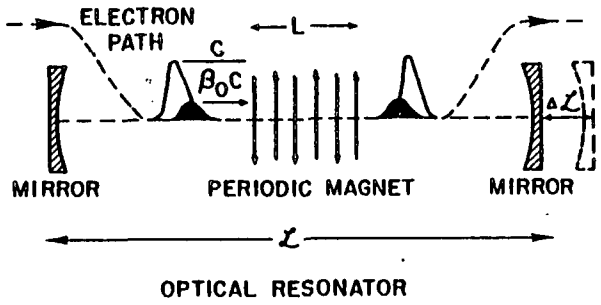

OPTICAL RESONATOR

Fig. 1. A succession of electron pulses is injected into the resonator to overlap a rebounding optical pulse. The synchronism of the pulses is adjusted by moving the end-mirror an amount $\Delta\mathcal{L}$. While "wiggling" through the transverse periodic magnet in the presence of the superimposed light, the electrons bunch within each optical wavelength to drive the radiation field.

be a problem as previously reported, but the steady-state operation may not lead to the expected electron trapping when desynchronism is not optimized. Optical subpulse structure is observed for both the tapered and untapered wigglers when fields are large. This may be an example of the Kroll-Rosenbluth[12] sideband instability proposed earlier. If so, we find that this instability is not limited to tapered wigglers, but can occur under much more general conditions than anticipated.

OSCILLATOR "START-UP" DISCUSSION. The Stanford linac produces a sequence of ~2 x 10^4 electron pulses spaced $\mathcal{L}' = 25$ m apart. Initially, no light is present in the resonator, but magnetic bremsstrahlung is emitted from electrons "wiggling" through the periodic magnet of wavelength $\lambda_o = 2\pi/k_o = 3.3$ cm, length $L = N\lambda_o = 5.3$ m, and field strength B = 2.3 kgauss.

The resonator mirror spacing must be sufficiently close to $\mathcal{L}'/2$ to ensure that the spontaneous emission of magnetic bremsstrahlung repeatedly builds on the same synchronized optical pulse. The build-up from the start of the electron pulse to just before laser saturation requires $n_T \sim 1800$ passes.[3]

The quantum mechanical forward transition rate for bremsstrahlung per unit solid angle $d\Omega$ into the dimensionless frequency interval $d\nu_k = 2\pi N d\omega/\omega$ is

$$\left.\frac{dW}{d\Omega d\nu_k}\right|_{\theta=0} = 2\alpha k_o c\left[\frac{\gamma K}{2\pi(1+K^2)}\ \frac{\sin(\nu_k/2)}{(\nu_k/2)}\right]^2 \qquad (1)$$

where $\lambda = 2\pi c/\omega = 2\pi/k \approx 3.3$ μm is the radiation wavelength, $\alpha = e^2/\hbar c$ is the fine structure constant, $K = eB\lambda_o/2\pi mc^2 = 0.71$, $\gamma mc^2 = 43$ MeV is the electron energy, and $\nu_k = L\{k_o - k(1+K^2)/2\gamma^2\}$ is the dimensionless frequency referenced to the magnet design and electron energy. For a long magnet, light is emitted into a narrow (~1/2N) frequency range about $\omega = 2\gamma^2 k_o c/(1+K^2)$. The number of photons emitted into $d\Omega d\nu_k$ by one electron in a single pass is L/c times the differential transition rate (1). The radiation cone for relativistic beams has a small angular width $\theta \lesssim \gamma^{-1}$ so $\int d\Omega \sim \pi\theta^2$. We estimate the solid angle collected by the solid angle of the Stanford end-mirror (~4 cm diameter) at an average distance of 6 m: $\theta \sim 2$ cm/600 cm = 3.3×10^{-3}. Both the classical and quantum mechanical gain calculations[13,14] show that photons with $\nu_k \leq 0$ lead to stimulated absorption and photons with $\nu_k \gtrsim 0$ lead to stimulated emission. Integrating over the positive gain modes gives W_T, the number of transitions per pass for one characteristic electron:

$$W_T = \pi N\alpha\{\gamma\theta K/(1 + K^2)\}^2 \ , \qquad (2)$$

where $W_T \approx 0.07$ for the Stanford experiments.[3] Note that for any value of the magnet field K, it is not at all likely that an electron emits even a single photon in the forward direction as it passes through one magnet period. Therefore, forward magnetic bremsstrahlung cannot be a classical process in free electron lasers even though a classical calculation gives the correct average rate. After several passes the radiation will spread out from the electron beam to begin to form the resonator mode. The density of the emitted photons is $\rho F W_T n$ where n is the number of passes, $F \approx .075$ is the "filling factor" = (electron beam area)/(average density optical mode area), and $\rho = 2 \times 10^{10}$ cm^{-3} is the Stanford electron density.

A particularly relevant volume element for photon counting is one of length $N\lambda$ and cross section λ^2. The classical gain process requires that N coherent wavelengths of light pass over an electron during a single pass through the magnet so that all electrons sample the volume element $N\lambda^3$. If optical phase fluctuations occur within the slippage distance $N\lambda$, a "gain" electron can become an "absorption" electron. Net gain results when the ensemble average of electrons drive the optical wave amplitude. After each pass the photon number η in the volume element $N\lambda^3$ increases by $\Delta\eta = \rho F N\lambda^3 W_T \approx 0.6$ photons/pass. Each volume element also suffers a measured[3] ~2.8% loss per pass due to the transmissive end-mirror. Together with some gain $g(\bar{\eta})$ that might be present in the laser, the growth of the average photon number $\bar{\eta}$ over many passes is described by

$$\frac{d\bar{\eta}}{dn} = \Delta\eta + (g(\bar{\eta}) - Q^{-1})\bar{\eta} \qquad (3)$$

where Q = 35 describes the 2.8% loss and n is the pass number.

The early growth of radiation when $\bar{\eta} \ll \Delta\eta/(g - Q^{-1})$ is given by $\bar{\eta}(n) \approx n\Delta\eta$ and is independent of either gain or loss. Gain $g \approx .05 - .06$ is measured* in the later stages of evolution in the Stanford experiment when $\bar{\eta} \approx 10^6$. But this gain cannot persist to arbitrarily weak fields because electrons will experience an optical phase uncertainty due to low photon number: $\delta\phi\delta\eta \gtrsim 1$. This decrease in optical coherence length $N_c\lambda$ in effect corresponds to a shorter magnet length and decreases gain. As an example, consider evolution at $\bar{\eta} \sim 20$ photons with Poisson statistics so that $\delta\eta = \bar{\eta}^{1/2} \sim 5$ and $\delta\phi \approx 0.6\pi$. These phase fluctuations would certainly decrease gain, but just how much is not yet clear. The classical low-gain formula in weak fields[8] is independent of $\bar{\eta}$ and therefore wrong for very low $\bar{\eta}$. $g(\bar{\eta})$ must decrease to zero as $\bar{\eta} \to 0$.

During normal gain, growth progresses to saturation at $\bar{\eta} \sim 3 \times 10^8$ photons, and has been analyzed classically. If the measured $g = .05$ is used in (3), the number of passes necessary for saturation is $n_T \sim 700$ which is lower than the value $n_T = 1800$ measured in the experiments. However, if we postulate that the average gain is diminished to $g = .035$ due to phase fluctuations at low photon number, then (3) gives $n_T \sim 2000$. A more careful analysis of just how $g(\bar{\eta})$ evolves at low photon number is needed, but since n_T is so sensitive to g just about any decrease will explain the observed n_T. For instance, in the next section the optical pulse shape is seen to evolve and exhibit different

*This gain[3] is lower than expected from the fundamental gain formula[8] because of short pulse effects, but can be calculated numerically as will be shown in the next section.

amounts of gain while taking on different shapes. This alone could explain why the specific gain measured at a single point in the evolution of the system is not consistent with the n_T observed. Regardless of these complications, our main point here is that $g(\bar{n})$ should decrease at low $\bar{n}$ due to quantum phase fluctuations. Although the full explanation of n_T remains as a more complicated problem, quantum fluctuations will increase n_T (by decreasing $g(\bar{n})$) over the classically calculated n_T.

STANFORD PULSE PROPAGATION. We now study optical pulse evolution after the electromagnetic wave has developed significant coherence. The goal is to calculate a final optical pulse shape which reproduces itself after many passes in steady state. The result is the "fixed point" or "limit cycle" solution to this complicated classical non-linear problem.

The derivation of the coupled non-linear wave equation and the self-consistent electron "pendulum" equation has been presented elsewhere[9-11] but is reviewed again here. The helical magnet is represented by $B(\cos k_o z, \sin k_o z, 0)$ on axis. If electrons are perfectly injected near the magnet axis (as we will assume) their helical motion is $\vec{\beta}_\perp = -(K/\gamma)\cdot(\cos k_o z, \sin k_o z, 0)$. The corresponding optical wave has the form $\vec{A}(\vec{x},t) = k^{-1}E(z,t)(\sin\Psi, \cos\Psi, 0)$ where $\vec{A}$ is the vector potential, $\omega = kc$ is the carrier frequency, $E(z,t)$ is the optical electric field strength, $\Psi = kz - \omega t + \phi(z,t)$, and $\phi(z,t)$ is the optical phase. After the coherence of this wave form is established, its amplitude E and phase ϕ can still evolve in shape and time.

In the presence of these fields the electron energy

γmc^2 changes according to $d\gamma/dt = (eKE/\gamma mc)\cos(\zeta + \phi)$ where the electron phase is $\zeta = (k + k_o)z - \omega t$. When the number of magnet periods is large the resulting changes in γ are small ($\delta\gamma/\gamma \lesssim 1/2N$). In this event the electron equation of motion becomes the pendulum equation:[8,15]

$$\ddot{\zeta}_{z'} = \dot{\nu}_{z'} = |a(z)|\cos(\zeta_{z'} + \phi(z)), \qquad (4)$$

where $z' = z + s(\tau - \frac{1}{2})$, $\tau = ct/L$, $\dot{(\ )} \equiv d(\ )/d\tau$, $\nu \equiv \dot{\zeta}$ is the electron's dimensionless velocity, $a = |a|e^{i\phi}$, $|a| = 4\pi NeKLE/\gamma_o^2 mc^2$ is the dimensionless optical field amplitude, and γ_o the initial electron energy. The position $z = z/\Delta$ and the "slippage" $s = N\lambda/\Delta$ have been normalized to Δ, the electron pulse half-width at half-maximum. The dimensionless time τ changes from 0 to 1 during one pass through the laser magnet. The height of the closed orbit separatrix in the dimensionless pendulum phase space (ζ,ν) is $2|a|^{\frac{1}{2}}$.

The optical wave is driven by the total beam current which is the sum of all single particle currents determined by (4). The resulting changes in $a(z)$ then act back self-consistently to alter the electron phase space paths. The *slowly varying amplitude and phase approximation* describes an envelope $a(z)$ that evolves slowly over optical wavelengths. The terms in Maxwell's wave equation involving double derivatives ($\ddot{E},\ddot{\phi},E'',\phi'',\dot{E}\dot{\phi}$, etc.) are negligible compared to terms involving single derivatives. The wave operator $(\partial/\partial z + c^{-1}\partial/\partial t)$ is made into a single derivative $L^{-1}\partial/\partial\tau$ by substituting $z = \tilde{z} + ct$ and $t = \tau L/c$ (the method of characteristics). Projecting out the slow driving current the wave equation becomes

$$\dot{a}(z) = -\langle re^{-i\zeta}\rangle_{z'}, \qquad (5)$$

where $r(z') = r_o[1-\frac{1}{2}(z')^2]$ is the dimensionless electron pulse shape with $z' = z + s(\tau - \frac{1}{2})$, $r_o = 8N(\pi eKL)^2\rho_o F/\gamma_o^3 mc^2$, and ρ_o is the actual peak electron density at position $z'=0$. The average value of $re^{-i\zeta}$ at the position z' is taken over sample electrons labeled by their initial phase space coordinates (ζ_o,ν_o) and is denoted by $\langle\ \rangle_{z'}$. As electrons evolve in the pendulum phase space, they can at most move a few optical wavelengths relative to the electron pulse centroid. This redistribution of charge affects $\langle e^{-i\zeta}\rangle$ locally, but is not sufficient to alter the pulse shape which is many wavelengths long. The electron pulse shape given by $r(z)$ remains fixed throughout the evolution $\tau = 0 \to 1$, but drifts back in the coordinate z by a distance s. We have taken $r(z)$ to be parabolic with a half-width at half-maximum of unity ($r(1) = \frac{1}{2}r_o$). Previous pulse propagation studies[10,11] used Gaussian shapes for $r(z)$, but real pulses from accelerators are probably better described by a shape without extended tails. Furthermore, a real three-dimensional pulse becomes narrower in the transverse dimension as the on-axis density decreases away from its peak. The narrower regions of the beam have increased diffraction losses (the optical wavefront spreads beyond the transverse width of the end-mirror), making the cutoff parabolic density an even more reasonable representation of the system. The coupled nonlinear equations (4) and (5) form the basis of our problem. They are valid for low gain and high gain systems ($r \lesssim 10^3$) in both weak and strong optical fields ($10^{-3} \lesssim |a| \lesssim 10^4$).

A "fresh" electron pulse enters the resonator cavity on each round trip bounce of the optical pulse. The new electrons are uniformly spread over ζ_o between $-\pi/2$ and $3\pi/2$ covering one closed orbit section of the separatrix. The separatrix is given by the locus of phase space points

(ζ_s,ν_s) at z satisfying $\nu_s^2 = 2|a(z)|(1 + \sin(\zeta_s + \phi(z))$. The Stanford beam is nearly monoenergetic so that each electron starts with the same initial dimensionless velocity $\nu_o = 2.6$ called the resonance parameter. This gives maximum gain $g = (a^2_{final}/a_o^2 - 1) = 0.13r_o$ for low current ($r_o \lesssim 20$) and initially weak uniform fields a_o ($\lesssim 1$). Alternatively, selecting $\nu_o = 2.6$ can be thought of as predicting the carrier wave frequency ω which will first establish coherence by means of mode competition. After the electrons are started at $\tau = 0$ the pendulum equation (4) forces them to "bunch" in response to the presence of the optical wave. When this bunching is around $\zeta \approx \pi$ the optical wave grows according to (5). To illustrate the electron phase space dynamics, Fig. 2 shows twenty sample electrons starting at $\nu_o = 2.6$ in strong fields $a_o = 30$ with $r_o = 1$. Here the pulse structure is ignored ($\Delta \to \infty$). Maximum gain $g(\tau)$ occurs near $\tau \sim \frac{1}{2}$ and "over-bunching" actually absorbs light near $\tau \sim 1$. The net gain and phase shift are diminished in strong fields causing saturation.

It has been shown[16] that the form of equations (4) and (5) applies to a linearly polarized magnet and its on-axis harmonics as well as to the helical magnet. The proper transformation to the f^{th} harmonic in a linearly polarized magnet is $|a| \to \frac{1}{2}|a|$ in (4); $\zeta \to f\zeta$ in both (4) and (5); and $K^2 \to K^2[J_\ell(f\xi) - J_{\ell+1}(f\xi)]^2$ in both $|a|$ and r_o where $\xi = K^2/4(1 + \frac{1}{2}K^2)$ and $\ell = (f - 1)/2$.

Integration of (4) and (5) with respect to τ starts with a wave form on the n^{th} pass and gives a new modified wave form for the $(n + 1)^{th}$ pass. Only two parameters govern this change: the nominal gain $r_o = 1.6$ and the slippage $s = 1.2$ for Stanford. After passing through the laser magnet, the optical pulse then strikes the resonator mirrors. The

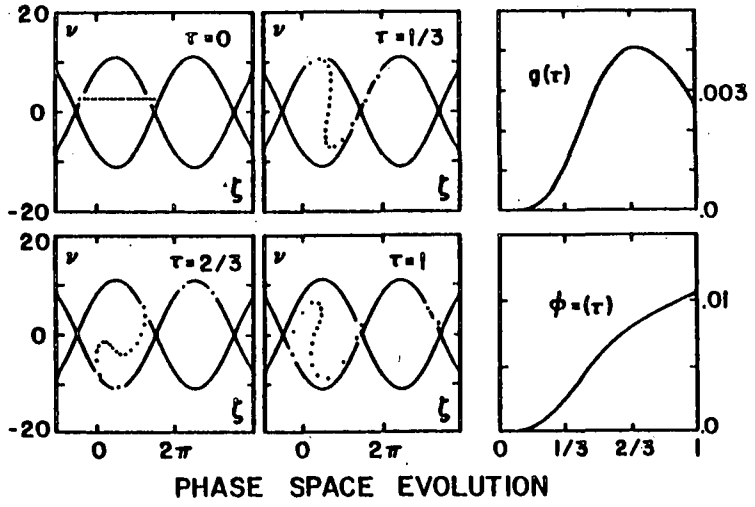

Fig. 2. Twenty sample electrons representing a current density $r_o = 1$ start at $\tau = 0$ with dimensionless velocity $\hat{v}_o$ in the self-consistent pendulum phase space (ζ,ν). The self-consistent separatrix is drawn for reference to the evolving phase space paths. For strong fields $a_o = 30$ there is bunching near $\zeta \sim \pi$ at $\tau \sim \frac{1}{2}$. However, because the electrons perform a full synchrotron orbit about $\zeta \sim \pi/2$ there is a decrease in gain $g(\tau)$ at $\tau = 1$. The phase shift $\phi(\tau)$ is also shown.

end mirror has some small transmission which is described by a resonator Q such that $a^2(n) \propto e^{-n/Q}$ in the absence of gain. A value of Q = 35 is measured at Stanford.

In the Stanford experiment one of the resonator mirrors can be moved to adjust the synchronism between the electron and optical pulses. The length adjustment $\Delta\mathcal{L}$ is again normalized to Δ and defines the desynchronism $d = \Delta\mathcal{L}/\Delta$. With no gain or loss the optical pulse would advance by a distance 2d with respect to the electron pulse on each pass. The many experimental parameters of the Stanford pulse problem[3] have been grouped together leaving only four independent

dimensionless variables: $r_o = 1.6$, $Q = 35$, $s = 1.2$, and d spanning the range $0 \to 0.1$.

The procedure for solving (4) and (5) is to start the oscillator from coherent weak fields ($a_o \simeq 1$) with either a Gaussian or uniform optical pulse shape. The goal of iteration is to find an optical pulse profile which reproduces itself on successive passes n. This is either the "fixed point" or "limit cycle" solution to our non-linear pulse problem. Typically a solution is reached after about 500 passes, and we observe the pulse to about 1000 passes. The role of the phase profile $\phi(z)$ is to change the optical pulse frequency. When $\phi(z)$ acquires a linear slope in z, this can be directly interpreted as a change in the optical wave number and hence the resonant parameter through $\delta\nu = -s\,\phi'(z)$. We define $\nu_k = \nu_o + \delta\nu$ as the modified resonance parameter. Typically we find $\delta\nu$ moves the laser from $\nu_o = 2.6$ to $\nu_k \sim 7$ which gives higher gain in strong fields. The final "fixed point" behavior is independent of the starting field strength a_o and resonance parameter ν_o since we can alter these variables and arrive at the same solution.

It is instructive to consider the gain curves $g(\nu_o)$. We again ignore the pulse structure here. In weak fields ($a_o \lesssim 1$) and for low gain ($r_o \lesssim 1$) $g(\nu_o) = r_o(1 - \cos\nu_o - \frac{1}{2}\nu_o \sin\nu_o)/\nu_o^3$. Figure 3 plots low gains g/r_o over the range $-50 \leq \nu_o < 25$ for field strengths from $a_o = .1$ to 100. When $a_o \gtrsim 10$, the gain curves distort, so that peak gain decreases (this is saturation) and occurs at increasing ν_o. For these curves alone, we should expect that steady-state occurs when a_o is somewhere between 10 and 100 and ν_k is between 2.6 and 10. This is what we will in fact find.

Our first observation is that the steady-state solution for $d = 0$ is $|a(z)| = 0$. Figure 4 illustrates this effect.

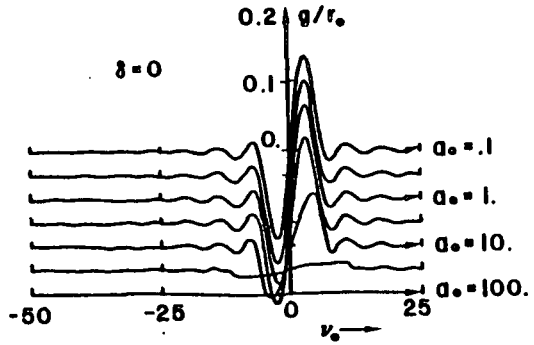

Fig. 3. Gain curves $g(\nu_o)$ are plotted in units of $r_\bullet$ for various optical field strengths $a_o = .1 \to 100$. For moderate gain ($r_\bullet \lesssim 10$), the curves are antisymmetric about resonance ($\nu_o = 0$). In weak fields ($a_o \lesssim 1$) peak gain occurs at $\nu_o = 2.6$, but in strong fields peak gain is found at $\nu_o \sim 7$. The laser oscillator evolves along the points of maximum gain. ($\delta = 0$ indicates that this is an untapered wiggler).

It is surprising that exact synchronism (d = 0) of the electron and optical pulses results in no power from the free electron laser oscillator. The fundamental reason for the desynchronism effect is clearly seen in Fig. 4. Even in the strong fields gain does not develop until $\tau \sim \frac{1}{2}$. This delay means that the leading edge of the optical pulse experiences little gain and in fact a net loss after absorption. The trailing edge of the optical pulse overtakes the electrons after bunching has occurred so that higher gain is experienced. The net result is that the optical pulse is reshaped so that its centroid moves back on each pass through the laser magnet. Effectively the optical pulse is traveling slower than the speed of light even though the individual photons are traveling at the speed of light. Figure 4 shows the distortion and subsequent decay of a pulse

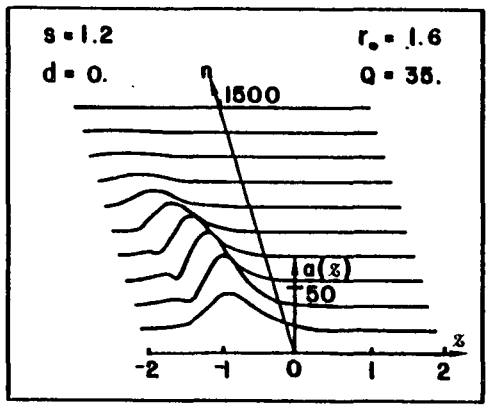

Fig. 4. The amplitude of the optical pulse shape a(z) is plotted at $\tau = 1$ every 150 passes through the resonator up to n = 1500 passes. The fields start at $|a| = 1$, and are diven by the parabolic current density $r(z') = r_o(1 - \frac{1}{2}(z')^2)$ where $z' = z + s(\tau - \frac{1}{2})$ With no desynchronism d = 0, the light moves away from the electrons and eventually decays with the resonator Q. The fixed point solution is therefore zero.

evolving with d = 0. The optical pulse a(z) is plotted at $\tau = 1$ after each 150 passes up to 1500 passes. The electron pulse peak moves from $z = s/2$ to $-s/2$ on each pass, and has a half-width at half-maximum of unity.

To achieve non-zero steady state power, we must have $d > 0$. Then electrons continue to add light to the trailing edge of the optical pulse, but the desynchronism mechanism moves the light forward to support the front edge. The laser characteristics are significantly modified as d increases. Figure 5 shows a plot of the steady-state optical pulse energy $\int_{-\infty}^{\infty} a^2(z)dz$ versus d, called the "desynchronism curve". Near d = 0 the peak power grows rapidly with d.

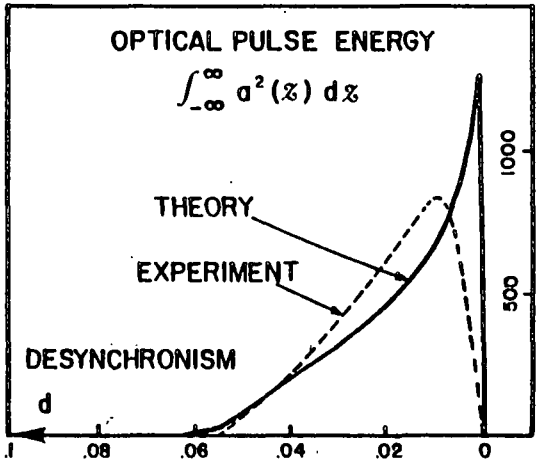

Fig. 5. The steady-state optical pulse energy, or laser output power, is non-zero only over a small range in desynchronism d > 0. Maximum energy occurs when d ≈ 0, then steadily decreases as d increases. The experimental desynchronism curve agrees very well with theory in overall width but differs somewhat in shape.

When d is too large the desynchronism mechanism moves the pulse power forward too fast for gain to support the trailing edge of the pulse so that the pulse energy decreases back to zero. The character of the steady-state optical power spectrum, the optical pulse shape, and the electron velocity distribution all change with the operating desynchronism d.

Figure 6 shows the evolution to steady-state after n = 1500 passes for small desynchronism d = .001. The optical pulse a(z) is only one-fourth the length of the electron pulse and has multiple peaks which can have high field strengths $|a| \sim 50$. This is a remarkably short optical

pulse of 0.25 mm length with high power ~10^9 watts in the Stanford case. The multiple peaks in a(z) are caused by "ringing" synchrotron oscillations in the electron phase space following the large optical spike. They are spaced a distance slightly less than s in strong fields. We measure the final electron z-velocities at τ = 1 by their final

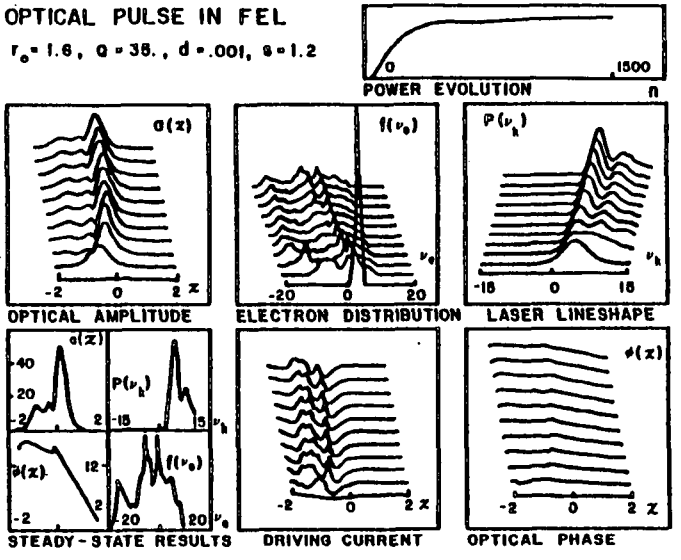

Fig. 6. At small desynchronism d = .001, the Stanford parameters produce an optical pulse shape a(z) whose length is four times shorter than the electron pulse and has a large peak field. This gives a broad power spectrum $P(\nu_k)$ centered at $\nu_k \sim 6$, and a broad electron velocity distribution $f(\nu_e)$ due to the high field strength. The driving current continually reshapes the optical pulse to compensate for desynchronism, and the phase profile $\phi(z)$ shifts $P(\nu_k)$. The pulse energy (or laser power) reaches steady state after $n \sim 10^3$ passes, and the final results are shown on the lower left.

dimensionless velocity $\nu_e = L[(k + k_o)\beta_z - k]$, and $f(\nu_e)$ is the distribution of ν_e's. The width of $f(\nu_e)$ is generally given by the height of the separatrix $4|a|^{\frac{1}{2}} \approx 30$ in this case, and is characteristically wide for small d. The Stanford experiment also shows wide $f(\nu_e)$ for d, but does not show the sharp peak structure because of insufficient resolution in their spectrometer. The large peak at $\nu_e \approx -15$ is observed and the overall width of $f(\nu_e)$ is in good agreement with experiment. The Fourier transform of the pulse structure gives its power spectrum $P(\nu_k)$. Each component is measured by $\nu_k = \nu_o - s\phi'(z)$. $P(\nu_k)$ is relatively wide and centered around the $\nu_k \sim 6$. The shift in ν_k from ν_o accomplished by a sloping phase profile $\phi(z)$ shown in the lower right of Figure 6. We interpret the experimental results as giving $\delta\nu_k \sim 2$ centered at $\nu_k \sim 4$, but there is some uncertainty in determining resonance. The current driving $|a(z)|$ at $\tau = 1$ is shown in the bottom-center. This shows how the oscillating current can cause multiple peaks. The final pulse profile $|a(z)|$, $\phi(z)$, power spectrum, and electron velocity distribution are shown at the lower left.

In Figure 7 is shown the optical pulse evolution resulting from larger desynchronism d = .003. It is significantly broader with multiple peaks of weaker fields $|a| \sim 25$ spaced slightly larger than s. The optical pulse centroid is ahead of the electron pulse. The power spectrum and electron velocity distribution are both narrower than for the small d case. The limit cycle behavior is the most prominent feature of this example. This is observed in the Stanford experiment and has not been previously reported theoretically. It is remarkable that a given pulse shape can disappear and reproduce itself hundreds of passes later. The pulse energy

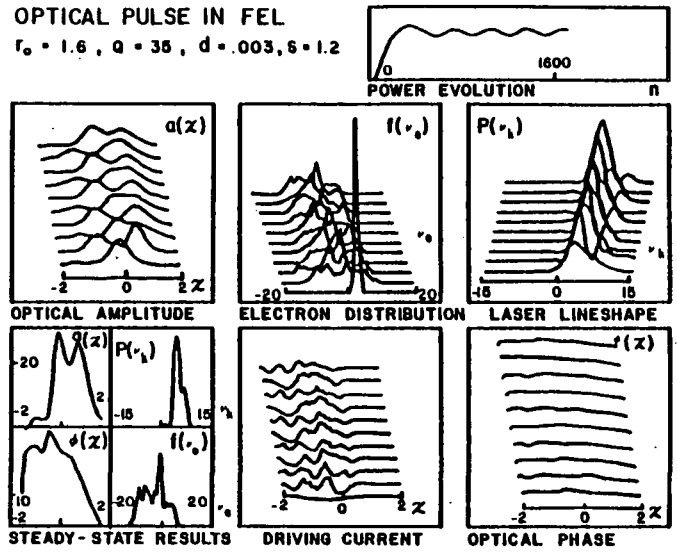

Fig. 7. With d = .003 we see clear limit-cycle behavior of the laser pulse energy. Subpulses in a(z) start at the trailing edge and pass through the pulse profile to continually modify its shape.

or power oscillations are quite periodic in the upper-right plot. The power variations are caused by "marching subpulses" which start at the trailing edge and pass through to the front of the optical pulse over hundreds of passes. Higher pulse energy occurs when there are two peaks, and diminishes when only one peak is present.

At large desynchronism d = .042 the optical pulse has much weaker fields and is three times longer than the electron pulse $\delta z \sim 6$. This is depicted in Figure 8. Its centroid runs farther ahead of the electron pulse with little or no subpulse structure. Much of the pulse's area lies

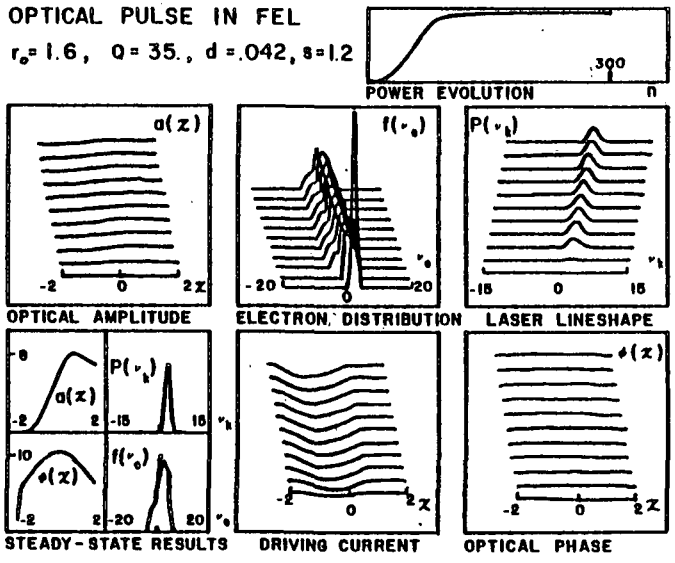

Fig. 8. With large desynchronism d = .042, the steady-state pulse energy is small and the fields are weak. The optical pulse is now three times longer than the electron pulse. The electron velocity distribution $f(\nu_e)$ is narrow as is the power spectrum $P(\nu_k)$, which is centered about $\nu_k \sim 3$.

outside of the "window" shown and decays away exponentially with Q^{-1} since it is decoupled from the electrons ($r(z) = 0$ for $z \geq s/2 + \sqrt{2}$). The rate of the decay is given by $|a(z^*)| \exp(-z/4Qd)$ where $z^* = 2$ is the last point calculated in Fig. 8. Since there is no subpulse structure, there is no limit cycle behavior and the power spectrum is narrow $\delta\nu_k \sim 2$. Since the fields are weak the power spectrum remains centered near $\nu_k \sim 3$. A power spectrum width of $\delta\nu_k \sim 1$ is observed experimentally. The resulting electron velocity distribution is narrower ($\delta\nu_e \sim 5$) with a single

peak. This is in part because of weaker fields, but also because electrons drop back out of the optical pulse at about $\tau \sim \frac{1}{2}$ on each pass. The single peaked $f(\nu_e)$ with width $\delta\nu_e \sim 6$ is observed experimentally.

In total, the characteristic trends presented in the examples of Figs. 6, 7, and 8 are in excellent agreement with the experimental results available at this time. Even the quantitative agreement is good, but cannot be perfect because of a few minor experimental uncertainties. The simple set of equations (4) and (5) are rich in the variety of solutions they can present and many of these are now verified by the recent Stanford experiments.

PULSE PROPAGATION IN TAPERED WIGGLERS. The original proposal for a variable parameter wiggler magnet in a free electron laser was made by J.M.J. Madey concurrent with his original proposal for the free electron laser.[17-19] This proposal makes use of a fundamental advantage of free electron lasers. The periodic magnetic field can be constructed in a variety of ways to meet various needs. The magnetic field strength, the magnet wavelength, or both may be varied along the magnet length to achieve the desired result. All of these variations were explored theoretically early in the development of free-electron lasers with the goal of improving free electron laser characteristics for storage-ring operation. However, after the development of the pendulum equation[8] accelerator physicists realized the similarity between the free electron laser and a linear accelerator.[20,21] Based on this understanding, it was proposed that an increasing wavelength magnet could trap electrons and decelerate electrons, and thereby

persistently drive a large amplitude optical wave.

The modified electron equation for a variable parameter magnet is derived by starting from a new form for the magnetic field $\vec{B}_m = B_o(z)(\cos\alpha, \sin\alpha, 0)$ where $\alpha = \int_0^z k_o(z')dz'$ and $\lambda_o(z) = 2\pi/k_o(z)$. For algebraic convenience we take a special case where $K = eB_o(z)\lambda_o(z)/2\pi mc^2$ is constant even though B_o and λ_o can vary with z. The derivation proceeds as before to give the same energy transfer equation, but a somewhat different definition of the electron phase: now $\zeta = \int_0^z k_o(z')dz' + kz - \omega t$ and $\nu = \dot{\zeta}$, $\dot{(\ )} = d(\ )/d\tau$, and $\tau = tc/L$ as before. The new feature in $\nu = L[(k_o(\tau) + k)\beta_z - k] \approx L[k_o(\tau) - k(1 + K^2)/2\gamma^2]$ is an evolving magnet wavenumber $k_o(\tau)$. Electrons trapped near resonance ($\nu \approx 0$) by a large amplitude optical field must follow a decreasing $\lambda_o(\tau)$ by decelerating, thereby lowering γ. Their energy loss drives the optical wave.

If the electron energy extraction is large, corresponding to a large change in $\lambda_o(\tau)$, then the equations of motion are best left in the form above using γ. If the amount of taper is more modest, the fractional energy changes can be small, but still much larger than for the untapered wiggler. In this case the electron energy can be eliminated from the tapered wiggler equations ($\gamma \approx \gamma_o$) to give

$$\ddot{\zeta}_{z'} = \dot{\nu}_{z'} = \delta + |a(z)|\cos(\zeta_{z'} + \phi(z)) \qquad (6)$$

where $z' = z + s(\tau - \frac{1}{2})$. The modified pendulum equation (6) has a new additive term $\delta \equiv Lk_o'(\tau)$. If the amount of taper is small, δ is nearly constant and $\delta \approx 2\pi N\Delta\lambda_o/\lambda_o$ where $\Delta\lambda_o/\lambda_o$ is the fractional decrease in λ_o. The wave equation retains precisely the same form as (5) in the case of the tapered wiggler and only the pendulum equation is modified.

The main new feature in the pendulum equation, the term δ, leads to significantly altered evolution. If the optical field is absent or very weak ($|a| \approx 0$), all electrons evolve according to $\nu = \nu_o + \tau\delta$ and $\zeta = \zeta_o + \tau\nu_o + \frac{1}{2}\tau^2\delta$. Their phase space paths are given by parabolas $\nu^2 = \nu_o^2 + 2\delta(\zeta - \zeta_o)$. When $|a|$ evolves slowly compared to the electron evolution, as is typical, we can consider the self-consistent phase space paths given by $\frac{1}{2}\nu^2 - [\zeta\delta + |a|\sin(\zeta + \phi)] = \text{constant}$. These paths evolve slowly with $|a|$ and ϕ, but instantaneously are a good guide. The corresponding potential $V(\zeta) = -[\zeta\delta + |a|\sin(\zeta + \phi)]$ gives (6) through $\ddot{\zeta} = -\partial V(\zeta)/\partial\zeta$. $V(\zeta)$ is "tilted" toward positive ζ and has ripples caused by $|a|\sin(\zeta + \phi)$. These ripples act as electron traps when $|a|$ is large enough.

In strong fields ($|a| \gtrsim \sqrt{2}\delta$) the phase space parabolas are distorted so that electrons near $\nu_o \approx 0$ and $\zeta_o \approx \pi$ can be trapped. This is shown in Fig. 9 where pulse structure is ignored and $\delta = 5\pi$, $\nu_o = 0$ for twenty sample electrons representing a current density $r_o = 1$, and $a_o = 25$. This example could be a N = 50 period magnet with a 5% decrease in magnet wavelength λ_o from $\tau = 0 \to 1$. The untrapped electrons eventually become random in phase, while the trapped electrons remain near $\zeta \approx \pi$ to drive the optical wave through $\hat{a} = -r\langle e^{-i\zeta}\rangle$. The wave growth, or gain $g(\tau)$, is shown at the right with the accompanying optical phase shift $\phi(\tau)$. Since $g(\tau)$ helps determine how the optical pulse is reshaped on each pass, we can generally expect tapered wigglers to act differently than untapered wigglers. Note that the main feature of tapered wigglers is the presence of a term like δ. For more severe tapers, the actual time dependence of δ and γ only modifies the central ideas

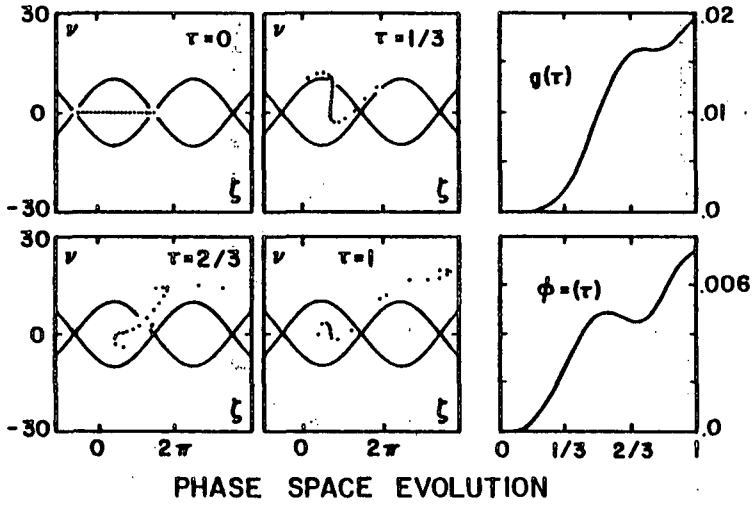

Fig. 9. Twenty sample electrons representing a current density $r_o = 1$ start on resonance in the self-consistent phase space (ζ,ν) of a tapered wiggler with $\delta = 5\pi$. About half the electrons are trapped near resonance by strong optical fields $a_o = 30$. The wave is driven in a non-uniform way as shown by the gain $g(\tau)$ and shifting phase $\phi(\tau)$.

described above.

The coupled equations (5) and (6) can be solved analytically when gain is low ($r_o \lesssim 1$), fields are weak ($|a| \lesssim 1$), and pulse structure is ignored. The gain and phase are

$$g/r_o = \int_0^1\int_0^\tau\int_0^{\tau'} \sin[\nu_o(\tau - \tau'') + \tfrac{1}{2}\delta(\tau^2 - \tau''^2)]d\tau''d\tau'd\tau$$

$$\Delta\phi/r_o = \int_0^1\int_0^\tau\int_0^{\tau'} \cos[\nu_o(\tau - \tau'') + \tfrac{1}{2}\delta(\tau^2 - \tau''^2)]d\tau''d\tau'd\tau. \qquad (7)$$

These solutions are more general than earlier work[22] and are shown among the curves presented in Fig. 10 ($a_o = 0.1$ to 1). The integrals can be written in terms of Fresnel integrals,[23] but the result is no more transparent than (7). In Fig. 10 gain curves are plotted in units of r_o with $\delta = 5\pi \approx 2\pi N\Delta\lambda_o/\lambda_o$. Maximum gain now occurs at a negative resonance parameter ($\nu_o \approx -\frac{1}{2}\delta$), and is less than the available gain in an untapered wiggler.

The advantage of tapered wigglers comes at large a_o. In the untapered case, saturation occurs when $|a|$ is large

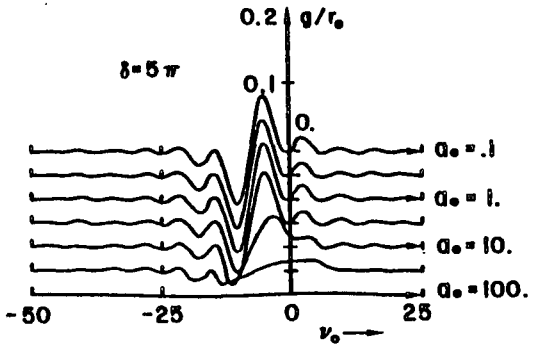

Fig. 10. Gain curves $g(\nu_o)$ are plotted in units of r_o for a tapered wiggler with $\delta = 5\pi$. Peak gain in weak fields ($a_o = .1$ to 1.) now occurs at negative $\nu_o \approx -\frac{1}{2}\delta$. In strong fields where trapping occurs ($a_o \gtrsim \sqrt{2\delta}$), peak gain occurs on resonance $\nu_o = 0$. Note that there is sufficient weak field gain available for oscillator start-up.

causing bunching to center about $\zeta \sim \pi/2$. But when $\delta > 0$ and $|a| > \sqrt{2\delta}$ in the tapered case the trapping near resonance causes electrons to be centered about $\zeta \sim \pi$. At high fields

the tapered wiggler exhibits gain superior to that of the untapered wiggler so that more energy can be extracted from the electron beam. Figure 10 shows the evolution of gain from weak to strong fields. Gain decreases with increasing a_o just as in the $\delta = 0$ case, but comparison with Fig. 3 shows more gain is available at strong fields ($a_o \gtrsim 25$). The point of maximum gain moves to $\nu_o \approx 0$ in strong fields since trapping occurs at resonance. We should anticipate that a tapered wiggler laser oscillator will start at wavelengths corresponding to $\nu_k \approx -\frac{1}{2}\delta$ and then move to $\nu_k \approx 0$. We will observe this in the numerical solutions to the pulse problem.

In Fig. 11, gain curves for the same field strengths are shown with $\delta = 10\pi$. This could be a N = 50 period magnet with 10% taper. The result is even more distortion of the weak field gain curve. There are now several peaks which have competitive gains. Unlike the $\delta = 5\pi$ examples, it appears that weak coherent fields may build up in many modes. It is not clear what will happen to some of these modes in the evolution of gain to strong fields. The modes starting at $\nu_o \approx -8$ move to resonance, but the modes starting at $\nu_o \approx -22$ could not really reach resonance in an obvious way. We therefore leave this example for further study and restrict ourselves to the more modestly tapered wiggler example $\delta = 5\pi$. Note also that in both of these examples there is always more weak field gain available than strong field gain. There is no start-up problem in modestly tapered wigglers as often reported; the gain is just not on resonance. With larger δ, weak field gain can become small enough to cause problems, but it should be appreciated that these examples still represent a significant improvement

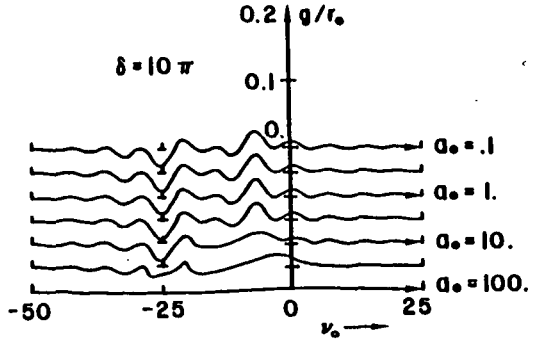

Fig. 11. Gain curves $g(\nu_o)$ for a more severely tapered wiggler ($\delta = 10\pi$) show significantly less gain in weak fields, and have several competitive gain maxima. Such a system may give experimental difficulties.

over tapered wiggler energy extraction.

In order to facilitate comparison with an untapered wiggler, we choose parameters similar to the Stanford system: $r_o = 2$, $Q = 35$, and $s = 1$ with a modest taper $\delta = 5\pi$. If we imposed a 1.5% taper on the Stanford laser magnet the nominal extraction efficiency would be increased by a factor of 5 and give $\delta = 5\pi$.

We solve the $\delta = 5\pi$ oscillator problem in the same manner as in the previous section. Electrons are injected with $\nu_o = -2\pi$ to give nearly maximum gain in weak fields. Figure 12 shows twenty sample electrons ($r_o = 1$) evolving in weak fields $a_o = 1$. Starting at $\nu_o = -2\pi$, they follow quasi-parabolic phase space paths toward and past resonance. Some bunching develops so that gain is achieved near $\tau \approx 1$. However, absorption occurs first at $\tau \approx 2/3$.

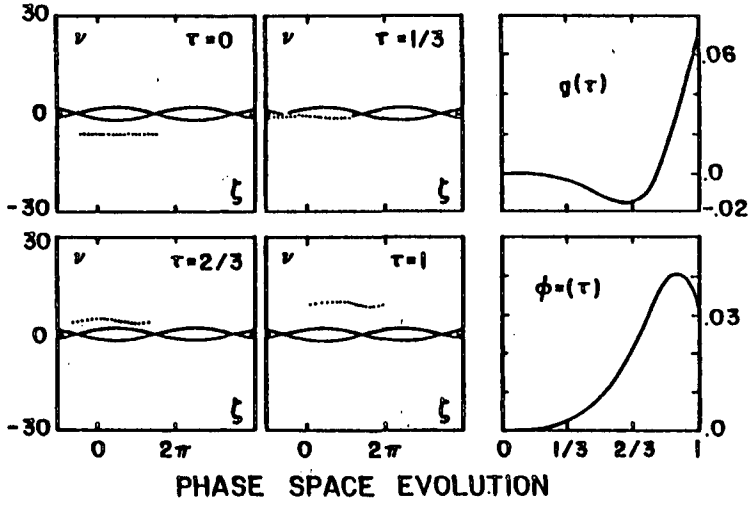

Fig. 12. Phase space evolution shows how gain is achieved in weak fields in a tapered wiggler with $\delta = 5\pi$. Twenty sample electrons start at $\nu_o = -2\pi$ representing a current density of $r_o = 1$. Electrons follow nearly parabolic phase space paths, but bunch due to the weak field $a_o = 1$. $g(\tau)$ shows there is actually absorption at $\tau \approx 2/3$ followed by final gain.

An optical pulse with no desynchronism d = 0 disappears after ~1000 passes as in the $\delta = 0$ case. The evolution is similar to that shown in Fig. 4.

With a small amount of desynchronism d = .001, we find that the laser slowly grows to high power ($|a| \sim 40$). See Fig. 13. The energy distribution $f(\nu_e)$ shows a double peak indicating some electrons are trapped in the optical potential. Note the power spectrum has shifted from $\nu_k = -2\pi$ to resonance $\nu_k \approx 0$ as expected. This is again accomplished by the optical phase profile $\phi(z)$ developing

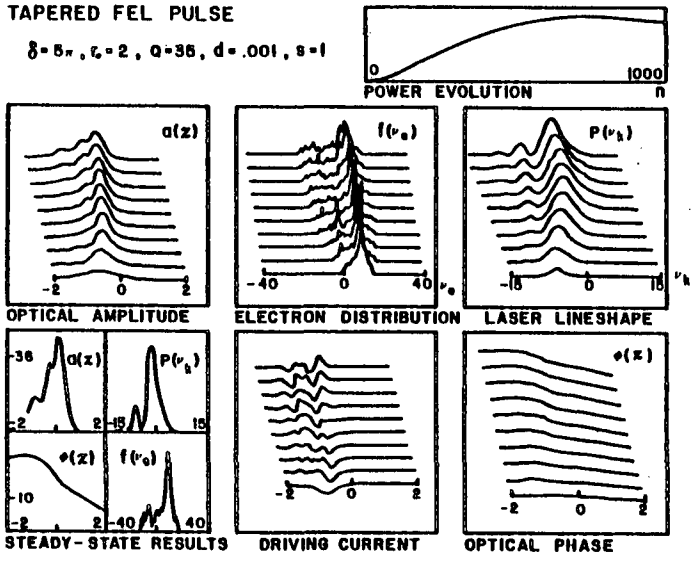

Fig. 13. Tapered wiggler pulse evolution with $\delta = 5\pi$ and small desynchronism d = .001 results in a short optical pulse a(z) with subpulse structure. Trapping is evident in the final electron distribution $f(\nu_e)$ when fields are strong. The power spectrum $P(\nu_k)$ is broad and its center smoothly evolves from $\nu_k = -2\pi$ to resonance $\nu_k = 0$ as strong fields begin to trap electrons. This example corresponds to the Stanford laser with a 1½% taper of the magnet wavelength during $\tau = 0 \rightarrow 1$, and 25% more current ($r_o = 2$).

the slope shown in the lower right. As in the untapered case, a complicated pulse structure a(z) develops due to the driving current. The final results are shown on the lower left. The subpulse structure indicates the "ringing" of the electron synchrotron oscillations within the trapping potential. This

can also be caused by untrapped electrons absorbing light as they pass by $\zeta \sim 0$ in a bunch. The narrow subpulse structure causes a broad power spectrum with sideband structure. As indicated by the pulse energy or power evolution (upper right), this computation may not as yet have reached steady state after 1000 passes.

In the next example, we consider a larger amount of desynchronism d = .005. See Fig. 14. The optical pulse centroid is in front of the electron pulse. The optical

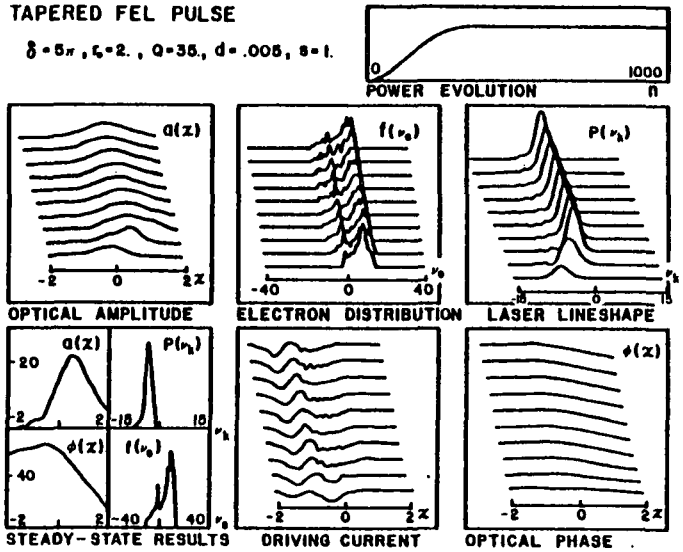

Fig. 14. Tapered wiggler pulse evolution with $\delta = 5\pi$ and large desynchronism d = .005 results in a weaker and longer optical pulse with no structure. Only modest trapping occurs because the fields are weaker and because most electrons drop back out of the optical pulse at $\tau \sim \frac{1}{2}$. The power spectrum $P(\nu_k)$ is narrow.

pulse is broad with no structure so the power spectrum is narrow. Again it is clear that as the fields become strong the maximum gain drives the waves toward resonance, but the fields in this case never become strong enough for efficient trapping and never reach resonance. Steady state operation is reached more quickly for larger d. For even larger d, there is less steady-state power and fields a(z) are so weak that trapping cannot take place. There is sufficient gain to sustain the pulse however, and the results are similar in character to the $\delta = 0$ case shown in Fig. 8.

The desynchronism curve for tapered wigglers has the same shape as the untapered case shown in Fig. 5. A direct comparison with Fig. 5 taking $\delta = 0 \rightarrow 5\pi$ gives a desynchronism curve which has half the width in d and about half the peak power. For this short pulse example, the tapered wiggler performance was inferior to the untapered wiggler.

ACKNOWLEDGEMENTS. The author wishes to acknowledge support from the Air Force Office of Scientific Research, Grant AFOSR-81-0061 and NASA Grant NAG 2-48, and many helpful discussions with R.A. Freedman, J. Richardson and J.M.J. Madey.

REFERENCES

1. D.A.G. Deacon, L.R. Elias, J.M.J. Madey, G.J. Ramian, H.A. Schwettman, and T.I. Smith, *Phys. Rev. Lett.* 38 (1977) 892.
2. J.M.J. Madey *et al.*, Final Technical Report to ERDA, Contracts EY-76-S-03-0326 PA 48 and PA 49 (1977).
3. J.N. Eckstein, J.M.J. Madey, K. Robinson, and T.I. Smith, Stanford HEPL Report #894, to be published in this volume.

4. *Physics of Quantum Electronics*, vol. 7, (Addison-Wesley, 1980) eds. S.F. Jacobs, H.S. Pilloff, M. Sargent, M.O. Scully, and R. Spitzer.
5. *IEEE J. Quantum Electron.*, QE-17, Special issue on free electron lasers, August (1981), guest ed. A. Szöke.
6. F.A. Hopf, T.G. Kuper, G.J. Moore, and M.O. Scully, Chapter 3, reference 4.
7. G. Dattoli, A. Marino, A. Renieri, and F. Romanelli, *IEEE J. Quantum Electron.*, QE-17 (1981) 1371.
8. W.B. Colson, *Phys. Lett.* 64A (1977) 190.
9. W.B. Colson and S.K. Ride, *Phys. Lett.* 76A (1980) 379.
10. W.B. Colson, Chapter 13, reference 4.
11. W.B. Colson, *Proc. Int. Summer School of Quantum Electronics*, A. Renieri and S. Martellucci, eds. New York:Plenum, 1981.
12. N.M. Kroll and M.N. Rosenbluth, Chapter 6, reference 4.
13. W.B. Colson, *Phys. Lett.* 59A (1976) 187.
14. W.B. Colson, *Ph.D. Thesis*, Stanford University (1977), Univ. Microfilms Int., Pub. #78-02, 145.
15. W.H. Louisell, J.F. Lam, D.A. Copeland, and W.B. Colson, *Phys. Rev. A* 19 (1979) 288.
16. W.B. Colson, *IEEE J. Quantum Electron.*, QE-17 (1981) 1417.
17. J.M.J. Madey, U.S. Patent #3,822,410 (1974).
18. W.B. Colson, J.M.J. Madey, and T.I. Smith, Stanford Patent Disclosure S78-32 (1978).
19. J.M.J. Madey, D.A.G. Deacon, L.R. Elias, and T.I. Smith, *Nuovo Cimento* 51B (1979) 53.
20. N.M. Kroll, P.L. Morton and M.N. Rosenbluth, Chapter 4, reference 4.
21. N.M. Kroll, P.L. Morton, and M.N. Rosenbluth, *IEEE J. Quantum Electron.* QE-17 (1981) 1436.

IEEE JOURNAL OF QUANTUM
ELECTRONICS, VOL.QE-19, No.3
March 1983 , p. 272

Quantum/Classical Mode Evolution in Free Electron Laser Oscillators

P. Bosco, W. B. Colson, and Roger A. Freedman

Quantum Institute and Department of Physics

University of California

Santa Barbara, California 93106

ABSTRACT

The problem of oscillator evolution and mode competition in free electron lasers is studied. Relativistic quantum field theory is used to calculate electron wave functions, the angular distribution of spontaneous emission, and the transition rates for stimulated emission and absorption in each mode. The photon rate equation for the weak-field regime is presented. This rate equation is applied to oscillator evolution with a conventional undulator, a two-stage optical klystron, and a tapered undulator. The effects of noise are briefly discussed.

1. Introduction

A free electron laser (FEL) amplifies coherent radiation stored in a resonant optical cavity by means of a relativistic electron beam passing through an undulating transverse magnetic field (Fig. 1) [1-3]. From a classical point of view the electrons execute transverse oscillations which enhances their coupling to the radiation fields through the Lorentz force [4-8]. From a quantum mechanical point of view, the electron wave function is modulated by the undulating field: this distortion in the presence of radiation allows stimulated inverse Compton scattering to occur [9-15]. References [16-17] are collections of works on the FEL from many points of view.

Madey's original paper [1] led to the practical realization of the first FEL

and made use of the Weizsäcker-Williams method to calculate the quantum mechanical transition rates and to describe the gain. When classical approaches were subsequently introduced [4], they proved both to be adequate in describing the important features of the FEL and to be more tractable in dealing with the strong optical field regime [5,6,12-13,18-23]. For weak optical fields both quantum and classical approaches give similar results for comparable effort.

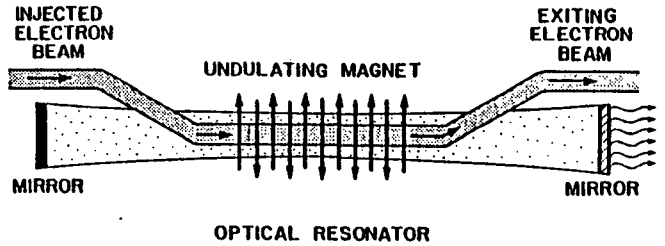

Figure 1. Relativistic electrons enter the FEL optical resonator, interact with the magnetic field of the undulator and with the stored optical radiation, and leave the resonator after a single pass.

Some of the quantum calculations presented in the literature have worked in a relativistic moving frame [24,25], with results similar to those found in the laboratory frame. Other authors have used quantum mechanics to study photon statistics in an FEL [26,27], including interesting problems such as the rise of long range coherence in the radiation field [28,29]. Other quantum approaches have made use of the Bloch equations [30] by exploiting some similarities between conventional lasers and the FEL. Finally some papers have dealt with single mode Compton scattering [31,32].

What has not been done either classically or quantum mechanically is to describe the early stages of the evolution and competition between modes of radiation stored in an FEL oscillator. While some work has examined the mode behavior in strong fields [33], the weak-field problem is important for understanding the onset of laser operation in an FEL. Our analysis is based on a rate

equation for the photon distribution function beginning from a fully quantum mechanical foundation in weak optical fields [11,12]. This is obtained using quantum electrodynamics: standard diagrammatic expansions are used to determine the rates for spontaneous emission and for stimulated emission and absorption. The rate equation is used to calculate the photon distribution function over many passes both below threshold and above threshold in the weak-field regime. The simplicity of the rate equation makes it possible to study various magnet designs, including the conventional undulator, the tapered undulator and the optical klystron. Since Planck's constant does not occur in the final rate equation, our results are classical and could have been derived from classical arguments. The motivation for using a quantum formalism is to eventually extend the calculations to include noise. The connections with the classical picture are pointed out in the paper whenever possible.

In section 2 we solve the Dirac equation to second order in the static field for electrons in an undulator. In section 3 we study the quantum mechanical spontaneous emission rates. In section 4 stimulated emission and absorption is investigated, and the resultant rate equation is stated explicitly in section 5. In section 6 the rate equation is used for the various magnet designs to obtain the multimode gain. The effects of noise are briefly discussed and found to be negligible.

2. Electron wave functions

The character of radiation from a free electron laser is determined by electron wave functions in the undulator structure. In this section these wave functions are calculated using the Dirac integral equation:

$$\psi(x) = \psi^{(0)}(x) + ie\int d^4x' G^{\text{Dirac}}(x-x')\,\gamma\cdot A^M(x')\psi(x') \quad , \tag{2.1}$$

where $G^{\text{Dirac}}(x-x') = -\int \frac{d^4q}{(2\pi)^4}\frac{e^{iq\cdot(x-x')}}{(i\gamma\cdot q+m)}$, and $\psi^{(0)}(x) = \frac{e^{ip\cdot x}}{\sqrt{V}}U(p,\sigma)$.

We use notation as in Sakurai [34] so that $x_\mu = (\vec{x},it)$, $\gamma_\mu = (\vec{\gamma},\gamma_4)$, and $\gamma\cdot q = \gamma_\mu q_\mu$ with repeated indices summed. The speed of light and Planck's constant over 2π are set equal to unity, the electron mass is m, the electron charge magnitude is $e=|e|$, and $A^M_\mu = (\vec{A}^M,0)$ is the vector potential of the undulator magnetic field. The unscattered electron wave function $\psi^{(0)}(x)$ is taken to be a plane wave: $p_\mu = (\vec{p},ip_4) = (\vec{p},i\gamma m)$ is the unscattered electron four-momentum, γ is the electron Lorentz factor, and $U(p,\sigma)$ is the four-component Dirac spinor. The normalization volume V is chosen to have longitudinal dimension L equal to the undulator length. We use $m\to m-i\varepsilon$ to properly define the Green's function $G^{\text{Dirac}}(x-x')$.

To incorporate the static magnetic field into the Dirac equation we have the vector potential

$$\vec{A}^M(x) = \frac{B\lambda_0}{4\pi}[\vartheta(z+L/2)-\vartheta(z-L/2)](\vec{a}e^{ik_0z} + \vec{a}^*e^{-ik_0z}) \quad , \tag{2.2}$$

where the peak magnetic field strength is B and the magnet wavelength is $\lambda_0 = 2\pi/k_0$. The complex polarization vector of the magnet $\vec{a}$ is transverse ($\vec{a}\cdot\hat{z} = 0$) and is not necessarily a unit vector. For example, a helical magnet has $\vec{a} = -(i,1,0)$ and a linearly polarized magnet has $\vec{a} = (1,0,0)$. The undulator magnet extends for a length $L = N\lambda_0$ where the number of periods $N \gg 1$. It is assumed that electrons sample the field only near the z-axis so that (2.2) is accurate [35]. Farther off the undulator axis the transverse field lines bend to satisfy Maxwell's equations. A typical undulator design has $\lambda_0 = 3.0$ cm, $B = 2500$ kilogauss, and $L = 150$ cm so that $N = 50$.

A single iteration of the Dirac equation estimates the full wave function $\psi(x)$ on the right-hand side of (2.1) with the noninteracting wave function $\psi^{(0)}(x)$. The result is [12]

$$\psi^{(1)}(x) = \frac{-ik\dot{m}}{2(2\pi)^4}\int d^4x'\int d^4q\,\frac{e^{iq\cdot(x-x')}}{(i\gamma\cdot q+m)}\left\{\gamma\cdot a e^{ik_0z'}+\gamma\cdot a^* e^{-ik_0z'}\right\}\frac{e^{ip\cdot x'}\,U(p,\sigma)}{\sqrt{V}}, \tag{2.3}$$

where $K = eB\lambda_0/2\pi m$. The integrals over x',y', and t' give δ-functions. The electron is allowed to interact with the magnet for an infinite time, but because the magnet length L is finite the integral over z' does not give a δ-function. The first order result is

$$\psi^{(1)}(x) = \left[\frac{-iKLm}{4\pi}\right]\int dq\,\frac{\sin[(q-k_0)L/2]}{[(q-k_0)L/2]} \times \left\{\frac{e^{iqz}\gamma\cdot a}{i(\gamma\cdot p+q\gamma_3)+m} + \frac{e^{-iqz}\gamma\cdot a^*}{i(\gamma\cdot p-q\gamma_3)+m}\right\}\psi^{(0)}(x) \quad . \tag{2.4}$$

where q is the z-momentum transferred to the electron. The most probable momentum transfer is k_0 with a fractional spread of $\approx N^{-1}$. Since $N \gg 1$ there is a narrow range of momentum transfers from the magnet to the electrons.

Iterating once more produces the second-order result [12]:

$$\begin{aligned}\psi^{(2)}(x) = &\left[\frac{-iKLm}{4\pi}\right]^2\int dq\int dq'\cdot\frac{\sin[(q-k_0)L/2]}{[(q-k_0)L/2]}\,\frac{\sin[(q'-k_0)L/2]}{[(q'-k_0)L/2]} \\ &\times\left\{\frac{e^{i(q+q')z}\gamma\cdot a}{i(\gamma\cdot p+q\gamma_3+q'\gamma_3)+m}\,\frac{e^{iqz}\gamma\cdot a}{i(\gamma\cdot p+q\gamma_3)+m}+\right. \\ &+\frac{e^{-i(q+q')z}\gamma\cdot a^*}{i(\gamma\cdot p-q\gamma_3-q'\gamma_3)+m}\,\frac{e^{-iqz}\gamma\cdot a^*}{i(\gamma\cdot p-q\gamma_3)+m}+ \\ &+\frac{e^{i(q-q')z}\gamma\cdot a}{i(\gamma\cdot p+q\gamma_3-q'\gamma_3)+m}\,\frac{e^{-iqz}\gamma\cdot a^*}{i(\gamma\cdot p-q\gamma_3)+m}+ \\ &\left.+\frac{e^{-i(q-q')z}\gamma\cdot a^*}{i(\gamma\cdot p-q\gamma_3+q'\gamma_3)+m}\,\frac{e^{iqz}\gamma\cdot a}{i(\gamma\cdot p+q\gamma_3)+m}\right\}\psi^{(0)}(x).\end{aligned} \tag{2.5}$$

The pattern of higher order terms is clear. These lengthy expressions may be written symbolically in terms of Feynman diagrams as shown in Fig. 2. The directional interactions correspond to positive or negative momentum transfer from the magnet. It will be evident later that one direction of momentum transfer is kinematically associated with emission of radiation and the other

with absorption. The strength of each such interaction is proportional to $Km/p = K/\gamma$. In practice K is never much larger than unity and γ is always large, so that $K/\gamma \ll 1$ and perturbation theory is valid. In principle the electron wave functions can be written to any order in K/γ with spin effects included.

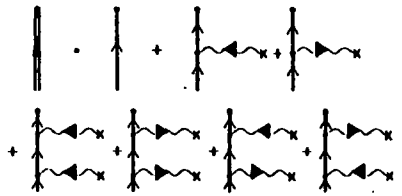

Figure 2. In the diagrammatic expansion for the electron wave function $\psi(x)$, solid lines ending in circles represent the noninteracting electron wave function $\psi^{(0)}(x)$. Other solid lines represent electron Green's functions G^{Dirac}. Wiggly lines with directional arrows denote interactions with the undulator field in which momentum is transferred either to or from the undulator.

It is also possible to write the Dirac equation in differential form including all orders in K/γ. We ignore the boundary conditions due to the finite length L of the magnet and concentrate on the character of the higher order effects in K/γ. We write the four-component first-order differential equation as two two-component second-order differential equations for the upper and lower components of the wave function $\psi(x)$. The two-component wave functions differ only by the magnitude of the spin energy. The spin-dependent and spin-independent terms proportional to K/γ differ by a factor $k_0/\gamma m$ which is $\approx 10^{-12}$ for typical parameters, so that the spin-dependent terms may be neglected [12,36]. The two second-order differential equations are then identical and are just the one-dimensional Klein-Gordon equation with a sinusoidal potential,i.e. the Mathieu equation. For a linearly polarized magnet this equation is

$$\left\{\frac{d^2}{(k_0dz)^2} - \frac{K^2}{\gamma^2}\cos^2(k_0z) + \frac{\gamma^2-1}{\gamma^2}\right\}\xi(z) = 0 \quad . \tag{2.6}$$

To zeroth order in fields ($K/\gamma = 0$) the solutions are plane waves representing electrons propagating unperturbed along the magnet axis.

Since deviations from linear motion along the z-axis of the magnet are small, an eikonal or WKB approximation is suggested as a limiting case of Mathieu's equation. Expanding to second-order in the small parameter K/γ gives [12]

$$\xi_l(z) = C_l\left\{1 + \frac{K^2}{8\gamma^2}\cos(2k_0 z) + \cdots\right\}\exp\left\{\pm il\left\{k_0 z - \frac{K^2}{8\gamma^2}\sin(2k_0 z) + \cdots\right\}\right\}, \quad (2.7)$$

where l is an integer labeling the energy level. The electron wave function (2.7) is modulated in amplitude and frequency due to its interaction with the linearly polarized magnet. Classically, the electrons undergo periodic acceleration which modifies their z-momentum so that their energy remains constant. In a helical magnet the acceleration is constant in magnitude along z so that there is no modulation of the electron wave function.

The energy eigenvalues are

$$E_l = \left\{(lk_0)^2 + m^2 + \frac{K^2 m^2}{2} + \cdots\right\}^{\frac{1}{2}} . \quad (2.8)$$

The electron has acquired an effective mass $m^* = m(1+K^2/2+\cdots)^{\frac{1}{2}}$. We may understand this as follows. When an electron emits or absorbs radiation it recoils. The electrons in the undulator magnet "resist" this action more than do free electrons since they are constrained to follow a transverse oscillatory path. In a helical magnet the mass correction is twice as large because the average transverse acceleration is twice as large. Henceforth we will assume that K is sufficiently small that we may neglect this correction to the electron mass. The discrete eigenvalues result from requiring that the wave functions remain invariant under translation by an integral number of magnet wavelengths λ_0. However, for relativistic electrons in a typical magnet $l \approx 10^{12}$. This gives essentially

a continuum of states indicating that a classical approach is accurate. Furthermore, if we were to impose the finite length boundary conditions on the wave function the magnet would only include $\approx 10^2$ periods. It would therefore be impossible to resolve energy level differences of one part in 10^{12}. From now on we will therefore consider the electron energy to be a continuum variable.

The current density $\vec{j} = ie\bar{\psi}\vec{\gamma}\psi$ can be found from the wave functions in (2.4) or (2.7). To lowest order in K the current density in a linearly polarized magnet is proportional to $[-(K/\gamma)\cos(k_0 z), 0, \beta_z]$ where $\beta_z = 1 - 1/2\gamma^2$. The current density is modulated in the x-direction in proportion to K. This agrees with the classical current found from the Lorentz force equations in the presence of the magnet field alone. The procedure of finding the electron trajectories in the magnetic field is the classical counterpart to solving for the electron wave functions in the magnetic field.

3. Quantum mechanical spontaneous emission

In this section we derive the transition rate, angular distribution, and frequency dependence of spontaneous emission from an electron in an undulator. This radiative process is magnetic bremsstrahlung, and is fundamentally the same process as occurs in the spontaneous decay of excited atomic states. A distinction, however, is that the electrons in the excited atoms of conventional lasers make transitions over discrete states, while the electrons in an FEL make transitions over a continuum of states. The external magnetic field in the FEL is necessary for emission to occur, since otherwise energy and momentum cannot be conserved in the process.

The emission and absorption of photons is described by the creation and annihilation operators $c^\dagger_{\vec{k}\lambda}$ and $c_{\vec{k}\lambda}$ for photons of wave vector $\vec{k}$ and helicity λ. The number of photons per mode is given by the photon distribution function

$$\eta(\vec{k},\lambda) = \langle \mathcal{E}^{\dagger}_{\vec{k}\lambda} \mathcal{E}_{\vec{k}\lambda} \rangle \quad . \tag{3.1}$$

which is just the expectation value of the photon number operator for the mode $(\vec{k},\lambda)$. The total number of photons present in all modes is then

$$N_{\text{photon}} = \frac{V}{(2\pi)^3} \int d^3k \; \eta(\vec{k},\lambda) \quad . \tag{3.2}$$

In the calculation of spontaneous emission we assume that no photons are initially present.

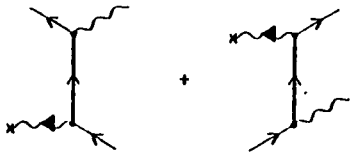

Figure 3. Feynman diagrams for spontaneous emission are shown to lowest order in the electron-undulator and electron-photon interactions. Wiggly lines without directional arrows represent real photons. Vertices are denoted by circles.

The Feynman diagrams that describe spontaneous emission to lowest non-vanishing order in the undulator field strength are shown in Fig. 3. The zero order term in K does not contribute to emission since it does not conserve energy and momentum. The resulting S-matrix is

$$S^{(1)}_{fi} = -ie^2 \left[\frac{2\pi}{k\,V^{\beta}}\right]^{\frac{1}{2}} \bar{U}(p',\sigma') \times \left\{ \gamma\cdot\varepsilon_{\lambda} \frac{1}{i\gamma\cdot(p'-k)+m} \gamma\cdot A^{M}(p'+k-p) + \right. \tag{3.3}$$

$$\left. \gamma\cdot A^{M}(p'+k-p) \frac{1}{i\gamma\cdot(p'+k)+m} \gamma\cdot\varepsilon_{\lambda} \right\} U(p,\sigma) \quad .$$

where

$$A^{M}_{\mu}(q) = (2\pi)^3 \delta(q_x)\delta(q_y)\delta(q_0) \frac{B\lambda_0}{4\pi} \left[a_{\mu} \frac{\sin[(q-k_0)L/2]}{[(q-k_0)L/2]} + a^{*}_{\mu} \frac{\sin[(q+k_0)L/2]}{[(q+k_0)L/2]} \right] \tag{3.4}$$

is the Fourier transform of the undulator vector potential (2.2). The initial and final electron four-momenta are p_{μ} and p'_{μ}. $k_{\mu} = (\vec{k},ik)$ is the photon four-momentum, and $(\varepsilon_{\lambda})_{\mu} = (\vec{\varepsilon}_{\lambda},0)$ where $\vec{\varepsilon}_{\lambda}$ is the photon polarization vector. Kinematically only the second term in $A^{M}_{\mu}(q)$, corresponding to a momentum transfer from the undulator field to the electron, contributes to spontaneous emission.

From (3.3), we find the square of the T-matrix:

$$|T^{(1)}_{fi}|^2 = \left[\frac{(2\pi)^3 e^2 K^2 L}{4k\,V^2}\right] \delta(q_x)\delta(q_y) |\bar{U}(p',\sigma')\,\bar{O}\,U(p,\sigma)|^2 \, s(\nu^{(e)}) \quad . \tag{3.5}$$

The matrix $\bar{O}$ is just the quantity in brackets $\{\cdots\}$ in (3.3) with A^{M}_{μ} replaced by a_{μ}. The momentum transfer from the undulator is $\vec{q} = \vec{p}' + \vec{k} - \vec{p}$ which must vanish in the x and y directions. The range of momentum transfers possible in the z direction gives the spontaneous emission line shape

$$s(\nu^{(e)}) = \frac{\sin^2(\nu^{(e)}/2)}{(\nu^{(e)}/2)^2} \approx \frac{\sin^2(\nu_0/2)}{(\nu_0/2)^2} \quad , \tag{3.6}$$

where

$$\nu^{(e)} = L(k_0 - p'_z - k_z + p_z)$$

$$\approx L(\, k_0 - k\,(\,1-\beta_z\,)) \equiv \nu_0 \quad . \tag{3.7}$$

The approximate expression for $\nu^{(e)}$ is valid in the relativistic limit. The function $s(\nu^{(e)})$ is maximum for a momentum transfer from the undulator field of $\vec{q} = k_0 z$, at which point the resonance parameter $\nu^{(e)}$ vanishes. The characteristic width of $s(\nu_0)$ in ν_0 is π, corresponding to a fractional line width $\delta k/k \approx (2N)^{-1}$. The photon wave number at the line center (i. e., at "resonance") is

$$k_{res} = \frac{k_0}{(1-\beta_z\cos\vartheta)} + O\left[\frac{K^2}{\gamma^2}\right] \quad . \tag{3.8}$$

This expression agrees with the classical result. In the forward direction $k_{res} = 2\gamma^2 k_0$, which shows the large Doppler shift of the radiation wave number

relative to k_0.

The transition rate is found by multiplying (3.5) by the density of final states, which we take to correspond to a free final electron and a plane wave photon. The spin sums are rather involved and a simple form is available only for the case in which the electron moves along the z direction before entering the undulator. In that case we find [12]

$$\frac{d^2w}{d\Omega d\nu_0} = \frac{r_0^2 B^2}{16\pi^2 k_0 \gamma^2}\left\{\frac{|\beta_z(\varepsilon_\lambda\cdot z)\,(\hat{\kappa}\cdot\hat{a}) + (\varepsilon_\lambda\cdot\hat{a})\,(1-\beta_z\cos\vartheta)|^2}{(1-\beta_z\cos\vartheta)^4}\right\} s(\nu_0) \quad , (3.9)$$

where $r_0 = e^2/m$ is the classical electron radius and ϑ is the angle between the z direction and the photon wave vector $\vec{k} = \hat{\kappa}\, k$. On axis, the radiation is polarized in the same sense as the undulator polarization $\hat{a}$, but the polarization changes off axis. Due to the strong angular dependence of the denominator in (3.9), the radiation emerges within a narrow forward cone with characteristic opening angle $\approx \gamma^{-1}$ around the undulator axis. Within this cone the transition rate (3.9), the resonant wave number k_{res} and the optical polarization all change slowly with ϑ.

A simple interpretation of the spontaneous emission process is as follows [12]. The number of photons emitted per pass by an electron is found by multiplying (3.9) by the emission time $L = N\lambda_0$ and integrating over the line shape $s(\nu_0)$. Approximating the transition rate in the integrand by its value at $\vartheta = 0$ and estimating the solid angle integral $\int d\Omega$ by $\pi/4\gamma^2$ (the solid angle of the radiation cone) gives

$$\frac{\text{no. of photons}}{\text{pass}} = \left\{\frac{B^2}{8\pi k_0}\right\}(\pi r_0^2 L) \quad . \qquad (3.10)$$

The first term is the energy density of the static field divided by k_0, the energy of each virtual photon stored in the static field. The second term is the classical volume swept out by the electron while moving through the undulator. Thus the

total number of spontaneous photons emitted per pass is just the number of virtual photons swept out by the electron in the undulator. For typical FELs the number of photons emitted per pass is ≈ 0.1 per electron.

Typically not all photons emitted in a pass are stored in the FEL resonator cavity. The rigorous mode overlap problem is lengthy, but a good estimate is to use the solid angle subtended by the fundamental cavity mode. The characteristic angular spread of a Gaussian mode is $(kz_0)^{-1}$ where z_0 is the Rayleigh length of the cavity [37]. The resulting solid angle for a Gaussian mode is π/kz_0. This is smaller than the solid angle $\pi/4\gamma^2$ of the total emission cone by a factor $\lambda_0/\pi z_0$. Since this factor is $\ll 1$ for typical resonator designs, only a small fraction of the spontaneous emission remains within the resonator cavity.

All the results obtained above using quantum field theory can also be derived by using the WKB wave functions calculated in the previous section. The resulting T-matrix then includes the electron-undulator interaction to higher order in K. This result is not readily obtainable using diagrammatic techniques since an infinite class of diagrams must be considered. The transition rate in the forward direction obtained from the WKB wave functions is identical to (3.9) with $\vartheta = 0$ except for an extra multiplicative factor $[J_0(Z) - J_1(Z)]^2$, where J_0 and J_1 are Bessel functions and $Z = K^2/4(1 + K^2/2)$ [12,38].

4. Stimulated emission and absorption

In a free electron laser oscillator, the spontaneous radiation is stored in a resonant cavity formed by mirrors placed beyond either end of the undulator on the common axis of the undulator and electron beam. New electrons which enter the undulator on subsequent passes may then interact with this stored radiation, so that stimulated emission or absorption occurs. Photons may be present at a variety of wave numbers as expressed by the photon distribution function $\eta(\vec{k},\lambda)$.

The Feynman diagrams for stimulated emission are shown in Fig. 4a to lowest order in K. The square of the associated T-matrix is the same as (3.5) except for an additional factor of $\eta(\vec{k},\lambda)$ which arises from the action of the photon creation operator on the initial state. The differential probability per unit time for stimulated emission is then

$$dw^{(e)} = \left\{\frac{(2\pi)^2 e^2 K^2 m^2 L\,|\,\bar{U}(p',\sigma')\bar{O}U(p,\sigma)\,|^2}{4kV^2}\right\} s(\nu^{(e)})\,[\eta(\vec{k},\lambda)+1]$$

$$\times (2\pi)^2\delta(\sqrt{p'^2+m^2}+k-\sqrt{p^2+m^2}) \qquad (4.1)$$

$$\times \delta(p_x'+k_x-p_x)\delta(p_y'+k_y-p_y) \quad .$$

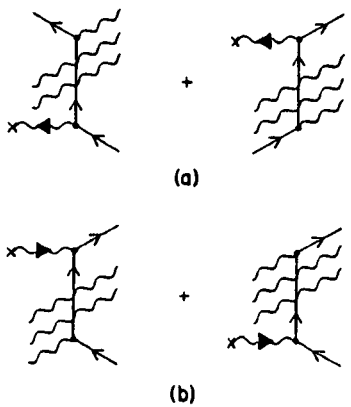

Figure 4. (a) Feynman diagrams for stimulated emission are shown to lowest order in the electron-undulator and electron-photon interactions. Photons other than that emitted by the electron do not interact directly with the electron. (b) As (a) but for absorption. Photons other than that absorbed by the electron do not interact directly with the electron.

We now specialize to the case where $\vec{p}$ and $\vec{k}$ are along the undulator axis, and assume that the electrons are highly relativistic. This is a good approximation for high quality electron beams and for resonators with a large Rayleigh length. The stimulated emission rate per wave number is then found by integrating (4.1) over the density of final states for the electron, summing over

the final electron spin, and averaging over the initial electron spin. The result is [12]

$$w^{(e)}(p,k,\lambda) = \left\{\frac{2\pi^2 N e^2 K^2 |\varepsilon_\lambda\cdot\vec{a}\,|^2}{k^2 V}\right\} s(\nu^{(e)})\,[\eta(k,\lambda)+1] \quad , \qquad (4.2)$$

where, as in (3.7),

$$\nu^{(e)} = L[k_0 - (k/2\gamma^2)(1+(k/p))] = \nu_0 - 2\pi Nk/p \quad . \qquad (4.3)$$

In this expression we have retained terms in the small quantity k/p (typically $\approx 10^{-10}$) only in the argument $\nu^{(e)}$ of the function $s(\nu^{(e)})$. All other terms in k/p are smaller by a factor $N>>1$. In the calculation of spontaneous emission in the preceding section, terms in k/p were dropped altogether. As shown below, however, k/p must be retained in the kinematic factor $\nu^{(e)}$ in order to to properly describe gain.

In order to find the rate equation for the photon distribution function, we also require the rate for absorption. The lowest-order Feynman diagrams for this process are shown in Fig. 4b. The calculation of the rate for absorption is similar to the calculation of the stimulated emission rate. The differences are:

(1) $[\eta(\vec{k},\lambda)+1]$ is replaced by $\eta(\vec{k},\lambda)$, since it is now the photon annihilation operator that acts on the initial state;

(2) the four-momentum transfer, which was given by $q_\mu = p'_\mu + k_\mu - p_\mu$ for the case of emission, is now $q_\mu = p'_\mu - k_\mu - p_\mu$; and

(3) only the first term in (3.4) for $A^M_\mu(q)$ contributes to absorption. The resulting expression for the forward absorption rate is [12]

$$w^{(a)}(p,k,\lambda) = \left\{\frac{2\pi^2 N e^2 K^2 |\varepsilon_\lambda\cdot\vec{a}\,|^2}{k^2 V}\right\} s(\nu^{(a)})\,\eta(k,\lambda) \quad , \qquad (4.4)$$

where

$$\nu^{(a)} = L[k_0 - (k/2\gamma^2)(1-(k/p))] = \nu_0 + 2\pi Nk/p \quad . \qquad (4.5)$$

The difference in kinematics between the emission and the absorption rates appears in the sign of the small quantity k/p appearing in $\nu^{(e)}$ and $\nu^{(a)}$. This results in a slight difference between the emission and absorption rates for fixed k, k_0, and p. The magnet wave number k_0 and initial electron momentum p are fixed by design, but the FEL oscillator contains a range of photon wave numbers k. The rates for emission and absorption and the difference between these rates vary with k, so that the net gain is a function of wave number. This is embodied in the photon rate equation.

5. Photon rate equation

The number of photons evolves due to emission and absorption by the electron beam. The rate of change of $\eta(k,\lambda)$ is found by integrating the difference of (4.2) and (4.4) over the electron momentum distribution function $N_e(p)$:

$$\frac{d\eta(k,\lambda)}{dt} = \int dp\ N_e(p)\ [\ w^{(e)}(p,k,\lambda) - w^{(a)}(p,k,\lambda)\ ] \quad . \tag{5.1}$$

We only consider the evolution of the expectation value of the photon number operator $c^{\dagger}_{k\lambda}c_{k\lambda}$ and not the expectation values of the creation operator $c^{\dagger}_{k\lambda}$ or the annihilation operator $c_{k\lambda}$. The commutation relations are therefore neglected so that we ignore quantum fluctuations. In addition, gain must be small since we do not follow the evolution of the optical phase through $c^{\dagger}_{k\lambda}$ and $c_{k\lambda}$ [39]. Most present and proposed FELs indeed have small gain per pass and small quantum fluctuations.

The electron momentum distribution function $N_e(p)$ also changes with time due to emission and absorption. A continuum of states is available to the electrons so that the number of electrons per state is low and Fermi statistics do not restrict transitions. Almost invariably $N_e(p)$ has an initial width large compared to k and has no structure on the order of k. These attributes are not changed by repeated emission and absorption during a single pass, which act

only to redistribute electrons in momentum. Furthermore, the initial width of $N_e(p)$ is typically small compared to the characteristic width in p of $[\ w^{(e)}(p,k,\lambda) - w^{(a)}(p,k,\lambda)\ ]$ in (5.1). Thus we may regard $N_e(p)$ as a narrow function of p. Repeated emission and absorption during a single pass can significantly modify $N_e(p)$ when $\eta(k,\lambda)$ is large, since the transition rates increase with $\eta(k,\lambda)$. When $\eta(k,\lambda)$ becomes sufficiently large that $N_e(p)$ acquires a fractional width in momentum $\delta p/p \approx (2N)^{-1}$, saturation occurs. Our analysis is therefore restricted to weak optical fields (small $\eta(k,\lambda)$) below the saturation limit. This regime includes most of the dynamical evolution of an FEL oscillator. With these approximations, the rate equation (5.1) becomes

$$\frac{d\eta(k,\lambda)}{dt} = N_e\ [\ w^{(e)}(p,k,\lambda) - w^{(a)}(p,k,\lambda)\ ] \quad , \tag{5.2}$$

where N_e is the total number of electrons within the quantization volume V. Making use of (4.2) and (4.4), this may be written as

$$\frac{d\eta(k,\lambda)}{dt} = \left\{\frac{N_e 2\pi^2 N e^2 K^2 |\varepsilon_\lambda \cdot \vec{a}\,|^2}{k^2 V}\right\}\left\{s(\nu^{(e)})\ [\ \eta(k,\lambda) + 1\ ] - s(\nu^{(a)})\eta(k,\lambda)\right\} \quad . \tag{5.3}$$

Since the optical gain per pass is low, $\eta(k,\lambda)$ changes only slightly during a single pass and the electron distribution remains constant over each pass. We then rewrite (5.3) as an equation for the change of the photon distribution function over many passes through the undulator. We note from (4.3) and (4.5) that $\nu^{(e)}$ and $\nu^{(a)}$ differ only by the small quantity $-4\pi Nk/p$, so that a first-order Taylor expansion may be used in (5.3). The resulting rate equation is

$$\frac{d\eta(k,\lambda,n)}{dn} = j\left\{\frac{m\lambda_0}{64\pi^2 N\gamma}\ s(\nu_0) + g(\nu_0)\ \eta(k,\lambda,n)\right\} \quad , \tag{5.4}$$

where n is the pass number. The dimensionless electron current density j is, in cgs units,

$$j = \left\{\frac{4\pi^2 N e^2 K^2 L^2 |\varepsilon_\lambda \cdot \vec{a}\,|^2}{\gamma^3 mc^2}\right\}\left\{\frac{N_e}{V}\right\} \quad . \tag{5.5}$$

which is the same as occurs in classical calculations [IEEE]. The function $g(\nu_0)$ arises from the Taylor expansion of $s(\nu_0)$:

$$g(\nu_0) = -\frac{1}{2}\frac{ds(\nu_0)}{d\nu_0} = \frac{(2 - 2\cos\nu_0 - \nu_0\sin\nu_0)}{\nu_0^3} \quad . \tag{5.6}$$

Equation (5.4) contains both a term due to spontaneous emission [independent of $\eta(k,\lambda,n)$] as well as a gain term [proportional to $\eta(k,\lambda,n)$] which arises from the difference between the rates for stimulated emission and absorption. This latter term is present as a consequence of the slight kinematical difference between the emission and absorption process. Were this difference absent, there would be no gain. The spontaneous and gain terms depend in different ways on the relationship between the electron energy and photon wave number expressed by the resonance parameter ν_0. From (3.6), the increase in $\eta(k,\lambda,n)$ due to spontaneous emission is greatest for $\nu_0 = 0$, while from (5.6) the increase due to the dominance of stimulated emission over absorption is greatest for $\nu_0 \approx 2.6$, corresponding to a wave number lower than that which is optimum for spontaneous emission. As the photon number grows to

$$\eta_{th} \approx \frac{mc\lambda_0}{64\pi^2 N\gamma h} \tag{5.7}$$

(in cgs units), the stimulated gain term becomes important. This is the FEL threshold condition. Below threshold ($\eta \ll \eta_{th}$) $\eta(k,\lambda,n)$ grows linearly, increasing by $\eta_{th}s(\nu_0)$ on each pass. Above threshold ($\eta \gg \eta_{th}$) growth is exponential and the fractional gain per pass is given by $jg(\nu_0)$, in agreement with classical calculations of the gain in weak optical fields [5,12]. We note that both the spontaneous and gain terms in (5.4) are identical to the classical results. The relation (5.6) between $s(\nu_0)$ and $g(\nu_0)$ is a restatement of a theorem due to Madey [1,40]; like that theorem, it is only valid for weak optical fields that are well approximated by forward plane waves [41].

The solution to (5.4) is [12]

$$\eta(k,\lambda,n) = \frac{\eta_{th}s(\nu_0)}{g(\nu_0)}\left\{e^{jg(\nu_0)n} - 1\right\} \quad . \tag{5.8}$$

Initially ($n = 0$) no photons are present. When the gain function $g(\nu_0)$ is positive, (5.8) gives first linear and then exponential growth of the photon number. When $g(\nu_0)$ is zero, the growth is linear and arises from spontaneous emission only. For negative $g(\nu_0)$ the photon number tends to an asymptotic value for which the emission and absorption rates are equal. We discuss these characteristics of the solution (5.8) in more detail below.

6. Oscillator evolution

In this section we use the solution (5.8) for the photon distribution function to study the light stored in an FEL oscillator. The total energy of the photons in all modes stored in the volume V is $E_{photon} = (2\pi)^{-3}V\int d^3k\ \hbar ck\ \eta(\vec{k},\lambda,n)$ (in cgs units). Since the characteristic solid angle for a Gaussian mode is $\int d\Omega \approx \pi/kz_0$ is small for large $z_0 \gg L$, it is appropriate to replace $\eta(\vec{k},\lambda,n)$ in this integral by the corresponding function $\eta(k,\lambda,n)$ for on-axis photons given by (5.8). We may then write the optical power per unit area as $P_{photon} = E_{photon}c/V \approx \hbar c^2(2\pi)^{-3}(\pi/kz_0)\int dk\ k^3\ \eta(k,\lambda,n)$ in cgs units. For oscillators with smaller values of z_0 ($\approx L$) the optical phase changes substantially over the length of the undulator, leading to changes in the resonance parameter and in the functions $s(\nu_0)$ and $g(\nu_0)$ [41].

We extend our study to include oscillator evolution for magnet designs other than the simple undulator by replacing $s(\nu_0)$ and $g(\nu_0)$ with the corresponding functions describing each alternate magnet design. We consider the additional examples of the two-stage optical klystron and the tapered undulator. We also discuss the effect of spontaneous noise and shot noise on oscilla-

tor evolution. In all of this the resonator losses are assumed to be negligibly small compared to the gain. Greater losses can easily be included by subtracting the losses from $g(\nu_0)$ in (5.8).

(a) Conventional undulator

In Fig. 5 we show $s(\nu_0)$, $g(\nu_0)$, and the corresponding evolution of $\eta(k,\lambda,n)$ for a linearly polarized undulator ($|\varepsilon_\lambda \cdot \vec{a}|^2 = 1$) with $N = 50$, $\lambda_0 = 3.0$ cm, $\gamma = 50$, and a dimensionless electron current density $j = 1.0$. This value of j would arise from the typical values $K = 0.3$ and $N_e / V \approx 10^{11}$ cm^{-3}. With these parameters the center of the spontaneous line ($\nu_0 = 0$) corresponds to an optical wavelength $\lambda = 6.0\,\mu$m. Other choices of parameters give somewhat different numerical results, but the qualitative conclusions of Fig. 5 are unchanged.

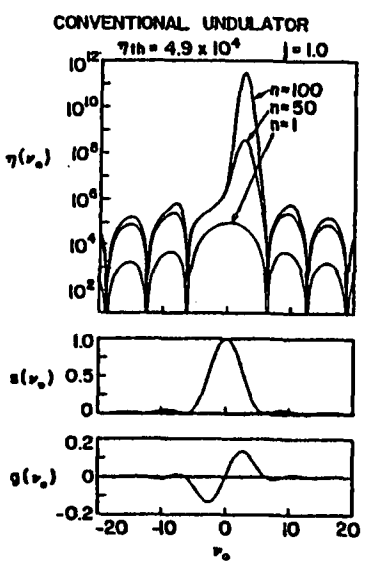

Figure 5. The mode evolution for an FEL oscillator using a conventional periodic undulator shows a definite peak after 100 passes. Here $j = 1.0$, $N = 50$, $\gamma = 50$, and $\lambda_0 = 3.0$ cm, so that $\eta_{th} = 4.92 \times 10^4$. Upper graphs: $\eta(\nu_0)$ for pass numbers $n = 1$, 50, and 100. Middle graph: spontaneous emission function $s(\nu_0)$. Lower graph: gain function $g(\nu_0)$. The range of ν_0 depicted is from -20 to 20. The maximum gain per pass is 13.5 per cent at $\nu_0 = 2.6$.

As the pass number increases, the radiation becomes increasingly monochromatic due to mode competition. The line center moves towards the maximum gain point $\nu_0 \approx 2.6$, at which point the gain per pass is 13.5 percent. After only 100 passes, however, the center of the line is at a slightly lower value of ν_0 since the number of spontaneous photons is greater near $\nu_0 = 0$. The most negative value of $g(\nu_0)$ occurs at $\nu_0 = -2.6$: near this point the competing processes of spontaneous emission and net absorption have nearly come to steady state after 100 passes, giving a relatively small asymptotic value of $\eta(k,\lambda,n)$.

We note that while other values of ν_0 besides the peak value of ≈ 2.6 produce positive gain, the gain at these other values is sufficiently small that after 100 passes these sidebands are suppressed by six orders of magnitude. This is emphasized in Fig. 6 in which the photon distribution function after 50 and 100 passes is shown on a linear scale. For an optical cavity with $z_0 = 5L$ the optical power per unit area after 100 passes is approximately 2.1 kW/cm^2, essentially 100 percent of which is within the central peak of Fig. 5.

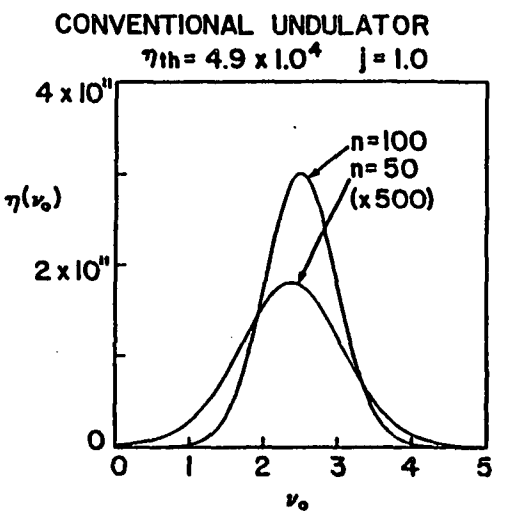

Figure 6. A comparison of central region of $\eta(\nu_0)$ for an FEL oscillator using a conventional periodic undulator after pass numbers $n = 50$ and 100 shows significant laser line narrowing due to mode competition. The range of ν_0 depicted is from 0 to 5.

In the preceding section we noted that our analysis is only valid if the value of $\eta(k,\lambda,n)$ is below saturation, so that the fractional change in momentum of an electron after one pass is small compared to $(2N)^{-1}$. To determine the saturation limit, we find the average momentum change per electron by equating the momentum gain of the photons in a single pass to the momentum loss of the electron beam. The resulting restriction is, in cgs units,

$$\eta(k,\lambda,n) \ll \eta_{sat} \approx \frac{m^2\lambda_0 z_0 c^3}{64\pi^2 h e^2 K^2 N^3 \gamma^2 |\varepsilon_\lambda \cdot \vec{a}|^2 g(\nu_{max})\Delta\nu_0} \quad . \tag{6.1}$$

where $g(\nu_{max})$ is the maximum value of $g(\nu_0)$ and $\Delta\nu_0$ is the width of the peak in g. For the parameters used here $\eta_{sat} \approx 10^{15}$. Thus the calculation depicted in Figs. 5 and 6, in which $\eta(k,\lambda,n)$ is always less than 10^{12}, is well within the range of validity of our approximations.

(b) Two-stage optical klystron

An alternative magnet design to the conventional undulator is the two-stage optical klystron [42,43]. In an optical klystron the undulator magnet is divided into two separate sections between which is placed either a long drift space or a shorter dispersive magnet. In either case the spontaneous emission function $s(\nu_0)$ changes shape due to interference between emission from the two sections, so that the variation with ν_0 becomes more rapid as shown in Fig. 7. Consequently the gain function $g(\nu_0)$, which from (5.6) is proportional to the derivative of $s(\nu_0)$, has larger maxima and the gain is enhanced. This is particularly useful when the gain of a conventional undulator would be unacceptably low.

We study oscillator evolution for an optical klystron by replacing the function $s(\nu_0)$ in (5.8) by the corresponding function for an optical klystron as calculated classically [42]. For magnet sections of equal length, this is

$$s_{OK}(\nu_0) = \frac{[1-\cos(\nu_0/2)]\,[1+\cos(\nu_0/2+\chi)]}{(\nu_0/2)^2} \quad . \tag{6.2}$$

where $\chi = N_d[\,(\nu_0/2N) - 2\pi\,]$ and N_d equals the number of optical wavelengths which pass over an electron during its traversal of the dispersive section or drift space [43]. For $N_d = 0$, (6.2) reduces to the original form (3.6). As N_d increases, $s_{OK}(\nu_0)$ varies more rapidly with ν_0. The corresponding gain function then has greater maxima:

$$\begin{aligned} g_{OK}(\nu_0) = -\frac{1}{2}\frac{ds_{OK}(\nu_0)}{d\nu_0} = \{\,&2-\cos\chi-\cos(\nu_0+\chi)-(\nu_0/2)\sin(\nu_0+\chi) \\ &-2\cos(\nu_0/2)+2\cos((\nu_0/2)+\chi)-(\nu_0/2)\sin(\nu_0/2)+(\nu_0/2)\sin((\nu_0/2)+\chi) \\ &+(\nu_0/2)(N_d/N)[\sin((\nu_0/2)+\chi)-(1/2)\sin(\nu_0+\chi)-(1/2)\sin\chi]\}(\nu_0)^{-3} \quad . \end{aligned} \tag{6.3}$$

Note that if N_d is an integer we may drop the term $-2\pi N_d$ in the definition of χ since this term does not change s_{OK} or g_{OK}.

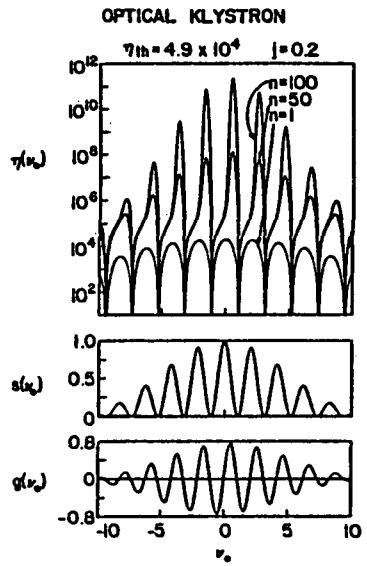

Figure 7. The mode competition in a two-stage optical klystron FEL with N_d = 250 shows many more gain peaks than in the periodic undulator in Fig. 5. Here j = 0.2, N = 50, γ = 50, and λ_0 = 3.0 cm, so that η_{th} = 4.92 x 10^4. The range of ν_0 depicted is from -10 to 10. The maximum gain per pass is 15 per cent at ν_0 = 0.5.

In Fig. 7 we show the evolution of the photon distribution function for an optical klystron. This example is identical to the conventional undulator dep-

icted in Fig. 5 but with the value of j reduced to 0.2. A dispersive section has been introduced with $N_d = 5N = 250$ to bring the peak gain per pass up to the value obtained with the conventional undulator. The sidebands to either side of the central peak in Fig. 7 are larger and more closely spaced than for the conventional undulator. This is due to the higher sideband gain and more rapid variation of $g(\nu_0)$. For this example only 63 percent of the optical power present after 100 passes is within the maximum gain peak centered at $\nu_0 \approx 0.5$. Furthermore the power within this central peak is only 14 percent of the peak power obtained with the conventional undulator. This reduction is due in part to the narrowness of the peak and in part to the reduced value of $s(\nu_0)$ at the peak gain point. The adjacent sidebands are suppressed by less than an order of magnitude, compared to six orders of magnitude for the conventional undulator. After many more passes, mode selection will be more complete and sidebands will be further suppressed, but before mode selection is complete the laser will reach the strong optical regime and saturation. In strong fields the gain function $g(\nu_0)$ is altered and the mode selection problem changes.

(c) Tapered undulator

Another type of magnet design is the tapered undulator (or "tapered wiggler") [23]. This design is intended to increase the gain in strong fields above that obtained with a conventional undulator, thereby increasing the saturation limit. This can be done by decreasing ("tapering") the magnet wavelength λ_0 along z, by decreasing the magnetic field strength, or by supplying a longitudinal accelerating electric field. Each method results in a change of the electron energy for resonance ($\nu_0 = 0$) for fixed wave number k. When the optical field is strong, some electrons can become trapped in phase with the optical field, resulting in enhanced energy transfer from the electrons to the optical field.

As with the optical klystron, we study the evolution of a tapered undulator FEL oscillator by replacing the spontaneous emission and gain functions in (5.8) by the corresponding quantities for a tapered undulator. The spontaneous emission function $s_{taper}(\nu_0)$ may be written as an opaque expression involving a number of Fresnel integrals [44,45] which we do not present here. With increasing amounts of taper $s_{taper}(\nu_0)$ becomes broader and the peak value decreases as shown in Fig. 8. Again the gain function is obtained from the spontaneous emission function by differentiation. Because of the broadening of the spontaneous emission function, the maximum slope of the line shape and hence the maximum amount of gain in weak fields is therefore reduced relative to a conventional undulator. Thus we expect a tapered undulator to perform less well during the early weak-field stages of oscillator operation than does a conventional undulator.

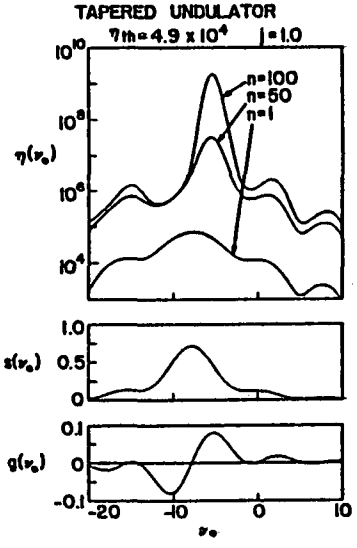

Figure 8. The mode competition in a tapered undulator FEL with a five per cent taper of the undulator wavelength λ_0 shows behavior distinct from that in Figs. 6 and 7. Here $j = 1.0$, $N = 50$, $\gamma = 50$, and $\lambda_0 = 3.0$ cm, so that $\eta_{th} = 4.92 \times 10^4$. The range of ν_0 depicted is from -20 to 10. The maximum gain per pass is 8 per cent at $\nu_0 = -5.4$.

In Fig. 8 we show the evolution of the photon distribution function for an undulator identical to that used in Fig. 5 but with a five percent taper in λ_0 from

the beginning to the end of the undulator. In this example we have assumed that both λ_0 and the undulator field strength B vary along the length of the undulator so that K remains constant. After 100 passes the optical power is less than the value with a conventional undulator by two orders of magnitude. After 500 passes the optical power becomes comparable to the power obtained after 100 passes with a conventional undulator. Unlike the situation with an optical klystron, the sidebands in this case remain small so that the stored light is quite monochromatic in weak fields. With larger amounts of tapering, the sidebands are enhanced and can remain comparable to the main peak after $\approx$ 100 passes.

(c) Quantum fluctuations and shot noise

The gain and spontaneous emission rates in the previous examples have been taken to be constant with pass number. In fact there are fluctuations due to quantum and shot noise that will vary the shapes of $s(\nu_0)$ and $g(\nu_0)$ on each pass. We show here that typically these fluctuations are small.

From (5.4) and (5.7), at low photon number the growth of the photon distribution function is given by $d\eta(k,\lambda,n)/dn \approx \eta_{th} j s(\nu_0)$. The photon distribution function integrated over the density of states gives the number of photons as in (3.2). The solid angle in d^3k is again the actual solid angle $\int d\Omega = \pi/kz_0$ captured between the spherical mirrors of the resonator. The cross-sectional area of the mode waist is $\pi w_0^2 = 2\pi z_0/k$. Since the mode area doubles in each distance z_0 we can estimate the interaction volume in (3.2) as $V \approx L(\pi w_0^2 L/2z_0) = \pi L^2/k$. The wave number interval dk in (3.2) can be rewritten in terms of the resonance parameter: $d\nu = 2\pi N dk/k$, where $k \approx 2\gamma^2 k_0$ near resonance. This gives a convenient formula for the number of photons entering the resonator each pass:

$$\frac{d^2N_{\text{photon}}}{dn\,d\nu_0} \approx \frac{L\gamma^2}{4\pi z_0}\frac{d\eta}{dn} \approx \frac{L\gamma^2}{4\pi z_0} j\,\eta_{th}\,s(\nu_0) \qquad (6.4)$$

The full range $d\nu_0 \approx 2\pi$ about resonance is excited by spontaneous emission, but the range of interest for gain is only $d\nu_0 \approx 1$ about $\nu_0 = 2.6$. For typical free electron laser resonator designs $L/2z_0$ is of order unity, $j \approx 1$, $\gamma \approx 50$, and $\eta_{th} \approx 5\times10^{-4}$. This results in a large number of photons ($\approx 10^7$) even after a single pass through the laser. Assuming that Poisson statistics apply [27], the fractional fluctuations in the photon number are small ($\approx 3\times10^{-4}$).

The optical mode length corresponding to the frequency interval in $d\nu_0 \approx 1$ is $20\pi N/k$. The number of electrons in that length is given by the volume element $\pi w_0^2(20\pi N/k)$ times the electron density. Typically this number is $\approx 10^9$. The shot noise associated with such a large number of electrons will be small.

Acknowledgements

We are grateful for support from NASA grant NAG 2-48, Air Force grant AFOSR-81-0081, and Office of Naval Research grant N00014-81-K-0809.

References

1. J. M. J. Madey, "Stimulated emission of bremsstrahlung in a periodic magnetic field", *J. Appl. Phys.*, vol. 42, pp. 1906-1913, 1971.

2. D. A. G. Deacon, L. R. Elias, J. M. J. Madey, G. J. Ramian, H. A. Schwettman, and T. I. Smith, "First operation of free electron laser," *Phys. Rev. Lett.*, vol. 38, pp. 892-894, 1977.

3. S. Benson, D. A. G. Deacon, J. N. Eckstein, J. M. J. Madey, K. Robinson, T. I. Smith, and R. Taber, "Optical autocorrelation function of a 3.2-μm free electron laser", *Phys. Rev. Lett.*, vol. 48, pp. 235-238, 1982.

4. F. A. Hopf, P. Meystre, and M. O. Scully, "Classical theory of a free-electron laser," *Phys. Rev. Lett.*, vol. 37, pp. 1215-1218, 1976.

5. W.B. Colson, "One-body dynamics in a free electron laser," *Phys. Lett.*, vol. 64A, pp. 190-192, 1977.

6. A. A. Kolomensky and A. N. Lebedev, "Stimulated radiation of relativistic electrons and physical processes in the 'free electron laser'", P. N. Lebedev Physics Institute preprint no. 127.

7. A. Bambini and A. Renieri, "The free electron laser: A single-particle classical model," *Lett. Nuovo Cimento*, vol. 21, pp. 399-404, 1978.

8. V. N. Baier and A. I. Milstein, "To the theory of a free-electron laser," *Phys. Lett.*, vol. 65A, pp. 319-322, 1978.

9. R. H. Pantell, G. Soncini, and H. E. Puthoff, "Stimulated photon-electron scattering", *IEEE J. Quantum Electron.*, vol. QE-4, pp. 905-907, 1968.

10. V. P. Sukhatme and P. A. Wolff, "Stimulated Compton scattering as a radiation source - theoretical limitations," *J. Appl. Phys.*, vol. 44, pp. 2331-2334, 1973.

11. W. B. Colson, "Theory for a free electron laser," *Phys. Lett.*, vol. 59A, pp. 187-190, 1976.

12. W. B. Colson, "Free electron laser theory," Ph.D. dissertation, Stanford University, 1977.

13. V. A. Dubrovskii and B. G. Tsikin, "Stimulation of scattering in a Compton laser by decelerated waves (semiclassical theory)", *Sov. J. Quantum Electron.*, vol. 7, pp. 832-836, 1977.

14. W. Becker, "On the frequency of a free-electron laser", *Phys. Lett.*, vol. 65A, pp. 317-318, 1978.

15. S. J. Glass and H. Mendlowitz, "One-photon emission in periodic magnetic fields", *Phys. Lett.*, vol. 63A, pp. 191-192, 1977.

16. *Physics of Quantum Electronics*, vols. 5 (1978), 7 (1980), 8 and 9 (1982), Addison-Wesley.

17. Special issue on free-electron lasers, *IEEE J. Quantum Electron.*, vol. QE-17, ed. A. Szöke, 1981.

18. W. Becker, "Saturation behavior of the free-electron laser from barrier reflection", *Phys. Lett.*, vol. 74A, pp. 66-68, 1979.

19. J. K. McIver and M. V. Fedorov, "Quantum theory of stimulated processes in a free-electron laser in a strong field," *Zh. Eksp. Teor. Fiz.*, vol. 76, pp. 1996-2010, 1979 [English translation: *Sov. Phys. JETP*, vol. 49, pp. 1012-1019, 1979].

20. M. V. Fedorov and J. K. McIver, "Multiphoton stimulated Compton scattering", *Optics Comm.*, vol. 32, pp. 179-182, 1980.

21. M. V. Fedorov, "Free-electron lasers: amplification, multiphoton transitions, saturation, and geometry," *IEEE J. Quantum Electron.*, vol. QE-17, pp. 1359-1363, 1981.

22. J. M. J. Madey, "Stimulated emission of radiation in periodically deflected electron beam," *U.S. Patent #3,822,410*, 1974.

23. N. M. Kroll, P. L. Morton, and M. N. Rosenbluth, "Free-electron lasers with variable parameter wigglers," *IEEE J. Quantum Electron.*, vol. QE-17, pp. 1436-1468, 1981.

24. A. Bambini and S. Stenholm, "Quantum description of free electrons in the laser", *Optics Comm.*, vol. 30, pp. 391-393, 1979.

25. A. Bambini and S. Stenholm, "Unification of free electron laser theories", *Optica Acta*, vol. 27, pp. 201-213, 1980.

26. W. Becker, "Multiphoton analysis of the free electron laser", *Optics Comm.*, vol. 33, pp. 69-74, 1980.

27. W. Becker and M. S. Zubairy, "Photon statistics of a free-electron laser," *Phys. Rev.*, vol. A25, pp. 2200-2207, 1982.

28. R. Bonifacio, "Coherent states of a free electron laser," *Optics Comm.*, vol. 32, pp. 440-442, 1980.

29. G. Dattoli, A. Renieri, F. Romanelli, and R. Bonifacio, "On the coherent states of a free electron laser," *Optics Comm.*, vol. 34, pp. 240-244, 1980.

30. G. Dattoli, "A Bloch-like model of the free electron laser," *Lett. Nuovo Cimento*, vol. 27, pp. 247-251, 1980.

31. R. T. Deck and P. G. Gill, "Quantum theory of magnetic bremsstrahlung gain," *Phys. Rev.*, vol. A26, pp. 423-437, 1982.

32. W. Becker, "Unified quantum theory of free-electron devices", preprint.

33. G. Dattoli, A. Marino, A. Renieri, and F. Romanelli, "Progress in the Hamiltonian picture of the free-electron laser," *IEEE J. Quantum Electron.*, vol. QE-17, pp. 1371-1387, 1981.

34. J. J. Sakurai, *Advanced Quantum Mechanics*, Addison-Wesley, 1967.

35. P. Diament, "Electron orbits and stability in realizable and unrealizable wigglers of free-electron lasers," *Phys. Rev.*, vol. A23, pp. 2537-2552, 1981.

36. W. Becker and H. Mitter, "Quantum theory of a free electron laser," *Z. Phys.*, vol. 35B, pp. 399-404, 1979.

37. A. Yariv, *Quantum Electronics*, Wiley, 1975.

38. W. Becker, "Increasing the frequency of a free electron laser by means of a linearly polarized magnetic field", *Z. Phys.*, vol. 42B, pp. 87-94, 1981.

39. W. B. Colson, "The nonlinear wave equation for higher harmonics in free-electron lasers," *IEEE J. Quantum Electron.*, vol. QE-17, pp. 1417-1427, 1981.

40. J. M. J. Madey, "Relationship between mean radiated energy, mean squared radiated energy and spontaneous power spectrum in a power series expansion of the equations of motion in a free-electron laser," *Nuovo Cimento*, vol. 50B, pp. 64-88, 1979.

41. W. B. Colson and P. Elleaume, "Electron dynamics in free electron laser resonator modes," *Appl. Phys.*, in press.

42. C. Shih and A. Yariv, "Electron rebunching and radiation gain in two-element free-electron lasers," *Physics of Quantum Electronics*, vol. 7, pp. 473-490, Addison-Wesley, 1980.

43. P. Elleaume, "Optical klystron spontaneous emission and gain," *Physics of Quantum Electronics*, vol. 8, pp. 119-152, Addison-Wesley, 1982.

44. C. C. Shih and M. Z. Caponi, "Theory of multicomponent wiggler free-electron lasers in the small-signal regime," *Phys. Rev.*, vol. A26, pp. 438-450, 1982.

45. P. Bosco and W. B. Colson, to be published.

Phys. Rev. A 27, June 1 (1983) P. 319

Spontaneous Radiation from Relativistic Electrons in a Tapered Undulator

P. Bosco and W. B. Colson

Department of Physics and Quantum Institute

University of California

Santa Barbara, California 93106

ABSTRACT

The spectrum, angular distribution, polarization and coherence properties of the radiation emitted by relativistic electrons undulating through a quasiperiodic tapered magnetic field are studied. Tapering the wavelength and/or field strength along the undulator's axis has the effect of spreading the spectral line to higher frequencies; interference over this broader spectral range results in a more complex line shape. The angular dependence, on the other hand, is not affected by the amount of taper. The polarization of the radiation in the forward direction is determined by the transverse polarization of the undulator, but the polarization changes off axis. The radiation patterns predicted here are distinct from those of untapered undulators, and their detection is now feasible. They will provide useful diagnostics of electron trajectories and threshold behavior in free-electron-laser oscillators using tapered undulators.

PACS: 41.70

Introduction

Charged particles traveling along the axis of a static, undulating, magnetic field execute transverse oscillations. The resulting acceleration radiation from relativistic electrons ("magnetic bremsstrahlung" [1-7]) is emitted into a narrow cone in the forward direction. The Doppler shifted spectrum is peaked at a much higher frequency than the electron oscillation frequency. The polarization of the radiation in the forward direction is determined by the configuration of the undulating magnetic field and resulting particle motion; a helical array of magnets produces circularly polarized light while a linear array produces linearly polarized light. As the detector is moved off axis the emission spectrum shifts down in frequency, decreases, and the polarization changes [4-7]. A trajectory with many, small transverse excursions produces a spectrum with a few narrow peaks at the low-order harmonics. The magnetic field generating this type of radiation is called an "undulator", while the term "wiggler" is reserved for magnetic fields with only a few periods and larger excursions which generate broad band synchrotron radiation [4,5].

In a free electron laser (FEL) [8,9], the magnetic bremsstrahlung is stored in an optical resonator to provide feedback for subsequent stimulated magnetic bremsstrahlung. The optical gain at various frequencies, angles and harmonics, depends on the undulator design and the resulting electron trajectories through the undulator. The evolution from spontaneous to stimulated emission also depends on that design. These important characteristics are known for the simple periodic undulator, but less is known about the tapered undulator which represents an important modification for high power FEL operation [10-12]. In a tapered undulator the magnet's wavelength and/or field strength are varied along its length to preserve the same Doppler shift while the electrons lose energy to the optical field. This improves the energy extraction efficiency from

the electrons when operating at high optical power levels. A physical picture of this process can be given in terms of electron trapping and deceleration in the potential "bucket" generated by the combined action of the laser and the static fields [11,12].

However, the same tapered undulator design that improves energy extraction efficiency in strong optical fields reduces the electron-optical coupling in weak fields. This is caused by the broader spectral range of the tapered undulator, and the details of the reduced coupling can be investigated directly from the spontaneous emission spectrum. Furthermore, in any real experimental situation one must include a study of the spectrum off axis since resonator modes extend over a finite range of angles. Detailed knowledge of the emission spectrum can be a useful diagnostic tool in determining the paths of electrons through the undulator. The forward emission spectrum in the fundamental line from a linearly tapered undulator has been calculated analytically [13]. We present the spectrum's full angular distribution in higher harmonics for a wide range of tapers. The polarization of the emitted radiation is also examined. For helical undulators we show that the polarization changes from circular to linear at a well defined angle, regardless of the tapering. Because of its analytical simplicity the focus is mainly on the helical undulator design, but some results are presented for the linearly polarized field design to highlight their differences.

I. Electron Trajectories

The spontaneous emission spectrum is determined by the electron trajectories in the undulator. Neglecting radiation losses ($\dot{\gamma} = 0$), the equation of motion for an electron in a magnetic field is

$$\frac{d\vec{\beta}}{dt} = -\frac{e}{\gamma mc}\left(\vec{\beta}\times\vec{B}\right) \tag{1.1}$$

where $e = |e|$ is the electron charge, m is the electron mass, $c\vec{\beta}$ is the electron velocity, γmc^2 is the electron energy, and c is the speed of light.

A circularly polarized magnetic field inside the undulator has the form

$$\vec{B} = B(z)\,[\,\cos\Psi(z),\ \sin\Psi(z),\ 0\,] \tag{1.2}$$

where $\Psi(z) = \int_0^z dz'\,k_0(z') = [1 + \eta\, z/2L(\eta)]\,k_0 z$, $\lambda_0(z) = 2\pi/k_0(z)$ is the undulator's wavelength at z, and $\lambda_0 = 2\pi/k_0$ is the undulator's wavelength at $z = 0$. The parameter η describes a linear taper of the undulator's wave vector. The length of the undulator $L(\eta)$ is a function of taper η and is the sum of all tapered wavelengths. This gives

$$L = \lambda_0 \sum_{i=1}^{N}\left[1 + \eta\left(\frac{i-1}{N-1}\right)\right]^{-1}$$

$$= \lambda_0\left\{N - \frac{\eta}{N-1}\left[\frac{N(N-1)}{2}\right] + \frac{\eta^2}{(N-1)^2}\left[\frac{N(N-1)(2N-1)}{6}\right] - \cdots\right\}$$

$$= N\lambda_0\left\{1 - \frac{\eta}{2} + \frac{\eta^2}{6}\left[\frac{2N-1}{N-1}\right] - \frac{\eta^3}{4}\left[\frac{N}{N-1}\right] + \cdots\right\}\ , \tag{1.3}$$

where N is the number of undulator periods. For long undulators ($N \gg 1$)

$$L(\eta) \approx N\lambda_0 \sum_{k=0}^{\infty}\frac{(-\eta)^k}{k+1} = L_0\,\frac{\ln(1+\eta)}{\eta}\ . \tag{1.4}$$

where $L_0 = L(0) = N\lambda_0$ is the undulator length with no taper.

We consider the particular case in which the amplitude of the magnetic field is also a linear function of z such that $B(z) = B_0[1 + \eta z/L(\eta)]$ and the dimensionless ratio $K = eB(z)/k_0(z)mc^2$ is constant throughout the undulator. Typical values of K for an undulator are of order unity. (If $K \gg 1$, the array of magnets becomes a broad band "wiggler" [4,5]). Both $k_0(z)$ and $B(z)$ can be used to "tune" the Doppler shift along the undulator's length, but the special case where K is constant is analytically simpler. The Stanford undulator,

although untapered, gives typical values of $\lambda_o = 3.2$ cm and $B_o = 2.4$ kG, and uses a 40 MeV electron beam ($\gamma = 80$), so that $K = 0.7$. A typical tapered undulator has $L \approx 160$ cm and $\eta \approx 0.05$ with fields and wavelengths similar to the Stanford untapered case.

The transverse equations can be integrated immediately because K is constant.

$$\beta_x(t) = \frac{K}{\gamma}(1 - \cos\Psi) + \beta_x(0) \quad , \quad \beta_y(t) = -\frac{K}{\gamma}\sin\Psi + \beta_y(0) \qquad (1.5a)$$

$$\beta_z = \left[1 - \frac{(1 + K^2)}{\gamma^2} \right]^{\frac{1}{2}} = \beta_o = \text{const.} \qquad (1.5b)$$

The constants of integration $\beta_x(0)$ and $\beta_y(0)$ can be chosen to insure that the beam does not drift in the transverse directions. This requirement gives the conditions for "perfect injection"

$$\beta_x(0) = -\frac{K}{\gamma} \quad , \quad \beta_y(0) = 0 \quad , \qquad (1.5c)$$

Integrating (1.5b) gives $z(t) = c\beta_o t + z(0)$. The transverse oscillations are obtained by direct integration of (1.5a) using $z(t)$ in $\Psi(z)$:

$$\begin{aligned} x(t) &= -\frac{K\lambda_o s}{\gamma\beta_o}\Big[\cos(2\pi s^2)\,[C(q) - C(2s)] + \\ &\quad + \sin(2\pi s^2)\,[S(q) - S(2s)] \Big] + x(0) \quad , \\ y(t) &= -\frac{K\lambda_o s}{\gamma\beta_o}\Big[\cos(2\pi s^2)\,[S(q) - S(2s)] - \\ &\quad - \sin(2\pi s^2)\,[C(q) - C(2s)] \Big] + y(0) \quad , \end{aligned} \qquad (1.6)$$

where $s^2 = L(\eta)/2\eta\lambda_o$, $q = 2s\,[1 + \eta c\beta_o t / L(\eta)]$, $S(q)$ and $C(q)$ are Fresnel integrals and $z(0) = 0$ for simplicity. For undulators with a number of periods $N \gg 1$ and with $\eta \leq 1$ the arguments of the Fresnel integrals are large. Using their asymptotic expansions [14] and keeping only the leading term in q^{-1} we

obtain

$$\begin{aligned} x(\tau) &= -\frac{K\lambda_o}{2\pi\gamma}\left[\frac{\sin\Psi(\tau)}{(1 + \eta\tau)} \right] + x(0) \quad , \\ y(\tau) &= -\frac{K\lambda_o}{2\pi\gamma}\left[1 - \frac{\cos\Psi(\tau)}{(1 + \eta\tau)} \right] + y(0) \quad , \end{aligned} \qquad (1.7)$$

where

$$\Psi(\tau) = k_o\, L(\eta)\, \tau\, (1 + \eta\tau/2) \quad ,$$

and $\tau = c\beta_o t / L(\eta)$ so that $0 \leq \tau \leq 1$ for any trajectory. Both results (1.6) and (1.7) are new and relevant to the explicit angular dependence of the spectrum that will be calculated in Sec. IV.

The function $x(\tau)$ is plotted in Fig. 1 for the values $\eta = 1.0$, $x_o(0) = 0$, and $N = 10$ periods in the undulator. A similar plot would describe $y(\tau)$. Both the wavelength and the amplitude of the oscillations decrease while keeping K constant. A typical amplitude of the transverse oscillations is $K\lambda_o / 2\pi\gamma \approx 10^{-2}$ cm. There is an upper limit on $K/\gamma \leq 0.369$ for stable orbits in untapered undulators [15].

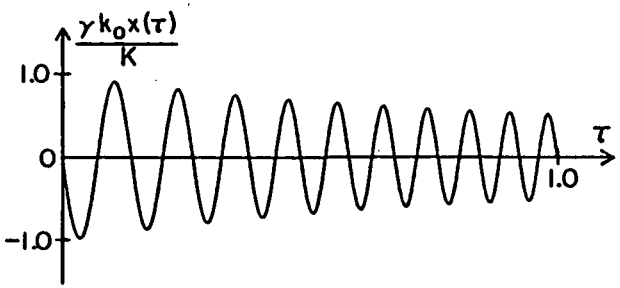

Fig. 1. Electron trajectories in a tapered undulator. The electron is shown to "undulate" in phase with the magnetic field. The amplitude and wavelength of the oscillations decrease to keep $K = eB(z)/k_o(z)mc^2$ constant along z.

To insure that all the electrons in a beam follow helical orbits along the same axis of the undulator, we must choose the initial position $x(0)$ and $y(0)$ so that $\int_0^1 x(\tau)\,d\tau = \int_0^1 y(\tau)\,d\tau = 0$. The integration can be performed numerically to find that for values of η less than unity $|x(0)| \le 0.057\ K\lambda_0/2\pi\gamma$, $|y(0)| \le 0.998\ K\lambda_0/2\pi\gamma$. Since typical electron beams have a $d \approx 1$ mm diameter this condition cannot be met for all electrons. Most electrons travel in parallel but identical helices. The characteristic emission angle for relativistic electrons is γ^{-1} so that the light emitted with wavelength λ adds coherently from all electrons within a beam of diameter d if $d \le \gamma\lambda$. This condition is not met for typical experiments since $\gamma\lambda \approx 0.2$ mm, and coherent emission is only possible over a narrower range of emission angles. Fortunately in an FEL, the high Q resonator selects a much narrower range of angles naturally so that all electrons participate coherently.

II. Total Energy Radiated

We can use the formula of Liénard [16] to express the total electromagnetic energy radiated:

$$E_{tot} = \int_{-\infty}^{\infty} \frac{2e^2\gamma^6}{3c}\left[\left(\frac{d\vec{\beta}}{dt}\right)^2 - \left(\vec{\beta}\times\frac{d\vec{\beta}}{dt}\right)^2\right]dt \quad . \tag{2.1}$$

Using (1.5) we obtain

$$E_{tot} = \frac{2}{3}e^2\gamma^2K^2k_o^2\beta_o\,L(\eta)(1+\eta+\eta^2/3) \quad . \tag{2.2}$$

For small amounts of tapering and using (1.4)

$$E_{tot} \approx \frac{2}{3}e^2\gamma^2K^2k_o^2\beta_o\,L_o\left[1+\frac{\eta}{2}+\frac{\eta^2}{6}\cdots\right] \quad . \tag{2.3}$$

Notice that E_{tot} increases in proportion to γ^2K^2 and increases with η because the electron is forced into a tighter spiraling motion. Typical numerical

values ($\gamma \approx 80$, $K \approx 0.7$, $L_o \approx 1.6$m, $\lambda_o \approx 3$cm) give $E_{tot} \approx 0.1$ eV. This justifies neglecting radiation losses in Sec. I since $E_{tot} \ll \gamma mc^2$.

III. Liénard-Wiechert Fields

The radiation fields from accelerating electrons can also be investigated by using the Liénard-Wiechert fields [16]. The electric field at the observation position $\vec{D} = D\hat{n} = D(\sin\vartheta\cos\varphi, \sin\vartheta\sin\varphi, \cos\vartheta)$ created by an electron at $\vec{r}(t)$ is

$$\vec{E}(\vec{D},t) = -\left\{\frac{e}{\kappa^3}\left[\frac{(\hat{n}-\vec{\beta})}{\gamma^2R^2} + \frac{\hat{n}\times((\hat{n}-\vec{\beta})\times(d\vec{\beta}/dt))}{cR}\right]\right\}_{ret} \tag{3.1}$$

where $\vec{R}(t') = \vec{D} - \vec{r}(t')$ and $\kappa = 1 - \hat{n}\cdot\vec{\beta}(t')$. The quantity in brackets is evaluated at the retarded time given by $t' = t - R(t')/c$. In the far field limit (R large) and in the forward direction ($\vartheta = 0$), $R(t') \approx (D - c\beta_o t')$. Using (1.7) and $\Psi(\tau)$ defined there, we get

$$\vec{E}(t)\Big|_{\vartheta=0} \approx \frac{4\gamma^3eKk_o\,(1+\eta\tau')}{(1+K^2)^2(D-\tau'L(\eta))}\,[\,\sin\Psi(\tau'),\ -\cos\Psi(\tau'),\ 0\,] \tag{3.2}$$

where

$$\tau' = \frac{2\gamma^2(ct-D)}{(1+K^2)L(\eta)} \quad ,\text{and} \quad \gamma \gg 1 \quad .$$

The radiation is substantially Doppler shifted to higher frequencies for relativistic electrons due to the γ^2 factor in Ψ. This feature gives the FEL its wide tunable range to short wavelengths. For typical parameters the emitted wavelength is $\sim 3\mu$. The effect of tapering is to introduce more Fourier components into the oscillation spectrum, thus complicating the line shape. The forward radiation is circularly polarized because of the helical undulator design.

It is interesting to investigate whether quantum effects might play a role in the emission process. The number of photons emitted by a single electron per pass through the undulator is approximately $E_{tot}/\hbar\omega$, ignoring emission into higher harmonics ($K \le 1$) and the taper ($\eta \ll 1$). The photon frequency from

(3.2) is $\omega \approx 2\gamma^2\omega_o$ where $\omega_o = ck_o$. Then using (2.3) $E_{tot}/\hbar\omega \leq 1$. The classical results must therefore be interpreted as representing the average energy emitted and the photon statistics left to another calculation.

Now consider the emission from a beam of N_e electrons. Interference effects due to the phase differences introduced by the initial position $\vec{r}_j(0)$ of the j^{th} electron have to be taken into consideration. The effects of the transverse distribution of initial positions has been discussed. The effects of the longitudinal distribution of initial electron phases $\zeta_j = 2\gamma^2 k_o z_j(0)/(1+K^2)$ is found by summing the contributions from all the electrons using (3.2)

$$\vec{E}_{tot}(t) = \sum_{j=1}^{N_e} \vec{E}_j(t) = \sum_{j=1}^{N_e} \frac{4\gamma^3 e K k_o (1+\eta\tau')}{(1+K^2)^2 (D-\tau' L(\eta))} \left| \sin(\Psi(\tau')+\zeta_j), -\cos(\Psi(\tau')+\zeta_j), 0 \right|$$

$$= \frac{4\gamma^3 e K k_o (1+\eta\tau') A}{(1+K^2)^2 (D-\tau' L(\eta))} \left| \sin(\Psi(\tau')+Z), -\cos(\Psi(\tau')+Z), 0 \right| \qquad (3.3)$$

where

$$A^2 = N_e + 2\sum_{i>j}^{N_e} \cos(\zeta_i - \zeta_j) \quad , \quad Z = \tan^{-1}\left| \frac{<\sin\zeta_j>}{<\cos\zeta_j>} \right| ,$$

and $< \cdots > \equiv N_e^{-1} \sum_{j=1}^{N_e} (\cdots)$. When $N_e \gg 1$ and the phases are completely random $A \approx \sqrt{N_e}$. The radiated power detected will then be proportional to N_e and during the initial stages of start-up in a resonator this is the relevant case. After enough radiation build-up, the optical field begins to bunch electrons in phase ζ_j ; so that the limit $E_{tot} \propto N_e$ is approached. In what follows, only the emission from a single electron is calculated, and the result is considered characteristic of the incoherent emission from the whole beam.

IV. Radiation Spectrum

The Fourier spectrum of the Liénard-Wiechert fields can be used to solve for the infinitesimal amount of electromagnetic energy d^2E emitted into the solid

angle $d\Omega$ within the frequency range $(\omega, \omega + d\omega)$ [Ref. 16]

$$\frac{d^2E}{d\Omega\, d\omega} = \frac{e^2\omega^2}{4\pi^2 c} \left| \int_{-\infty}^{+\infty} dt \left[\hat{n} \times (\hat{n} \times \vec{\beta}(t)) \right] \exp\left[i\omega \left(t - \hat{n}\cdot\vec{r}(t)/c \right) \right] \right|^2 \qquad (4.1)$$

Since an electron only accelerates inside the undulator, the limits of the time integration are $t = 0$ to $L(\eta)/\beta_o c$ ($\tau = 0$ to 1). For long helical undulators, the emission spectrum does not depend on the azimuthal angle φ, so that we take $\varphi = 0$ in $\hat{n}$. The initial position $\vec{r}(0)$ introduces a phase factor that does not affect the emission spectrum. Inserting $\vec{\beta}(\tau)$ from (1.5) and $\vec{r}(\tau)$ from (1.7) we obtain

$$\left.\frac{d^2E}{d\Omega d\omega}\right|_{\varphi=0} = \frac{e^2\omega^2 L^2(\eta)}{4\pi^2 c^3 \beta_o^2} \left| \int_0^1 d\tau \left\{ \mathcal{Z} \left[\frac{K}{\gamma}\cos^2\vartheta \cos\Psi(\tau) + \beta_o \sin\vartheta\cos\vartheta \right] + \mathcal{Y} \left[\frac{K}{\gamma}\sin\Psi(\tau) \right] + \mathcal{Z} \left[-\beta_o \sin^2\vartheta - \frac{K}{\gamma}\sin\vartheta\cos\vartheta\cos\Psi(\tau) \right] \right\} \times \exp\left\{ \frac{i\omega L(\eta)}{\beta_o c} \left[(1-\beta_o\cos\vartheta)\,\tau + \frac{K\sin\vartheta}{\gamma k_o L(\eta)} \left[\frac{\sin\Psi(\tau)}{(1+\eta\tau)} \right] \right] \right\} \right|^2 \qquad (4.2)$$

where $\Psi(\tau)$ is defined below (1.7). The analytical integration is carried out in the Appendix, but the result is not transparent. Instead we numerically obtain graphs of the spectral properties. Expression (4.2) reduces to the sum of the squares of six real integrals that can be more efficiently evaluated numerically than the result (A.3).

The spectrum's fundamental line shape in the forward direction is presented for a wide range of values of η in Sec. IV A. Then, in Sec. IV B, the angular features of the spectrum are examined in detail at a few selected values of η. The values for the physical parameters are $\lambda_o = 3.2$ cm, $K = 0.747$, $\gamma = 80$, and the number of undulator periods is $N = 50$.

A. The Forward Spectrum in the Fundamental

In Fig. 2 the forward emission spectrum of (4.2) is shown for the fundamental at selected values of η between 0.0 and 0.48. The figure shows that the line becomes broader and more structured, as η increases, while the center moves towards higher frequencies. These features can be understood if we think of a tapered undulator as a succession of untapered undulators, whose wavenumber increases over the same length, so that the convolution of their spectra gives a shifted line center at $\omega_o(1 + \eta/2)/(1 - \beta_o)$ for $\vartheta = 0$.

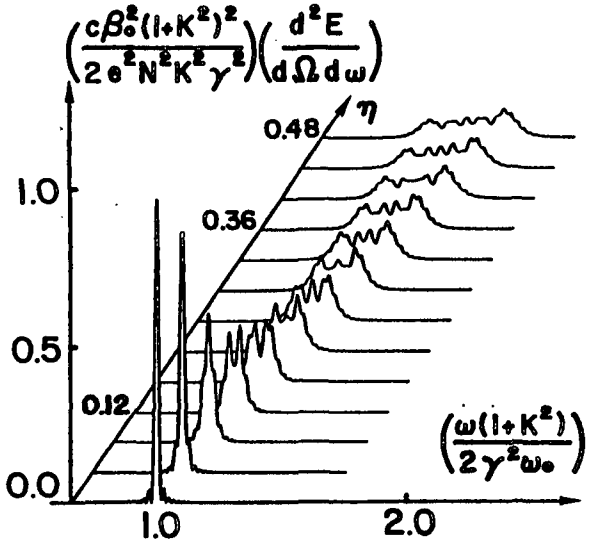

Fig. 2. The forward spectrum from a tapered undulator is shown with $0 \le \eta \le 0.48$, $f = 1$, and $\vartheta = 0$. The energy emitted is plotted in units of the forward power emission energy from an untapered undulator using the same electron energy and having the same physical parameters N, K, and λ_o.

For the tapered undulator the total spectral width can be approximated by the sum of the untapered linewidth $\approx \omega_o / N(1 - \beta_o)$, and the shift in the line center caused by tapering, which is $\approx \omega_o \eta / 2(1 - \beta_o)$. The resulting linewidth for tapered undulators is therefore $\approx \omega_o(1 + N\eta/2)/N(1 - \beta_o)$. This estimate

gives the range of frequencies over which the emitted energy drops to $\approx 5\%$ of the peak value. In Fig. 2 we show forward spectra for a range $0 \le N\eta/2 \le 12$. Note that the linewidth increases rapidly with increasing taper, because of the large number of periods. In Fig. 3 the emitted energy at the line center is plotted as a function of η. The decrease in peak emission observed between $\eta = 0.0$ and $\eta = 0.20$ is due to the rapid increase in the spectral width, together with the slower increase in the total energy radiated.

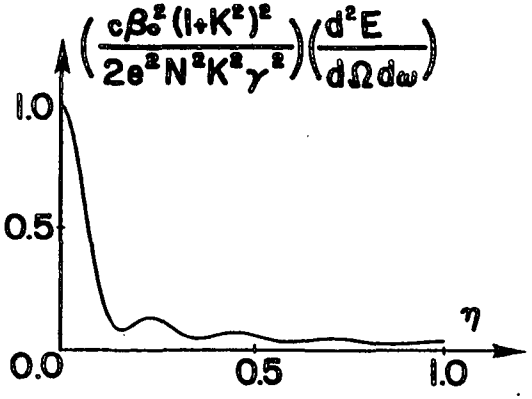

Fig. 3. The forward emission of the fundamental at the line center is plotted against the amount of taper η for $0 \le \eta \le 1$.

B. Angular Dependence (including higher harmonics)

The angular dependence of the radiation from a tapered undulator shows the same characteristic behavior as for of the untapered undulator [6,7]. Fig. 4 shows the radiated energy as a function of frequency and angle in the fundamental and first three higher harmonics for the taper $\eta = 0.05$. Note that the peak emission in each harmonic shifts down in frequency as the observation angle away from the undulator axis ϑ increases; the line shape remains substantially unchanged as the detector is moved off axis. The same physical arguments as presented in Sec. IV A show that the peak emission falls on a locus of points in

the $(\omega\,,\,\vartheta)$ plane described by

$$\omega_f = \frac{f\,\omega_o(1+\eta/2)}{(1-\beta_o\cos\vartheta)} \tag{4.3}$$

and the linewidth in each harmonic is given by

$$\delta\omega_f \approx \frac{\omega_o[1+(Nf\eta/2)]}{N(1-\beta_o\cos\vartheta)} \tag{4.4}$$

where $f = 1, 2, 3, ..$ is the harmonic number ($f = 1$ is the fundamental).

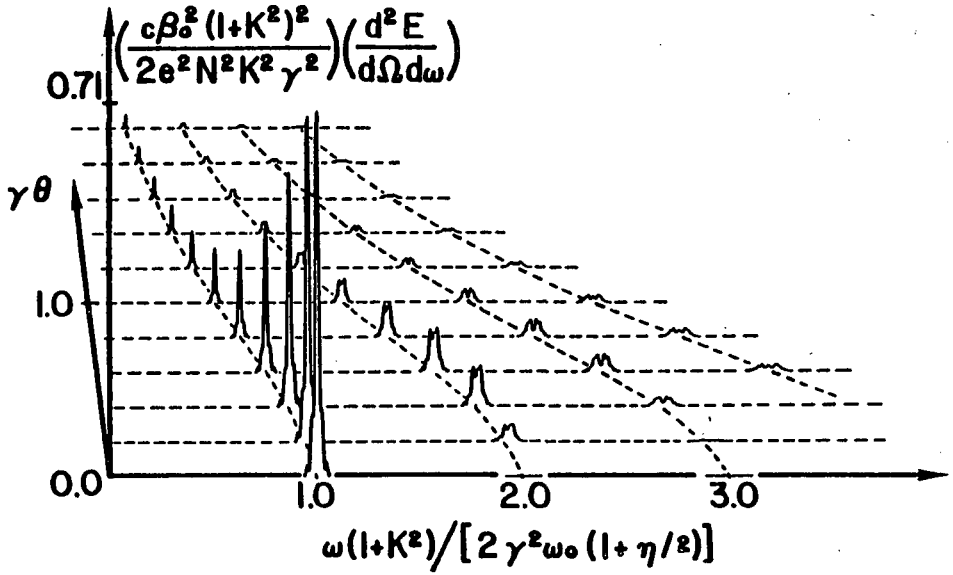

Fig. 4. The fundamental and first three higher harmonics of the emission spectrum from a tapered undulator with $\eta = 0.05$ are shown as a function of frequency ω and angle in units $\gamma\vartheta$.

An interesting aspect of (4.4) is that the linewidth depends on η and f only through their product. Therefore the spectrum in higher harmonics should have the same characteristic width as the one at lower harmonics with a higher amount of taper. Likewise reducing the tapering gives a line shape resembling

the spectrum in lower harmonics. In Fig. 5 we show the shape of various spectral lines, all calculated at the fixed characteristic emission angle $\vartheta = \gamma^{-1}$. They are arranged in a square "matrix" whose rows correspond to various taperings ($\eta = 0.05\,,\,0.10\,,\,0.15\,,\,0.20$) and whose columns correspond to the fundamental and the first three higher harmonics ($f = 1, 2, 3, 4$). The emission energy and frequency scales are the same for all graphs, to allow for direct comparison. Notice that the matrix is nearly symmetric about the diagonal, in that the line shapes corresponding to the same value of $f\eta$ are similar.

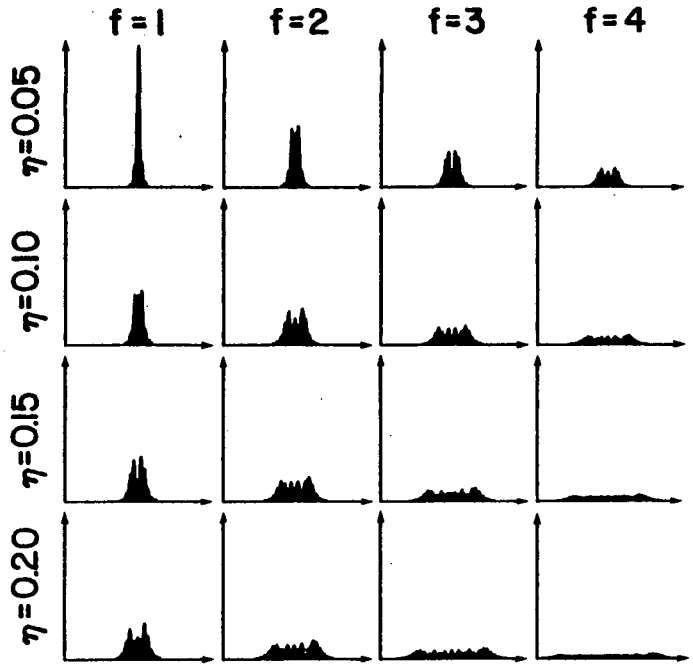

Fig. 5. The spectral line shapes $d^2E(\omega)/d\omega\,d\Omega$ are shown for $\eta = 0.05$, 0.10, 0.15, 0.20 and $f = 1, 2, 3, 4$. Line shapes corresponding to the same value of $f\eta$ are seen to be similar.

As in the case of a circularly polarized untapered undulator [6,7], the tapered undulator generates no forward radiation in higher harmonics. In Fig. 6

we follow the radiated energy measured at the line center ω_f given in (4.3) as a function of ϑ for various harmonics and tapers. Each separate graph refers to the same harmonic number f = 1, 2, 3 and 4, and shows the angular dependence of the peak emission for different values of taper η. At each angle the peak energy radiated into the frequency interval around ω_f decreases monotonically as η increases owing to the line broadening in (4.4).

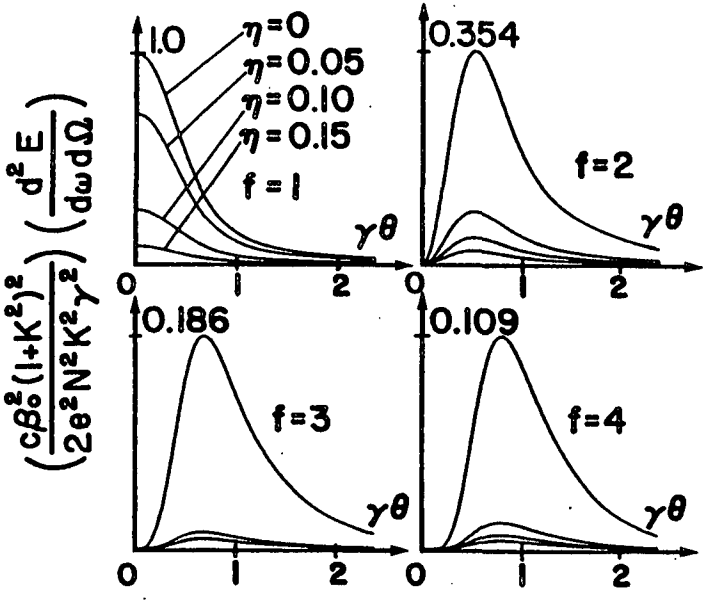

Fig. 6. The radiated energy measured at the line center frequency ω_f for the harmonics f = 1, 2, 3, and 4 is plotted against $\gamma\vartheta$ for taperings η = 0.0, 0.05, 0.10, and 0.15 for the case of a circularly polarized undulator.

For comparison in Fig. 7 we plot the same quantity in a linearly polarized undulator using the same physical parameters. There is now emission in the forward direction of each odd upper harmonic, f = 3, 5, 7,... owing to the longitudinal acceleration of the electrons [6,7].

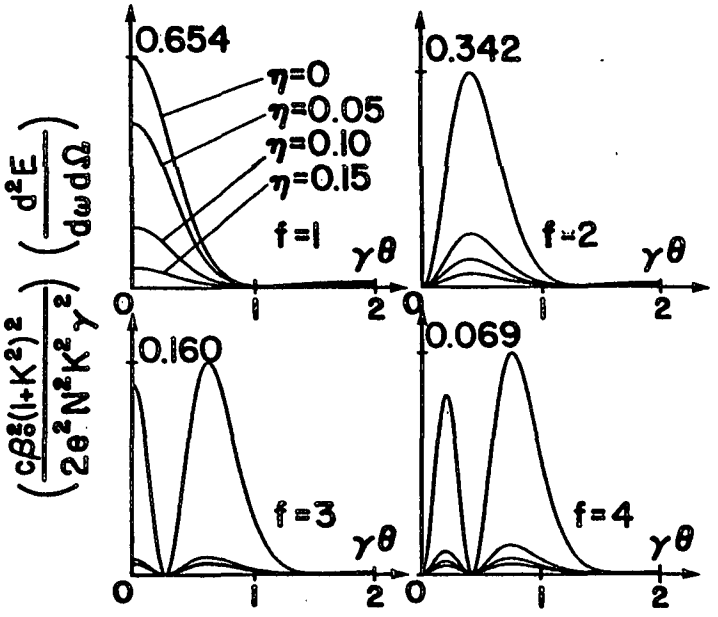

Fig. 7. The radiated energy measured at the line center frequency ω_f for the harmonics f = 1, 2, 3, and 4 is plotted against $\gamma\vartheta$ for taperings η = 0.0, 0.05, 0.10, 0.15 for the case of a linearly polarized undulator.

V. Polarization of the Spontaneous Emission

The polarization of the spontaneous radiation can be studied directly by using the Liénard-Wiechert fields (3.2). From (3.2) the ratio $|E_x|^2/|E_y|^2$ is seen to be unity at $\vartheta = 0$ and to vanish at the particular angle ϑ^* defined by

$$\gamma\vartheta^* = \cos^{-1}(\beta_0) \approx \sqrt{2}\,(1-\beta_0)^{1/2} = (1+K^2)^{1/2} \qquad (5.1)$$

for any value of taper η. For a typical value of $K = 0.7$, $\gamma\vartheta^* = 1.248$. As ϑ increases from 0 to ϑ^*, the radiation changes polarization from circular to linear independent of the amount of tapering.

The polarization of the spontaneous radiation calculated using (4.1) can be

found by projecting the integrand onto a unit polarization vector.

$$\hat{\varepsilon} = (\cos\vartheta \cos\Phi,\ \cos\vartheta \sin\Phi,\ -\sin\vartheta) \qquad (5.2)$$

The observation angle away from the undulator axis is ϑ and the polarization angle is Φ. The spectrum shown in Fig. 8 plots the radiated energy $d^2E(\hat{\varepsilon})/d\omega\, d\Omega$ from a tapered undulator with $\eta = 0.05$ as a function of ϑ measured at the line center of the fundamental for three different polarization angles $\Phi = 0, \pi/4, \pi/2$. The radiation off axis becomes progressively more polarized in the y-direction and at ϑ^* the emission becomes linearly polarized as described by (5.1).

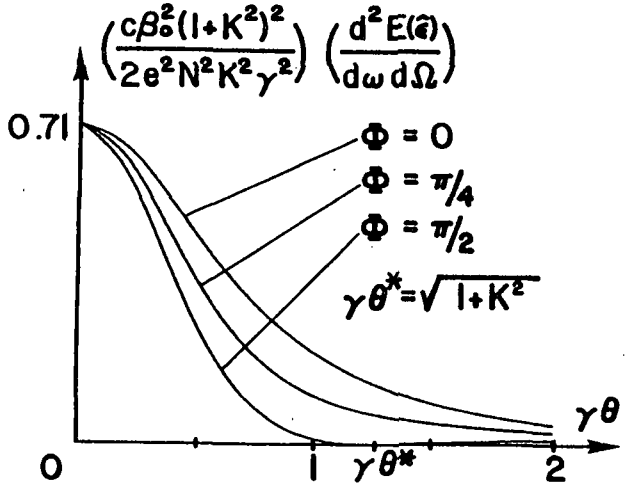

Fig. 8. The energy radiated $d^2E(\hat{\varepsilon})/d\omega\, d\Omega$ with polarization $\hat{\varepsilon}$ by a tapered undulator with $\eta = 0.05$ is shown as a function of $\gamma\vartheta$ at the line center in the fundamental. The radiation changes its polarization from circular to linear at the angle $\gamma\vartheta^* = \sqrt{1+K^2}$.

Conclusion

The results presented in this paper provide the first complete description of the spontaneous emission spectrum from a tapered undulator. The frequency and angular spectrum are presented for a wide range of taperings. The assumed linear dependence of $k_o(z)$ and K = const simplify the calculations but show the same general features expected of a wide range of tapered undulators. Practical designs are likely to be more complex to optimize the electron beam energy extraction during high power laser operation. The differences will show in the detailed shapes of the spectral lines while the angular distribution and the total energy emitted will remain comparable. These results should be useful to experimentalists working on tapered FEL designs.

Acknowledgements

We thank K. Speer, R. Freedman and G. Dattoli for helpful conversations. We are grateful for research support by NASA Grant NAG-2-48 and by Air Force Office of Scientific Research Grant AFOSR-81-0061.

Appendix

To perform the τ-integral in (4.2) we need to rewrite the integrand. Consider the second term in the exponential of (4.2) and expand in plane waves with Bessel function coefficients [14] to write

$$\exp\left\{\frac{i\omega K\sin\vartheta}{\beta_o\omega_o\gamma}\left[\frac{\sin\Psi(\tau)}{(1+\eta\tau)}\right]\right\} = \sum_{n=-\infty}^{\infty} J_n\left[\frac{\mu(\omega,\vartheta)}{1+\eta\tau}\right]\exp(in\Psi(\tau)) \qquad (A.1)$$

where $\mu = \omega K \sin\vartheta/\beta_o\omega_o\gamma$. The right hand side of (A.1) can be rewritten as follows [14]

$$\sum_{n=-\infty}^{\infty}\frac{\exp[in\Psi(\tau)]}{(1+\eta\tau)^n}\sum_{k=0}^{\infty}\frac{J_{n+k}(\mu)\,\mu^k}{2^k k!}\left[1-\frac{1}{(1+\eta\tau)^2}\right]^k . \qquad (A.2)$$

If $\vartheta = 0$ only the $k=0$ term survives, the double series reduces to unity, and the spectrum can then be expressed in terms of Fresnel integrals. If $\vartheta > 0$ the

τ–integrals in (4.2) can be expressed in the general form

$$\sum_{n=-\infty}^{\infty}\sum_{k=0}^{\infty}\frac{J_{n+k}(\mu)\mu^k}{2^{k+1}k!}\int_0^1 d\tau[e^{i\Psi(\tau)}\pm e^{-i\Psi(\tau)}]e^{in\Psi(\tau)}e^{i\omega(\omega,\vartheta)\tau}\frac{(\eta\tau)^k(2+\eta\tau)^k}{(1+\eta\tau)^{n+2k}} \quad (A.3)$$

where $w = \omega L(\eta)(1 - \beta_0 \cos\vartheta)/\beta_0 c$. When the tapering parameter $\eta \ll 1$ (as is typically the case) an expansion in η will have terms of the form

$$\int_0^1 d\tau\, \tau^k \exp\{ i [(n \pm 1)\Psi(\tau) + w(\omega,\vartheta)\, \tau]\} \quad . \quad (A.4)$$

Since $\Psi(\tau)$ is quadratic in τ , all resulting integrals can be performed analytically [14] and only the first few terms in the power series expansion need be retained.

References

1. G. A. Schott, *Electromagnetic Radiation* (Cambridge University Press, London ,1912).

2. J. Schwinger, Phys. Rev. **75** , 1912 (1949).

3. H. Motz, J. of Appl. Phys. **22** , 527 (1951).

4. D. F. Alferov, Yu. A. Bashmakov and E..G. Bessonov, Zh. Tekh. Fiz. **43** , 2126 (1973) [Sov. Phys. Tech. Phys. **18** , 1336 (1974)].

5. B. Kincaid, J. of Appl. Phys. **48** , 2684 (1977).

6. W. B. Colson, Ph.D. Dissertation (Stanford University, 1977)(unpublished).

7. W. B. Colson, Phys. Lett. **59A** , 187 (1976).

8. J.M.J. Madey, J.of Appl. Phys. **42** , 1906 (1971).

9. D.A.G. Deacon, L. R. Elias, J.M.J. Madey, G. J. Ramian, H. A. Schwettman and T. I. Smith, Phys. Rev. Lett. **38** , 892 (1977).

10. J.M.J. Madey, U.S. Patent No. 3,822,410 (1974).

11. N. M. Kroll, P. L. Morton and M. N. Rosenbluth, *Phys. of Quantum Electron.* **7** , 89 (1980).

12. P. Sprangle, C.-M. Tang, and W. B. Manheimer, Phys. Rev. Lett. **43** , 1932 (1979).

13. C. C. Shih and M. Z. Caponi, Phys. Rev. **A26** , 438 (1982).

14. M. Abramowitz and I. A. Stegun, *Handbook of Mathematical Functions* (Dover, New York, 1964).

15. P. Diament, Phys. Rev. **A23** , 2537 (1981).

16. J. D. Jackson, *Classical Electrodynamics* (Wiley, New York, 1975), Ch. 14.